Vol. 157 No. 1, February 1, 1984 ISSN 0003-2670

ANALYTICA CHIMICA ACTA

International journal devoted to all branches of analytical chemistry

ELSEVIER

ANALYTICA CHIMICA ACTA

International journal devoted to all branches of analytical chemistry
Revue internationale consacrée à tous les domaines de la chimie analytique
Internationale Zeitschrift für alle Gebiete der analytischen Chemie

PUBLICATION SCHEDULE FOR 1984

	J	F	M	A	M	J	J	A	S	O	N	D
Analytica Chimica Acta	156	157/1	157/2	158	159	160	161	162	163	164	165	166

Scope. *Analytica Chimica Acta* publishes original papers, short communications, and reviews dealing with every aspect of modern chemical analysis, both fundamental and applied.

Submission of Papers. Manuscripts (three copies) should be submitted as designated below for rapid and efficient handling:

Papers from the Americas to: Professor Harry L. Pardue, Department of Chemistry, Purdue University, West Lafayette, IN 47907, U.S.A.

Papers from all Other countries to: Dr. A. M. G. Macdonald, Department of Chemistry, The University, P.O. Box 363, Birmingham B15 2TT, England. Papers dealing particularly with computer techniques to: Professor J. T. Clerc, Universität Bern, Pharmazeutisches Institut, Baltzerstrasse 5, CH-3012 Bern, Switzerland.

Submission of an article is understood to imply that the article is original and unpublished and is not being considered for publication elsewhere. Upon acceptance of an article by the journal, authors will be asked to transfer the copyright of the article to the publisher. This transfer will ensure the widest dissemination of information.

Information for Authors. Papers in English, French and German are published. There are no page charges. Manuscripts should conform in layout and style to the papers published in this Volume. Authors should consult Vol. 150/2 for detailed information. Reprints of this information are available from the Editors or from: Elsevier Editorial Services Ltd., Mayfield House, 256 Banbury Road, Oxford OX2 7DH (Great Britain).

Reprints. Fifty reprints will be supplied free of charge. Additional reprints (minimum 100) can be ordered. An order form containing price quotations will be sent to the authors together with the proofs of their article.

Advertisements. Advertisement rates are available from the publisher.

Subscriptions. Subscriptions should be sent to: Elsevier Science Publishers B.V., Journals Department, P.O. Box 211, 1000 AE Amsterdam, The Netherlands. Tel: 5803 911, Telex: 18582.

Publication. *Analytica Chimica Acta* appears in 11 volumes in 1984. The subscription for 1984 (Vols. 156–166) is Dfl. 2145.00 plus Dfl. 231.00 (p.p.h.) (total approx. U.S. $950.40). All earlier volumes (Vols. 1–155) except Vols. 23 and 28 are available at Dfl. 200.00 (U.S. $80.00), plus Dfl. 15.00 (U.S. $6.00) p.p.h., per volume.

Our p.p.h. (postage, packing and handling) charge includes surface delivery of all issues, except to subscribers in the U.S.A., Canada and India who receive all issues by air delivery (S.A.L. — Surface Air Lifted) at no extra cost. For the rest of the world, airmail and S.A.L. charges are available upon request.

Claims for issues not received should be made within three months of publication of the issues. If not they cannot be honoured free of charge.

For further information, or a free sample copy of this or any other Elsevier Science Publishers journal, readers in the U.S.A. and Canada can contact the following address: Elsevier Science Publishing Co., Inc., Journal Information Center, 52 Vanderbilt Avenue, New York, NY 10017, U.S.A., Tel: (212) 867-9040.

ANALYTICA CHIMICA ACTA
VOL. 157 (1984)

ANALYTICA CHIMICA ACTA

International journal devoted to all branches of analytical chemistry

ELSEVIER Amsterdam–Oxford–New York–Tokyo

Anal. Chim. Acta, Vol. 157 (1984)

0003-2670/84/$03.0(

Printed in The Netherlands

Analytica Chimica Acta, 157 (1984) 1—16
Elsevier Science Publishers B.V., Amsterdam — Printed in The Netherlands

THE ELECTROCHEMICAL REDUCTION AND DETERMINATION OF REDUCED NICOTINAMIDE ADENINE DINUCLEOTIDE IN ACIDIC MEDIA

ANDREW WEBBER, MUMTAZ SHAH[a] and JANET OSTERYOUNG*

Department of Chemistry, State University of New York at Buffalo, Buffalo, NY 14214 (U.S.A.)

(Received 25th July 1983)

SUMMARY

The apparent reduction of reduced nicotinamide adenine dinucleotide (NADH) in acidic media at a static mercury drop electrode was investigated. A simple, quick pretreatment procedure was developed to convert the NADH to its acid-hydrated form. This adsorbs on the mercury surface during a film deposition time and the film is then reduced. The adsorption is diffusion-controlled and hence the peak currents for square-wave and linear-scan voltammetry are proportional to $Ct_p^{1/2}Af$ and $Ct_p^{1/2}Av$, respectively, where t_p is the effective film deposition time, C the concentration of NADH, A the electrode area, f the square-wave frequency, and v the linear scan rate. Several electrochemical techniques were compared for the determination of NADH; the method of choice is square-wave voltammetry, although staircase or linear scan voltammetry can also be used. The detection limit is less than 7 nM, and the range of linear response covers 2—3 orders of magnitude of NADH concentration.

The interconversion of NAD^+ and NADH is of immense importance in both biochemical and clinical laboratories (e.g., in the determination of alcohol or lactate dehydrogenase in serum). Many methods have been developed for the determination of NADH. Most are either spectroscopic or, more recently, electrochemical. The simplest is probably u.v. spectrophotometry which is, however, rather insensitive. Direct fluorimetry [1] is much better and has been developed by, among others, Chance and coworkers [2, 3] for in vivo and in vitro studies, particularly in the examination of the surfaces of various internal organs.

Most spectrometric methods used to quantify NADH are indirect and thus require additional steps of various degrees of complexity and cost. These indirect methods include colorimetry [4—7], u.v. spectrophotometry [8], fluorimetry [9], chemiluminescence [10], bioluminescence [11], mass spectrometry [12], radioimmunoassay [13], liquid scintillation [14] and photokinetic assay [15]. Some of these methods, especially when coupled

---

[a]Present address: School of Pharmacy, University of Georgia, Athens, GA 30602, U.S.A.

0003-2670/84/$03.00

with enzymatic cycling [5, 8, 9, 14], are very sensitive. However, enzymatic methods pose problems with regard to cost, stability and reproducibility.

Electrochemical techniques are generally sensitive and rapid, and, in contrast with spectrophotometric methods, are unaffected by turbidity of the solution. Indirect electrochemical methods for NADH involving the determination of hexacyanoferrate(II) [16] or other reactants [17—20] have been described. Direct electrochemical methods have been developed utilizing the anodic oxidation of NADH at solid electrodes [21—28]. A detection limit of 5 μM has been claimed using cyclic voltammetry for the oxidation at a carbon anode coated with adsorbed NAD^+ [26]. The amperometric method [23, 25, 28] seems to have a detection limit of 10 μM [21, 25]; interferences limit the usefulness of this method for liquids of biological origin [27, 28]. In addition, electrode fouling occurs at low pH values [23] or with high concentrations of NADH [21, 23, 28]. Thus, apart from the electrochemical methods, only u.v. spectrophotometry and fluorimetry offer a method for direct determinations of NADH.

The use of rapid-scan square-wave voltammetry was recently reported [29] for the direct determination of NADH in aqueous 0.1 M succinic acid solution at low concentrations (0.1 $\mu g\ ml^{-1}$). The method differed in concept from the other electrochemical methods in that the (apparent) reduction of NADH at a mercury electrode was involved. The purpose of this work is to examine the effect of various experimental parameters on this rather unusual reduction, in order to understand the electrode process and to explore and improve the quantitative method already suggested. The results provide a method for determination of NADH using square-wave voltammetry which yields detection limits below 7 nM. In a subsequent paper, work with similar compounds is discussed and, in conjunction with the present conclusions, enables a mechanism to be proposed for the reduction process.

EXPERIMENTAL

Materials

Sigma-Grade NADH obtained as preweighed vials of the disodium salt were used as received (0.2, 1.0 and 10 mg vials, lot numbers 654-F1, 662-F2 and 611-F1). Succinic acid (Fisher Certified) was twice recrystallized from water and dried in vacuo at 100°C for 24 h. Acetic acid (Baker, Ultrex grade), hydrochloric acid (Baker, Instra-analyzed), benzoic acid (Eastman Kodak, ACS Reagent Grade), oxalic acid (Fisher Certified), Triton X-100 (Fisher) and Baker-Analyzed formic acid (88%), malonic acid, sodium chloride, 1.0 M hydrochloric acid and 1.0 M sodium hydroxide solutions were used as received. Distilled water was purified by a Millipore Milli-Q water purification system. Ultraviolet (u.v.) spectrophotometry was done at room temperature using a Beckman DB-G spectrophotometer linked to a Bascom Turner 2120 digital plotter. The computer-controlled system for running electrochemical experiments and subsequent data analysis is described elsewhere [30].

Solutions of varying pH, ionic strength, and concentration of free succinic acid were prepared with the aid of a Metrohm E635 Dosimat and 636 Titroprocessor. This system was also used for pH measurements. The Davies equation was used [31] to estimate the activity coefficients used in the calculation of the necessary amounts of succinic acid, sodium hydroxide, and sodium chloride required for each solution. The results of these calculations are given in Table 1 along with the experimental pH values of the solutions. The principle behind this selection of media was to define a reference solution (in this case pH 3.8 (calc), 1.0 M ionic strength and 0.1 M free succinic acid) and then to prepare three series of solutions in which only one of these parameters was varied. The peak at −0.75 V in the electrolyte used in our first report [29] appears to be due to an impurity in the succinic acid, as no such peak was seen in the background scans of the solutions used in this study. From Table 1, the experimental pH values differ slightly from the calculated ones. This is because the Davies equation, used for calculating the activity coefficients, is an approximation [31]. The series of solutions of differing ionic strength vary slightly in pH, but the series in which the concentration of free succinic acid is varied is at both constant ionic strength and pH.

TABLE 1

Succinic acid buffer solutions

Calculated values[a]			Formalities[b]			Measured pH
pH	Ionic strength (M)	Conc. free succinic acid (M)	Succinic acid (F)	NaCl (F)	NaOH (F)	
3.0	1.00	0.10	0.109	0.991	0.0076	2.73
3.4	1.00	0.10	0.122	0.997	0.0222	3.17
3.8[c]	1.00	0.10	0.157	0.939	0.0589	3.57
4.2	1.00	0.10	0.251	0.827	0.162	4.00
4.6	1.00	0.10	0.521	0.437	0.492	4.48
3.8	0.25	0.10	0.162	0.184	0.0636	3.77
3.8	0.50	0.10	0.162	0.433	0.0643	3.69
3.8[c]	1.00	0.10	0.157	0.939	0.0589	3.57
3.8	1.50	0.10	0.151	1.447	0.0517	3.44
3.8	2.00	0.10	0.144	1.954	0.0447	3.33
3.8	1.00	0.025	0.039	0.985	0.0146	3.57
3.8	1.00	0.050	0.079	0.970	0.0294	3.57
3.8[c]	1.00	0.100	0.157	0.939	0.0589	3.57
3.8	1.00	0.150	0.236	0.909	0.0885	3.57
3.8	1.00	0.200	0.315	0.878	0.118	3.57

[a]Calculated from the literature pK_a values of succinic acid (4.16 and 5.61) and the dissociation constant of water using the Davies equation for estimation of activity coefficients. [b]Actual amount of the three components added. [c]This is the same reference solution repeated here to show the way in which each of the three parameters is varied, in turn.

Procedure

All voltammograms were obtained using an EG & G PARC Model 303 static mercury drop electrode and solutions were deoxygenated by purging with purified argon that was saturated with water. The cell contents were maintained at 25.0 ± 0.1°C. Four capillaries were used with the following mercury drop areas: A, 0.0177 cm^2; B, 0.0166 cm^2; C, 0.0156 cm^2 and D, 0.0182 cm^2. For comparison of results obtained using different capillaries, all currents are normalized to 0.0177 cm^2 drop area. All potentials were measured and are reported vs. a saturated calomel electrode (SCE) placed in a bridge tube containing the reference solution of succinic acid. The cell contents were separated from those of the bridge by a Vycor tip.

Unless otherwise stated, all square-wave voltammograms were recorded under the following conditions; initial potential (E_{in}) −0.55 V, final potential −1.40 V, step height 5 mV, frequency 30 Hz, square-wave amplitude 25 mV, delay time (time potential was held at −0.55 V prior to application of the potential waveform) 10 s. The average of four successive scans (each recorded on a fresh mercury drop) was taken. Data analysis was greatly facilitated by the computer-controlled system used. An example of a typical sequence is given in Fig. 1. Subtraction of the background from the voltammogram obtained in the presence of NADH (or, more precisely, its acid-decomposition products) yields voltammogram 1b. In square-wave voltammetry, the net current should be the same as the background current at potentials sufficiently far from the peak. This is not the case for curve 1b because the nitrogen-containing heterocycles of the sample catalyze the background reaction, proton reduction. Thus the net current from the reaction of interest is approximated by subtracting the current indicated by the tangent (dashed line) of Fig. 1b. This gives the final result, 1c, from which

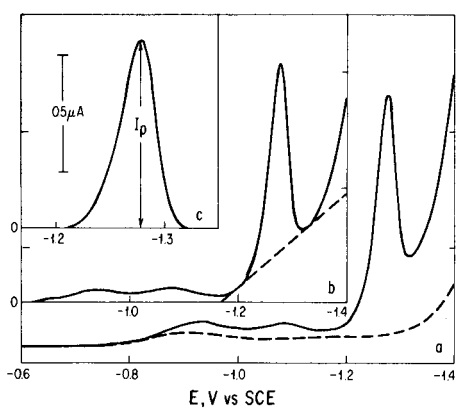

Fig. 1. Square-wave voltammetry of 2.8 μM pretreated NADH in the reference succinate buffer. (a) Dotted line is the background current. (b) Solid line is after background subtraction and dotted line is the line drawn through either side of the base of the peak. (c) After subtraction of the dotted line from the solid line in (b). Electrode A; square-wave parameters were the typical values given in the Procedure.

the peak potential (E_p) and current (I_p) are measured. The effect of subtracting the background (dotted line of Fig. 1a) from the voltammogram is quite small; as long as the tangent subtraction is done, no difference in the accuracy is expected if this step is omitted.

Quantities are generally reported as $\bar{x} \pm$ s.d.; for linear regressions the correlation coefficient, r, the number of data points, N, and the standard error of the estimate, S_{y_x}, are usually included.

RESULTS AND DISCUSSION

The main concern of this paper is the effect of chemical and electrochemical conditions on the faradaic response when NADH is added to acidic solutions. After discussion of the dependence on pH and the other constituents of the solution, the dependence on the parameters of the square-wave technique is described, and finally the responses for a variety of other commonly used voltammetric and polarographic techniques are considered.

It should be emphasized at the outset that NADH is highly unstable in acidic media and that most of the solutions used in this work cannot actually contain appreciable amounts of undecomposed NADH. Accordingly, NADH was added to solutions of different pH and the variation in peak current with time was examined (Fig. 2). There is an initial rise in the peak current followed by a slower decay. Both processes are faster at lower pH values. The reduction peak appears to be associated with an initial rapid formation of the electroactive species followed by some kind of slow decay. Table 2 shows the data obtained. Because of the time dependence, measurements done in any of these media would be inaccurate unless the peak currents were measured at the same time after addition of each sample to a fresh

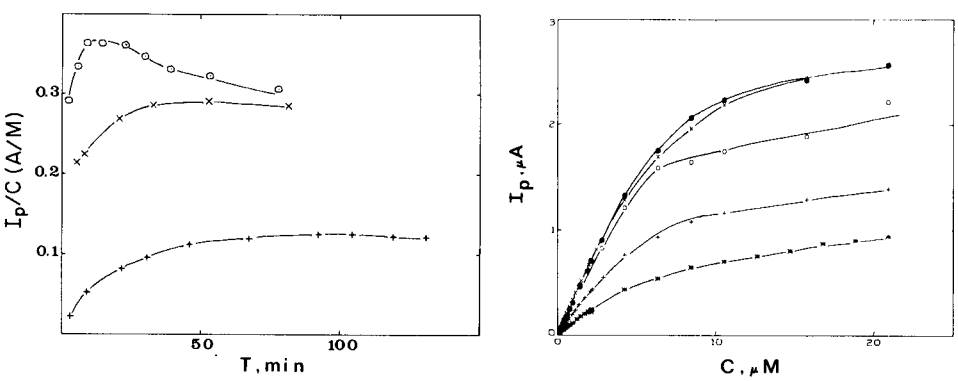

Fig. 2. Plot of peak current, normalized to a concentration of 1 μM, of (I) against time in solutions at different pH: (○) 2.7; (×) 3.6; (+) 4.5. (I) concentration was 1.3 μM for pH 2.7 and 3.6, and 2.8 μM for pH 4.5. Electrode A.

Fig. 3. Plots of peak current vs. concentration of pretreated NADH for succinate buffers at different pH: (●) 2.7; (×) 3.2; (○) 3.6 (standard solution); (+) 4.0; (*) 4.5. Electrode A.

TABLE 2

Degradation of NADH in acidic solution

Measured pH	Rise time[a] (min)	Decay rate[b] (% h^{-1})	k[c] (10^{-3} s^{-1})	$t_{0.9}$[c] (min)
2.73[d]	10	15	4.1	9.4
3.57[d]	30	4	1.2	31
3.66[e]	55	—	0.95	40
4.48[d]	90	5	—	—

[a]Time for square-wave peak current to reach its maximum value; average of two runs. [b]Decay rate of square-wave peak current; from the linear regression of I_p vs. t after the rise time, decay rate = slope/intercept. [c]From plots of ln A_{340} vs. time; solutions initially 85 μM in NADH. [d]0.1 M free succinic acid, 1.0 M ionic strength. [e]0.1 M free acetic acid, 0.25 M ionic strength.

electrolyte. In particular, the method of standard additions would pose problems; by the time the current response for each new addition had reached its maximum value, that due to the NADH previously added would have decayed to a significant degree.

Hydration of NADH

The general consensus of previous work done on the acid-catalyzed degradation of NADH and its analogs [32—40] is that the first step is hydration of the 5,6-double bond in the nicotinamide ring giving (I). The species (I) then undergoes a series of much slower degradation steps. The pseudo-first-order rate constant for the decay of NADH to (I) has been determined

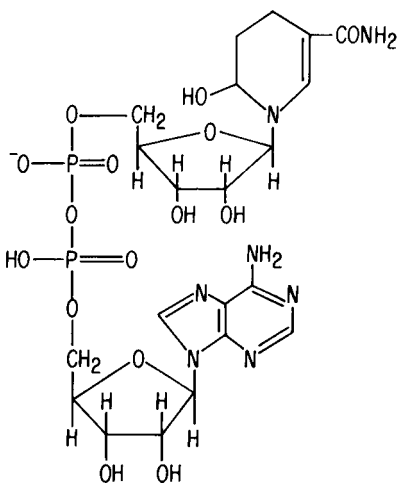

(I)

under a variety of conditions. Some typical values are: at pH 4.1, $k = 5.9 \times 10^{-4}$ s^{-1} ($t_{1/2}$ = 20 min); at pH 7.1, $k = 7.0 \times 10^{-6}$ s^{-1} ($t_{1/2}$ = 27 h) [38].

However, the rate of the reaction has been found to depend on the nature of the buffer as well as the pH. So, rather than estimate k from the literature, the decay with time was monitored by the absorbance of NADH at 340 nm. The results, given in Table 2, show that the initial increase in peak current on addition of NADH to these media can be attributed to the transformation of NADH to (I). The voltammetric data are insufficient to estimate a first-order rate constant for the growth of the peak current but, so as to enable a rough comparison, the $t_{0.9}$ (the time it takes for 90% of the NADH to decompose) is given in Table 2; this time is similar to the time needed for the square-wave peak current to reach its maximum value. Thus it seems clear that the faradaic reaction is actually the reduction of (I).

Pretreatment procedure

The variation in peak current with time makes it difficult to examine the effects of other experimental parameters on the system. A simple pretreatment procedure was therefore developed to eliminate these kinetic effects. The NADH was first dissolved in 10 ml of pH 2.7 solution; and after 15 min, when the NADH had been converted to (I), 2 ml of 1.0 M NaOH was added to bring the pH to 6.1. Adjusting the pH to 6.1 freezes the pH-dependent reaction(s) that are responsible for hydration of (I) and the decay in peak current at longer times. When samples from such a stock solution are added to solutions of various pH, the initial waiting period for the peak to develop is eliminated. Plots of peak current vs. time show only a decay in the peak current with rates of 14% h^{-1} at pH 2.7, 5.7% h^{-1} at pH 3.6 and 1.3% h^{-1} at pH 4.5. These decay rates are similar to those given in Table 2 for the same solutions. Replicate determinations in fresh electrolytes of samples taken from the same stock solution at various times showed hardly any variation in peak current. Stock solutions were discarded after 5 h; they may be stable for longer.

Elimination of the initial increase in peak current should enable accurate determinations to be done by using h.p.l.c. separation because the slow decay of 5% h^{-1} would not matter as long as standards and samples were treated under similar conditions (e.g., the same retention times). However, for determinations by direct voltammetry, the decay rate of the peak current should be taken into account. So, in the following series of experiments using the method of standard additions of pretreated NADH, the cell contents were discarded and the calibration was resumed with a fresh electrolyte after 30 min (pH 2.7 and 3.2) or 60 min (pH 3.6, 4.0 and 4.5). The decrease in peak currents of the final samples, caused by decay of the samples added earlier, is estimated to be 1—2%.

A series of measurements on 2.1 μM NADH in the pH 4.0 solution, using stock solutions from different sample vials of NADH, gave a relative standard deviation of the peak current of 1.8%.

Effect of pH value, ionic strength and free succinic acid concentration

The peak currents for (I) are much larger than expected for a diffusion-controlled process. One possible explanation is a catalytic mechanism involving succinic acid. In the preliminary report [29], data obtained from solutions in which the pH value, ionic strength, and concentration of free succinic acid were varied simultaneously showed a linear relationship between the peak current and the concentration of free succinic acid. Moreover, no response was seen in oxalic acid solutions. Catalytic currents generally increase with buffer capacity and decrease with increasing ionic strength. Therefore, the effects of independently varying pH, ionic strength, and the concentration of free succinic acid (i.e., the buffer capacity) were examined.

Calibration curves at various pH values (but constant ionic strength and concentration of free succinic acid) are shown in Fig. 3. At low concentration, the plots are linear but at higher concentrations they become curved. Solutions with pH values higher than 3.6 yield much smaller peak currents, but the peak current decays faster with time at lower pH values, so pH 3.6 seems to be the optimum value for the determination of (I). Concentrations as low as 40 nM were readily quantified at pH values of 2.7 and 3.6 using the standard conditions outlined in the experimental section. Table 3 gives the results of a least-squares fit of a line to the initial portions of the calibration plots of Fig. 3. The excellent correlation coefficients at low pH values and the near zero intercepts demonstrate that determinations at these concentrations (0.04—2 μM) are quite straightforward and precise. The peak potential is independent of concentration over the linear range of the plot of peak current vs. concentration, but shifts to more negative potentials as more (I) is added. The average peak potentials at low concentrations are given in Table 3. A plot of peak potential vs. pH value is linear with a slope of 60.4 ± 0.8 mV (S_{yx} = 1.0 mV, N = 5, r = 0.9998). The exact relationship is expressed by the equation

TABLE 3

Calibration data for NADH in solutions of various pH values[a]

Measured pH	Average E_p (V vs. SCE)	Slope (mA M^{-1})	Intercept (nA)	S_{yx} (nA)	r	N	Conc. range[b] (μM)
2.73	—1.227	317 ± 2	1.5 ± 2.8	9.6	0.9997	20	0—4.3
3.17	—1.254	330 ± 2	9.8 ± 2.2	6.3	0.9997	20	0—2.5
3.57	—1.276	316 ± 1	1.4 ± 0.8	5.2	0.99991	17	0—2.0
4.00	—1.302	213 ± 3	3.0 ± 2.0	4.0	0.9993	10	0—1.4
4.48	—1.330	112 ± 3	12 ± 3	7.3	0.996	16	0—2.0

[a]All solutions were 1.0 M ionic strength, 0.1 M free succinic acid. NADH was pretreated as described in the text. N is the number of concentrations, r is the correlation coefficient, S_{yx} is the standard error of the estimate. [b]Linear range and range over which peak potential is independent of concentration.

$$E_p(\text{V vs. SCE}) = -1.062 - 0.060\ \text{pH} \quad (1)$$

The strong dependence of peak current on pH and the shift in peak potential with pH indicates that at least one protonation step is involved in the electrode reaction. Similar experiments were done with solutions in which either ionic strength or free succinic acid concentration was varied (cf. Table 1). The results, presented in Tables 4 and 5, show that the peak current is independent of both parameters. The peak potential does vary with ionic strength but this is almost wholly accounted for by the fact that the pH values of the solutions are not the same. These data show clearly that there is no specific interaction between succinic acid and the decomposition products of NADH, and that the electrode process is not catalytic in nature.

Other acidic media

Because it appeared that succinic acid did not play a special role in the reaction, samples of pretreated NADH, i.e., (I), were examined in the following solvent systems: (a) acetic acid (0.1 M, 0.115 F), NaCl (0.235 F), NaOH (0.0149 F); (b) benzoic acid (0.01 M, 0.0115 F), NaCl (0.244 F), NaOH

TABLE 4

Calibration data for NADH in solutions of various ionic strengths[a]

Ionic strength (M)	E_p calc.[b] (V vs. SCE)	Average E_p (V vs. SCE)	Measured pH	Slope (mA M^{-1})	Intercept (nA)	S_{yx} (nA)	r	N	Conc. range (μM)
0.25	−1.290	−1.295	3.77	318 ± 3	1.5 ± 1.9	8.3	0.9996	9	0—1.0
0.50	−1.285	−1.289	3.69	321 ± 3	4.0 ± 2.0	3.9	0.9997	10	0—1.5
1.00	−1.277	−1.276	3.57	316 ± 1	1.4 ± 0.8	5.2	0.99991	17	0—2.0
1.50	−1.270	−1.270	3.44	299 ± 2	5.8 ± 1.4	7.7	0.99987	12	0—1.8
2.00	−1.263	−1.263	3.33	304 ± 2	2.4 ± 2.2	4.7	0.9998	11	0—2.7

[a]All solutions were 0.1 M free succinic acid. NADH was pretreated as described in the text. See Table 3 for meanings of the headings. [b]E_p calculated from $E_p = -1.062 - 0.060$ pH.

TABLE 5

Calibration data for NADH in solutions containing various concentrations of succinic acid[a]

$[H_2A]$ (M)	E_p (V vs. SCE)	Slope (mA M^{-1})	Intercept (nA)	S_{yx} (nA)	r	N	Concentrations range (μM)
0.025	−1.282	325 ± 5	15 ± 5	8.4	0.9992	10	0—1.9
0.05	−1.280	323 ± 3	7.8 ± 3.1	5.4	0.9997	11	0—1.9
0.10	−1.276	316 ± 1	1.4 ± 0.8	5.2	0.99991	17	0—2.0
0.15	−1.273	305 ± 6	8.0 ± 4.7	8.4	0.9989	8	0—1.4
0.20	−1.274	272 ± 3[b]	13 ± 4	6.6	0.9993	11	0—1.9

[a]All solutions were 1.0 M ionic strength, pH 3.57. [b]At a lower concentration the slope increased and became 334 from 0 to 0.4 μM (r = 0.99998, 3 concentrations).

(0.0053 F); (c) formic acid (0.1 M, 0.252 F), NaCl (0.0985 F), NaOH (0.151 F); (d) malonic acid (0.01 M, 0.142 F), NaCl (0.110 F), NaOH (0.136 F); (e) oxalic acid (0.0001 M, 0.102 F), NaCl (0.0467 F), NaOH (0.152 F); (f) hydrochloric acid (0.000215 F), NaCl (0.258 F). The measured pH values for these systems are listed in Table 6; F refers to the concentration added while M refers to the calculated molar concentration of free acid. Each solution was calculated to have a pH of 3.8 and an ionic strength of 0.25 M (except for the hydrochloric acid solution with ionic strength 0.26 M).

Table 6 shows the sensitivities and peak potentials for measurements in each solvent. Results are similar to those observed in the succinic acid media; thus only the pH is important to the electrode process. Using hydrochloric acid at pH 3.8 raises the question of buffer capacity. The concentration of protons in this solution is 100—100,000 times that of acid-decomposed NADH, which suggests that the solution should be effectively buffered. This turns out to be incorrect as discussed below. This is the reason why the plot of I_p vs. C in hydrochloric acid levels out at much lower concentrations than in the other media. Because pure acetic acid is readily available and provides good buffer solutions in the desired pH range, and because these solutions have very low background currents, acetate buffers were used for much of the following work.

It was previously reported [29] that no response was observed in 0.1 F oxalic acid solutions. With the oxalic acid solution described above, a peak can be detected. However, the onset of catalytic proton reduction appears at more positive potentials than in the other solutions, and the peak appears only as a small shoulder on this background current. Even using background subtraction, it is only at quite high concentrations that the peak is clearly discernible.

TABLE 6

Calibration data for NADH in various acidic media[a]

Acid	Measured pH	E_p calc.[b] (V vs. SCE)	Average E_p (V vs. SCE)	Slope (mA M^{-1})	Intercept (nA)	S_{yx} (nA)	r	N
Acetic	3.66	—1.283	—1.291	366 ± 1	—1.3 ± 0.8	1.1	0.99997	6
Benzoic	3.75	—1.288	—1.292	268 ± 2	1.9 ± 1.6	2.4	0.9998	7
Formic	3.69	—1.285	—1.290	380 ± 4	1.0 ± 2.4	3.3	0.9998	6
Malonic	3.80	—1.292	—1.297	348 ± 4	9.5 ± 4.3	7.5	0.9995	11
Succinic[c]	3.77	—1.290	—1.295	318 ± 3	1.5 ± 1.9	8.3	0.9996	9
Oxalic[d]	3.81	—1.292	—1.297	326	—	—	—	1
Hydrochloric	3.70	—1.286	—1.309	312 ± 15	4.8 ± 5.5	6.5	0.998	6

[a]All solutions were 0.25 M ionic strength, see text for further details. Range of concentrations is 0—1.0 μM, except for malonic and benzoic acid where the range is 0—2.0 μM. [b]E_p calc. is that calculated from the measured pH value and Eqn. 1. [c]This is the same as the first entry in Table 4. [d]Because of high background currents data were taken from one measurement at a concentration of 2.1 μM.

Reactant adsorption

A calibration experiment over the concentration range 1—100 μM pretreated NADH in 0.5 M ionic strength solution (pH 3.7 and 0.1 M free succinic acid) showed that the peak current leveled off completely and became independent of concentration above 20 μM. This is consistent with the process being the reduction of an adsorbed species which at concentrations above 20 μM completely covers the electrode surface. Figure 4 shows the effect of addition of Triton X-100 to the sample solution. The peak completely disappears and the voltammogram is identical to that obtained with no (I) added. (Addition of Triton X-100 to the electrolyte shifts the peak in the background at —0.9 V to more negative potentials and changes the shape to that of a wave. Presumably, this peak is due to some adsorbed impurity in the electrolyte.) Further additions of Triton X-100 have no effect on the voltammograms. It appears, then, that the strongly adsorbing Triton X-100 displaces the NADH decomposition product(s) from the electrode surface.

Dependence on square-wave parameters

The peak current was found to depend markedly on the delay time during which the potential is held at the initial value before application of the potential waveform. The longer the delay time (i.e., the older the drop) the larger the peak current. The background current is unaffected by the delay time, so detection limits should be improved by the use of longer delay times. A plot of peak current, I_p, for a 1.1 μM pretreated NADH solution in the 1.5 M ionic strength succinic acid solution against $t_p^{1/2}$, where t_p is the

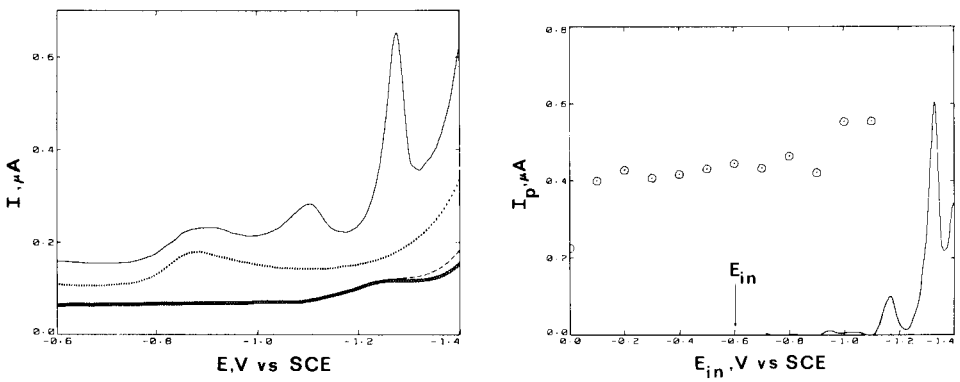

Fig. 4. Square-wave voltammograms of 1.06 μM pretreated NADH in the 1.5 M ionic strength succinate buffer with and without 0.0007% Triton X-100 present. Usual square-wave parameters; electrode B. (•) Background voltammogram; (—) with (I) added; (○) background with Triton X-100 added; (---) with both NADH and Triton X-100 added.

Fig. 5. Plot of peak current of 0.19 μM, pretreated NADH in acetate buffer against E_{in}. f = 180 Hz, t_d = 20 s, ΔE_s = 5 mV and the square wave amplitude is 25 mV. Voltammogram at lower right is with E_{in} = —0.6 V. Electrode D.

time after initiation of drop growth at which the electrode potential equals the peak potential, is linear (with f = 30 Hz and ΔE_s = 5 mV, slope = 88.1 ± 0.9 nA $s^{-1/2}$, intercept = −4.2 ± 3.8 nA, S_{yx} = 7.8 nA, N = 11, r = 0.9995). This time, t_p, depends on the delay time, t_d, the potential range, $E_p - E_{in}$, and the scan rate, $f\Delta E_s$, where f is the square-wave frequency and ΔE_s is the step height, and is given by Eqn. 2

$$t_p = t_d + (E_p - E_{in})/f\Delta E_s \quad (2)$$

Data obtained using two different values of E_{in} (−0.55 and −1.0 V) gave results independent of choice of E_{in}. A plot of log I_p vs. log t_p gives a line having a slope of 0.509 ± 0.009 (N = 11, r = 0.998). This dependence of I_p on t_p is that expected for diffusion-controlled adsorption of the electroactive species on the electrode surface. The adsorption is rapid (it is a diffusion-limited process) and independent of electrode potential in the range −0.5 to −1.0 V, as shown in Fig. 5. Long delay times and high frequencies are used to ensure that $t_p^{1/2}$ is virtually constant and that the electrode has not become completely covered with the adsorbed species. Assuming that peak current is proportional to surface coverage, it is evident from Fig. 5 that the reactant is adsorbed almost equally over virtually the entire potential range.

These observations suggested that stirring the solution (by purging with argon) during the delay time would also increase the sensitivity by increasing mass transport to the electrode. Use of both longer delay times (50 s) and purging with argon enabled determinations to be done at concentrations as low as 7 nM in the 0.025 M free succinic acid solution with sensitivity 12.1 times larger than that obtained when using the usual conditions (10-s delay time and no purging). The detection limit for this method (in effect, cathodic stripping square-wave voltammetry) is therefore less than 7 nM if longer delay times, of the order of minutes, are used. Obviously, more efficient and reproducible stirring could further enhance the response. This mechanism has important implications for use of the method in conjunction with h.p.l.c. separation. In this case the solution is passed over the electrode in a continuous stream at constant flow rate, which should give high and reproducible sensitivity.

As expected for the reduction of an adsorbed species, the peak current is directly proportional to the square-wave frequency; for 0.19 μM pretreated NADH in the acetic acid buffer, $\partial\log(I_p/t_p^{1/2})/\partial\log(f)$ = 1.03 ± 0.01 (N = 10, r = 0.9997). (For a diffusion-controlled process, I_p is proportional to $f^{1/2}$.) Plotting $I_p/Ct_p^{1/2}$ vs. f gives a slope of 3.40 ± 0.04 mA $s^{1/2}$ M^{-1} with an intercept of −5.1 ± 2.6 mA $s^{-1/2}$ M^{-1} (S_{yx} = 5.9 mA $s^{-1/2}$ M^{-1}, N = 11, r = 0.9995). At practical frequencies, the intercept is negligible and therefore $I_p = 3.40\,Cft_p^{1/2}$ mA (where C is in M, t_p is in s and f is s^{-1}). The peak potential depends linearly on log f with a slope of −39.4 ± 0.6 mV (S_{yx} = 0.8 mV, N = 10, r = 0.9991). The effect of experimental parameters on the peak current and peak potential will be discussed further in the subsequent paper.

Other electrochemical techniques

A solution of 0.77 μM pretreated NADH in the acetate buffer was examined by sampled-d.c., normal-pulse, and differential-pulse polarography and by both square-wave and staircase voltammetry. In each case the delay time (or drop time) was 10 s.

Sampled d.c. At this concentration virtually nothing is seen in the potential region of the major peak observed when square-wave voltammetry is used.

Normal pulse. For this mode (Fig. 6), a peak is seen which is quite large at short pulse times. This is further evidence of reactant adsorption. However, because the current is, as expected, proportional to the square root of drop time, achieving good sensitivities requires long experiment times. At 10 s per drop, a scan of 400 mV with 5-mV resolution would take 13 min in contrast with the 12 s required in the square-wave mode. Thus the normal pulse mode is tedious by comparison.

Differential pulse. There is no response at all using a pulse amplitude of 25 mV. This is to be expected, because during the waiting period before pulse application the adsorbed material reacts. Only in the limit of very large pulse amplitudes (i.e., effectively the normal pulse experiment) is the peak seen. This lack of signal in differential pulse should be a general phenomenon characteristic of any system following this mechanism.

Staircase voltammetry (Fig. 7). When long delay times are used, a peak is seen which is smaller than that observed with square-wave voltammetry at the same sampling frequency. The charging currents with this technique are, however, very large and background subtraction is required. The charging

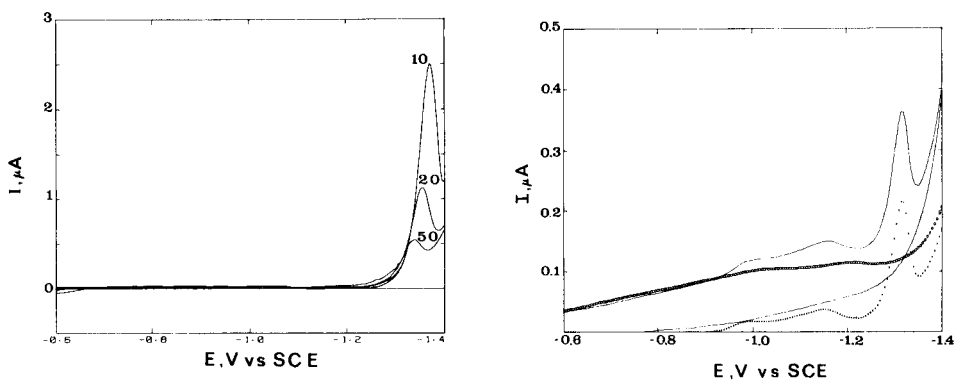

Fig. 6. Normal-pulse polarograms of 0.77 μM pretreated NADH in the acetate buffer after background subtraction. Drop time 10 s, current sampling time 1.67 ms; the numbers are the pulse times (ms). Electrode C.

Fig. 7. Staircase voltammogram of 0.77 μM pretreated NADH in the acetic acid solution. The backward portion is omitted for clarity for the curves with circles. (○) Background voltammogram; (—) with NADH added; (●) after background subtraction. t_d = 10 s, E_{in} = −0.55 V, f = 30 Hz, ΔE_s = 5 mV (effective sweep rate 150 mV s^{-1}). Electrode C.

currents expected for linear-scan voltammetry would be even larger, and therefore in linear-scan voltammetry background subtraction should be absolutely essential. In this respect, square-wave voltammetry is superior because background subtraction does not affect the result significantly. As was found for square-wave voltammetry, a plot of log I_p vs. log t_p (defined by Eqn. 2) has a slope of 0.53 ± 0.02 (N = 5, r = 0.9990). Similarly, a plot of I_p against $t_p^{1/2}$ (with staircase width 1/30 s and step height 5 mV) is linear with a slope of 44.2 ± 1.2 nA $s^{-1/2}$ and an intercept of −9.5 ± 4.5 nA (S_{yx} = 2.2 nA, N = 5, r = 0.9990). This is, as mentioned previously, in accord with diffusion-controlled adsorption.

A 0.19 μM solution of pretreated NADH in the acetate buffer was examined by staircase voltammetry at various frequencies (sweep rates). The peak currents are directly proportional to the sweep rate, $\partial\log(I_p/t_p^{1/2})/\partial\log(\nu)$ = 1.00 ± 0.01, (N = 9, r = 0.9996), again in accord with the reduction of an adsorbed species. (Previously [29], $\partial\log(I_p)/\partial\log(\nu)$ = 0.67 was reported for linear-scan voltammetry. The apparent contradiction is attributable to the extreme difficulty of accurate background subtraction in the linear-scan case.) A plot of $I_p/Ct_p^{1/2}$ vs. f gave a line with a slope of 1.74 ± 0.02 mA $s^{1/2}$ M^{-1} and an intercept of 1.1 ± 1.4 mA $s^{-1/2}$ M^{-1} (S_{yx} = 3.2 mA $s^{-1/2}$ M^{-1}, N = 11, r = 0.9996). This is about one-half the sensitivity of square-wave voltammetry (slope = 3.40 mA $s^{1/2}$ M^{-1}). When the frequency, f, is replaced by the sweep rate, ν, for the cyclic staircase data, the sensitivity is $I_p/t_p^{1/2}C\nu$ = 0.349 A $s^{1/2}$ M^{-1} V^{-1}. As for square-wave voltammetry, the peak potential depends linearly on log f with a slope of 38.9 ± 0.2 (S_{yx} = 0.3 mV, N = 10, r = 0.99990).

CONCLUSIONS

By virtue of small background currents, good sensitivity, low detection limits, and short measurement times, square-wave voltammetry is the voltammetric technique of choice for this determination. However, staircase and linear-scan voltammetry can also be used. These techniques must be used in studying the electrode mechanism because no theoretical basis for interpreting square-wave voltammetric data in the case of adsorption-controlled processes exists at present. Normal-pulse voltammetry is less useful because of the long measurement times required, while differential-pulse voltammetry gives no signal.

The electrode process involves totally irreversible reduction of the adsorbed acid-decomposition product of NADH; because the adsorption is diffusion-controlled, greater sensitivity is obtained when long delay times or forced convection are employed.

A certain amount of caution must be exercised when using this method so that high concentration, long delay times, or convection do not result in saturation of the electrode surface with the adsorbed species. (Saturation occurs in unstirred solution for $Ct_p^{1/2} > 69$ μM $s^{1/2}$.) The method of standard

additions would reveal if complete surface coverage were to be reached, because the plot of peak current against concentration would be nonlinear. In addition, the peak potential would differ from that found in the case of partial coverage of the electrode.

If samples of biological origin are to be examined, interference from surfactants (e.g., in serum) would require separation of (I) from such compounds and also from other interfering nucleotides. The separation of NADH and (I) from other nucleosides and nucleotides in biological matrices has already been reported [41—45]; indeed, this is one method used for the study of acid-decomposition reactions of NADH [41, 43]. Use of this method for detection in a flow system (e.g., high-performance liquid chromatography) would seem to be particularly advantageous. Amperometric methods at solid electrodes suffer from electrode fouling [21, 23, 28], while the use of mercury as the electrode means that a clean drop can be used for every measurement. The detection limit for this procedure is two orders of magnitude lower than that given in our preliminary report [29], and the range of linear response covers almost three orders of magnitude (7 nM—5 μM).

Philip Elving discussed with us the chemistry of NADH, and Marek Wojciechowski assisted with experiments. We are grateful to both. This work was supported by the National Science Foundation under Grant Nos. CHE 7917543 and CHE 8305748.

REFERENCES

1 O. H. Lowry, N. R. Roberts and J. I. Kapphahn, J. Biol. Chem., 224 (1957) 1047.
2 D. E. F. Harrison and B. Chance, Appl. Microbiol., 19 (1970) 446.
3 G. Austin, R. Jutzy, B. Chance and C. Barlow, in P. J. Dutton, J. A. Leigh and A. Scarpa, Frontiers in Biological Energetics, Vol. 2, Academic Press, New York, NY, 1982, pp. 1445—1455.
4 J. F. Whitaker, Clin. Chim. Acta, 24 (1969) 23.
5 C. L. Woodley and N. K. Gupta, Anal. Biochem., 43 (1971) 341.
6 M. M. Nachlas, S. I. Margulies, J. D. Goldberg and A. M. Seligman, Anal. Biochem., 1 (1960) 317.
7 D. Kupfer and T. Munsell, Anal. Biochem., 25 (1968) 10.
8 M. P. Schulman, N. K. Gupta, A. Omachi, G. Hoffman and W. E. Marshall, Anal. Biochem., 60 (1974) 302.
9 F. M. Matschinsky and R. Thalmann, Laryngoscope, 77 (1967) 292.
10 D. C. Williams III and W. R. Seitz, Anal. Chem., 48 (1976) 1478.
11 P. E. Stanley, Anal. Biochem., 39 (1971) 441.
12 J. C. Weaver, M. K. Mason, J. A. Jarrell and J. W. Peterson, Biochim. Biophys. Acta, 438 (1976) 296.
13 R. Bredehorst, H. Lengyel and H. Hilz, Eur. J. Biochem., 99 (1979) 401.
14 G. S. Serif and F. R. Butcher, Anal. Biochem., 15 (1966) 278.
15 S. E. Brolin, E. Borglund, L. Tegner and G. Wettermark, Anal. Biochem., 42 (1971) 124.
16 L. C. Thomas and G. D. Christian, Anal. Chim. Acta, 82 (1976) 265.

17 A. L. Greenbaum, J. B. Clark and P. McLean, Biochem. J., 95 (1965) 161.
18 F. S. Cheng and G. D. Christian, Anal. Chem., 49 (1977) 1785.
19 D. Pfeiffer, F. Scheller, M. Janchen and K. Bertermann, Biochimie, 62 (1980) 587.
20 M. D. Smith and C. L. Olsen, Anal. Chem., 46 (1974) 1544.
21 W. J. Blaedel and R. A. Jenkins, Anal. Chem., 47 (1975) 1337.
22 W. J. Blaedel and G. A. Mabbott, Anal. Chem., 50 (1978) 933.
23 T. C. Wallace and R. W. Coughlin, Anal. Biochem., 80 (1977) 133.
24 L. C. Thomas and G. D. Christian, Anal. Chim. Acta, 78 (1975) 271.
25 G. G. Guilbault and T. Cserfalvi, Anal. Lett., 9 (1976) 277.
26 J. Moiroux and P. J. Elving, Anal. Chem., 51 (1979) 346.
27 G. D. Christian, Ion & Enzyme Electrodes in Biology and Medicine. International Workshop, University Park Press, Baltimore, MD, 1976, pp. 173—181.
28 T. C. Wallace, M. B. Leh and R. W. Couglin, Biotechnol. Bioeng., 19 (1977) 901.
29 M. Shah and J. Osteryoung, Anal. Chem., 54 (1982) 586.
30 T. R. Brumleve, J. J. O'Dea, R. A. Osteryoung and J. Osteryoung, Anal. Chem., 53 (1981) 702.
31 R. W. Ramette, Chemical Equilibrium and Analysis, Addison Wesley, Reading, MA, 1981, pp. 94—98.
32 A. G. Anderson, Jr. and G. Berkelhammer, J. Am. Chem. Soc., 80 (1958) 992.
33 C. C. Johnston, J. L. Gardner, C. H. Suelter and D. E. Metzler, Biochemistry, 2 (1963) 689.
34 S. G. A. Alivisatos, F. Ungar and G. J. Abraham, Biochemistry, 4 (1965) 2616.
35 D. W. Miles, D. W. Urry and H. Eyring, Biochemistry, 7 (1968) 2333.
36 N. J. Oppenheimer, Biochem. Biophys. Res. Commun., 50 (1973) 683.
37 C. O. Schmakel, K. S. V. Santhanam and P. J. Elving, J. Electrochem. Soc., 121 (1974) 1033.
38 R. D. Braun, K. S. V. Santhanam and P. J. Elving, J. Am. Chem. Soc., 97 (1975) 2591.
39 C. O. Schmakel, K. S. V. Santhanam and P. J. Elving, J. Am. Chem. Soc., 97 (1975) 5083.
40 S. L. Johnson and P. T. Tuazon, Biochemistry, 16 (1977) 1175.
41 J. R. Miksic and P. R. Brown, J. Chromatogr., 142 (1977) 641.
42 C. Bernofsky, Physiol. Chem. Phys., 10 (1978) 193.
43 C. Bernofsky, Physiol. Chem. Phys., 13 (1981) 3.
44 P. R. Brown, J. Chromatogr., 52 (1970) 257.
45 O. C. Ingebretsen, A. M. Bakken, L. Segadal and M. Farstad, J. Chromatogr., 242 (1982) 119.

Analytica Chimica Acta, 157 (1984) 17—29
Elsevier Science Publishers B.V., Amsterdam — Printed in The Netherlands

CATHODIC REDUCTION OF NICOTINAMIDE ADENINE DINUCLEOTIDE AND OTHER ADENINE-CONTAINING COMPOUNDS IN ACIDIC MEDIA

ANDREW WEBBER and JANET OSTERYOUNG*

Department of Chemistry, State University of New York at Buffalo, Buffalo, NY 14214 (U.S.A.)

(Received 25th July 1983)

SUMMARY

Both nicotinamide adenine dinucleotide (NAD^+) and acid-hydrated NADH, as well as adenine, adenosine, adenosine mono-, di-, and tri-phosphate and adenosine diphosphoribose, undergo four-electron reductions of the protonated adenine ring in acidic media. The values of αn_a (transfer coefficient times the number of electrons involved in the rate-determining step), n (total number of electron transferred), and p (number of protons involved in the rate-determining step) agree well with values previously reported for adenine. Cathodic stripping voltammetry of an adsorbed film can be applied to these compounds. Rapid scan rates are required to eliminate the slow desorption step at −1.1 V vs. SCE for some of these compounds. Hydration of the nicotinamide ring of NADH appears to inhibit this desorption step, but does not appear to be related directly to the electroactivity of the hydration product.

The redox behavior of nicotinamide adenine dinucleotide (NAD^+) and its reduced product (NADH) is important from both an analytical and mechanistic view. Greater understanding of the electrochemical mechanisms of these compounds can help comprehension of the nature of the NAD^+/NADH couple in the electron-transport chain in biological systems. Use of this couple to determine, indirectly, other compounds such as ethanol is also of growing interest. Recently [1, 2], the electrochemical determination of NADH at low concentrations by cathodic stripping voltammetry of an adsorbed film was reported. Adenine-containing compounds and other related pyrimidines (e.g., cytosine, cytidine) are of great biological and clinical importance [3—5], and quantitative methods for these compounds as sensitive as stripping voltammetry are extremely tedious and time-consuming. Whereas fluorescence spectrometry can be used to determine NADH at low concentrations, it cannot be used, at least directly, for the other adenine-containing compounds because they do not fluoresce.

In the previous paper [2], it was shown that it is the primary acid-degradation product of NADH (I) that is actually responsible for the reduction process. It is fortunate that it is the primary acid-degradation product that is

0003-2670/84/$03.00

the electroactive species, because there still exists considerable controversy about the nature of the secondary products.

The peak currents in square-wave and staircase voltammetry were found to be governed by diffusion-controlled adsorption of (I) during the effective delay time, t_p, that the electrode potential is held at —0.6 V vs. SCE before the potential is scanned negatively and the adsorbed film of (I) is reduced. Because it is not immediately obvious just what the electroactive site of (I) is, both adenine and reduced nicotinamide analogs of (I) were examined, and the parameters that define the electrode process for both (I) and the analogs under identical conditions were evaluated.

Thus the purpose of this report is to study the actual electrode mechanism for the electrochemical reduction reported in the previous paper and to examine briefly other adenine- and nicotinamide-containing compounds to determine whether the quantitative method based on cathodic stripping voltammetry can also be applied to these substances. The compounds examined were NAD^+, NADH, adenine, adenosine, AMP, ADP, ADPR, ATP, and NMNH (see below).

EXPERIMENTAL

Materials

In addition to the chemicals used previously [2], adenine, adenosine, adenosine-5′-monophosphate sodium salt (AMP), adenosine-5′-diphosphate sodium salt (ADP), adenosine-5′-triphosphate disodium salt (ATP), adenosine-5′-diphosphoribose sodium salt (ADPR), reduced β-nicotinamide mononucleotide sodium salt (NMNH) and β-nicotinamide adenine dinucleotide (NAD^+; lot number 625-F1) from Sigma Chemical Co. were used as received.

Procedure

Two acetate buffers were prepared as described previously [2]. The ionic strength was 0.25 M, the concentration of undissociated acetic acid was 0.1 M, and the measured pH values were 3.7 and 4.4. An EG&G PARC Model 303 static mercury drop electrode (SMDE) was used for all voltammetry. The area of the mercury drops was 0.0182 cm^2. All potentials were measured and are reported vs. a saturated calomel electrode (SCE) placed in a bridge tube containing the pH 3.7 acetate buffer. The cell contents were separated from those of the bridge by a Vycor tip. All experiments were done at 25 ± 0.1°C. The computer-controlled system for running the electrochemical experiments and subsequent data analysis is described elsewhere [6].

RESULTS AND DISCUSSION

Estimation of n *and* αn_a *for (I)*

Staircase voltammetry was used to obtain values of n and αn_a for (I). Staircase voltammetry is virtually identical to linear scan voltammetry under the

conditions used in this work [2, 7]. The following relationships for the peak current (I_p), peak potential (E_p) and the charge, Q, under the peak have been proven to apply to cases of diffusion-controlled adsorption of a reactant [8]

$$Q = nFA\Gamma; I_p = n\alpha n_a \Gamma A\nu F^2/eRT$$

$$E_p = E^{0'} - (RT/F\alpha n_a) \ln (\alpha n_a F\nu/RTk^0); \delta = 62.5/\alpha n_a \text{ mV}$$

where D is the diffusion coefficient of the reactant, ν is the sweep rate, n is the total number of electrons transferred, α is the transfer coefficient, n_a is the number of electrons transferred in the rate-determining step, Γ is the coverage, δ is the peak width, and k^0 is the standard rate constant of the surface reaction. (The equation for δ is incorrectly printed in [8]).

From the equation for E_p,

$$\partial E_p/\partial \log \nu = \partial E_p/\partial \log f = 59.15/\alpha n_a \text{ (mV)}$$

and, obviously, $I_p/Q = \alpha n_a F\nu/eRT$. Thus, αn_a can be estimated from δ, $\partial E_p/\partial \log f$ and from I_p/Q. Estimation of αn_a from the I_p/Q relation does not require knowledge of Γ, n, or A. These methods give values of 1.41 ± 0.04, 1.50 ± 0.02 and 1.66 ± 0.03, respectively, for reduction of (I). The reaction is also pH-dependent, with $\partial E_p/\partial \text{pH} = 60 = 59\, p/\alpha n_a$ mV over the pH range 2.7—4.5. This gives a value of p, the number of protons involved in the rate-determining step, of 1.5.

Phillips [9] has shown that the coverage for spherical electrodes in the case of diffusion-controlled adsorption is given by

$$\Gamma = 1.128C(Dt_p)^{1/2} + CDt_p/r \quad (1)$$

where r is the radius of the mercury drop and the concentration, C, is in mol cm^{-3}. We use this in place of Koryta's equation [10] employed by Laviron [8]. The second term of the equation can be neglected for small values of t_p [11]. Substituting this relation for Γ into $Q = nFA\Gamma$ gives

$$n = Q/1.128\, FAC(Dt_p)^{1/2} \quad (2)$$

Using the ratio $Q/t_p^{1/2}$ for 0.194 μM (I) in acetate buffer (pH value 3.7) and a value of 3.3×10^{-6} cm^2 s^{-1} for D [12] then (2) gives a value for n of 4.08 ± 0.06.

Comparison with adenine-containing compounds

In acidic media, adenine is protonated at the N(1) nitrogen [13—18]. The cathodic reduction of protonated adenine has been extensively studied by, among others, Elving and co-workers [13, 17, 19—21] and the relationships for the effect of the pH value of the electrolyte on $E_{1/2}$ (polarography at the dropping mercury electrode, DME), E_p (cyclic voltammetry at the hanging mercury drop electrode, HMDE) and E_s (a.c. voltammetry at the HMDE) are: $E_{1/2}$ = (—0.975 — 0.090 pH) V [19], $E_{1/2}$ = (—0.975 — 0.084 pH) V [13, 17, 18], E_p = (—1.060 — 0.080 pH) V [20], and E_s = (—1.090 — 0.067 pH) V

[20]. The more negative values of E_p and E_s are attributed to the effect of accumulation of the reduction product in the region of the electrode when a HMDE is used [22]. Thus, the E_p and E_s values should be compared to the present data for (I) obtained at an SMDE. Referring to Eqn. (1) [2], they agree well.

Other similarities in the reduction of (I) and adenine are that the reduction of adenine is irreversible and that the peak current is fairly independent of pH value between pH 1 and 3.5, but then decreases with increasing pH value and disappears altogether at pH values above 6 [13, 19, 20, 21]. This is due to the low concentration of the protonated, electroactive form of adenine present in solution at pH values higher than the pK_a value of adenine (4.1 [13, 15, 16]) and is behavior typical for the reduction of the acid form of a conjugate acid-base system [13, 14, 21]. Similar behavior has also been observed for adenine nucleosides, nucleotides, and oligonucleotides [11, 14, 21, 23].

The reduction of adenine, on the time-scale of the electrochemical techniques used in this study, is a $4e^-/4H^+$ reaction [13, 17, 19]. The values of αn_a for this process have been found to increase with decreasing concentration of the adenine species [21] [as was found here for the reduction of (I)] up to a value of 1.3, which is close to that for the reduction of (I) at the low concentrations used here. Another value for αn_a quoted for adenine is 1.09 ± 0.07 [13]. Moreover, the value of p has been given as 1.20 ± 0.25 [21] and 1.54 ± 0.08 [13] which, in view of the uncertainties involved, agrees well with the value of 1.5 for (I) found in this study. This, the value of 4 for n, and the agreement of reduction potentials, indicates that the electrode process in the reduction of (I) is actually that of the protonated adenine ring.

Detailed discussion of the mechanism of reduction of the adenine moiety is beyond the scope of this work. However, it is worth commenting on the meaning of the apparent value of αn_a and the pH-dependence described in the preceding section. Of course, the treatment of the above expressions for Q, I_p, E_p, δ, etc. is for a simple irreversible surface reduction. The pH-dependence and the similar, well-studied reduction of adenine indicate clearly that this is not the case for the reduction of (I). However, by analogy with the extensive work on pH-dependence of polarographic half-wave potentials, the results of the preceding section can be interpreted as arising from two reversible proton additions and one reversible electron addition preceding the rate-determining slow transfer of one electron. In that case (see e.g. Scheme 5.4 of Heyrovsky and Vavricka [24]) it seems intuitively reasonable that the quantity "αn_a" be identified as $1 + \alpha_2$, where α_2 is the transfer coefficient for the second electron. Thus $\alpha_2 = 0.5$. The pH-dependence of the peak potential, 60 mV per pH unit, suggests that the slow step is in fact a concerted process involving one proton and one electron.

Adsorption of (I) and adenine-containing compounds

The adsorption and resulting accumulation of (I) on the surface of the electrode is important to its determination. The adsorption of adenine, its

nucleosides, nucleotides, and oligonucleotides on mercury electrodes has been the subject of much interest [11, 13—18, 20, 21, 23, 25—32], and the site of adsorption has been found to be the adenine ring in every case. Indeed, the adenine moiety has been found to be responsible for both the adsorption of NADH [23, 26] and NAD^+ [18, 23, 29], and it would seem reasonable to assume that, whatever the actual reduction site of (I), the molecules are adsorbed via the adenine ring. This adsorption has been used in a cathodic stripping procedure for adenine [33—35] [very different from the cathodic stripping procedure developed for (I)] in which the adenine actually reacts with the mercury surface in basic media at anodic potentials to form an insoluble complex that is then reduced. Addition of Triton X-100 to solutions containing adenine suppresses both this cathodic stripping peak [35] and the maximum observed in the polarographic reduction of adenine [13, 22]. This behavior resembles earlier results [2] for the reduction of adsorbed (I).

Adenine and its derivatives exhibit adsorption over a broad potential range centered at −0.6 V and extending to 0.0 and −1.0 V [11, 15, 16, 18, 27, 28, 31]. The change in the a.c. voltammograms that occurs at −1.1 V has been attributed to a slow desorption-readsorption process [14—16, 21, 27, 30]. This is quite similar to the behavior of (I) shown in the earlier Fig. 5 [2], except that there is no evidence of desorption of (I) at −1.1 V.

The concentration at which the electrode surface becomes saturated with the reactant is related to the area occupied by the adsorbed species and the effective delay time (t_p). Adenine nucleotides and oligonucleotides occupy only a slightly greater area than adenine itself [11, 16, 27, 28, 30]. This suggests that the nucleotides adsorb in the *syn*-conformer [30], with the sugar group sticking out into the bulk solution. The experimental value for the area occupied by adsorbed NAD^+ in the folded configuration, and presumably (I), on mercury surfaces is only 90—130 $Å^2$ per molecule [18, 32]. Calculated values for NAD^+ are 85 or 125 $Å^2$ per molecule, depending on whether the adenine and nicotinamide rings are parallel or perpendicular to each other. A plot of net square-wave peak current vs. concentration of (I) with t_p = 12 s levels off at about 20 μM. Substituting these values in Eqn. 1 gives a value of the maximum coverage for adsorbed (I) of 1.63×10^{-10} mol cm^{-2}, or 102 $Å^2$ per molecule. In view of the error in estimating the exact concentration at which the plot I_p vs. C levels off, this is in excellent agreement with the data for NAD^+.

It has been established that the nicotinamide and adenine rings in NADH, and presumably (I), are in close proximity [32, 36, 37] and can therefore influence each other (i.e., the molecule exists in a folded conformation). The value for the area occupied by each adsorbed molecule of (I) is in accord with a folded configuration, and is about half that calculated for an unfolded configuration of NAD^+, 190 $Å^2$ [32]. Fluorescence studies [38] of NADH have established that the adenine moiety adsorbs at least part of the radiation and transfers it to the nicotinamide ring, and pulse radiolysis data support

the hypothesis that initial attack on NAD^+ occurs at the adenine ring, which then transfers the electron to the nicotinamide ring [39]. The idea of electron transfer from the adenine to the nicotinamide ring in the electrochemical reduction of NAD^+ has been proposed [23, 29, 32], although the evidence for this is inconclusive. Accordingly, one would expect that other adenine species, including NADH itself, would also give a response similar to that of (I) when examined by cathodic rapid-scan square-wave voltammetry.

Other compounds at μM level

Adenine, adenosine, AMP (adenosine-5′-monophosphate), ADP (adenosine-5′-diphosphate), ADPR (adenosine diphosphoribose), ATP (adenosine-5′-triphosphate), NMNH (reduced β-nicotinamide mononucleotide), and NAD^+ (β-nicotinamide adenine dinucleotide) were examined at μM concentrations in pH 3.7 acetate buffer using cyclic-staircase and square-wave voltammetry. Representative data are presented in Table 1. Except for NAD^+, which is discussed later, none showed a reduction peak in the potential region of interest when frequencies of 30—180 Hz were used (0.15—0.9 V s^{-1}). This apparent lack of electrochemical activity was surprising because, except for NMNH, these compounds are known to adsorb strongly at —0.6 V (the initial potential) and reduce in acidic media at ca. —1.3 V vs. SCE. The explanation becomes apparent when one increases the sweep rate of the cyclic-staircase or square-wave voltammetric scan by increasing the frequency. Taking ADP as an example, at frequencies greater than 300 Hz (1.5 V s^{-1}), a peak appears which has all of the characteristics of a diffusion-controlled adsorption process (I_p proportional to $Cft_p^{1/2}$, see Table 1). This effect is illustrated in Fig. 1A and B. The square-wave voltammograms of (I) (Fig. 1B), when normalized with respect to f, are virtually identical in size and shape at both low (30 Hz) and high frequencies (400 Hz). In the case of ADP (Fig. 1A) the normalized peak at 15 Hz is much smaller than that at 610 Hz. The a.c. voltammetric behavior of these adenine species indicates that while adsorption occurs at —0.6 V, a slow desorption-rearrangement process occurs at ca. —1.0 V, just prior to their reduction at —1.3 V [14, 18]. Hence, when low frequencies are used, the adsorbed material desorbs and diffuses away from the electrode when the potential reaches —1.0 V and no reduction peak is seen at —1.3 V. When high frequencies are used, the material does not have enough time to desorb and is detected when the potential reaches —1.3 V. Thus, (I), but neither NADH nor the other adenine compounds, is electroactive at low frequencies, because the desorption process for (I) must either not occur at all, or else be much slower than that of the other compounds. So the hydration of the nicotinamide ring of NADH appears to affect the kinetics of the desorption step at —1.0 V.

Other compounds at higher levels of concentration

Most of the adenine-containing compounds give a four-electron diffusion-controlled peak or wave at higher concentrations when studied by normal

TABLE I

Square-wave voltammetric data for reduction of μM solutions of ADP, NAD^+ and (I)[a]

Relation	Variable	ADP	NAD^+	(I)[b]
I_p vs. $t_p^{1/2}$	Slope	0.83 ± 0.02 μA $s^{-1/2}$	114 ± 2 nA $s^{-1/2}$	88.1 ± 0.9 nA $s^{-1/2}$
	Intercept	0.07 ± 0.06 μA	−10 ± 12 nA	−4.2 ± 3.8 nA
	r	0.9994	0.9993	0.9995
	n	5	6	11
	S_{yx}	0.09 μA	18 nA	7.8 nA
	Remarks:	$I_p/Cft_p^{1/2}$ = 1.69 mA $s^{1/2}$ M^{-1}, f = 550 Hz, C = 1.16 μM.	Linear for 3 concentrations. Example given for 1.13 μM. f = 30 Hz.	C = 1.06 μM, f = 30 Hz, pH 3.4 succinate buffer.
$I_p/t_p^{1/2}$ vs. C	Slope (mA $s^{-1/2}$ M^{-1})		99.9 ± 0.1	82.0 ± 0.3
	Intercept (nA $s^{-1/2}$)		0.5 ± 0.3	0.4 ± 0.2
	r		1.00000	0.99991
	n		4	17
	S_{yx} (nA $s^{-1/2}$)		0.5	1.3
	Remarks:		$I_p/Cft_p^{1/2}$ = 3.33 mA $s^{1/2}$ M^{-1}	pH 3.6 succinate buffer, t_d = 10 s, f = 30 Hz.
$I_p/t_p^{1/2}$ vs. f	Slope (nA $s^{1/2}$)	1.92 ± 0.03	3.53 ± 0.03	0.664 ± 0.007
	Intercept	−0.19 ± 0.01 μA $s^{-1/2}$	−3.2 ± 3.0 nA $s^{-1/2}$	−0.99 ± 0.52 nA $s^{-1/2}$
	r	0.9993	0.9997	0.9995
	n	10	9	10
	S_{yx} (nA $s^{-1/2}$)	16	5.8	1.1
	Remarks:	f > 200 Hz, t_d = 10 s, C = 1.16 μM.	t_d = 10 s, C = 1.13 μM.	$I_p/Cft_p^{1/2}$ = 3.40 mA $s^{1/2}$ M^{-1}, C = 0.19 μM.
E_p vs. log f	Slope (mV)	−42.7 ± 0.3	−40.0 ± 0.3	−39.4 ± 0.6
	Intercept (mV)	−1225.7 ± 0.8	−1233.5 ± 0.5	−1238.9 ± 1.0
	r	0.9997	0.9998	0.9991
	n	12	8	10
	S_{yx} (mV)	0.4	0.4	0.8
	Remarks:[c]	C = 1.16 μM, αn_a = 1.39, $\partial E_p/\partial t_p$ = 0	C = 1.13 μM, αn_a = 1.48.	C = 0.19 μM, αn_a = 1.50, $\partial E_p/\partial t_p$ = 0, $\partial E_p/\partial C$ = 0.

[a]Unless otherwise stated, all data obtained in pH 3.7 acetate buffer. [b]See [2] for details. [c]αn_a from the slope and $\partial E_p/\partial \log \nu = 59.15/\alpha n_a$ (mV).

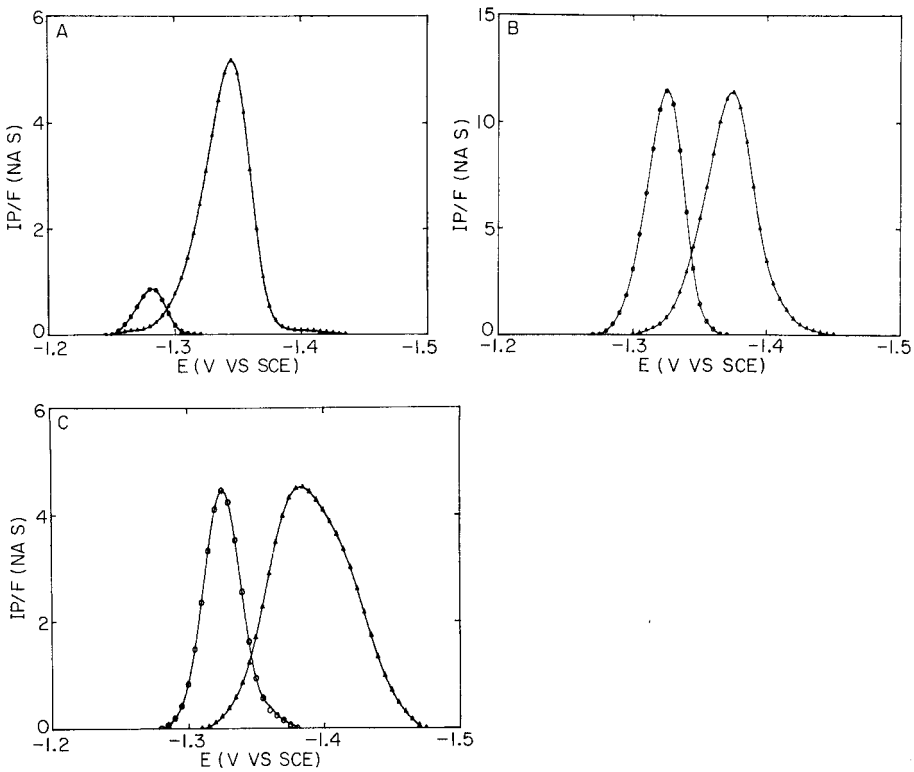

Fig. 1. Normalized square-wave voltammograms at various frequencies for ADP, (I), and NADH. The delay time at −0.6 V is 10 s, the step height is 5 mV and the amplitude 25 mV. (A) 1.16 μM ADP in pH 3.7 acetate buffer: (•) 15 Hz; (▲) 610 Hz. (B) 2.56 μM (I) in pH 4.4 acetate buffer after decomposition of NADH is essentially complete: (•) 30 Hz; (▲) 400 Hz. (C) 2.56 μM mixture of (I) and undecomposed NADH in pH 4.4 acetate buffer: (•) 30 Hz; (▲) 400 Hz.

pulse polarography (n.p.p.), cyclic-staircase and square-wave voltammetry, in agreement with the literature [13, 14, 19]. The data are summarized in Table 2 to facilitate comparison with the data for (I) under identical conditions (the data in the literature presents $E_{1/2}$ and E_p values as a function of pH but ignore the variation in these parameters with concentration, sweep rate (frequency), drop time, and pulse time; therefore it was necessary to obtain data for all of these compounds). Both NAD^+ and (I) exhibit mixed adsorption and diffusion-controlled behavior at these concentrations, so they are not included. The apparent values of αn_a and values of n from the different techniques are in good agreement with each other and, in the case of ADP, with the parameters obtained at low concentrations given in Table 1. The large uncertainties associated with the diffusion coefficients of all of these compounds (except for NAD^+ and NADH) is the most probable reason for

TABLE 2

Adenine compounds at higher concentrations[a]

Compounds	Square-wave			Cyclic-staircase			N.p.p.[b]	
	$I_p/Cf^{1/2}$ (μA s$^{1/2}$ mM^{-1})	αn_a[c]	$-E_p$ (mV vs. SCE)	$I_p/Cf^{1/2}$ (μA s$^{1/2}$ mM^{-1})	αn_a[d]	n[e]	$\partial E_{1/2}/\partial \log t$ (mV)	n[f]
Adenine	8.1 ± 0.1	1.30	1283 ± 23 log f	7.3 ± 0.1	0.94 ± 0.11	4.8	g	g
Adenosine	7.5 ± 0.3	1.62	1306 ± 18 log f	6.3 ± 0.2	1.08 ± 0.06	4.8	g	g
AMP	6.3 ± 0.1	1.43	1327 ± 21 log f	6.0 ± 0.1	1.08 ± 0.09	4.4	24.9 ± 2.9	4.5
ADP	6.0 ± 0.1	1.26	1334 ± 23 log f	5.7 ± 0.1	1.00 ± 0.05	4.6	23.8 ± 0.7	4.5
ADPR	4.3 ± 0.1	1.53	1347 ± 19 log f	5.3 ± 0.3	0.89 ± 0.07	4.6	20.3 ± 1.2	4.5
ATP	5.4 ± 0.2	1.24	1347 ± 24 log f	4.9 ± 0.1	1.00 ± 0.05	4.9	25.6 ± 1.1	4.9
(II)	0.05	0.70	923 ± 42 log f	0.28	0.56 ± 0.05	0.95	14.9	0.4

[a]Usually 0.05—3 mM concentrations. Standard deviations and correlation coefficients are omitted but are similar to those given in Table 1. I_p is proportional to $Cf^{1/2}$ and I_{lim} to $1/t^{1/2}$ (where t is the pulse time). This is evidence of diffusion control. The following diffusion coefficients were used for calculations of n (compound, $D \times 10^6$ cm^2 s^{-1}): adenine, 12.3 [13]; adenosine, 9.5 [13]; AMP, 10.6 [13]; ADP, 9.0 [19]; ATP, 6.9 [19]; ADPR as ADP; (II) assumed to be the same as NMN, 1.7 [36]. NAD^+ and (I) show adsorption-controlled behavior at high concentrations.

[b]Plots of E vs. $\log((I_{lim} - I)/I_{lim})$ gave values for αn_a for adenine, adenosine, AMP, ADP, ADPR and ATP from 1.1 to 1.6. However, the maxima, even at long pulse times, distorted the plots and so these values for αn_a are not listed.

[c]From $\partial E_p/\partial \log f = 29.6/\alpha n_a$ mV [40].

[d]From $(E_p - E_{p/2}) = 47.7/\alpha n_a$ mV [40]. Average values given; αn_a values decrease with increasing concentration.

[e]The average value of αn_a is substituted into the equation for the peak current for a diffusion-controlled irreversible process [40].

[f]The value of n from the slope of the I_{lim} vs. $t^{-1/2}$ plot and using the equation derived from the Cottrell equation for a diffusion-controlled process [40].

[g]Insufficient data because of the presence of maxima, even at long pulse times.

the slightly higher values of n than the expected value of four. The diffusion coefficients are reported to decrease with increasing concentration [17—19] and are approximately three times those based on the Stokes—Einstein law [2, 18]. In addition, the estimation of n is adversely affected by: (a) the uncertainty in the apparent value of αn_a if cyclic-staircase peak currents are used and (b) the presence of adsorption maxima (and accompanying depression of limiting current) in the normal-pulse polarograms. The apparent values of αn_a determined from the peak width of cyclic voltammograms do indeed decrease with increasing concentration, as previously reported [21].

Reduced β-nicotinamide mononucleotide

The mononucleotide, NMNH, does not adsorb on mercury [41, 42] and so no response is observed at low concentrations. At higher levels, a diffusion-controlled reduction wave is seen which actually increases with time and corresponds to the reduction of the primary acid degradation product, (II), of NMNH [42, 43]. A plot of ln $(I_{p\,max} - I_p)$ vs. time (where $I_{p\,max}$ is the maximum square-wave peak current attained on addition to the solution) in

pH 3.7 acetate buffer is linear and gives a first-order rate constant for the formation of (II) of $1.1 \pm 0.1 \times 10^{-3}$ s^{-1}. This is in excellent agreement with that for the rate of decay of NMNH at pH 4.1 in the literature (0.82×10^{-3} s^{-1}, determined from the decay in the oxidation peak of NMNH [43]; the rate constant is expected to be slightly lower than the value determined at pH 3.7).

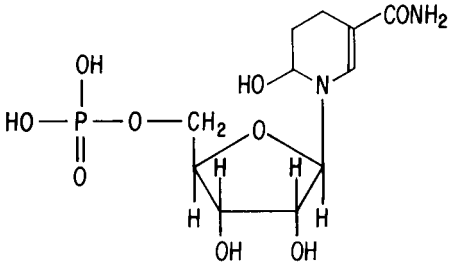

(II)

Data in Table 2 show clearly that the values of αn_a, n and, in particular, the potential for the reduction of (II) all differ markedly from the behavior of the peak at −1.3 V for the reduction of (I). In contrast, comparison of the data for (I) with that for the adenine species in Tables 1 and 2 shows excellent agreement. This confirms our belief that the electroactive site of (I) is the protonated adenine ring and not the nicotinamide group. The reduction of (II) was not investigated further. The reduction peak at ca. −1.0 V of (I) may be related to reduction of the nicotinamide group; however, this small peak appears to be irreproducible and has not been studied in detail. Braun et al. [43] have reported on a reduction wave of NADH at −0.94 to −0.98 V at pH 4.1, which they attribute to the reduction of (I). This appears to be the small wave at −1.0 V and not the process studied in the present work (−1.308 V vs SCE at pH 4.1).

Undecomposed NADH

Because the electrode process is attributed to the adenine ring of (I), one would expect that both NADH and NAD^+ (both of which adsorb strongly on mercury surfaces [23, 26]) should behave similarly. It is impossible to study NADH in acidic media without at least some (I) being present. However, by using pH 4.4 acetate buffer and running square-wave voltammograms immediately after the NADH was added and the solution deoxygenated, it was possible to examine a solution that contained approximately a 60:40 ratio of undecomposed NADH to (I). After waiting approximately 1.5 h, the NADH had all decomposed and the major component of the solution was then (I). Square-wave voltammograms at low and high frequencies were run in both solutions. After normalization to unit frequency, the voltammograms when only (I) is present merely shift along the potential axis as the frequency is changed, and I_p is proportional to f. The normalized peak height and peak width hardly change, as expected (Fig. 1B).

In the mixture at low frequencies, only (I) is detected (Fig. 1C). The peak has the same potential and width as in Fig. 1B (no NADH present), and the

peak current is proportional to the frequency. However, it maintains this proportionality throughout the entire range of frequencies used (15—800 Hz). At low frequencies, the I_p/f value is about 40% of that when only (I) is present, because only about 40% of the NADH is hydrated. At high frequencies, NADH itself is detected but, instead of the normalized peak height increasing, the peak width almost doubles, as is evident in the high-frequency voltammogram of Fig. 1C. So, at high frequencies, the desorption of NADH is indeed prevented and it is reduced at potentials slightly negative of those for (I). In no case were two peaks observed. In the pH range where the reduction occurs, NADH is always undergoing significant decomposition to (I), so this method of detection has limited value for the direct determination of NADH. This work does, however, explain why (I) but not NADH was detected in our earlier work at low frequencies. It also demonstrates that the reaction of the nicotinamide ring to form (I) does not affect the reduction of the protonated adenine ring, but merely inhibits the desorption of (I) at —1.0 V.

NAD^+

As mentioned previously, NAD^+ gives a response similar to that of (I) and the reduction process is presumably the reduction of the protonated adenine ring. This has been briefly studied by Elving and coworkers [26, 29]. The characteristics of the square-wave voltammetry peak for the reduction of NAD^+ at μM concentrations are the same as those for (I), as shown in Table 1. The reduction is irreversible at all frequencies used; the peak current corresponds to a diffusion-controlled adsorption process. Plots of I_p vs. $t_p^{1/2}$ at various concentrations level off at values of $Ct_p^{1/2}$ greater than 57 $\mu M\ s^{1/2}$. This gives a value for the area occupied by each adsorbed molecule of approximately 115 $Å^2$, which agrees well with reported values [18, 32]. Using a value of 3.3×10^{-6} $cm^2\ s^{-1}$ for the diffusion coefficient of NAD^+ [44] in Eqn. 1 gives a value for Γ as a function of the bulk concentration of NAD^+. Placing this in the equation for I_p, and using the I_p/C slope of 0.237 A M^{-1} from cyclic-staircase data (t_p = 14.5 s, f = 30 Hz, ν = 0.15 V s^{-1}, αn_a = 1.48) gives a value of 4.6 for n. A plot of Q vs. C for NAD^+ is linear (ν = 0.15 V s^{-1}, t_p = 14.9 s, slope = 60.8 ± 0.8 C $cm^3\ mol^{-1}$, intercept = —2.6 ± 2.7 nC, S_{yx} = 5.9 nC, r = 0.9995, N = 7) and using Eqn. 2 gives a value of 3.76 ± 0.05 for n. If the full form of Eqn. 1 is used, n = 4.37 ± 0.06. This further supports the mechanism of a four-electron reduction of the adenine group being responsible for the wave at —1.3 V in acidic media. The peak for NAD^+ at ca. —1.0 V is probably the one-electron reduction of the nicotinamide ring to $NAD^{\cdot}$. Because this peak is much smaller than that for the four-electron reduction of the protonated adenine ring investigated here, it is less useful for quantitative purposes. From an analytical viewpoint, the relevant facts are that (a) NAD^+ is stable in acidic media, (b) this method is as sensitive for NAD^+ as for (I), and (c) NAD^+ does not fluoresce, and so a method with a sensitivity as high as that of stripping voltammetry is particularly desirable. The behavior

of NAD^+ has been studied so extensively that these reductions were not examined further.

CONCLUSION

Square-wave stripping of an adsorbed reactant can be used for determination of a range of adenine compounds with a detection limit of ca. 2×10^{-9} M. This method should be applicable to virtually any electroactive compound that strongly adsorbs on mercury surfaces. This method should have great potential in the pharmaceutical and bioanalytical field in general, because many of the compounds of interest are known or suspected to adsorb strongly in their biological environments. Wang and Freiha recently [45] demonstrated that the drug chlorpromazine can be determined in urine by a similar method. The drug adsorbs onto a carbon paste electrode in a flow-injection apparatus and is detected by differential-pulse voltammetry.

Under appropriate conditions, any of these adenine species when present alone and possibly the total concentration of adenine-containing species can be determined. If the method is used directly, samples must not contain surfactants that would compete with the analyte for the electrode surface. Serum samples, for example, would require separation of the sample constituents.

A flow system such as that provided by h.p.l.c. gives stable, reproducible forced-convection. As a result of increasing the rate of transport of the analyte to the electrode surface, the sensitivity is increased [2]. Flow-injection techniques provide the same advantage of reproducible convection, but would be subject to interference because of competitive adsorption. In this respect, it is noted that instruments for square-wave voltammetry are becoming commercially available. Such a scanning technique for detection in h.p.l.c. gives three-dimensional plots similar to those obtained using rapid scanning u.v.-visible spectrophotometry. One need merely replace the wavelength axis by potential and the absorbance axis by current. Square-wave voltammetry is fast, sensitive and in every case yields peak-shaped responses (returning to zero currents on either side of the peak) and so is particularly well-suited to applications in this field.

We are grateful to Philip Elving for helpful discussions concerning the chemistry of NADH and to Marek Wojciechowski and John O'Dea for technical assistance. Some preliminary experiments with adenine compounds were done by Mumtaz Shah. This work was supported by the National Science Foundation under Grant Nos. CHE-7917543 and CHE-8305748.

REFERENCES

1 M. Shah and J. Osteryoung, Anal. Chem., 54 (1982) 586.
2 A. Webber, M. Shah and J. Osteryoung, Anal. Chim. Acta, (1984) in press.
3 W. E. C. Wacker, D. U. Ulmer and B. L. Vallee, New Eng. J. Med., 255 (1956) 449.

4 O. C. Ingebretsen, A. M. Bakker, L. Segadal and M. Farstad, J. Chromatogr., 242 (1982) 119.
5 M. C. Capogrossi, M. R. Holdiness and Z. H. Israili, J. Chromatogr., 227 (1982) 168.
6 T. R. Brumleve, J. J. O'Dea, R. A. Osteryoung and J. Osteryoung, Anal. Chem., 53 (1981) 702.
7 D. R. Ferrier and R. R. Schroeder, J. Electroanal. Chem., 45 (1973) 343.
8 E. Laviron, J. Electroanal. Chem., 52 (1974) 355.
9 S. L. Phillips, J. Electroanal. Chem., 12 (1966) 294.
10 J. Koryta, Collect. Czech. Chem. Commun., 18 (1953) 206.
11 P. Valenta and D. Krznaric, J. Electroanal. Chem., 75 (1977) 437.
12 Z. Samec and P. J. Elving, J. Electroanal. Chem., 144 (1983) 217.
13 B. Janik and P. J. Elving, J. Electrochem. Soc., 116 (1969) 1087.
14 J. W. Webb, B. Janik and P. J. Elving, J. Am. Chem. Soc., 95 (1973) 8495.
15 D. Krznaric, P. Valenta and H. W. Nürnberg, J. Electroanal. Chem., 65 (1975) 863.
16 H. Kinoshita, S. D. Christian and G. Dryhurst, J. Electroanal. Chem., 83 (1977) 151.
17 T. E. Cummings, M. A. Jensen and P. J. Elving, Bioelectrochem. Bioenerg., 4 (1977) 425.
18 W. T. Bresnahan, J. Moiroux, Z. Samec and P. J. Elving, Bioelectrochem. Bioenerg., 7 (1980) 125; J. Electroanal. Chem., 116 (1980) 125.
19 D. L. Smith and P. J. Elving, J. Am. Chem. Soc., 84 (1962) 1412; Anal. Chem., 34 (1962) 930.
20 G. Dryhurst and P. J. Elving, Talanta, 16 (1969) 855.
21 B. Janik and P. J. Elving, J. Am. Chem. Soc., 92 (1970) 235.
22 B. Janik and P. J. Elving, J. Electrochem. Soc., 117 (1970) 457.
23 W. T. Bresnahan and P. J. Elving, J. Am. Chem. Soc., 103 (1981) 2379.
24 M. Heyrovský and S. Vavřička, J. Electroanal. Chem., 36 (1972) 203.
25 V. Vetterl, J. Electroanal. Chem., 19 (1968) 169; Biophysik, 5 (1968) 255.
26 C. O. Schmakel, K. S. V. Santhanam and P. J. Elving, J. Am. Chem. Soc., 97 (1975) 5083.
27 P. Valenta, H. W. Nürnberg and D. Krznaric, Bioelectrochem. Bioenerg., 3 (1976) 418.
28 D. Krznaric, P. Valenta, H. W. Nürnberg and M. Branica, J. Electroanal. Chem., 93 (1978) 41.
29 C. O. Schmakel, M. A. Jensen and P. J. Elving, Bioelectrochem. Bioenerg., 5 (1978) 625.
30 V. Brabec, M. H. Kim, S. D. Christian and G. Dryhurst, J. Electroanal. Chem., 100 (1979) 111.
31 M. Katz, T. E. Cummings and P. J. Elving, Ber. Bunsenges. Phys. Chem., 83 (1979) 614.
32 P. J. Elving, W. T. Bresnahan, J. Moiroux and Z. Samec, Bioelectrochem. Bioenerg., 9 (1982) 365; J. Electroanal. Chem., 141 (1982) 365.
33 E. Palecek, Anal. Biochem., 108 (1980) 129; Anal. Lett., 13 (1980) 331.
34 E. Palecek, F. Jelen, M. A. Hung and J. Lasovsky, Bioelectrochem. Bioenerg., 8 (1981) 621; J. Electroanal. Chem., 128 (1981) 621.
35 E. Palecek, J. Osteryoung and R. A. Osteryoung, Anal. Chem., 54 (1982) 1389.
36 O. Jardetzky and N. G. Wade-Jardetzky, J. Biol. Chem., 241 (1966) 85.
37 R. W. Sarma and R. J. Mynott, J. Am. Chem. Soc., 95 (1973) 7470.
38 G. Weber, Nature, 180 (1957) 1409.
39 E. J. Land and A. J. Swallow, Biochim. Biophys. Acta, 162 (1968) 327.
40 A. J. Bard and L. R. Faulkner, Electrochemical Methods, Wiley, New York, 1980, p. 222 and p. 187.
41 K. S. V. Santhanam, C. O. Schmakel and P. J. Elving, Bioelectrochem. Bioenerg., 1 (1974) 147.
42 C. O. Schmakel, K. S. V. Santhanam and P. J. Elving, J. Electrochem. Soc., 121 (1974) 1033.
43 R. D. Braun, K. S. V. Santhanam and P. J. Elving, J. Am. Chem. Soc., 97 (1975) 2591.
44 Z. Samec, W. T. Bresnahan and P. J. Elving, J. Electroanal. Chem., 133 (1982) 1.
45 J. Wang and B. A. Freiha, Anal. Chem., 55 (1983) 1285.

Analytica Chimica Acta, 157 (1984) 31—36
Elsevier Science Publishers B.V., Amsterdam — Printed in The Netherlands

POLAROGRAPHIC REDUCTION OF 2,4,6-TRINITROBENZENE-1-SULPHONIC ACID AND SOME 2,4,6-TRINITROPHENYL-AMINO ACID DERIVATIVES

M. A. AL-HAJJAJI

Chemistry Department, College of Science, King Saud University, Riyadh (Saudi Arabia)

(Received 5th July 1983)

SUMMARY

The rapid d.c. polarography of 2,4,6-trinitrobenzene-1-sulphonic acid and its derivatives with serine (I), threonine (II), glycine (III) and histidine (IV) revealed a 3-wave reduction and a marked pH dependence of the reduction potential. The polarographic waves of the derivatives (2.5×10^{-4} M) showed appreciable changes when sulphite ions were present, with the development of a new wave at more negative potential in $\geqslant 0.01$ M sulphite solutions at pH 7.0. The $E_{1/2}$ values of these waves in pH 7.0 supporting electrolyte were: (I) −1000; (II) −1007; (III) −1021; (IV) −949 mV (vs. Ag/AgCl, sat. KCl). These waves were used to determine the amino acids investigated ($1—4 \times 10^{-4}$ M) in the presence of excess of 2,4,6-trinitrobenzene-1-sulphonic acid, with good precision (2%).

Polarography is one of many techniques that have been utilized for the determination of amino acids. The direct polarographic determination of these compounds via reduction cannot be achieved unless a reducible group is present. Indirect methods are therefore used, e.g., the liberation of soluble copper(II)—amino acid complexes from insoluble copper(II) compounds [1]. The decrease in the phthalaldehyde polarographic wave [2] and the introduction of polarographically active groups through substitution with 1-fluoro-2,4-dinitrobenzene [3, 4] have also been used.

2,4,6-Trinitrobenzene-1-sulphonic acid (TNBS) is a well known spectrophotometric reagent for the determination of compounds containing primary amino groups [5], and is said to yield more precise and sensitive results than ninhydrin [6]. It reacts stoichiometrically and rapidly in alkaline solutions with most amino acids, yielding 2,4,6-trinitrophenyl (TNP-) derivatives [7]. This report describes the polarographic behaviour of TNBS and its derivatives with glycine, threonine, serine and histidine in various supporting electrolytes. A set of conditions was established that allowed the determination of amino acids as their trinitrophenyl derivatives in the presence of excess of TNBS reagent.

0003-2670/84/$03.00

EXPERIMENTAL

Apparatus and reagents

A Metrohm Polarecord Model 506 polarograph was used to record all d.c. polarograms, in the rapid mode which facilitates control of drop lifetime (0.6 s) plus current integration over the whole drop life, apart from the first 20 ms during which drop growth is irregular. The three-electrode cell assembly used consisted of an Ag/AgCl reference electrode (saturated KCl), a platinum auxiliary electrode and a dropping mercury electrode (DME) which had the following characteristics: corrected mercury column height, 54.5 cm and mercury flow rate, 0.9050 mg s^{-1}. The water-jacketed polarographic cell was maintained at 25 ± 0.1°C; the polarographic scans started from 0 V.

The chemicals used were of analytical-reagent grade. 2,4,6-Trinitrobenzene-1-sulphonic acid (BDH) was used as received. Buffer solutions were prepared in double-distilled, deionized water and their ionic strength was adjusted to 0.5 M with potassium chloride. Their pH was then checked using a Metrohm 632 pH meter. Unless otherwise mentioned, all compounds were investigated as 2.5×10^{-4} M solutions. The TNP-amino acid derivatives were prepared by the method of Okuyama and Satake [7] and were purified by recrystallization. The elemental analysis of the recrystallized derivatives showed excellent agreement with the theoretical percentages of carbon, hydrogen and nitrogen. Stock solutions (0.01 M) of the derivatives in methanol and of TNBS in water were stored away from light at 4°C for a maximum period of one week.

Determination of amino acids in the presence of excess of TNBS

The trinitrophenylation reaction was done [8] in a total volume of 10 ml in a 25-ml volumetric flask using 2.5 ml of aqueous TNBS solution (0.01 M) followed by 0.25—1.00 ml of amino acid solution (0.01 M). At zero time, 5.0 ml of borate buffer (0.025 M, pH 9.3) was added and the reaction mixture was diluted to 10 ml with double-distilled water. The reaction was allowed to proceed for 30 min. The solution was then diluted to the mark with sodium sulphite solution (0.017 M) in phosphate buffer (0.1 M, pH 6.4). The final pH was found to be about 7. The polarographic waves were recorded directly with no need for nitrogen bubbling. Blanks were measured in the same way, the amino acid solution being replaced with double-distilled water.

RESULTS AND DISCUSSION

Polarograms of TNBS were recorded at different pH values. The half-wave potentials ($E_{1/2}$) are shown in Table 1. At pH $\leqslant$7, the compound produced three polarographic waves of equal height (Fig. 1). The separation of these waves increased as the pH increased [9]. Above pH 7, the second wave

TABLE 1

Effect of pH on $E_{1/2}$ (mV vs. Ag/AgCl) of the polarographic waves of TNBS and some TNP-amino acid derivatives

Compound	$E_{1/2}$ at different pH								
	3.0	4.0	4.6	5.0	5.6	6.0	6.6	7.0	8.0
TNBS	−44	−76	−94	−116	−132	−146	−166	−186	−226
	−157	−210	−248	−282	−306	−332	−360	−388	—[a]
	−283	−384	−408	−448	−482	−562	−596	−620	—[a]
TNP-threonine[b]	−12	−68	−94	−124	−148	−172	−206	−236	−292
TNP-glycine[b]	−25	−76	−104	−126	−148	−166	−198	−228	−278
TNP-serine[b]	−20	−72	−96	−126	−146	−168	−196	−228	−288
TNP-histidine[b]	+2	−42	−72	−94	−118	−138	−160	−188	−276

[a]Waves could not be evaluated because of the appearance of a maximum. [b]First wave only; the second and third waves were insufficiently separated.

produced an acute maximum that made the evaluation of the second and following wave(s) impossible. It was necessary, therefore, to add a maximum suppressor to the supporting electrolyte in alkaline solutions. As gelatine reacted with the compound, other surface-active agents (starch, sodium dodecylbenzene sulphate, dextrin and polyvinyl alcohol) were tried. Only polyvinyl alcohol was successful in removing this maximum, at relatively high concentration (0.01%, pH 8.0). Sodium dodecylbenzene sulphate and starch were even less suitable as they caused disturbances in the polarogram while dextrin was ineffective. Polyvinyl alcohol (0.01%) itself distorted the second and third waves of TNBS at pH 6.6. All the results reported here were therefore obtained in the absence of maximum suppressors.

The plots of $E_{1/2}$ vs. pH (from Table 1) for each of the three waves were linear. No inflection at pH 4—5 was observed, similarly to nitrophenols [9]. This is consistent with the presence of the sulphonate ion, and precludes the formation of hydroxylammonium ions in acidic solution. The increased separation of the waves of TNBS with increasing pH cannot therefore be attributed to the change of electronegativity of hydroxylamine groups with

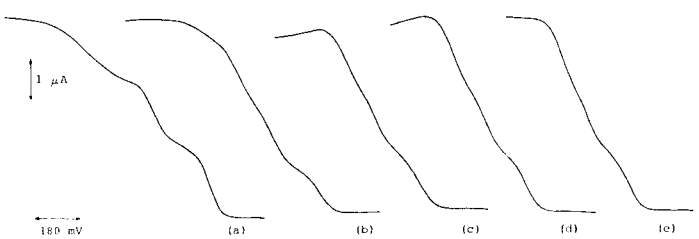

Fig. 1. Polarograms of 2.5 × 10^{-4} M solutions at pH 7.0: (a) TNBS; (b) TNP-histidine; (c) TNP-serine; (d) TNP-glycine; (e) TNP-threonine.

increasing pH, but may be due to the decreased acidity of the sulphonic acid derivative as it loses its nitro groups by reduction, leading to a change in the electronegativity of the sulphonate group. The increase in pH will thus encourage the ionization of the sulphonate group and influence the successive reduction of the nitro groups.

The polarographic behaviour of the trinitrophenyl-amino acid derivatives was similar in that all the derivatives produced three waves at pH 3—7 although the waves were less distinct (Fig. 1). Again the separation of the first wave from the second and third waves increased as the pH increased. The latter waves remained very close together and were practically unaffected by pH change. This similarity in behaviour could be the result of steric effects of the bulky amino acid residue on the nitro groups present in the 2- and 6- positions [10]. All the investigated derivatives except TNP-histidine produced acute maxima at alkaline pH. The latter was also different in that its reduction in acidic solution was easier than that of the other derivatives, perhaps because of the basic nature of the histidine residue compared to other amino acids.

Comparison of the diffusion currents for picric acid with those measured for TNBS and the TNP-amino acid derivatives in acidic solutions (0.1 M HCl, 0.4 M KCl) indicated that TNBS was reduced with the consumption of 14 electrons, which means that two of the nitro groups were converted to hydroxylamine groups while the third was reduced further to an amino group. The derivatives, however, showed a consumption of 17 electrons. Hence it is most probable that two of the nitro groups are reduced to amino groups while the third is reduced to a hydrazo group, similar to picric acid reduction in acidic media [11]. The direct application of the Ilkovič equation, using the diffusion coefficient of benzoate ion, gave approximately the same results. Accordingly, this equation was applied to the approximate determination of the number of electrons involved in the reduction in neutral solutions (phosphate buffer, pH 7.0, ionic strength 0.5 M). The number was found to be 12 electrons for TNBS and the TNP-amino acid derivatives, indicating the possibility that all three nitro groups are reduced to hydroxylamine groups.

These results indicate the similarity in the polarographic behaviour of TNBS and its derivatives with amino acids, as all the compounds bear the same polarographically active nitro groups. The TNP-amino acid derivatives, however, are known to form complexes with sulphite ions [12]. The polarographic reduction of the sulphite complexes of the investigated TNP-amino acid derivatives was examined at pH $\geqslant$6.6, because it is known that sulphite rather than hydrogen sulphite is the complexing species [12] and to avoid the reduction wave(s) of sulphurous acid [13, 14] which would otherwise interfere with the polarographic reduction waves of the investigated compounds. The sulphite anodic wave (at pH $>$6.0) [14] did not interfere, as it occurred well before the reduction of all the above derivatives. The effect of various concentrations of sulphite solutions on the polarographic wave of

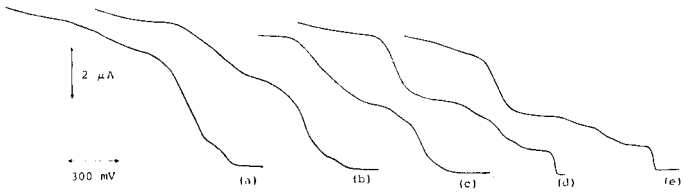

Fig. 2. Effect of various concentrations of sulphite (pH 7.0) on polarographic waves of TNP-histidine (2.5×10^{-4} M): (a) 1.25×10^{-4} M; (b) 2.50×10^{-4} M; (c) 5.00×10^{-4} M; (d) 0.01 M; (e) 0.10 M.

TNP-histidine is shown in Fig. 2. All other derivatives showed similar responses. The changes in the polarographic waves ceased at sulphite concentrations $\geqslant 0.01$ M with the development of a new wave at a more negative potential: —949 mV for TNP-histidine, —1000 mV for TNP-serine, —1007 mV for TNP-threonine and —1021 mV for TNP-glycine. This new wave was selective for TNP-amino acid derivatives and did not appear in solutions containing picric acid or TNBS. Although the addition of sulphite ions to TNBS gave a pink solution that has been reported to be due to complex formation [15], polarograms of TNBS in the presence and absence of sulphite ions were identical.

The height of the sulphite complex wave (at ca. 1000 mV) in all the investigated derivatives at constant sulphite concentration (pH 7.0) was linearly dependent on the square root of the corrected height of the mercury column, which means that it is a diffusion-controlled process. At pH >7, the wave split into two waves but the total height remained constant and equal to the height of the original wave at pH 7.0. The appearance of this wave, which is separated from the waves of TNBS at pH 7.0 permitted the determination of amino acids after their trinitrophenylation with TNBS even in the presence of excess of reagent. Figure 3 shows polarograms which can be used to prepare a calibration graph for the determination of $1—4 \times 10^{-4}$ M histidine after its conversion to the trinitrophenyl derivative with 10^{-3} M TNBS. To avoid the troublesome maximum from excess of TNBS and the splitting of

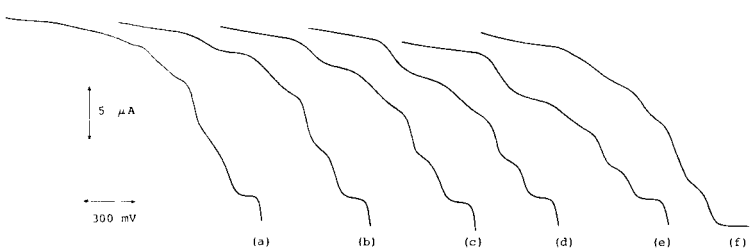

Fig. 3. Polarograms for the calibration of the determination of histidine in the presence of excess of TNBS (10^{-3} M) and 0.01 M sulphite solution at pH 7.0: (a) 0.0 M; (b) 1×10^{-4} M; (c) 2×10^{-4} M; (d) 3×10^{-4} M; (e) 4×10^{-4} M; (f) 4×10^{-4} M histidine without sulphite.

the TNP-amino acid-sulphite complex wave, the pH of the reaction mixture (9.3) must be lowered to 7.0; then sulphite solution is added and the polarogram is recorded. The importance of adding excess of sulphite is demonstrated in Fig. 3(f); an ill-defined wave was obtained compared to the well-defined wave that appears at −960 mV in polarogram (e) for the same amount of histidine under the same conditions but in the presence of 0.01 M sulphite solution. The precision of the method was good; the relative standard deviation for 2×10^{-4} M histidine (10 measurements) was 2%.

The method is being extended to include amines, peptides and proteins. Possible advantages of this method are in the determination of amino acids in solutions that are not amenable to spectrophotometry because they are turbid or highly coloured, and the lack of high blanks, as the picric acid formed during the reaction in basic solutions does not interfere in the measurement as it does not form a sulphite complex.

The author acknowledges the excellent technical assistance of Mr. Khalid M. Mirza.

REFERENCES

1 T. S. G. Jones, Biochem. J., 42 (1948) 59.
2 D. R. Norton and N. H. Furman, Anal. Chem., 26 (1954) 1116.
3 I. A. Vaintraub, Biokhimiya, 25 (1960) 688.
4 P. E. Wenger, D. M. Monnier and S. Faraggi, Anal. Chim. Acta, 13 (1955) 89.
5 K. Satake, T. Okuyama, M. Ohashi and T. Shinoda, J. Biochem., 47 (1960) 654.
6 C. A. Adams, T. C. Robberts and K. C. Butler, Anal. Biochem., 70 (1976) 181.
7 T. Okuyama and K. Satake, J. Biochem., 47 (1960) 454.
8 S. L. Snyder and P. Z. Sobocinski, Anal. Biochem., 64 (1975) 284.
9 J. Pearson, Trans. Faraday Soc., 44 (1948) 683, 692.
10 P. Zuman, The Elucidation of Organic Electrode Processes, Academic Press, New York, 1969, p. 150.
11 J. J. Lingane, J. Am. Chem. Soc., 67 (1945) 1916.
12 A. R. Goldfarb, Biochemistry, 5 (1966) 2570.
13 B. Gosman, Collect. Czech. Chem. Commun., 2 (1930) 185.
14 I. M. Kolthoff and C. S. Miller, J. Am. Chem. Soc., 63 (1944) 2818, 1405.
15 R. Fields, in Methods in Enzymology, Academic Press, New York, Vol. 25, Part B, 1972, p. 464.

Analytica Chimica Acta, 157 (1984) 37—44
Elsevier Science Publishers B.V., Amsterdam — Printed in The Netherlands

THE DIFFERENTIAL PULSE POLAROGRAPHIC DETERMINATION OF CHROMIUM IN GALLIUM ARSENIDE

P. LANZA

Istituto di Tecnologie Chimiche Speciali, Università di Bologna (Italy)

M. TADDIA

Istituto Chimico "G. Ciamician", Università di Bologna (Italy)

(Received 1st July 1983)

SUMMARY

The method described for the determination of chromium in gallium arsenide is based on the catalytic current produced by nitrate in the electrolytic reduction of the chromium(VI)—diethylenetriaminepentaacetate complex. Matrix effects, primarily caused by gallium, are discussed in detail. The method is suitable for determinations of chromium at levels as low as about 1 $\mu g\ g^{-1}$ with about 50 mg of sample; the r.s.d. is better than 10%.

Gallium arsenide is of widespread interest because it supplements the properties of germanium and silicon semiconductors for certain combinations of electrical performance. For instance, fast digital integrated circuits, low- and high-power field effect transistors, and fast coupled devices are often made on semi-insulating gallium arsenide substrates. Chromium is a common dopant for this material. The range of the chromium content in semi-insulating gallium arsenide extends from about 5×10^{13} to 1×10^{14} atom cm^{-3} (1—2 ng g^{-1}) for undoped material, to concentrations typically approaching 1×10^{17}—5×10^{17} (2—10 $\mu g\ g^{-1}$) in the Cr-doped material.

Numerous papers dealing with the determination of several elements in gallium arsenide by polarographic techniques, mainly by anodic stripping, have appeared in recent years. Very few of these, however, have dealt with the determination of chromium. Idrisova and Lebedeva [1] published a method for determining chromium at 10—20 $\mu g\ g^{-1}$ levels in gallium arsenide by d.c. polarography; this technique does not offer the required sensitivity for controlling chromium-doped semi-insulating products. Anodic or cathodic stripping voltammetry would provide better sensitivity, but chromium is ill-suited to this technique [2].

Tanaka and Ito [3] first observed that Cr(III) or Cr(VI), in a supporting electrolyte containing EDTA and nitrate ions, give exceptionally high polarographic currents, from a catalytic effect caused by reoxidation of the electrolytic Cr(II)—EDTA product. More recently, Zarebski [4] observed an

0003-2670/84/$03.00

outstanding catalytic activity of chromium with other polyaminopolycarboxylic acids such as diethylenetriaminepentaacetic acid (DTPA) and 1,2-diaminocyclohexanetetraacetic acid (DCTA). The catalytic process lowers the determination limit to about 10^{-7} M for both Cr(III) and Cr(VI) in an EDTA—KNO_3 supporting electrolyte and 10^{-7} M Cr(III) or 2×10^{-8} M Cr(VI) in DTPA—KNO_3 solutions.

Recently, Ferri et al. [5] used a slightly acidic supporting electrolyte containing DTPA and lithium nitrate and obtained very encouraging results, determining chromium in gallium arsenide with a detection limit of about 0.1 $\mu g\ g^{-1}$ by differential pulse polarography (d.p.p.). The greatly enhanced sensitivity arising from the catalytic properties of such chromium complexes offers interesting possibilities for analytical applications. In order to evaluate the real possibilities, however, far more knowledge is needed, especially with regard to possible interferences on this polarographic process.

Ranly and Neeb [6] made an extensive study of the influence of several foreign elements on the determination of chromium in supporting electrolytes containing various polyaminocarboxylic acids by d.p.p. and other polarographic techniques, but they did not study these effects on the catalytic current. Ferri et al. [5] investigated the effects of some ten elements but nothing has been reported on the possible effects of the matrix itself. This paper reports a more detailed investigation of the matrix effect in the determination of chromium in gallium arsenide.

EXPERIMENTAL

Apparatus

An AMEL Model 472 Multipolarograph was used. The instrumental conditions included: drop time 2 s; scan rate 2 mV s^{-1}; pulse height —50 mV. Quoted potentials are referred to the SCE. In order to minimize contact between mercury and the test solution, the polarographic cell was cone-shaped, with a ground-glass joint (5-cm diameter) for the cell cover and a small sidearm just under the joint; the bottom of the cell tapered to a small stopcock for removal of mercury. Measurements were made at room temperature (22 ± 0.5°C).

For sample processing, PTFE test tubes (30 × 110 mm) were used; these tubes were fitted with T29/32 adapters with inlet and outlet tubes for air circulation over the processed solution. Air filtered through a Millipore membrane (GSWP, 0.22 μm pore size) helped to accelerate the drying process. Air reflux condensers were fitted for prolonged heating of the solutions.

Reagents

Electronic-grade or analytical-grade reagents were used (C. Erba). The DTPA solutions were prepared by dissolving the required quantity of the free acid with two equivalents of sodium hydroxide per mole. Stock

chromium(III) or Cr(VI) standard solutions were atomic absorption standards (Normex, C. Erba). Solutions were stored in polyethylene bottles, previously cleaned by soaking for several days with concentrated hydrochloric acid and then thorough rinsing with distilled water.

Preliminary studies

In the preliminary study of the polarographic and chemical behaviour of the Cr(VI)/DTPA/nitrate system, the supporting electrolyte was 0.1 M in Na_2DTPA, 0.2 M in sodium acetate and 2.0 M in KNO_3. This solution (later referred to as the base solution) had a pH of about 4.8, and was adjusted to the required pH values by addition of 2 M sodium hydroxide. In this solution, the DTPA concentration is somewhat higher than those suggested by earlier workers [3—5]; the higher DTPA content was chosen in order to guarantee a sufficient excess of the ligand even in gallium arsenide solutions containing rather large quantities of Ga(III) ions.

Some fundamental parameters such as pH and nitrate concentration were studied. The effect of the pH value on the height of the Cr(VI) peak is shown in Fig. 1. The peak current (I_p) increased in exactly linear proportion with the concentration of nitrate in the range 0—2.5 M.

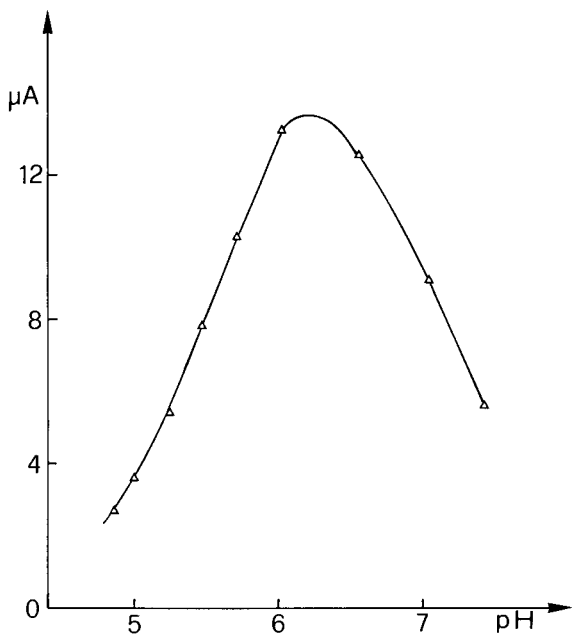

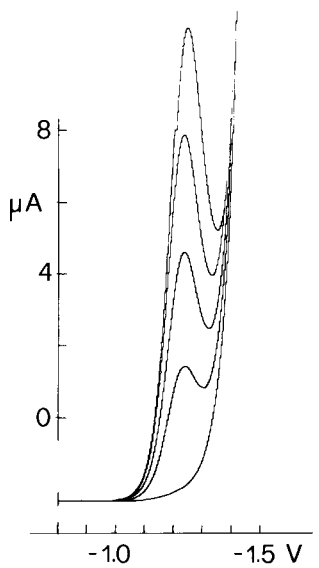

Fig. 1. Effect of pH on the catalytic current from 20 ng ml^{-1} Cr(VI).

Fig. 2. D.p.p. polarograms obtained with 0, 4.42, 8.79, 13.13 and 17.42 ng ml^{-1} Cr(VI) under the recommended conditions.

Solutions containing Cr(VI) were almost stable if stored without contact with mercury. In the presence of mercury, there was a noticeable reduction of Cr(VI) to Cr(III). Reaction with mercury was practically eliminated by minimizing the contact surface of the mercury with the solution by a suitable design of the polarographic cell. Mercury drops collected in the stem of the tap at the foot of the cell and could be run off as required.

The shape of the polarograms is shown in Fig. 2, which shows the peaks obtained when Cr(VI) was added to the above base solution at pH 6.20. The catalytic current partly merges with the discharge current of the base electrolyte and the d.p. polarogram develops a peak shape only at Cr(VI) concentrations greater than 3—4 ng ml^{-1}. The peak potential for the described experimental condition is E_p = —1.24 V (SCE). The peak height, measured from the base solution current, is in strictly linear proportion to the Cr(VI) concentration up to at least 100 ng ml^{-1}. Even at the lowest tested concentrations (0—5 ng ml^{-1}), the peak currents, corrected for the base solution blank, gave a reproducible linear calibration graph. For the reported experimental conditions 1 ng ml^{-1} Cr(VI) gives a peak current of about 0.73 μA over a blank current of about 0.3 μA.

Processing of the gallium arsenide samples

Dissolution by acidic treatment and composition of the residue. The dissolution of gallium arsenide with concentrated nitric and hydrochloric acid in various proportions seems to be the commonly accepted procedure. In this method, 10—100 mg of pulverized GaAs was placed in a teflon test tube and mixed with 2 ml of 36% hydrochloric acid and 0.5 ml of 70% nitric acid. The reaction started spontaneously and proceeded, even without heating, to complete dissolution. The solution was evaporated to dryness by heating in a thermoregulated aluminium block at 130°C under a flow of filtered air. After 60—90 min, a white, spongy residue remained in the test tube. This white residue was scarcely soluble in water, but was easily soluble in acidic or alkaline solutions.

In order to define its composition, the residue was examined by x-ray diffraction, and the gallium arsenate pattern was identified.

Arsenate was determined in the residue by a conventional iodimetric method. Three experiments gave contents of 87.7%, 86.1% and 86.4% as $GaAsO_4$. In the samples, large quantities of hydrochloric acid were still present.

Cr(III) → Cr(VI) oxidation. After the dissolution and drying process, chromium is present in the residue as Cr(III). The different behaviours of Cr(III) and Cr(VI) in solutions containing DTPA and nitrate were pointed out by Ferri et al. [5]. It was confirmed here that Cr(III) had little catalytic activity compared to the activity of Cr(VI). This is in contrast to the behaviour in EDTA-containing solutions, where both Cr(III) and Cr(VI) showed almost the same activity [4]. The use of DTPA, therefore, required all chromium to be oxidized to chromate. For this purpose, the residue was

treated in the same teflon tube with 4 ml of 1 M sodium hydroxide and 1 ml of 36% hydrogen peroxide.

The solution was boiled at reflux for about 90 min in order to ensure the complete decomposition of the hydrogen peroxide. After cooling to room temperature, the solution was mixed with about 20 ml of base solution and adjusted to pH 6.2 ± 0.1 with a few drops of 1 M sodium hydroxide or 1 M nitric acid. Suitable controls, done by adding Cr(III) to undoped gallium arsenide samples, showed quantitative recovery of the element.

Dissolution by alkaline treatment. Gallium arsenide is easily soluble in alkaline solutions containing oxidizing agents. Finely pulverized gallium arsenide dissolved without difficulty on gentle heating with diluted sodium hydroxide solution containing hydrogen peroxide:

$$GaAs + 4NaOH + 4H_2O_2 \rightarrow NaGaO_2 + Na_3AsO_4 + 6H_2O$$

The alkaline treatment offers some advantages in comparison with the commoner acidic procedure; it is faster and the reagent blanks are smaller.

In the procedure, 10—70 mg of pulverized sample in a teflon tube was mixed with 4 ml of 0.5 M sodium hydroxide and 1 ml of 36% hydrogen peroxide. The mixture was refluxed in a heating block for about 90 min. The solution, cooled to room temperature, is simply added to the base solution for polarography.

Recommended procedure

Prepare the base solution containing 0.1 M DTPA, 0.2 M sodium hydroxide, 0.2 M acetate, and 2.0 M potassium nitrate (pH 4.8 ± 0.1).

Dissolve 10—70 mg of powdered gallium arsenide in 4 ml of 0.5 M sodium hydroxide and 1 ml of 36% hydrogen peroxide in a weighed (±0.01 g) teflon tube, by refluxing in a heating block at 130°C for 90 min. This ensures complete oxidation of Cr(III) to Cr(VI) and elimination of peroxide. Cool to room temperature and add 20 ml of base solution. Adjust, if necessary, to pH 6.2 ± 0.1 with a few drops of 1 M sodium hydroxide or 1 M nitric acid. Weigh the tube again and calculate the volume of the final solution (d = 1.114 g cm^{-3}).

Transfer 20 ml of the solution to the polarographic cell, deaerate for 10 min and record the d.p. polarogram from —0.8 to —1.4 V. Add to the cell three successive 0.100-ml aliquots of 1.00 μg ml^{-1} Cr(VI) standard solution and record the polarogram after each addition. Measure the peak heights over the blank current and calculate the results by the standard additions method (see below).

The results must be corrected for the chromium content of the reagents used (NaOH and H_2O_2). This quantity can be obtained by following the above procedure without the sample. Under the conditions used here, the blank content in the final solution was estimated to be 0.25 ± 0.04 ng ml^{-1} Cr(VI), corresponding to about 6 ± 1 ng of chromium in the reagents used in each determination. Any chromium in the base solution is present essen-

tially in the Cr(III) state and does not interfere. However, the base solution should be checked by processing an aliquot of the solution, after adjustment of the pH to 6.2 ± 0.1.

RESULTS AND DISCUSSION

Matrix effect

The presence of the products of the sample treatment, particularly gallium arsenate, causes significant lowering of the Cr(VI) peaks. The magnitude of this effect is shown in Fig. 3, which presents some calibration graphs obtained for solutions containing varied concentrations of the matrix product, quoted as GaAs molarity (equivalent to $GaAsO_4$ molarity). The slopes of the Cr(VI) calibration graphs decreased as the GaAs molarity was increased to 3×10^{-2} M. An interesting aspect of the matrix effect is illustrated in Fig. 4, which shows the peak heights obtained with different amounts of GaAs doped with 1, 2 or 4 ng g^{-1} chromium. The maxima on the curves are noteworthy; these appear when the matrix effect overcomes the current increment caused by the added chromium in the sample. Acid or alkaline treatment of gallium arsenide did not make any difference with regard to matrix effects.

In a further study of the matrix effect, the influence of gallium- and arsenate-containing species on the chromium peak was investigated separately.

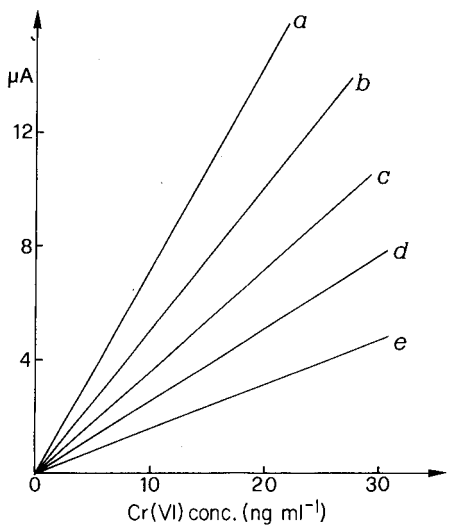

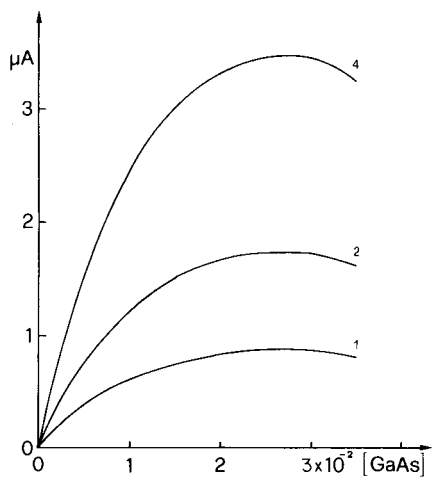

Fig. 3. Influence of the matrix products on the peak height. Calibration graphs obtained in solution containing varied concentrations of matrix products expressed as [GaAs]: (a) 0 mM; (b) 6.1 mM; (c) 16.6 mM; (d) 21.9 mM; (e) 35.0 mM.

Fig. 4. Peaks current as a function of the concentration of the matrix products in samples containing various concentrations (ng g^{-1}) of chromium; the concentrations are indicated on the curves.

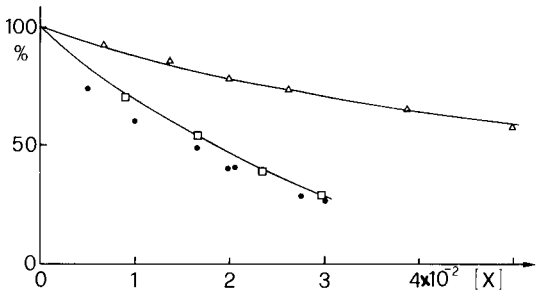

Fig. 5. Effects of various interferences: (△) As(V); (□) Ga(III); (•) GaAs.

For this purpose, potassium arsenate or gallium chloride was added to solutions containing 20 ng ml^{-1} Cr(VI), while the nitrate and DTPA concentrations were kept constant. The results are reported in Fig. 5, which also shows some points obtained in the same working conditions with undoped gallium arsenide. These experiments indicate that the matrix effect is essentially due to the presence of gallium, whereas the As(V) compounds show a more minor interference.

All the above-mentioned experiments prove that the peak heights depend on many factors such as nitrate content, pH value and, above all, the matrix concentration. Thus, in practical work, a single calibration graph cannot be satisfactory and it appears necessary to resort to the standard additions method.

Application of the method

The proposed method was used for determining chromium in four samples supplied by the Istituto Materiali Speciali (MASPEC, C.N.R., Parma). The results reported in Table 1, show good agreement with the results obtained independently by atomic absorption spectrometry.

Chromium can be determined by the present procedure in samples of gallium arsenide at levels as low as 1 $\mu g\ g^{-1}$, with relative standard deviations of 5—10%. One could, of course, process larger quantities of sample, provided

TABLE 1

Comparison of results obtained by the proposed method and a.a.s.

Sample	D.p.p.				A.a.s.			
	Mean ($\mu g\ g^{-1}$)	S.d.	*N*	R.s.d. (%)	Mean ($\mu g\ g^{-1}$)	S.d.	*N*	R.s.d. (%)
GaAs TEC	4.0	0.26	7	6.5	3.5	0.4	3	11.4
GaAs 32A	4.0	0.35	7	7.5	3.9	0.2	3	5.1
GaAs 32B	2.0	0.04	4	2.0	2.1	0.15	4	7.1
GaAs TS	2.3	0.16	7	6.9	2.4	0.2	3	8.3

that a suitable excess of sodium hydroxide over the stoichiometric quantity is used. However, because of the matrix effect, the polarographic peaks would not increase proportionally (see Fig. 4) and the advantages would not be real.

It appears that the sensitivity and the limit of determination are essentially fixed by the rather high current of the supporting electrolyte at the peak potential. Because of this, the catalytic effect cannot provide all its own potential advantages. For this reason, not even a preliminary elimination of the matrix, e.g., by liquid-liquid extraction, could further enhance the sensitivity.

A noteworthy point is the necessity of ensuring a suitable excess of DTPA, in addition to the quantity bound by the gallium of the matrix. Gallium(III) forms very stable complexes with DTPA [7]. As 100 mg of GaAs requires about 7 ml of 0.1 M DTPA, the concentration of ligand suggested for the base solution is not excessive.

Even with the limitations emphasized, however, the catalytic properties of the Cr—DTPA complexes can offer a very valuable procedure.

This work was supported by Consiglio Nazionale delle Ricerche (C.N.R.), under a contract related to the Progetto Finalizzato per la Chimica Fine e Secondaria.

REFERENCES

1 R. A. Idrisova and O. V. Lebedeva, Zavod. Lab., 38 (1972) 1187.
2 F. Vydra, K. Štulík and E. Juláková, Electrochemical Stripping Analysis, Ellis Horwood, London, 1976.
3 N. Tanaka and T. Ito, Bull. Chem. Soc. Jpn., 39 (1966) 1043.
4 J. Zarebski, Chem. Anal. (Warsaw), 22 (1977) 1037.
5 D. Ferri, F. Zignani and P. L. Buldini, Fresenius Z. Anal. Chem., 313 (1982) 539.
6 W. Ranly and R. Neeb, Fresenius Z. Anal. Chem., 292 (1978) 370.
7 E. Bottari and G. Anderegg, Helv. Chim. Acta, 50 (1967) 2349.

Analytica Chimica Acta, 157 (1984) 45—51
Elsevier Science Publishers B.V., Amsterdam — Printed in The Netherlands

A LACTATE ELECTRODE WITH LACTATE OXIDASE IMMOBILIZED ON NYLON NET FOR BLOOD SERUM SAMPLES IN FLOW SYSTEMS

M. MASCINI*, D. MOSCONE and G. PALLESCHI

Dipartimento di Scienze e Tecnologie Chimiche, II Università di Roma, Tor Vergata, 00173 Rome (Italy)

(Received 28th July 1983)

SUMMARY

Commercially available lactate oxidase from *Mycobacterium smegmatis* is immobilized on a nylon net which is fixed on an oxygen probe to provide a simple L-lactate sensor. A citrate buffer, pH 6.0, is the only reagent required. The high activity of the enzyme obtained with this immobilization process permits the use of only 20—100 μl of plasma; diluted with citrate buffer to 2 ml, the sample is pumped through a flow cell. The high dilution offsets inhibitory effects of some anions present in blood such as oxalate, hydrogencarbonate and chloride. The response of the sensor is linear over the range 0.2—2×10^{-4} M L-acetate. The lifetime is about two months. Effects of pH, temperature and different buffers are described and results on serum samples are reported.

The determination of L-lactate in blood is clinically important because its concentration indicates pathological states (e.g., shock, respiratory insufficiency, heart disease). Its concentration is considered the best biochemical criterion for judging the severity of circulatory deficiencies. Electrochemical detectors for L-lactate have been based on the selectivity of lactate dehydrogenase (LDH) [1—6] or on lactate oxidase (EC 1.1.3.2) from *Pediococcus* sp. [7—10].

Recently, a different lactate oxidase (decarboxylating; EC 1.13.12.4) [11] became commercially available. The reaction is

$$\text{Lactate} + O_2 \xrightarrow{\text{Lactate oxidase}} \text{Acetate} + CO_2 + H_2O$$

This paper reports the features of this enzyme immobilized on a nylon net [12], coupled with an oxygen electrode, and the performance of the sensor for serum samples in a flow cell. This enzyme requires only the oxygen provided by the buffer with which samples are diluted and no other chemical is required, in contrast to most LDH methods. The technique of immobilizing the enzyme on nylon nets was preferred for flow systems because of the mechanical stability and ruggedness of the nylon net [12, 13] and the reliability of the procedure.

0003-2670/84/$03.00

EXPERIMENTAL

Materials

Lactate oxidase (15 U mg^{-1}) from *Mycobacterium smegmatis* (EC 1.13.12.4) was obtained from Boehringer, Mannheim; commercial lyophilized human sera were obtained from Boehringer and Dade. Human fresh serum samples were obtained from a local hospital and from diabetic patients during the treatment on an artificial pancreas.

L-Lactate (lithium salt; Sigma) was used as standard. All other reagents and buffers were of the purest grade available (Carlo Erba, Milano, Italy). The nylon net used (A. Bozzone, Appiano Gentile, Italy) has a mesh of 120 cm^{-2} with a thickness of 100 μm and a free surface of 35%.

The oxygen probe was a pO_2 electrode (Instrumentation Laboratory; 0.1 M KCl internal solution, 12 μm teflon membrane, platinum cathode and silver anode). An IL Model 213 meter was used with an Omniscribe recorder (Houston Instruments) for measuring the current.

Procedures

Immobilization of the enzyme. The chemical procedure for immobilizing enzymes on nylon net was derived from the method of Hornby and Morris [14] and details have been reported [12]. About 0.5—2 mg of enzyme was used for each membrane which had an area of about 1 cm^2. The nylon net was secured to the oxygen probe together with the teflon membrane and the probe was fixed in a flow-through cell with an estimated volume of 40 μl, as previously described [13].

Determination of L-lactate. For the determination of L-lactate, the serum samples were diluted 20 or 50 times with 0.1 M citrate buffer, pH 6.0, and passed through the flow cell at a rate of 1 ml min^{-1} with a peristaltic pump. Usually, 2 ml of sample was pumped. The decrease in the electric current caused by the decrease in dissolved oxygen in the vicinity of the electrode surface was measured.

Before and after each sample, the 0.1 M citrate buffer was pumped at the same flow rate. The electrode was stored overnight in 0.1 M citrate buffer, pH 6.0, at 4° C.

RESULTS AND DISCUSSION

Characteristics of the sensor

The activity of the L-lactate oxidase immobilized on nylon net was measured with an oxygen electrode. For this purpose, a 10^{-2} M lactate solution was prepared in 0.1 M citrate buffer, pH 6.0, the nylon net with the immobilized enzyme was immersed in the stirred solution, and the decrease in oxygen concentration was recorded. From the decrease, the specific activity was calculated. Values in the range 80—100 nmol min^{-1} cm^{-2} were obtained.

Table 1 shows the effect of varying the loading of enzyme on the specific activity of the nylon net membrane (2 cm^2) at 25°C. It can be seen that doubling the loading from 1 to 2 mg (15—30 IU) doubles the activity of the membrane, but increasing the enzyme loading further does not affect the activity. Therefore, 2 mg of enzyme (30 IU) was the amount used in the rest of the work.

The lifetime of the enzyme membrane was over two months. During such periods, more than 500 measurements were done on standard and reconstituted human serum and on plasma samples from the hospital. This seems to be the longest lifetime ever reported for a lactate electrode. The activity of the lactate sensor with immobilized enzyme on nylon net during a two-month period is shown in Fig. 1. The lifetime is compared with that of a lactate sensor prepared with the same amount of lactate oxidase physically immobilized on the oxygen sensor by a thin (50 μm) dialysis cellulose membrane (Thomas and Co.). The lifetime of the lactate sensor with the enzyme physically entrapped was quite short, although initially the activity was higher than that of the nylon net sensor, presumably because of some inactivation of the enzyme during the chemical immobilization.

The reproducibility of the response to L-lactate was evaluated. A lactate standard in citrate buffer was pumped through the system several times on different days. The within-day reproducibility was fair, being in the range 1—2% r.s.d., but the absolute value of the current decrease varied from day to day so that a daily or twice-daily standardization of the lactate probe is advisable.

Several chemicals inhibit the enzyme [15, 16]. Figure 2 shows calibration graphs obtained for L-lactate in 0.1 M citrate buffer, pH 6.0, and in 0.1 M phosphate buffer, pH 7.0; the normal range of lactate in diluted blood is also indicated. The correlation coefficients for such calibration lines were always around 0.997, but the inhibitory effect of phosphate is very evident. The effect was transient and reversible; when the phosphate solution was eliminated, the enzyme activity was restored.

In Fig. 3, the effects of pH and different buffers are shown. The inhibiting effect of some anions is evident. Citrate is the best buffer for the enzymatic reaction, phosphate inhibition is evident but reversible, but the phthalate inhibition is severe, being irreversible at pH < 5.0 at which pH the enzyme lost all activity.

Other inhibitory effects were observed from chemicals commonly present in blood samples: chloride at concentrations $\geqslant 10^{-1}$ M and hydrogencarbonate

TABLE 1

Specific activity (nmol min^{-1} cm^{-2}) of lactate oxidase immobilized on nylon net (Surface 2 cm^2, 25°C, citrate buffer pH 6.0)

Enzyme loading (mg)	1	1.8	2.3	3.0
Spec. activity	50	100	130	100

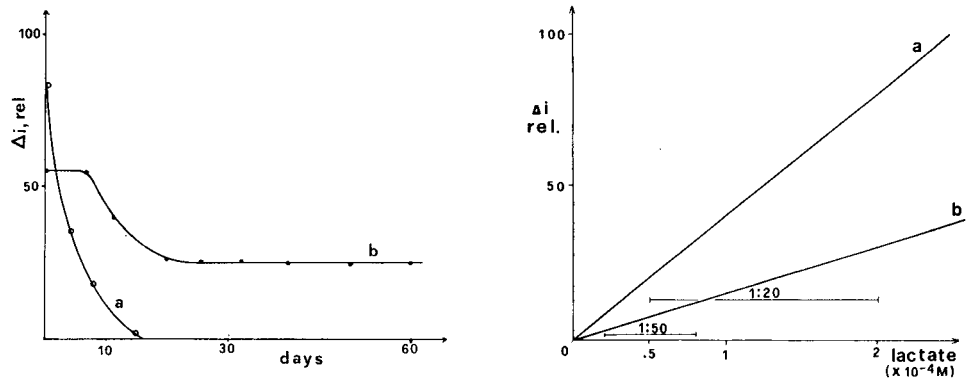

Fig. 1. Lifetime of lactate sensors with 1 mg of immobilized enzyme: (a) physically retained with a dialysis membrane; (b) chemically immobilized on nylon net. Conditions: 2 × 10^{-4} M lactate in 0.1 M citrate buffer, pH 6.0.

Fig. 2. Calibration graphs for the lactate sensor in (a) 0.1 M citrate buffer, pH 6.0; (b) 0.1 M phosphate buffer, pH 7.0. Horizontal lines show the normal range for serum diluted 1:50 and 1:20.

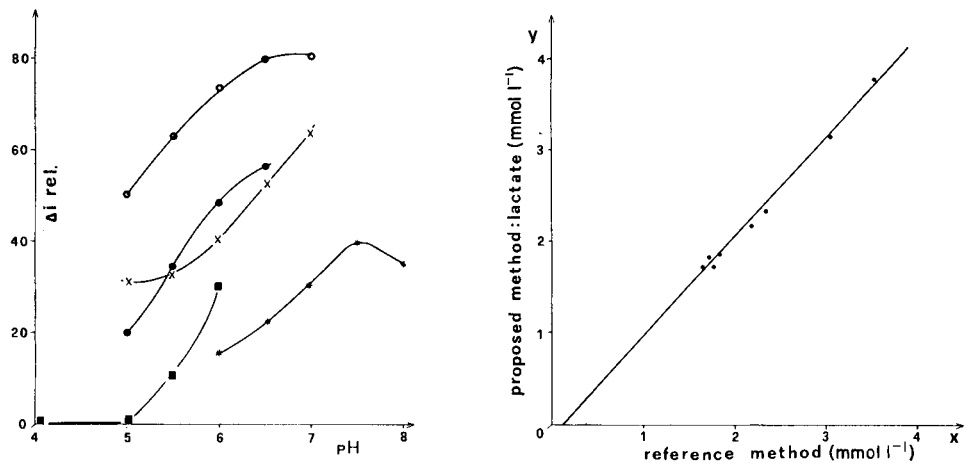

Fig. 3. Effect of pH and buffer anion: (○) 0.1 M citrate; (●) 0.1 M succinate; (×) 0.1 M maleate; (■) 0.1 M phthalate; (*) 0.1 M phosphate. Conditions: 2 × 10^{-4} M lactate, 25°C, 2 mg of enzyme.

Fig. 4. Correlation of lactate determination with the proposed method for reconstituted human sera.

at $\geqslant 10^{-2}$ M inhibited the enzyme somewhat (≈10%); oxalate at $\geqslant 10^{-4}$ M showed a drastic inhibition. All these inhibitions were transient and the enzyme recovered its features when the solution was replaced by citrate buffer. Table 2 lists the inhibitory effects for some anions present in normal serum samples. It should be noted that when the serum samples are diluted

TABLE 2

Inhibitory effect of some anions present in serum samples as a function of their concentration
(10^{-4} M L-lactate, citrate buffer pH 6.0, 25°C)

HCO_3^- added (M)	0.5×10^{-4}	1.25×10^{-3}	2.5×10^{-2}
Inhibition (%)	0	13	60
Cl^- added (M)	2×10^{-2}	5×10^{-2}	0.1
Inhibition (%)	0	12	20
$C_2O_4^{2-}$ added (M)	10^{-7}	10^{-6}	10^{-5}
Inhibition (%)	0	0	13
Pyruvate added (M)	—	10^{-6}	10^{-5}
Inhibition (%)	—	0	0

1:20 or even 1:50, all anions fall to the concentration range at which the interference is not detectable.

Temperature effects were studied in the range 20—45°C. The plot of response vs. temperature did not show the usual bell shape, but an increase of about 10% every 3°C. To improve the reproducibility of the performance of the oxygen probe, the cell was thermostated at 25 ± 0.1°C.

Application to serum samples

Table 3 lists the results obtained for several reconstituted sera along with the values and range reported by the manufacturers. Figure 4 shows the correlation of the above experiment; the equation of the line is $y = 1.094x - 0.128$ with a correlation coefficient of 0.995 ($n = 8$).

Figure 5 reports the recordings obtained for L-lactate standard solutions, reconstituted human serum samples and the same samples spiked with L-lactate standards. Each sample was changed manually after 2 min, i.e., 2 ml of each sample was pumped at a rate of 1 ml min^{-1}.

Recovery experiments for lactate added to a pooled serum obtained from a local hospital are reported in Table 4. The results are good. Table 5 lists the results obtained for some fresh human sera collected from the local hospital and compares them with results from a conventional enzymatic (LDH) spectrophotometric procedure. The correlation plot had the equation $y = 1.02x + 0.2$ with a correlation coefficient of 0.935.

Conclusion

The lactate sensor obtained by immobilizing the new commercially available enzyme, lactate oxidase from *Mycobacterium smegmatis*, has several advantages. It is suitable for determinations of L-lactate in serum samples or blood in a small flow-through cell; the immobilization process on nylon net covering an oxygen probe provides a lifetime of over two months. The nylon net has excellent mechanical features and the cell can be easily taken apart many times if necessary, without damage to the net.

TABLE 3

Lactate determination on reconstituted human sera commercially available

Type of serum	Lactate content (mmol l^{-1})		
	Manufacturer's data		
	Value	Range	Found[a]
Precinorm U 4-567	3.52	3.10—3.94	3.79
Monitrol I E	3.02	2.72—3.32	3.15
Precipath U 2-512	2.17	1.91—2.42	2.18
Precipath U 14-517	1.63	1.47—1.79	1.72
Precipath U 3-518	1.84	1.60—2.20	1.86
Precinorm U 09558	1.68	1.48—1.88	1.83
Monitrol II E	2.33	2.08—2.59	2.35
Precinorm U3-577	1.75	1.54—1.97	1.72

[a]Mean of three determinations.

TABLE 4

Recovery of L-lactate added to pooled serum

L-lactate (mmol l^{-1})		Recovery (%)	L-lactate (mmol l^{-1})		Recovery (%)
Added	Found		Added	Found	
0	1.72	—	4.53	6.26	100
2.27	4.02	101	5.66	7.60	104
3.40	5.13	100	6.80	8.46	99

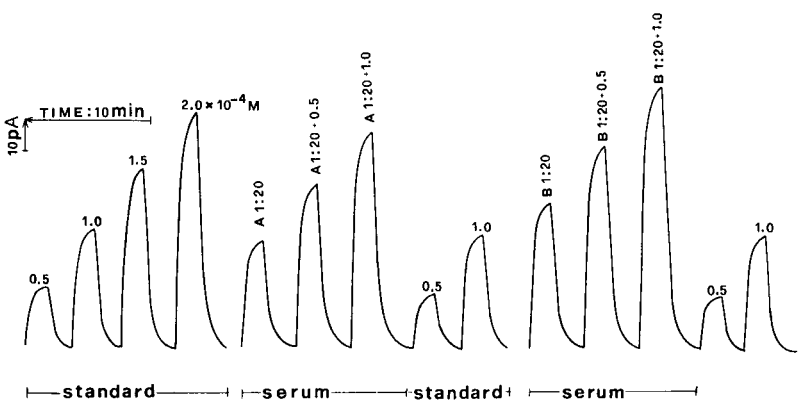

Fig. 5. Recording for standard solutions of lactate (0.5, 1.0, 1.5, 2.0 × 10^{-4} M), for reconstituted sera diluted (A and B) and for these sera spiked with standard (1:20 + 0.5 × 10^{-4} M, and 1:20 + 1.0 × 10^{-4} M).

TABLE 5

Comparison of results obtained for L-lactate in human sera obtained from a local hospital

Serum No.	Lactate found (mmol l^{-1})		Serum No.	Lactate found (mmol l^{-1})	
	Proposed method	Spectrophot. method		Proposed method	Spectrophot. method
1	2.15	2.10	5	2.51	2.03
2	2.66	2.40	6	2.70	2.31
3	2.81	2.53	7	3.40	3.20
4	2.85	2.40	8	2.28	2.10

The high activity of the immobilized enzyme on nylon net and the choice of an optimum buffer and pH allow serum samples to be diluted 1:50 or 1:20 for measurement. This dilution offsets the inhibitory effect of anions present in sera.

The new probe will be applied in the near future for the continuous analysis of blood samples in conjunction with an artificial pancreas in diabetic patients. The actual insulin infusion system is programmed on the basis of glucose values alone, but changes in the L-lactate parameter during treatment will also be studied. The ruggedness of the sensor is important in such situations.

REFERENCES

1 T. Shinbo, M. Sugiura and N. Kamo, Anal. Chem., 51 (1979) 100.
2 J. J. Kulys and G. J. S. Svirmickas, Anal. Chim. Acta, 109 (1979) 55; 117 (1980) 115.
3 W. J. Blaedel and R. A. Jenkins, Anal. Chem., 48 (1976) 1240; 52 (1980) 169.
4 T. Yao and S. Musha, Anal. Chim. Acta, 11 (1979) 203.
5 H. Durliat and M. Comtat, Anal. Chem., 52 (1980) 2109.
6 F. Cheng and G. Christian, Clin. Chim. Acta, 91 (1979) 295.
7 I. Karube, T. Matsunaga, N. Teraoka and S. Suzuki, Anal. Chim. Acta, 119 (1980) 271.
8 T. Matsunaga, I. Karube, N. Teraoka and S. Suzuki, Anal. Chim. Acta, 127 (1981) 245.
9 T. Matsunaga, I. Karube, N. Teraoka and S. Suzuki, Eur. J. Appl. Microbiol. Biotechnol., 16 (1982) 157.
10 F. Mitzutani, K. Sasaki and Y. Shimura, Anal. Chem., 55 (1983) 35.
11 J. G. Schindler and M. V. Gülich, Fresenius Z. Anal. Chem., 308 (1981) 434.
12 M. Mascini, M. Iannello, G. Palleschi, Anal. Chim. Acta, 146 (1983) 135.
13 M. Mascini, G. Palleschi, Anal. Chim. Acta, 145 (1983) 213.
14 W. E. Hornby and D. L. Morris, in H. H. Weetall (Ed.), Immobilized Enzymes, Antigens, Antibodies and Peptides, Vol. 1, M. Dekker, New York, 1975, p. 141.
15 O. Lockridge, V. Massey and P. A. Sullivan, J. Biol. Chem., 247 (1972) 8097.
16 S. Ghisla and V. Massey, J. Biol. Chem., 250 (1975) 577.

Analytica Chimica Acta, 157 (1984) 53—63
Elsevier Science Publishers B.V., Amsterdam — Printed in The Netherlands

QUANTITATIVE ION CHROMATOGRAPHY WITH AN ULTRAVIOLET ABSORBANCE DETECTOR WITHOUT STANDARDS

STEVEN A. WILSON and EDWARD S. YEUNG*

Ames Laboratory and Department of Chemistry, Iowa State University, Ames, IA 50011 (U.S.A.)

(Received 25th July 1983)

SUMMARY

Samples of ions are studied by non-suppressed ion chromatography and an ultraviolet absorbance detector. When two eluents of similar properties but different absorptivities per normal concentration are used in succession, two distinct chromatograms are obtained for the same sample. This information can be used to predict the number of equivalents of each ion present, as well as its absorptivity. In conjunction with elution-time studies, molar concentrations can also be obtained. The procedure does not require knowledge of the identity or any physical properties of the ionic species, and is applicable to ions with arbitrary absorption strengths.

Ion chromatography has made substantial advances in the last few years [1—3], partly because of the development of new detection methods. Much interest has been centered around non-suppressed ion chromatography because of the smaller void volumes possible and the greater simplicity in the system. Even though the conductimetric detector works quite well there, several optical methods, including indirect photometric [4], indirect refractive index [5], and direct photometric [6] methods, have been suggested to improve the overall detectability and to allow the use of more nearly standard liquid chromatographic instrumentation. An interesting question is whether there exists a sensitive absolute method for quantitation in ion chromatography so that the concentrations of ions can be determined as they elute from the column without prior identification and therefore without using standards.

Recently [7], it has been demonstrated that analytes can be quantified without identification in liquid chromatography (l.c.) by using the refractive index detector, and the method has been applied in gel-permeation chromatography [8]. The concept can be extended to the absorbance detector in liquid chromatography (l.c.) and is particularly applicable to ion chromatography. In the simplest case of a chromatographic peak registered by an absorbance detector in l.c., the response, ΔA, is related to the molar absorptivities of the eluent, ϵ_1, and the solute, ϵ_x, by Beer's Law. If m_x and m_1 are the number of moles of the analyte (solute) and the eluent, respectively, in

0003-2670/84/$03.00

the detection cell of volume V (l) and unit pathlength (1 cm), then the observed absorbance is A as determined by

$$A = (\epsilon_x m_x/V) + (\epsilon_1 m_1/V) \quad (1)$$

For most forms of l.c., it is more convenient to work with concentrations in volume fractions, V_x and $(1 - V_x)$, for the solute and the eluent, respectively. If the molar volumes of the solute and the eluent are v_x and v_1, then

$$A = (\epsilon_x V_x/v_x) + [\epsilon_1(1 - V_x)/v_1] \quad (2)$$

where the substitution $m_i = V_i V/v_i$ has been made for each component. When the detection cell contains only the eluent, $A = \epsilon_1/v_1$ because V_x is zero. In l.c., normally a differential absorbance detector is used so that a response, ΔA, is measured with respect to this "baseline". So,

$$\Delta A = V_x[(\epsilon_x/v_x) - (\epsilon_1/v_1)] \quad (3)$$

The only assumption invoked in Eqn. 3 is that of an ideal solution between the eluent and the solute, but such an assumption is needed in all l.c. work anyway, in order to relate the concentration observed at the detector to that of the injected sample, which is often present in an unpredictable matrix. Equation 3 has exactly the same form as Eqn. 8 in [7], and allows the application of the quantitative scheme described there to the absorbance detector in l.c. A subtle point is that unlike the refractive index detector, which gives a non-linear response with respect to concentration, no assumptions of low concentration are needed in deriving Eqn. 3, to the limit of the working range of Beer's Law.

Very briefly, one can consider Eqn. 3 as having two unknowns, V_x and f_x, where f_x is defined to be ϵ_x/v_x. If one injects the same sample into the l.c. system using two eluents with different molar absorptivities, ϵ_1 and ϵ_2, two different peak areas will be obtained for each separated peak. There are then available two equations of the form in Eqn. 3 to solve for the two unknowns, provided that ϵ_x is the same in both eluents. The concentration as well as the volume-weighted molar absorptivity of the analyte can be thus determined without analyte identification and without the use of standards. If the two eluents can be eluted using each other as the chromatographic mobile phase, one can follow the earlier procedure [7] and use Eqn. 16 [7] to calculate the concentration of the analyte without knowing even the molar absorptivities of the two eluents, and without calibrating the response of the detector.

In ion chromatography, some modifications must be made to Eqns. 2 and 3. In general, the major component of the eluent is always non-absorbing (e.g., water). Equation 1 should then refer only to the eluent ions, 1, and the solute ions, x. The principles of electroneutrality and equivalence of exchange imply that the total number of equivalents of the eluting ion and the solute ion remain fixed, because the number of co-ions in the eluent is constant. It is thus more convenient to think in terms of concentrations in normality. The normality of the solute ion with charge, n_x, and the eluting

ion with charge, n_1, at the detector are then N_x and $(N_1 - N_x)$, respectively, because the normality of the solution is a constant. The concentration of the eluting ion at the eluent reservoir is in fact N_1. Equation 1 can then be rewritten as

$$A = [\epsilon_x N_x/n_x] + [\epsilon_1(N_1 - N_x)/n_1] \quad (4)$$

Again, because only a differential response, ΔA, is measured, Eqn. 4 becomes

$$\Delta A = N_x[(\epsilon_x/n_x) - (\epsilon_1/n_1)] \quad (5)$$

If the same sample is then studied with a different eluting ion, 2, such that ϵ_2/n_2 is quite different from ϵ_1/n_1, one obtains two independent equations of the form of Eqn. 5. The fact that the major component in each case is identical (e.g., water) guarantees that ϵ_x is identical in the two eluents. So, one can solve for the two unknowns, N_x and ϵ_x/n_x.

The use of Eqn. 5 requires that the molar absorptivities and the charge numbers of the two eluting ions be known. Sometimes, it is inconvenient to determine ϵ and n because more than one form of an eluting ion may be present simultaneously, e.g., the various dissociated forms of a polybasic weak acid. These eluents can naturally be used if the equilibrium is controlled by the solution pH. If each eluting ion elutes conveniently when the other is used as the eluent, the procedure leading to Eqn. 16 [7] can be used to determine the concentration of the solute ion without knowing the physical properties of the eluting ions. If the eluting ions do not conveniently elute each other, one can arbitrarily choose two additional ions, 3 and 4, to accomplish the same goal. The complete procedure is first to obtain peak areas, S, for the analyte ions in each of the two eluents. Because peak areas take into account all ions that pass through the detector, they are not affected by changes in retention time. Redefining $\epsilon_i/n_i \equiv F_i$ in Eqn. 5, one obtains

$$S_1K_1 = C_x(F_x - F_1) \quad (6)$$

$$S_2K_2 = C_x(F_x - F_2) \quad (7)$$

where K_i is a constant characteristic of the particular eluent, including the scale expansion used at the detector, the eluent flow rate, and the integration interval for the area. This K_i then allows the use of arbitrary units for the areas S, and gives the concentration, C_x, at injection rather than at the detector. As long as the same set of chromatographic conditions is used throughout for a given eluent, K is a true constant. For the peak areas obtained for ions 3 and 4 in the same two eluents

$$S_3K_1 = C_3(F_3 - F_1) \quad (8)$$

$$S_4K_2 = C_3(F_3 - F_2) \quad (9)$$

$$S_5K_1 = C_4(F_4 - F_1) \quad (10)$$

$$S_6K_2 = C_4(F_4 - F_2) \tag{11}$$

It is more convenient, but not necessary, to use the same concentration C for these two ions, so that $C = C_3 = C_4$. Equations 8—11 then give

$$K_2/K_1 = (S_3 - S_5)/(S_4 - S_6) \tag{12}$$

Now, Eqns. 8 and 9 give

$$(F_2 - F_1)/K_1 = [S_3 - (K_2/K_1)S_4]/C \tag{13}$$

Similarly, Eqns. 6 and 7 give

$$(F_2 - F_1)/K_1 = [S_1 - (K_2/K_1)S_2]/C_x \tag{14}$$

Combining Eqns. 12—14, the final result is

$$C_x = C[S_1 - S_2(S_3 - S_5)/(S_4 - S_6)]/[S_3 - S_4(S_3 - S_5)/(S_4 - S_6)] \tag{15}$$

Equation 15 implies that quantitative determination is possible without knowing any of the absorption properties of the eluents, the analyte ion, or the two "calibrating" ions. The only requirements are that the two absorptivity functions, F_3 and F_4, are quite different, so that $(S_3 - S_5)$ and $(S_4 - S_6)$ can both be determined with good precision, and that the two functions F_1 and F_2 are quite different (but not necessarily different from F_3 or F_4), so that the subtractions in the numerator and in the denominator of Eqn. 15 can retain significance. It is also noted that S_3 through S_6 need only be determined once for a given set of eluting ions 1 and 2.

Once C_x is known, one can calculate the absorptivity of the analyte ion if the absorptivities of the eluting ions are known, following the earlier procedure [8]. However, in ion chromatography, this is not convenient because the exact distribution of ionic forms of the eluting ion may not be well determined. One can obtain the same information if instead the absorptivities of the "calibrating" ions 3 and 4 are known. From Eqns. 9 and 11

$$K_2 = C(F_3 - F_4)/(S_4 - S_6) \tag{16}$$

From Eqns. 7 and 9

$$F_x - S_2K_2/C_x = F_3 - S_4K_2/C \tag{17}$$

Combining these equations gives

$$F_x = F_3 + (S_2C/C_x - S_4)(F_3 - F_4)/(S_4 - S_6) \tag{18}$$

EXPERIMENTAL

All reagents and eluents used were reagent-grade materials without further purification. Water is deionized and purified by a Millipore Milli-Q System. The chromatographic system used was conventional, consisting of a reciprocating pump (Milton Roy, Riviera Beach, FL; Model 196-0066), a 25-cm × 4.6-mm, 15-μm ion chromatographic column (Vydac, Hesperia, CA;

302-IC-4.6), a 25-cm × 4.6-mm, 10-μm C_{18} column (Alltech, Deerfield, IL), a 20-μl sample loop of a conventional injection valve (Rheodyne Model 7010), and an absorbance detector (Rainin, Woburn, MA; Model 153-00) operated at 254 nm. The reference cell was used in the static mode filled with the eluent being used. Flow rates between 0.79 and 1.36 ml min^{-1} were used.

The output of the ultraviolet (u.v.) detector (1 mV full scale) was connected to a digital voltmeter (Keithley Model 160B), the analog output of which was in turn connected to a computer (Digital Equipment Model PDP-11/10 with LPS-11 laboratory interface). The computer took readings typically every 0.05 s, and averaged each set of ten before storing the information. Typically about 100 of these averaged data points defined an analyte peak. The area was determined by summation of the adjusted values above a chosen baseline for each peak to account for a slight linear drift in the detector, and the values were used directly as S_i defined earlier. All areas were determined for multiple injections (three or more). The linearities of the detector and of the attenuation settings were measured by injections of successively diluted samples covering the ranges used in this work.

Absorbances of samples were measured with a conventional spectrophotometer (Shimadzu, Model UV-240).

RESULTS AND DISCUSSION

An important condition for deriving Eqn. 15 is that the detector response, even though it need not be calibrated, must be linear with respect to concentration. It has already been pointed out [9] that although commercial detectors in general behave properly at low absorbance levels, non-linearity of response appears even at moderate concentrations. In the particular detector used in this study, stray light and amplifier bias current could affect linearity when the absorbing eluent was used. Therefore the detector response was measured under chromatographic conditions by injecting five samples spanning a concentration range of a factor of 16 to cover all the scale expansions used in these experiments. The result was a straight line passing through the origin with a slope of 1.001 and a correlation coefficient of 0.9997 when the area, S_i, was plotted against the concentration, each normalized to the highest value. If the peak heights were used instead, the two highest concentrations fell off the line. This is expected because of band broadening from saturation in the chromatographic column. Equation 15 can thus be used with confidence. It should be noted that a unit slope is not a necessity in this scheme, because only the value K_2/K_1 is used.

The validity of Eqn. 3 was checked by following a procedure similar to that described earlier [7]. The two eluents used were cyclohexane and a 0.015 M solution of benzene in cyclohexane. A reversed-phase C_{18} column was used. This provided eluent absorbances of 0.0 and 1.1, respectively, in the 1-cm detector. Ideally, one wants the absorbances of the two eluents to

be as different as possible to assure good sensitivity. In practice, highly absorbing eluents block out too much light in the optical path, and stray light plus amplifier bias current become dominant backgrounds. Increasing the intensity of the light source or the amplification of the photoelectric detector is not of much help, because when the absorbance changes from 1 to 10, the fraction of light transmitted changes by a factor of 10^9. By then, other effects such as thermal lensing [10] will become significant. The absorbing eluent is thus chosen to have an absorbance of about unity. Samples of "unknowns" are prepared by well-defined dilutions of the absorbing eluent in the non-absorbing eluent in the range 10—100%. On applying Eqn. 16 [7], the "unknown" concentrations are predicted with an accuracy of ±2%, within the uncertainties of the area measurements. This indicates that Eqn. 3 holds even at these high volume fractions, in contrast to the case of the refractive index detector.

The verification of Eqn. 3 under conditions for reversed-phase chromatography does not imply that this scheme is useful for l.c. in general. An examination of Eqn. 3 shows that the detector response (ΔA) must have a numerically significant difference in the two eluents. For eluents having absorbances of 0.0 and 1.0, respectively, and a detector capable of measuring an absorbance change of 2×10^{-4} in either eluent, one essentially has a dynamic range of 5×10^3. So, the volume fraction of the analyte must be at least 2×10^{-4} at the detector. Considering an additional dilution factor for the concentration at injection, this is a relatively high concentration for the analyte. It is noteworthy that the situation is identical regardless of the molar absorptivity of the analyte. For comparison, the refractive index detector typically can detect changes in the order of 10^{-7} units. For two eluents with refractive index differences of 0.1 units, this is a dynamic range of 10^6. The useful concentration range is then extended by a factor of 200. So, we have the curious result that the refractive index detector offers lower detection limits than the absorbance detector for most l.c. applications of this quantitation scheme.

In ion chromatography, the situation is quite different. The major component in each eluent, e.g., water, plays no part in determining the response given by Eqns. 4 and 5. Each equivalent of an analyte replaces one equivalent of the eluting ion. The dynamic range for absorption measurements discussed above then refers to the fraction of eluting ion that is exchanged by the analyte ion. Because the former is usually already at a low concentration, the detection limit for the analyte can be quite impressive. In contrast, if a refractive index detector is used for ion chromatography [5], the difference in refractive index dictated by the two eluting ions is small because of the presence of the major component. The detection limit based on refractive index will be therefore no better in ion chromatography than in any other form of l.c.

To test the applicability of this scheme in ion chromatography, a 10^{-3} M solution of potassium hydrogenphthalate and a 10^{-3} M solution of potassium

citrate were chosen as the two eluents. The former had a measured absorbance of 1.31 and the latter had a measured absorbance of 1.6×10^{-4} at 254 nm in a 1-cm cell. Both were adjusted to pH 5.4 with potassium hydroxide to avoid changes in ϵ_x for the analytes caused by pH effects. At this pH, the eluents were each a mixture of different ionic species, the ratios of which were not measured. Because the absorptivities of the citrates are essentially zero, their exact distribution is not critical. For the phthalates, because the isosbestic point is not used, the pH is chosen in a self-buffered region to minimize changes as the analyte ion elutes. Care must be taken if a buffering agent is used, because there is a chance that charge balance at the detector involves the buffer ion as well and Eqn. 4 will not be strictly valid. If the ion-exchange mechanism involves a constant ratio of eluting versus buffer ions, Eqn. 4 can be used, but with a loss in sensitivity. The analyte ions chosen were IO_3^-, NO_2^-, Br^-, NO_3^-, and SO_4^{2-}, to provide a range of absorptivities and charge, and to have reasonably well-behaved elution on the column used. Figure 1 shows the chromatograms of two test mixtures eluted by phthalate ions, and Fig. 2 shows the chromatograms of the same mixtures eluted by citrate ions. The chromatograms show good separation for the ions, so that area determination should be reliable. Flow rates of 0.79 ml min^{-1} for the phthalate ions and 0.94 ml min^{-1} for the citrate ions were used. This, plus the difference in elution strengths of the ions, resulted in different elution times for the analytes. As mentioned earlier, the flow rates are included in the constants, K_1 and K_2, and should not affect quantitation. Because one can safely assume a fixed elution order for ions in the two eluents, the more involved "consistency" test discussed earlier [7] can be omitted. In the left display of Fig. 2, the scale is chosen to display the small peak of bromide. The iodate peak is actually within the range of digitization of the computer, and peaks at about 4X full scale.

The results of the experiments are summarized in Table 1. The areas

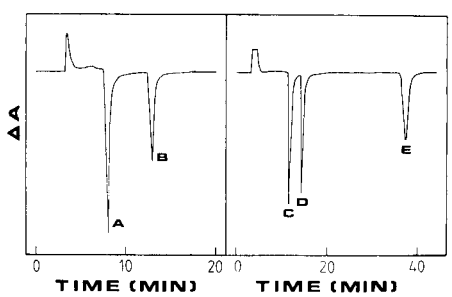

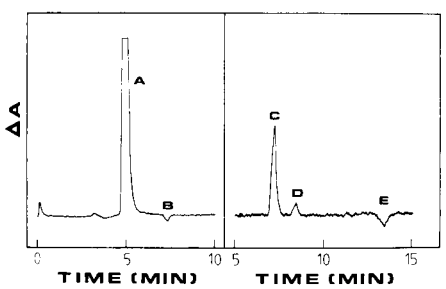

Fig. 1. Absorption chromatograms of two mixtures of ions with phthalate ions as the eluent. A, IO_3^-; B, Br^-; C, NO_2^-; D, NO_3^-; and E, SO_4^{2-}. Concentrations are as listed in Table 1. Full scale corresponds to an absorbance of 0.08.

Fig. 2. Absorption chromatograms of two mixtures of ions with citrate ions as the eluent. The concentrations and the labels of the peaks are as in Fig. 1. Full scale corresponds to absorbances of 0.005 and 0.0025 for the left and right displays, respectively.

TABLE 1

Quantitation of analytes

Ion	IO_3^-	Br^-	NO_2^-	NO_3^-	SO_4^{2-}
S_1[a]	−393800	−228200	−349100	−362900	−422600
S_2[b]	256200	−2130	15070	1860	−4310
True C_x (10^{-3} N)	1.14	0.62	0.97	1.01	1.20
True ϵ_x/n_x[c]	150	0	12	4.0	0
Calc. C_x[d,e] (10^{-3} N)	—	—	0.95	0.99	1.15
Calc. ϵ_x/n_x[d,f]	—	—	12.7	3.5	−0.1
Calc. C_x[g,e] (10^{-3} N)	1.07	0.64	—	—	1.18
Calc. ϵ_x/n_x[g,f]	143	1.0	—	—	0.8

[a]Integration interval is 2 s; 2048 = f.s. on 0.005 scale; phthalate eluent. [b]Integration interval is 0.5 s; 2048 = f.s. on 0.005 scale; citrate eluent. [c]Values obtained from [11]. [d]Iodate and bromide used as the "calibrating" ions. [e]Eqn. 15. [f]Eqn. 18. [g]Nitrite and nitrate used as the "calibrating" ions.

measured (three or more injections) by the computer for the two mixtures in each eluent are tabulated as S_1 and S_2. The integration interval in each eluting ion is different to allow optimized data collection over each chromatographic peak. The A/D interface used produced a value of 2048 for full-scale deflection, and all areas were normalized to the 0.005 scale on the detector. The actual absorbance corresponding to full-scale deflection, however, was not determined. For each of the ions, the normal concentration was calculated from the weight of material used in preparing the samples, and these are listed together with the known absorptivities of each ion. The concentrations of the last three ions were also checked by independent analysis. There are many combinations of ions that can be chosen as the "calibrating" ions 3 and 4. The results for two of these combinations are tabulated. To account for the fact that C_3 is not equal to C_4, the areas were first normalized to a concentration of $C = 1 \times 10^{-3}$ N for the two ions before applying Eqns. 15 and 18.

One has to be careful in applying Eqns. 15 and 18 to be sure that the subtractions result in significant numbers. This can be illustrated using iodate as ion 3 and bromide as ion 4. Using the areas in Table 1, one obtains for the normalized areas $(S_3 - S_5) = (-345400 + 368100) = 22700$, and $(S_4 - S_6) = (224700 + 3440) = 228100$. Considering that the areas are reliable to 2—3% for those in the 100 000's and to 10—15% for those in the 1000's, $(S_4 - S_6)$ is reliable to 2—3% but $(S_3 - S_5)$ is only reliable to 30—50%. The factor K_2/K_1, of the order of 0.1, is then only determined to an accuracy of 30—50%. However, because for the other three ions, S_2 is quite small compared to S_1, the numerator in Eqn. 15 essentially maintains the 2—3% reliability dictated by S_1 alone. For the denominator in Eqn. 15, one has the choice of using that form or the equivalent form of $[S_5 - S_6(K_2/K_1)]$. If the former is used, a slightly larger uncertainty will result because of the

relative magnitudes of S_3 and S_4, but the uncertainty is still only 3—4%. If the latter is used, one can improve the reliability again to 2—3%. It is therefore not surprising that the concentrations calculated for the "unknowns" in Table 1 are quite good, i.e., with errors less than 4%. If instead, nitrite is used as ion 3 and nitrate is used as ion 4, K_2/K_1 has a value of —0.043 with an uncertainty of a factor of 10. For predictions of the concentrations of bromide and sulfate, this is not a problem because S_2 is substantially smaller than S_1. For the case of iodate, the net uncertainty is of the order of 20%. This explains the results in Table 1, where bromide and sulfate are predicted with good accuracy and iodate is in error by 6%. This confirms the discussion earlier that for the best accuracy, F_3 and F_4 should be as different as possible. The present results would have been even better if an ion with higher absorptivity than iodate had been used as ion 3 and any non-absorbing ion as ion 4. A subtle point is that the reliability of the predictions is independent of the absorptivity of the analyte ion as long as it is within the linear range of the detector used.

To determine the absorptivities of the ions, one can either use Eqn. 16 to determine K_2 or use $K_1 = C(F_3 - F_4)/(S_3 - S_5)$. A slightly different set of indices will be present in Eqn. 18 in the latter case. From the concentration-weighted areas, one finds that $(S_4 - S_6)$ has much smaller uncertainties than $(S_3 - S_5)$ regardless of which pair of ions in Table 1 are chosen as ions 3 and 4. So, the former choice should be used. The predicted normal absorptivities are quite good when iodate and bromide are used for "calibration". The prediction for sulfate of —0.1 is close enough to zero to make the negative sign insignificant. The predicted absorptivities are also good when nitrate and nitrite are used, but not as good as the other values. This is because there is more uncertainty in the literature values [11] for the absorptivities of these two ions. In general, one wants to have F_3 and F_4 as different as possible to improve the reliability of Eqn. 18.

There is sufficient information to determine the absorptivities of the eluting ions as well. From Eqn. 9, $F_2 = F_3 - S_4K_2/C_3$. Using iodate as ion 3 and bromide as ion 4, one finds that $F_2 = 2.3$. The uncertainty is about 100% because of the subtraction of two numbers of the order of 150. This is consistent with the independent measurement of $F_2 = 0.2$ for the citrate solution used. From Eqn. 8, $F_1 = F_3 - S_3K_1/C_3$. One finds $F_1 = 2440$ compared to the value of 1370 measured independently. The literature value [11] of 1700 is for the monohydrogenated ion only, and cannot be used for comparison. The large discrepancy is due to the uncertainty in determining K_1, producing an uncertainty of 50%. Obviously, to obtain better values for the absorptivities of the eluting ions, one needs a larger difference in F_3 and F_4, so that extrapolation will not be over such an extended range.

To check the dynamic range of the method as well as some of the operating parameters, a series of chromatograms was obtained with nitrate as the analyte at five concentrations (at injection) of 8×10^{-3} N to 5×10^{-4} N, in steps of two. The injection loop used had a calibrated volume of 0.477 times

that of the 20-μl loop. The integration interval was chosen to be 4 times shorter than that used earlier, and the flow rate was a factor of 1.72 higher. So, the areas obtained for this series of samples were first multiplied by factors to normalize them to the same sample size, the same integration interval, and the same flow rate. Equation 15 was then used to predict the concentrations. The result was an average error of 3.9% with the mean, i.e., the least-square straight line using all five samples, deviating only 0.7% from the "true" value. This is particularly significant because these experiments were done one week after the initial series that produced the calibration. So, as long as these operating parameters can be related to those used earlier, the "calibration" remains good. Judging from the noise on the baseline on the most sensitive scales used for each eluent, it should be possible to measure an area for nitrate at a concentration of 1.25×10^{-5} N for a 5-μl injection. This corresponds to 4 ng of ions injected, and is comparable to the detection limits reported for indirect absorbance detection [4]. For analytical-scale l.c., injections of even 200 μl will not degrade the chromatographic resolution substantially, so that a concentration of 3×10^{-7} N should be adequate. This is consistent with the dynamic range of absorption detectors of 5×10^{3} and an eluting ion concentration of 10^{-3} N. It is possible to use another eluting ion, or phthalate ions at another absorption wavelength, so that F_1 is larger by as much as a factor of 10. The detection limit can then be improved accordingly, because the concentration of the eluting ion can then be decreased and yet maintain a background absorbance of about 1.0. For microscale l.c., the absolute detection limit can be improved because the elution volume of a given peak can be substantially smaller. An ion with a larger F_1 must be used to accommodate the typically shorter absorption pathlengths in order to benefit from this fact. A detection limit of 10 pg should be feasible. The detectability, just like the reliability of Eqn. 15, is independent of the absorptivity of the analyte.

The procedure above allows the determination of the number of equivalents of an analyte. Retention times in ion chromatography are related to charge numbers. Specifically, if the logarithm of the adjusted retention time is plotted against the logarithm of the concentration of the eluting ion, the slopes are in the ratios of the charge numbers of the ions [12]. Therefore, the elution of the same 5 ions was studied at other concentrations of the eluting ions. It was found that sulfate had a slope twice that of the other 4 ions. This implies that n_x can be independently determined for each without analyte identification. Molar concentrations can thus be derived from Table 1, as well as molar absorptivities.

Finally, the relationship between this scheme and some others needs to be discussed. The use of ion-interaction chromatography in conjunction with a u.v. detector [13] is an inselective method for quantifying ions. However, the absorbance of ion-interaction reagents can be affected differently by different analyte ions so that only approximate concentrations can be determined without standards. Indirect photometric methods for ion chroma-

tography [4] have truly constant sensitivity for all non-absorbing ions, but then one must assume or know that the analyte is in fact non-absorbing. Indirect refractive index detection can easily be adapted to this scheme for quantitation, but, as pointed out above, it is somewhat less sensitive than the current scheme even if properly optimized. The conductimetric detector for ion chromatography in principle can be used for quantitation without standards using a variation of the current scheme, but there are technical difficulties in measuring small conductance changes in a background of high conductivity. It is naturally possible, for example, to pass the chromatographic effluent into a strong-base anion-exchange resin in the hydroxide form and then relate the amount of hydroxide ions created to the normality of the analyte ion, but the procedure is tedious and suffers from possible degradation of the separatory power. In comparison with the refractive index scheme reported earlier [7, 8], the current absorbance scheme using Eqn. 3 gives exactly the same results for most forms of l.c., but with poorer sensitivity. When adapted to ion chromatography based on Eqn. 5, the sensitivity is impressive, but then the response is no longer truly universal, i.e., only analytes in ionic forms will be determined.

In summary, the quantitation scheme developed for l.c. uses the absorbance detector in a mode that does not require identification of the analyte and does not require knowing any of its physical properties. The scheme is verified using anion chromatography, but the extension to cations is straightforward.

The Ames Laboratory is operated for the U.S. Department of Energy by Iowa State University under Contract No. W-7405-eng-82. This work was supported by the Office of Basic Energy Sciences.

REFERENCES

1 H. Small, in J. F. Lawrence (Ed.), Trace Analysis, Vol. I, Academic Press, New York, 1982, p. 267.
2 J. S. Fritz, D. T. Gjerde and C. Pohlandt, Ion Chromatography, Huthig, New York, 1982.
3 H. Small, Anal. Chem., 55 (1983) 235A.
4 H. Small and T. E. Miller, Anal. Chem., 54 (1982) 462.
5 P. R. Haddad and A. L. Heckenberg, J. Chromatogr., 252 (1982) 177.
6 R. N. Reeve, J. Chromatogr., 177 (1979) 393.
7 R. E. Synovec and E. S. Yeung, Anal. Chem., 55 (1983) 1599.
8 R. E. Synovec and E. S. Yeung, J. Chromatogr., (1983) in press.
9 L. M. McDowell, W. E. Barber and P. W. Carr, Anal. Chem., 53 (1981) 1373.
10 R. L. Swofford, in G. M. Heiftje, J. C. Travis and F. E. Lytle (Eds.), Lasers and Chemical Analysis, Humana Press, Clifton, NJ, 1980, p. 143.
11 UV Atlas of Organic Compounds, Vol. V, Plenum, New York, 1971.
12 D. T. Gjerde, G. Schmuckler and J. S. Fritz, J. Chromatogr., 187 (1980) 35.
13 W. E. Barber and P. W. Carr, J. Chromatogr., 260 (1983) 89.

Analytica Chimica Acta, 157 (1984) 65—71
Elsevier Science Publishers B.V., Amsterdam — Printed in The Netherlands

DEPENDENCE OF SITE-SITE INTERACTIONS ON PORE DIAMETER ON AMINE-MODIFIED STATIONARY PHASES

C. H. LOCHMÜLLER* and W. B. HILL, JR.[a]

P. M. Gross Chemistry Laboratory, Duke University, Durham, NC 27706 (U.S.A.)

(Received 1st August 1983)

SUMMARY

m-Cresol purple stationary phases were prepared on a series of amine-silica substrates and studied by visible photoacoustic spectroscopy. Site-site interactions between residual, unreacted amines were shown to lower the pK_a of *m*-cresol groups and the magnitude of this effect was found to depend on the average pore diameter of the silica substrate. Two effects appeared to be operative: (1) solvent exclusion from small pores and (2) charge repulsion involving neighboring groups which effectively lowers the apparent pK_a. Surface "buffering" by unreacted amines may also occur in such systems.

The development and refinement of chemically-bonded stationary phases during the last decade have led to the widespread use of high-performance liquid chromatography. A more complete characterization of these stationary phases should lead to further understanding of the separation process which should result in enhanced resolution and efficiency. The unique characteristics of a stationary phase arise from a variety of factors including the production of the silica substrate, the chemical pretreatment and preparation of the bonded phase and the in situ modification by solvent (solvent-stationary phase interaction) [1, 2] and by other surface moieties (site-site interactions).

Investigations into the nature of amino stationary phases have utilized both chromatography and spectroscopy. Chromatographically, the influence of amino groups on other surface moieties has been used to explain the observed capacity changes of certain probe solutes [3, 4]. Spectroscopically, platinum(II) and rhodium(III) diamine complexes have been observed by ^{13}C-n.m.r. [5]. Both hydrogen ^{1}H-n.m.r. and infrared spectroscopies have been used in observing hydrogen bonding between surface-bound amines, and between amines and silanol groups [6—8]. The "web" structure of polymeric aminosilica substrates has also been observed by scanning electron microscopy [9]. Mimms et al. [10] observed a lowering of the pK_a of methyl red when immobilized on glass slides by using visible absorption

[a]Present address: Celanese Research Company, 86 Morris Avenue, Summit, NJ 07901, U.S.A.

0003-2670/84/$03.00

spectroscopy. Using visible photoacoustic spectroscopy, Lochmüller et al. [11] reported spectroscopic evidence which indicated that the response of the bonded phases to solvent acidity lagged behind the response of an appropriate solution model compound. This observation was attributed to a relatively-high surface group concentration, persistent site-site interactions, and solvent-stationary phase charge repulsion. Davidson et al. [12] also observed slight changes in the wavelength of maximum absorbance of picryl amido-bonded phase when residual amines were present.

In the present study, the interaction of surface-bound moieties with residual surface amines is investigated further by chemically-modifying amino-silica substrates with *m*-cresol purple. These pH-sensitive bonded phases were prepared on silica gels with pore sizes ranging from 8 to 3000 nm and their average pK_a values were determined by visible photoacoustic spectroscopy.

EXPERIMENTAL

Materials

The Spherosil silica gels (Analabs, North Haven, CT) and the Fractosil silica gels (American Scientific Products, McGaw Park, IL) were oven-dried (110°C) for 48 h prior to use. Other chemicals were 3-aminopropyldimethylethoxysilane (Petrarch Systems, Bristol, PA, U.S.A.), methyl orange, methyl red, *m*-cresol purple, oxalyl chloride and thionyl chloride (all from Aldrich Chemical Company). Toluene was distilled from calcium hydride over dry nitrogen and stored over sodium. The acetate buffers ranging from pH 4.0 to 6.0 (μ = 0.10) were prepared from analytical reagents according to the procedure of Boyd [13]. All other buffers were purchased from Fisher Scientific Company.

Preparation of stationary phases

The amine-bonded phases were prepared by refluxing dry toluene under dry nitrogen for 30 min, adding 1.0 g of dry silica gel, then 1.0 ml of 3-aminopropyldimethylethoxysilane in 10 ml of toluene dropwise for 20 min, and refluxing for 12 h under nitrogen with stirring. The silica product was filtered and washed consecutively with 60-ml aliquots of methanol and 60:40 methanol/water prior to Soxhlet-extraction with dry methanol for 48 h, and then dried at 40°C under vacuum for 3 h and stored in a vacuum desiccator until use. The sulfonyl chlorides of methyl orange and *m*-cresol purple were prepared by adding a 50% excess of thionyl chloride in dry toluene dropwise for 20 min into a refluxing mixture of toluene containing the indicator and refluxed for 12 h. The product was filtered with toluene to remove excess of thionyl chloride and recrystallized. Methyl red acid chloride was prepared in a similar manner, except that a 20% excess of oxalyl chloride was used. The bonded phases were prepared by refluxing 30 ml of dry toluene under dry nitrogen for 30 min, adding an equivalent

of pyridine followed by 1 g of the amine-bonded phase and a 100% excess of the appropriate sulfonyl chloride in toluene dropwise for 20 min, and refluxing for 12 h with stirring. The product was filtered consecutively with water, pH 7.0 buffer, pH 5.0 buffer, pH 7.0 buffer, and water until the filtrate remained colorless.

Spectroscopic studies

The visible transmission spectra were acquired using a Perkin-Elmer 576 ST double-beam spectrophotometer. The photoacoustic spectra were obtained using a Princeton Applied Research model 6001 spectrometer incorporating a 1-kW xenon arc lamp with a modulation frequency of 50 Hz, 2-mm slits (resolution of 8 nm) and a microprocessor. Sample preparation consisted of filtering the bonded phases in a buffer and transferring them to a cylindrical stainless steel cell in a sealed sample chamber. Typically, 10 scans were signal-averaged per sample.

Nonaqueous titration was used to determine the amine coverage of the bonded phases. Approximately 10 mg of bonded silica was added to 25 ml of anhydrous acetic acid, and after adding an excess of 8.58×10^{-4} M potassium hydrogenphthalate, the mixture was back-titrated with 10^{-2} M potassium hydroxide.

In order to determine the *m*-cresol purple coverage, the absorbance intensities at 579 nm were measured for known concentrations of *m*-cresol purple propylamide in 1.0 M potassium hydroxide at 21.6°C. The bonded phases were also dissolved in 50.0 ml of 1.0 M potassium hydroxide at 21.6°C, their absorbance intensities measured, and their coverages computed by fitting the resulting absorbances to the linear Beer—Lambert correlation.

RESULTS AND DISCUSSION

Bonded phases of methyl red propylamide, methyl orange propylamide, and *m*-cresol purple propylamide were studied by photoacoustic spectroscopy. The spectrum of a methyl red Spherosil XOB-075 phase displayed a wavelength maximum of 450 nm which remained unchanged between pH 7.0 and pH 2.0 (the pK_a of methyl red propylamide is 5.4) [14]. Within this same pH range, the spectrum of a methyl orange Spherosil XOB-075 phase also remained unchanged with a wavelength maximum of 420 nm (the pK_a of methyl orange propylamide is 3.8). The absorption maxima correspond to the unprotonated forms of these dyes indicating that the immobilized dyes remain essentially unprotonated even at pH 2.0.

The spectra of the *m*-cresol purple (MCP) silica phases exhibited a shift in their wavelength maxima between pH 5 and 6. The equilibrium of the model compound [14] is

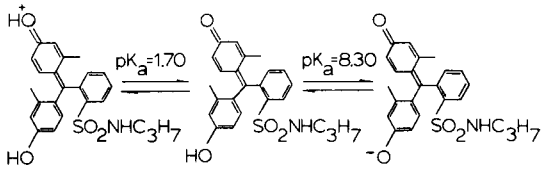

λ_{max} = 534 nm. λ_{max} = 408 nm. λ_{max} = 584 nm.

When compared with its free acid form, the *m*-cresol purple propylamide model compound displayed identical pK_a values. *m*-Cresol purple-bonded phases were prepared on both Spherosil and Fractosil silica substrates (Table 1). In pH 7.0 buffer, all had visible wavelength maxima of 592 nm except for Spherosil XOB-015, Spherosil XOC-005, and Fractosil 25000 which all had wavelength maxima at 440 nm.

The pK_a values of each of these bonded phases were determined by plotting the ratio of the intensities at 592 nm (purple) and 519 nm (red) against the pH of the buffer (Fig. 1). Because the ratio of the photoacoustic molar absorptivities of the unprotonated and protonated forms of the model compound was found to be 1.00 (±0.03), the equivalence point was taken to be the pH at which the intensity ratio was one. Table 1 lists the pK_a values for each of the MCP-bonded phases as well as some of their other physical characteristics. The molarity of the MCP moieties was determined on the assumption that they exist in a maximally extended conformation (11.7 Å). When the average pore diameter (D) $\geqslant$ 1250 Å, the pK_a values for both transitions were determined. The bonded phases with $D \leqslant 600$ Å exhibited a 73 nm shift (592 to 519 nm) on lowering the pH from 7.0 to 4.0 Figure 2

TABLE 1

The properties of *m*-cresol purple-bonded phases

Silica substrate	Average pore diameter (Å)	MCP surface concentration (10^{-3} M)	Residual amine-MCP ratio	Bonded-phase pK_a[a]
Frac. 200	190	3.0	57:1	4.85
Frac. 500	600	7.1	59:1	5.12
Frac. 25000	30000	110	4:1	8.55/0.65
Sph. XOA-400	80	0.78	50:1	5.89
Sph. XOA-200	150	1.6	20:1	5.73
Sph. XOA-075	300	3.2	64:1	5.77
Sph. XOB-030(A)	600	4.9	111:1	5.66
Sph. XOB-030(B)	600	3.8	92:1	5.72
Sph. XOB-015	1250	6.8	26:1	8.05/1.10
Sph. XOC-005	3000	3.8	89:1	8.31/0.02

[a]The bonded phase pK_a values for the 592—519 nm transition. For silica substrates with $D \geqslant 1250$ Å, both pK_a values were measured.

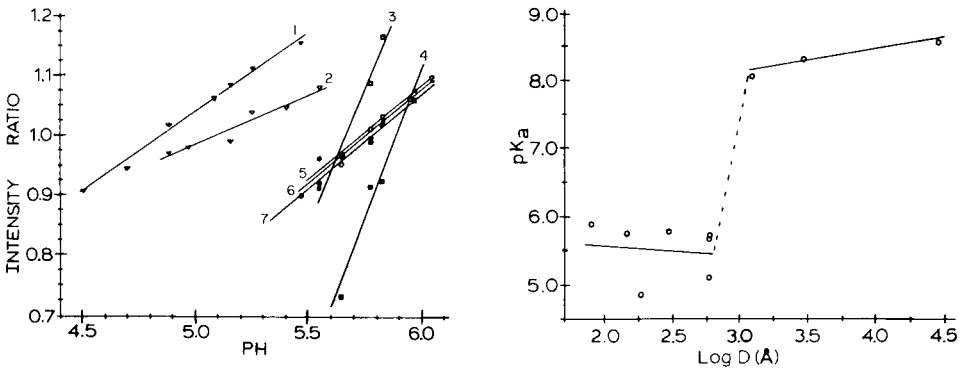

Fig. 1. Titrations of *m*-cresol purple-bonded phases with acetate buffers as the liquid phase and visible photoacoustic detection. Silica substrates: (1) Fractosil 200; (2) Fractosil 500; (3) Spherosil XOA-400; (4) Spherosil XOA-200; (5) Spherosil XOB-075; (6) Spherosil XOB-030(A); (7) Spherosil XOB-030(B).

Fig. 2. Dependence of the stationary phase pK_a on the average pore diameter.

shows that the relationship between D and pK_a changed between 600 Å and 1250 Å which suggested that the pore diameter directly affects the ability of the solvent to modify the immobilized molecule.

In an attempt to explain the existence of the absorbance at 592 nm on the MCP-bonded phases under neutral or weakly acidic conditions, the amine phases (which were the precursors to the MCP-bonded phases) were wetted with 1.0×10^{-5} M solutions of the MCP model compound in pH 5.0, 6.0 and 7.0 buffers, water and methanol. All of the resulting phases had wavelength maxima at 440 nm except those treated with methanol which gave wavelength maxima of 573 nm. When the underivatized silica gels were wetted with these same solutions, only the 440 nm transition was observed. These results suggested that the 592 nm transition resulted from the interaction of MCP with amines and not with silanol groups. For the MCP-bonded phases, the residual surface silanols would actually be expected to raise the bonded phase apparent pK_a because they are weak acids. However, because the residual amine-MCP ratio is at least 20:1 (see Table 1), the basicity of the amine should dominate the surface chemistry. The surface-bound amines may be deprotonating MCP, resulting in strong interactions between the protonated amine groups and the deprotonated MCP moieties. Therefore, the lower pK_a values for the MCP-bonded phases resulted from MCP-amine site-site interactions as well as from the buffering by the amine of the surface environment. Even though the MCP surface concentrations were high, the lack of any significant spectral skewing in either the protonated or unprotonated forms signified that nearly all of the surface-bound MCP is solvent-accessible. Furthermore, surface modification should "plug" fewer pores because the average pore diameters are much larger than the molecular diameter of MCP [15].

In contrast with the model compound, the pK_a transition of the MCP-bonded phase was from 592 to 519 nm. Under moderately acidic conditions, the wavelength maximum at 519 nm for the MCP-bonded phase could not have been the result of solvent modification because the pK_a of the model compound is 1.7 and because the pK_a values for the MCP-bonded phases with $D \geqslant 1250$ Å were even lower. The absorption spectra for solutions (ranging from 1.0×10^{-6} M to 3.0×10^{-3} M) of the MCP model compound had wavelength maxima around 440 nm in toluene, methanol, and acetone. Although this transition occurred in water, a new transition appeared at 512 nm as the concentration increased from 5.5×10^{-4} M to 8.7×10^{-3} M beginning at 1.0×10^{-3} M. A comparison of these results with the MCP-bonded phase surface concentrations (Table 1) indicated that the transition at 519 nm probably resulted from MCP site-site interactions. These high surface concentrations could have contributed to the observed bonded-phase pK_a value although no correlation between concentration and pK_a was found.

The Spherosil XOB-075 MCP-bonded phase was sonicated for 20 min with a series of solvents in order to determine the effect of solvent strength on the absorption spectrum. The 592-nm transition persisted for the phase when treated with water, methanol, acetonitrile, tetrahydrofuran, and toluene. The effect of surface-bound hydrogen chloride on the pK_a was minimal; the value remained unchanged even after sonicating with 2.5 M ammonia solution for 5 min. These results demonstrate that even solvents with adequate strength do not appreciably alter the MCP-amine surface interaction.

Although the amine-MCP site-site interactions lowered the pK_a values of the phases, the effectiveness of this interaction depended on the average pore diameter of the silica substrate as seen in Fig. 2. This break probably resulted from charge repulsion between the surface pore environment and the solvent. As D decreased, this repulsion as well as the amine-MCP interaction would be expected to increase. The immobilized moiety would then be more difficult to protonate which would result in the lowering of the apparent pK_a value of the bonded phase.

Conclusion

Although the effects of particle size and of modifier backbone structure have been extensively investigated in order to optimize the chromatographic process, the unique nature of the pore environment has rarely been considered. Although different types of stationary phases may vary as to the extent of site-site interactions in the pores, the pore chemistry of bound molecules will probably differ substantially from their solution models. If similar characteristics are desired in a bonded phase as were observed in some solution models, this study suggests that larger-than-average pores (perhaps 300—800 Å) should be considered. Both the acknowledgement and the further understanding of site-site interactions on silica substrates and their

dependence on pore size should lead to further refinement in stationary phase development.

This work was supported, in part, by the National Science Foundation under Grant CHE-8119600 (to CHL).

REFERENCES

1 R. K. Gilpin, M. E. Gangoda and A. E. Krishen, J. Chromatogr. Sci., 20 (1982) 345.
2 C. R. Yonker, T. A. Zwier and M. F. Burke, J. Chromatogr., 241 (1982) 269.
3 C. H. Lochmüller and W. B. Hill, Jr., J. Chromatogr. Sci., (1984) in press.
4 S. A. Matlin, A. Tito-Lloret, W. J. Lough, D. G. Bryan, T. Browne and S. Mehani, High Res. Chrom. Chrom. Commun., 4 (1981) 81.
5 S. Shinoda and Y. Saito, Inorg. Chim. Acta, 63 (1982) 23.
6 M. J. D. Low, A. G. Severdia and J. Chan, J. Catal., 71 (1981) 144.
7 M. J. Child, M. J. Heywood, S. Pulton, G. A. Vicary, G. H. Youg and C. H. Rochester, J. Colloid Interface Sci., 89 (1982) 202.
8 H. Ishida, C. Chiang and J. L. Koenig, Polymer, 23 (1982) 165.
9 A. D. Jones, I. W. Burns, S. G. Sellings and J. A. Cox, J. Chromatogr., 144 (1977) 169.
10 L. T. Mimms, M. A. McKnight and R. W. Murray, Anal. Chim. Acta, 89 (1974) 355.
11 C. H. Lochmüller, S. F. Marshall and D. R. Wilder, Anal. Chem., 52 (1980) 19.
12 R. S. Davidson, W. J. Lough, S. A. Matlin and C. L. Morrison, J. Chem. Soc. Chem. Commun., (1981) 517.
13 W. C. Boyd, J. Am. Chem. Soc., 67 (1945) 1035.
14 E. E. Sager, H. J. Keegan and S. F. Acree, J. Res. Natl. Bur. Stand., 31 (1943) 323.
15 K. K. Unger, Porous Silica; Its Properties and Use as Support in Column Liquid Chromatography, Elsevier, Amsterdam, 1979, pp. 104—108.

Analytica Chimica Acta, 157 (1984) 73—82
Elsevier Science Publishers B.V., Amsterdam — Printed in The Netherlands

APPLICATION OF STATIC SIGNAL-TO-NOISE THEORY TO THE DETECTION AND INTEGRATION OF DYNAMIC SIGNALS

WILLIAM J. TARASZEWSKI[a], DANIEL T. HAWORTH and BRUCE D. POLLARD*
Marquette University, Department of Chemistry, Milwaukee, WI 53233 (U.S.A.)
(Received 17th June 1983)

SUMMARY

Static, time-independent noise terms are combined to estimate the noise and signal-to-noise ratio (S/N) of dynamic, time-dependent methods. Simplified S/N equations for shot-noise-limited and flicker-noise-limited analyte signals with and without background signal noises are given. The intuitive aspects of peak integration are justified by these equations. For an ideal Gaussian peak, the equations are used to derive the chromatographic limit of detection (LOD). A comparison of the chromatographic detection limit with the detection limit for a static system using the same amount of sample predicts poorer chromatographic detection limits because of peak broadening. A possible determinate error in area measurement is shown to result when integration limits are chosen on the basis of the static detection limit.

Many studies of instrumental noise and its effects on quantitative results have been reported [1—5]. Sources of both shot and flicker noises have been investigated in order to improve signal-to-noise ratios (S/N) in various systems [6]. These studies have been concerned with noise characteristics of static systems, wherein signals are measured as a function of analyte concentration only. With the increasing importance of dynamic methods, such as gas chromatography/mass spectrometry, high-performance liquid chromatography and flow-injection sample processors, in which signals are functions of both concentration and time, comes the need for consideration of how signal-to-noise theory for essentially time-independent systems can be applied to transient systems.

This paper discusses the important parameters and presents equations for determining noise and S/N in dynamic systems as a function of the noise in their static system counterparts. Their implications are discussed. Although many of the optimal S/N conditions for dynamic systems can be predicted intuitively, the S/N equations presented here justify them quantitatively. The application of the equations is demonstrated by comparing the chromatographic limit of detection to that of a static system and by describing quantitatively for integrated peak measures the determinate errors caused by uncertainty in the integration limits.

[a]Present address: Pfizer Central Research, Eastern Point Road, Groton, CT 06340, U.S.A.

0003-2670/84/$03.00

THEORY

The basis of noise theory has been set down by Van der Ziel [7]. Alkemade, Winefordner, and their groups [1—4] have reviewed these fundamentals as they apply to noise and signal-to-noise ratios in analytical spectroscopy. Bower and Ingle [5] extended this work to include absorption spectrophotometry. Recently, O'Haver and Begley [8] applied signal-to-noise theory to derivative spectrometry. In all cases, the analyte concentration is assumed to be constant over many instrument response times or for the entire integration period. This is defined here as the static case. If the measurement system is properly designed, only shot and flicker (excess low frequency) noise contribute to the overall noise term as it appears in the S/N. Experimental studies of S/N have been reported in the time domain, for example by Pollard et al. [6] who determined the separate noise terms for a flame atomic fluorescence spectrometer, and in the frequency domain, for example by Belchamber and Horlick [9] who determined the noise/power spectrum for an inductively-coupled plasma.

Signal-to-noise theory for dynamic (time-dependent) signals has developed apart from static S/N theory. Much of the earlier work is related to gas chromatography. Kaiser [10] separated instrumental fluctuations into background and signal-carried noises. Smit and Walg [11] developed specific equations to describe the integrated background noise in both the time and frequency domains. Much of Smit's work has been centered around showing a S/N improvement for correlation chromatography [12]. Goedert and Guiochon [13] used computer simulations to show the effect of sampling rate, time constant of the instrument and baseline noise on the chromatographic retention time. Piepmeier [14] used noise expressions published by Hirschfeld [15] to find the optimum integration limits for transient spectroscopic absorption signals having different peak shapes.

Extending the static S/N theory to dynamic systems unifies the S/N studies mentioned above and provides a basis for optimizing new instruments. The approach will be to give a general equation for noise as a function of time but independent of the dynamic signal function. The equation can be applied to any signal function but as an example it will be applied to Gaussian-shaped chromatographic peaks.

Most dynamic signals are quantifiable by peak integration using some electronic device. Electronic integration usually consists of summing a series of sample measurements, X_i, taken at fixed intervals, t_i, over the integration time, t_{Int}. In integrating electronics, such as photon counters, the sampling interval is often chosen short enough to provide pseudo-continuous output. For such non-integrating electronics as a d.c. amplifier, the sampling period is limited to 4 τ_{R} where τ_{R} is the instrument response time. In either case the number of sample points, N, is $N = t_{\mathrm{Int}}/t_i$. The integrated signal, X_{Int}, is $X_{\mathrm{Int}} = \Sigma_{i=1}^{N} X_i$. It should be noted that, for integrating electronics, varying the sampling period would not alter the peak integral;

however, with non-integrating systems, a scaling factor would be necessary. The static response of the detector as a function of analyte concentration must be linear, as pointed out by Carr [16]. To eliminate superfluous constants, signal units are given in count rates as collected in photon or ion counting. The conversion of these units to relative intensities or other system-specific units is straightforward [4].

Noise terms can be combined according to certain precedents [6]. Shot-noise terms are uncorrelated and add to each other quadratically. Flicker-noise terms from the same source are, in the worst case, fully correlated and add linearly. Shot-noise terms and combined flicker-noise terms are independent so they are combined by quadratic addition. Thus, the total noise, σ_i, on any sample interval is

$$\sigma_i = \{[\sigma_{i,a}(s)]^2 + [\sigma_{i,b}(s)]^2 + [\sigma_{i,a}(f) + \sigma_{i,b}(f)]^2\}^{1/2} \quad (1)$$

(All symbols are defined in Table 1.) Substituting the square root of the corresponding signal for shot noise and the signal multiplied by a factor for flicker noise, the best estimate, s_i, of the noise on any interval is

$$s_i = [X_{i,a} + \bar{X}_{i,b} + (\xi_a X_{i,a} + \xi_b \bar{X}_{i,b})^2]^{1/2} \quad (2)$$

By analogy, the total noise on an integrated signal having N data can be estimated by

$$s_{Int} = [X_{Int,a} + N\bar{X}_{i,b} + (\xi_a X_{Int,a} + \xi_b N\bar{X}_{i,b})^2]^{1/2} \quad (3)$$

In practice, the noise depends on instrument design, condition, operating parameters and the analyte signal level. Usually the total noise is dominated by only one term so that Eqn. 3 can be simplified by deleting terms of minor significance. Table 2 shows the simplified noise estimate and the resulting S/N for each case.

In ideal cases, the analyte signal is present with little or no background. When the analyte signal is small, it will be shot-noise limited and the S/N will increase proportionally to the square root of the signal strength; if the calibration is linear, it is also proportional to the square root of the concentration. This implies that in this case it is preferable to integrate a dynamic signal for as long as any signal is present. However, if the analyte has a significant flicker factor, the limiting noise at higher signal levels will be analyte flicker noise. Table 2 indicates that when a signal noise is mainly analyte flicker noise, an increase in signal will not improve the S/N. This implies that fewer points (in the limiting case, only the peak maximum) need be acquired to maintain optimum S/N.

With most instrumentation there is some background signal present along with the analyte signal. The background is usually subtracted numerically or electronically by means of a baseline zero control. However, the noise generated by the background signal is not subtracted and contributes to the total signal uncertainty. When background noise (shot or flicker) is limiting, the optimal S/N will result when the integration time is as short as

TABLE 1

Notations used

Term	Definition
A_p	Area of a chromatographic peak
$A_{p,LOD}$	Area of a peak at the LOD
k	Statistical protection factor
LOD_{static}	Static system limit of detection
LOD_{chrom}	Chromatographic limit of detection
n	Number of data intervals during an injection
N	Number of data intervals during integration
s_i	Best estimate of noise during 1 data interval
s_{Int}	Best estimate of noise during integration
S	Static system sensitivity (calibration line slope)
t_i	Period of 1 data interval
t_{Int}	Integration time
t_r	Retention time
X_i	Total signal for 1 data interval
$X_{i,a}$	Analyte signal for 1 data interval
$\overline{X}_{i,b}$	Average background signal for 1 interval
X_{Int}	Total integrated signal (N intervals)
$X_{Int,a}$	Integrated analyte signal (N intervals)
$X_{max,a}$	Maximum analyte signal for 1 interval
$X_{t,a}$	Analyte signal at time t during a peak
y	Time in standard deviations (σ_p)
σ_i	Total noise (standard deviation) for 1 interval
$\sigma_{i,a}(s)$	Analyte shot noise for 1 interval
$\sigma_{i,a}(f)$	Analyte flicker noise for 1 interval
$\sigma_{i,b}$	Total background noise for 1 interval
$\sigma_{i,b}(s)$	Background shot noise for 1 interval
$\sigma_{i,b}(f)$	Background flicker noise for 1 interval
σ_p	Standard deviation of a Gaussian peak (in intervals)
ξ_a	Analyte flicker noise factor
ξ_b	Background flicker noise factor

TABLE 2

Dynamic signal limiting noise cases

Limiting noise	Noise (s_{Int})	S/N ($X_{Int,a}/s_{Int}$)
Analyte shot	$(X_{Int,a})^{1/2}$	$(X_{Int,a})^{1/2}$
Analyte flicker	$\xi_a X_{Int,a}$	ξ_a^{-1}
Background shot	$(N\,\overline{X}_{i,b})^{1/2}$	$X_{Int,a}/(N\,\overline{X}_{i,b})^{1/2}$
Background flicker	$\xi_b N\,\overline{X}_{i,b}$	$X_{Int,a}/\xi_b N\,\overline{X}_{i,b}$

possible (N is small). If the limiting noise is background shot noise, the S/N can be increased by making any instrumental adjustment that increases the analyte and background signals proportionally.

APPLICATIONS

In the previous section, equations for the dependence of S/N on the kind of noise on a dynamic signal and its background were presented. These are helpful in the design of new instruments, for the applications of methods to specific problems, and for intermethod comparison. To extend and illustrate these ideas, some specific applications are described.

Limit of detection: static vs. dynamic

Figures of merit, in particular the limit of detection (LOD), are important in the evaluation and comparison of instrumental methods. The detection limit is significant because it combines information about the background noise and the sensitivity (S) in a form that describes the smallest signal or concentration that can be significantly determined. The limit of detection is defined differently depending on the instrumental technique. In this section, static and dynamic limits of detection will be defined in terms of the noise equations given earlier. Then, for the ideal Gaussian peak shape, a relation between static and dynamic limits of detection for chromatographic systems will be developed.

The concentration detection limit for a static system using integrating electronics is defined as

$$\mathrm{LOD}_{\mathrm{static}} = k\,\sigma_{\mathrm{Int,\,b}}/(SN) \tag{4}$$

where $\sigma_{\mathrm{Int,\,b}}$ is the standard deviation of at least 16 blank measurements and k is a "protection factor", usually 2 or 3, related to Student's statistic. For the remainder of this paper, $k = 2$ will be used. Expressing the sensitivity in counts per interval (t_i) and concentration, and including N in the denominator facilitate the comparison of concentration detection limits at various integration times. The best estimate of the noise when no analyte signal is present, obtained from Eqn. 3, can be substituted into Eqn. 4 to obtain

$$\mathrm{LOD}_{\mathrm{static}} = 2[N\,\bar{X}_{i,\mathrm{b}} + (\xi_{\mathrm{b}} N\,\bar{X}_{i,\mathrm{b}})^2]^{1/2}\,S^{-1}\,N^{-1}. \tag{5}$$

In the shot-noise-limited case, the first term on the right-hand side dominates and lower detection limits can be realized with longer integration times. When the second term dominates, increasing the integration time will have no effect on the detection limit. Therefore, if there are no limitations on the amount of sample (some systems, e.g., flames, consume it), the integration time is best set for the point when flicker noise on the background begins to dominate.

The same situation does not exist in a dynamic system. In chromatography, for example, the injection time and sample volume limit the amount of available sample and the detector response is a function of the separation process as well as the analyte concentration. A pulse of sample is injected having a concentration that would give a static signal $X_{i,\mathrm{a}}$ for a time period $t_{inj} = n\,t_i$. In the ideal case, the chromatographic process transforms square

injection pulses into peaks having Gaussian distributions as described in their normalized form by

$$\int_{-\infty}^{\infty} [\sigma_p(2\pi)^{1/2}]^{-1} \exp[-(t - t_r)^2/2(\sigma_p t_i)^2]\, dt \tag{6}$$

where t_r is the retention time and σ_p is the standard deviation (1.18 σ_p is the half-width). In this application, Eqn. 6 will be multiplied by the actual peak area, A_p, and, because the sampling interval is a discrete yet small period of time, the analyte signal for any particular interval is described by

$$X_{t,a} = A_p/[\sigma_p(2\pi)^{1/2}] \exp[-(t - t_r)^2/2(\sigma_p t_i)^2] \tag{7}$$

At the centroid, where $t = t_r$, the maximum analyte signal is $X_{max,a} = A_p/(\sigma_p(2\pi)^{1/2})$. This can be rearranged and related to the static signal that would result from the amount of sample injected as $A_p = X_{max,a}\sigma_p(2\pi)^{1/2} = nX_{i,a}$.

The chromatographic limit of detection has been defined as that concentration giving a peak with amplitude twice the peak noise level [17]. From static noise theory, the signal amplitude corresponding to twice the peak noise (or the peak-to-peak noise; $2X_p = X_{p.p}$) is a good measure of 5 $\sigma_{i,b}$ [18]. Thus, at the limit of detection in chromatography $X_{max,a} = 5\ \sigma_{i,b}$. By substituting this equation into the expression for A_p, the area at the detection limit is

$$A_{p,LOD} = 5\ \sigma_{i,b}\sigma_p(2\pi)^{1/2} \tag{8}$$

It is interesting to note that, although a dynamic process may occur over many sampling intervals, it is both necessary and sufficient to exceed the background noise for only one interval for peak detection.

The chromatographic detection limit can be obtained by using the LOD area (Eqn. 8) and the static sensitivity (scaled by the injection pulse time)

$$LOD_{chrom} = 5\ \sigma_{i,b}\sigma_p(2\pi)^{1/2}\ S^{-1}\ n^{-1}. \tag{9}$$

In this form the chromatographic detection limit can be compared to its static counterpart. The static detection limit compared is one having an integration time equal to the injection time ($N = n$) because the same amount of sample is required for each. Starting with Eqn. 9 and Eqn. 4 and substituting the proper noise equations gives

$$LOD_{chrom}/LOD_{static} = 5[\bar{X}_{i,b} + (\xi_b \bar{X}_{i,b})^2]^{1/2}\ \sigma_p(2\pi)^{1/2}\ S^{-1}\ n^{-1}/$$
$$2[n\bar{X}_{i,b} + (\xi_b n\bar{X}_{i,b})^2]^{1/2}\ S^{-1}\ n^{-1} \tag{10}$$

This simplifies in the shot-noise-limiting case to

$$LOD_{chrom}/LOD_{static} = 5\ \sigma_p(2\pi)^{1/2}/2n^{1/2} \tag{11}$$

and in the flicker-noise-limiting case to

$$LOD_{chrom}/LOD_{static} = 5\ \sigma_p(2\pi)^{1/2}/2n \tag{12}$$

In both cases, the determining factor of the ratio is peak width. The chromatographic process widens the event width unless preconcentration is used to counteract dispersion. This has been demonstrated in methods such as h.p.l.c.-a.f.s. [19] and h.p.l.c.-i.c.p. [20] where static limits are very low but dynamic limits are larger. Thus, in the limit, the chromatographic detection limit can be expected to be at least six times worse than the static detection limit for the same quantity of sample.

Choosing integration limits

For the design of automated peak integrators, an understanding of how S/N theory relates to the application is important in optimizing accuracy and reproducibility. The many steps in integrating a peak include deciding when to start and stop integration, finding the peak maximum, and distinguishing unresolved peaks. Although S/N theory can be useful in all these, this discussion will focus on the start and stop points. Piepmeier [14] has described a relationship between the integration limits and the reproducibility of the integral that is dependent on peak shape. The questions to be considered here are how to determine when to start and stop integrating and what effect this choice has on the accuracy of the integral.

Unless there is prior knowledge of the peak position, the criterion for deciding when to start the integration process is a properly determined signal limit of detection. Whether it is based on the derivative of a "floating window" of points or a deviation from the baseline, the choice of when to start depends on the detection of a signal change that is statistically different from one which could be due to background noise alone. The proper choice of a detection limit equation depends, as usual, on the limiting noise. The time interval is determined by the number of points used in the start/stop detection algorithm.

Because peak integration should not start or stop before the signal exceeds the detection limit, some area on the wings of a low-level peak will be lost in the baseline noise. The percent of true area (%TA) found can be determined by dividing the area found by the ideal area as in

$$\%\mathrm{TA} = \left[\int_{-y}^{y} \exp(-K)\mathrm{d}t \Big/ \int_{-\infty}^{\infty} \exp(-K)\mathrm{d}t \right] \times 100 \qquad (13)$$

where $K = (t - t_r)^2/2\sigma_p^2$. The limits of integration, $\pm y$, correspond to the times at which the analyte signal becomes larger or smaller than the start/stop criteria.

Figure 1 is a graph of Eqn. 13 prepared with data from a standard table [21] using start/stop points in terms of standard deviations from the peak maximum. Table 3 lists a selection of these values along with the maximum signal of the peak in terms of the baseline noise obtained by substituting $2\ \sigma_{i,b}$ (the start/stop threshold) and y (the start/stop time) in units of σ_p into Eqn. 7 to obtain

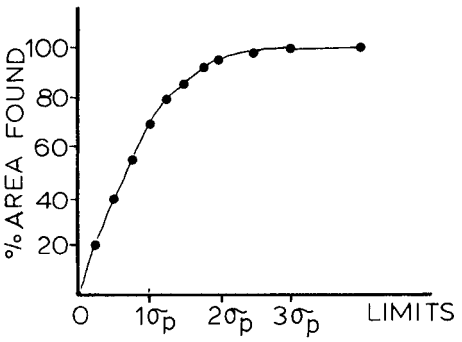

Fig. 1. Determinate errors in the peak integral.

TABLE 3

Determinate errors in integration

Start-stop point	Peak max	Actual area integrated (%)
Y (units of σ_p)	$X_{max,a}$	
±1.0	6 $\sigma_{i,b}$	68.3
±2.0	14 $\sigma_{i,b}$	95.4
±2.6	58 $\sigma_{i,b}$	99.0
±3.0	180 $\sigma_{i,b}$	99.7

$$2\,\sigma_{i,b} = [A_p/\sigma_p(2\pi)^{1/2}]\,\exp[-(y\sigma_p)^2/2\,\sigma_p^2] \tag{14}$$

This was simplified, solved for A_p, substituted into the expression for $X_{max,a}$, and simplified again, resulting in

$$X_{max,a} = 2\,\sigma_{i,b}/\exp[-y^2/2] \tag{15}$$

The areas in Table 3 should be easily recognized as the percentage of area between standard deviations in the normal distribution. Of more interest is the magnitude of the maximum signal relative to the background noise. Only when the maximum of the peak exceeds a value 58 times the baseline noise will the area obtained be within 1% of the true area. Depending on the kind of the baseline noise, this determinate error may or may not exceed the indeterminate error or reproducibility of the peak area. If it does, it will be manifested as a negative deviation in the lower portion of the calibration curve. Because chromatographic peaks are seldom ideal, this deviation can be pronounced, particularly in the case of tailing peaks. It can also be present when integrating small peaks on the wings of larger ones.

CONCLUSIONS

Equations for estimating the noise and S/N for a dynamic system using static noise terms have been presented. These equations verify what is known

intuitively. If the system is shot-noise limited, then the larger the analyte signal the better the S/N. Once a signal becomes analyte flicker-noise limited, there is no benefit to increasing the signal. If there is no long-term drift in the baseline, the reproducibilities of analyte flicker-noise-limited peak integrals and maximum values should be comparable. When the system is background-flicker-noise limited, making the dynamic event narrower will improve the S/N.

The applications related to chromatography demonstrate how figures of merit and other error-related quantities can be derived using the basic equations. The comparison of the chromatographic and the static limits of detection for the same amount of sample showed why detection limits for chromatographic methods are poorer than those achieved for static systems. This result demonstrates the need for high efficiency in the separation portion of any method. Integration limits for automated systems depend on the static detection limit of the detector. When the signals are small, determinate errors in integrals may occur because area in the wings of the event is lost in the noise.

The tenets of this paper apply to many instrumental systems. They have been helpful in studying the optimal data collection method for a gas chromatograph-mass spectrometer and optimizing a high-performance liquid chromatograph/atomic fluorescence spectrometer combination [19]. When the above conclusions are linked with the concept of sample/blank paired measurements, the best operating conditions can be predicted for flow systems with conventional detectors or with flame and plasma spectrometers.

REFERENCES

1 C. Th. Alkemade, W. Snelleman, G. D. Boutilier, B. D. Pollard, J. D. Winefordner, T. L. Chester and N. Omenetto, Spectrochim. Acta, Part B, 33 (1978) 383.
2 G. D. Boutilier, B. D. Pollard, J. D. Winefordner, T. L. Chester and N. Omenetto, Spectrochim. Acta, Part B, 33 (1978) 401.
3 C. Th. Alkemade, W. Snelleman, G. D. Boutilier and J. D. Winefordner, Spectrochim. Acta, Part B, 35 (1980) 261.
4 J. D. Winefordner, R. Avni, T. L. Chester, J. J. Fitzgerald, L. P. Hart, D. J. Johnson and F. W. Plankey, Spectrochim. Acta, Part B, 31 (1976) 1.
5 N. W. Bower and J. D. Ingle, Anal. Chem., 48 (1976) 686.
6 B. D. Pollard, A. H. Ullman and J. D. Winefordner, Anal. Chem., 53 (1981) 330.
7 A. Van der Ziel, Noise in Measurements, J. Wiley, New York, 1976.
8 T. C. O'Haver and T. Begley, Anal. Chem., 53 (1981) 1876.
9 R. M. Belchamber and G. Horlick, Spectrochim. Acta, Part B, 37 (1982) 17.
10 R. Kaiser, Chromatographia, 4 (1971) 123, 215.
11 H. C. Smit and H. L. Walg, Chromatographia, 8 (1975) 311.
12 T. T. Lub and H. C. Smit, Anal. Chim. Acta, 112 (1979) 341.
13 M. Goedert and G. Guiochon, Chromatographia, 6 (1973) 39, 76, 116.
14 E. H. Piepmeier, Anal. Chem., 48 (1976) 1296.
15 T. Hirschfeld, Appl. Spectrosc., 30 (1976) 67.
16 P. W. Carr, Anal. Chem., 52 (1980) 1746.

17 H. M. McNair and E. J. Bonelli, Basic Gas Chromatography, Varian, Palo Alto, CA, 1968.
18 J. D. Winefordner (Ed.), Trace Analysis, Wiley Chem Analysis Series, Vol. 46, Wiley Interscience, New York, 1976.
19 W. J. Taraszewski, Ph.D. Dissertation, Marquette University, 1982.
20 D. M. Fraley, D. Yates and S. E. Manahan, Anal. Chem., 51 (1979) 2225.
21 C. D. Hodgeman (Ed.), Handbook of Chemistry and Physics, 44th edn., Chemical Rubber Co., Cleveland, OH, 1963.

Analytica Chimica Acta, 157 (1984) 83—89
Elsevier Science Publishers B.V., Amsterdam — Printed in The Netherlands

EXTRACTION OF OSMIUM THIOCYANATE AND ITS SEPARATION FROM RUTHENIUM BY POLYURETHANE FOAM

SARGON J. AL-BAZI and ARTHUR CHOW*

Department of Chemistry, University of Manitoba, Winnipeg, Manitoba R3T 2N2 (Canada)

(Received 23rd May 1983)

SUMMARY

A detailed investigation of the conditions for formation and extraction of the thiocyanate complex of osmium by polyether-type polyurethane foam is reported. The complex which formed in solution was extracted through the "cation-chelation" mechanism and distribution coefficients of more than 10^4 were obtained. By using conditions which inhibit the formation of the osmium-thiocyanate complex, it was possible to leave 95% of osmium in the aqueous phase while extracting more than 95% of ruthenium into polyurethane foam.

One of the characteristic features of osmium is the formation of a non-polar tetroxide complex which has been extracted with chloroform as well as with carbon tetrachloride [1]. Many investigations have been reported for spectrophotometric quantitation of the thiocyanate complex of the metal starting with osmium tetroxide [2—6]. The use of several organophosphorus compounds [7—9], amines [10] and alcohols [11] for extraction of the chlorocomplex of osmium(IV) from hydrochloric acid solutions have been studied. The extractable species was shown to be $H_2OsCl_6 \cdot 4TBP$ in tri-n-butylphosphate (TBP) [8] and to be $2[TOA \cdot H^+] \cdot [OsCl_6^{2-}]$ in trioctylamine (TOA) [10].

Although the separation of osmium and ruthenium has been commonly achieved by the selective oxidation of osmium and distillation of the osmium tetroxide [12, 13], a few solvent extraction methods have also been reported [14, 15]. The most efficient extraction methods have been those which involve the formation of the extractable species of ruthenium with the complexing agent, while keeping osmium in the unextractable chloride form.

The purpose of the present work was to establish suitable conditions for the extraction of osmium(IV) from thiocyanate solutions by polyether-type polyurethane foam and to understand the mechanism of the distribution of the osmium-thiocyanate complex between foam and aqueous phase. A method for the separation of Os(IV) and Ru(III) from thiocyanate solution was also developed.

0003-2670/84/$03.00

EXPERIMENTAL

Apparatus and reagents

A Varian 634S u.v.-visible spectrophotometer was used for absorbance measurements and a Fisher Accumet model 520 meter was used for pH measurements.

Ammonium hexachloroosmate(IV) [$(NH_4)_2OsCl_6$] was supplied by Spex Industries (Metuchen, NJ) and ruthenium trichloride [$RuCl_3 \cdot 3H_2O$] by Johnson-Matthey Chemicals, Toronto. All other chemicals used were of analytical grade. Polyether-type polyurethane foam (1338 M; G. N. Jackson, Winnipeg, Manitoba) was washed by the procedure previously reported [16].

A stock solution of osmium containing 1.3×10^{-3} M osmium(IV) was freshly prepared for each experiment (to prevent the precipitation [17] of $OsO_2 \cdot 2H_2O$) by dissolving its salt in 0.1 M hydrochloric acid solution. A 5.0 M stock solution of potassium thiocyanate was prepared in doubly distilled and deionized water.

Extraction procedure

Aliquots (4.0 ml) of the stock solution of osmium(IV) chloride with potassium thiocyanate were placed in 100-ml volumetric flasks and the volume was diluted to approximately 60 ml. The solution was initially heated at 90°C, cooled to room temperature in ice water, and finally diluted to 100 ml after appropriate amounts of hydrochloric acid and ammonium chloride had been added. The procedure for the extraction of osmium from 95 ml of the solution by 99 ± 1 mg of foam and the calculations of percentage extracted (%E) as well as of distribution coefficient (D) were done as described previously [16]. Osmium as the thiocyanate complex was quantified spectrophotometrically. The technique was found to be applicable up to 8×10^{-5} M metal.

RESULTS AND DISCUSSION

On adding excess thiocyanate to an aqueous solution of hexachloroosmate(IV), a yellow-orange coloured osmium-thiocyanate complex with a maximum absorbance at 450 nm was formed. The reaction was exceedingly slow at room temperature and the complex was found to be stable for more than 24 h. A similar complex has been reported starting with osmium tetroxide [3—5] and it has been related to $Os(SCN)_6^{3-}$ [18, 19].

To establish the conditions for maximum formation of the osmium-thiocyanate complex in aqueous solution, approximately 30 ml of solution containing 5.0 ml of 5×10^{-4} M osmium and various amounts of potassium thiocyanate, hydrochloric acid, and lithium chloride was heated at 90°C, immediately cooled in ice water to room temperature, and finally diluted to 50 ml.

The effect of heating solutions at pH 2.8 ± 0.1 containing 4.8 ml of 5 M

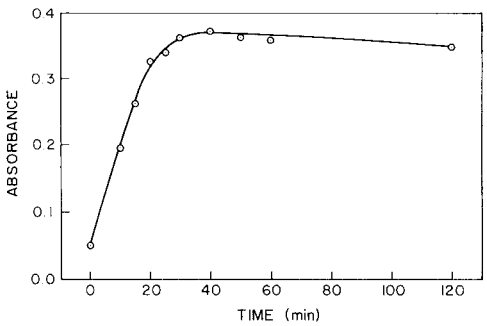

Fig. 1. Effect of heating time on the formation of osmium-thiocyanate complex.

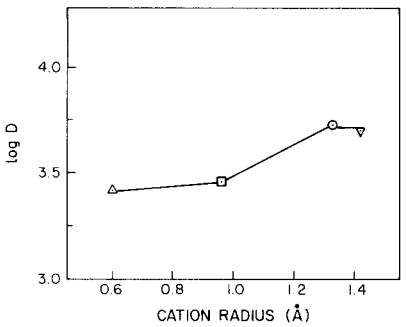

Fig. 2. Distribution of osmium-thiocyanate complex between foam and aqueous solution as a function of size of various monovalent cations. Conditions: 99 ± 1 mg foam, 95 ml of solution at pH 2.9 ± 0.1, 5×10^{-5} M in Os(IV), 0.3 M in KSCN, 0.5 M salt added after heating for 2 h. Cation: (△) Li^+; (□) Na^+; (○) K^+; (▽) NH_4^+.

thiocyanate and 15 ml of 10 M lithium chloride (Fig. 1) indicates that the absorbance at 450 nm increased to a maximum after 30 min and decreased slowly beyond this time. A 30-min heating period was used for further studies.

In the presence of as little as 1 ml of 6 M hydrochloric acid, it was found that a large amount of 5-amino-1,2,4-dithiazole-3-thione and hydrogen sulfide was formed after 10 min of heating and therefore, only mildly acidic conditions were used. Table 1 shows that the pH range 2.5—5.5 is optimum and this was used for further studies. The use of low acid concentrations (about 2×10^{-3} M) prior to heating has also been recommended by Shlenskaya and Khvostova [4] for the formation of osmium-thiocyanate complex starting from osmium tetroxide. Table 1 also shows that a minimum of 0.24 M thiocyanate (mole ratio of SCN/Os of 4570) is required for complete formation of the osmium-thiocyanate complex.

The effect of lithium chloride concentration in solutions at pH 2.7 ± 0.1

TABLE 1

Effect of pH and thiocyanate on the absorbance (A) of the osmium-thiocyanate complex

Effect of pH[a]									
pH	2.0	2.5	3.4	3.9	4.3	5.5	6.0	6.5	7.0
A	0.355	0.367	0.366	0.365	0.366	0.367	0.360	0.333	0.268
Effect of thiocyanate concentration[b]									
[SCN^-] (M)	0.10	0.15	0.19	0.24	0.29	0.34	0.39	0.48	0.58
A	0.308	0.343	0.363	0.366	0.371	0.374	0.372	0.366	0.364

[a]With a constant 0.3 M concentration of thiocyanate. [b]With a constant 3 M concentration of lithium chloride at pH 2.7.

containing 3 ml of 5 M thiocyanate showed that the absorbance at 450 nm was independent of the salt concentration up to 1.5 M and decreased by 4% for 2 M and by 14% for 3 M. The absorption spectra showed an increase in the absorbance in the region of 410 to 290 nm above 1.5 M lithium chloride, which corresponds to $OsCl_6^{2-}$ and thus chloride causes the interference in the formation of the osmium-thiocyanate complex.

The extraction of osmium(IV)

Preliminary investigations on the extraction of osmium-thiocyanate complex from solutions containing ammonium chloride or hydrochloric acid (added after heating the solution) by polyether-type polyurethane foam showed that the complex is extractable and turned reddish-brown on the foam.

When the extraction was done in the presence of both hydrogen peroxide and hydrochloric acid, the foam turned blue. Similar results were reported for the extraction of osmium(VIII) by peroxide-containing diethyl ether [14] and by other organic solvents [2, 3, 6] in the absence of hydrogen peroxide. The blue-coloured species was not stable, turning green and finally reddish-brown with time, indicating that the latter complex is the most stable form on the foam. The instability of the blue-coloured species was also reported by Qureshi and Mathur [3] through their extraction studies by isoamyl alcohol. Furthermore, a green-coloured organic phase was also observed by Wiersma and Lott [2] on investigating the extraction of osmium from thiocyanate solutions by diphenyl ether.

Under the optimum conditions for the formation of the yellow-orange osmium-thiocyanate complex (pH range 2.5—5.5, a minimum of 0.24 M potassium thiocyanate, and 30 min heating), several variations were studied to establish suitable conditions for its extraction by polyether-type polyurethane foam; the results are recorded in Table 2. The effect of hydrochloric acid added after heating the solution increased the extraction slightly up to 1 M and decreased it at higher concentrations. The absorbance at 450 nm was independent of acid up to 1 M, beyond which it decreased only by 6% for 2 M. The absorption spectra showed bands at 284 and 324 nm which indicates that thiocyanic acid and 5-amino-1,2,4-dithiazole-3-thione are formed in solutions containing high acid concentrations [20]; this would interfere with the extraction. In the presence of ammonium chloride, increasing hydrochloric acid concentration up to 1 M gave a slow decrease in the extraction. At low acid concentrations, the increased efficiency of the foam for osmium extraction in the presence of ammonium ions shows that this ion contributes to the distribution of the osmium-thiocyanate complex between the foam and the aqueous phase, most likely through the "cation-chelation" mechanism [21, 22]. The effect of ammonium ion (Table 2) was to increase the extraction up to 2 M ammonium chloride, where the extraction was also found to be independent of pH in the range 2.5—5.0. The osmium extraction decreased slightly with increasing

TABLE 2

Effect of hydrochloric acid, potassium thiocyanate, and ammonium chloride on the extraction of osmium

Conc. (M)[a]		Extraction (%)	pH	Conc. (M)		Extraction (%)
HCl	NH_4Cl			KSCN	NH_4Cl	
0.0	0.0	42	2.6	0.3	0.0	42
0.1	0.0	65	2.6	0.3	0.5	65
0.5	0.0	67	2.6	0.3	1.0	72
1.0	0.0	68	2.6	0.3	1.5	75
2.0	0.0	59	2.6	0.3	2.0	80
0.0	1.0	72	3.0	0.3	2.0	82
0.1	1.0	71	3.0	0.5	2.0	82
0.3	1.0	68	3.0	0.8	2.0	80
0.5	1.0	66	3.0	1.0	2.0	78
0.8	1.0	63	3.0	1.5	2.0	73
1.0	1.0	61	3.0	2.0	2.0	68

[a]0.3 M KSCN used in all cases.

thiocyanate concentration. Because the formation of thiocyanic acid and 5-amino-1,2,4-dithiazole-3-thione is not possible under these conditions, the decrease in the extraction of osmium-thiocyanate is most likely due to the interference of thiocyanate ion as has been shown for palladium [23].

Under the optimum conditions of pH 3.0 ± 0.1, 0.3 M thiocyanate and 2 M ammonium chloride with 30 min of heating, only 82% of the osmium was extracted by 99 ± 1 mg of foam from 95 ml of 5×10^{-5} M osmium(IV) solution. For solutions heated for longer times, the extraction increased gradually, reaching 90% after 1.25 h of heating and 97% ($\log D = 4.45$) after 3 h of heating; the absorbance at 450 nm decreased by 7% after 3 h. Furthermore, after extraction, the absorption spectrum of solutions heated for 30 min showed a broad absorbance in the region 530—320 nm with a maximum absorption at 450 nm, whereas solutions heated for 3 h did not. These results can be explained by assuming a kinetically slow equilibrium between two thiocyanate complexes of osmium which have different extraction efficiencies but very similar absorptivity in the same wavelength region. The existence of two thiocyanate complexes of osmium in solution has also been reported by Ayres [24]. By heating the solution, the equilibrium is shifted in the direction of the more extractable species.

In order to establish the mechanism of extraction of osmium-thiocyanate complex, the effect of chloride salts of the Li^+, Na^+, K^+ or NH_4^+ was studied. The extraction (Fig. 2) increases from 73% ($\log D = 3.41$) for lithium to 75% ($\log D = 3.46$) for sodium and to 85% ($\log D = 3.73$) for potassium and 84% ($\log D = 3.71$) for ammonium ions. The absorbance values at 450 nm were almost the same for all solutions, thus the influence of different cations is on the distribution of the complex between the foam and the aqueous solution,

rather than its formation. These results are similar to those obtained for the extraction of $Pd(SCN)_4^{2-}$ [16, 23], platinum(II) thiocyanate complex [25], and $Ru(SCN)_6^{3-}$ [26], and are in agreement with the "cation-chelation" mechanism reported previously [21, 22].

Separation of osmium and ruthenium

For the separation of osmium and ruthenium, it was decided to choose conditions carefully so that osmium would remain in solution. Because 5 min of heating at 90°C was sufficient for the maximum formation and extraction of ruthenium-thiocyanate complex [26], and because 3 h was required for osmium-thiocyanate complex, the shorter period should facilitate the separation. In addition, the presence of 3 M lithium chloride increased formation of the thiocyanate complex of ruthenium and decreased that of osmium. Therefore, by heating the solution of Os(IV) and Ru(III) for 5 min then rapidly cooling the solution to inhibit $Os(SCN)_6^{3-}$ formation, an effective separation of these two ions was possible. An immediate extraction with polyurethane foam for 1 h, adequate for ruthenium, also minimized the formation and extraction of the $Os(SCN)_6^{3-}$ complex.

Under these conditions, the effect of different concentrations of osmium on the extraction of ruthenium was investigated using a series of approximately 60-ml solutions at pH 2.4 ± 0.1 containing 2.0 ml of 2.5×10^{-3} M ruthenium, 12 ml of 5 M thiocyanate, 16.05 g of ammonium chloride and different amounts of 1.3×10^{-3} M osmium with heating at 90°C for 5 min. These solutions were then cooled in ice water to room temperature and diluted to 100 ml. Aliquots (95 ml) of these solutions were equilibrated with foam cubes each weighing 0.296 ± 0.005 g for 1 h. Under these conditions, less than 5% osmium was found to be extracted by polyurethane foam. Furthermore, the results given in Table 3 indicate that in the presence of three-fold excess of osmium, there was no effect on the extraction of ruthenium.

Conclusions

Polyurethane foam is highly efficient for the extraction of osmium as indicated by the distribution coefficient values as high as 10^4 obtained for foam relative to the 13—500 values reported for many organic solvents [1, 8, 10]. Furthermore, the affinity of polyurethane foam for osmium from slightly acidic thiocyanate solutions decreases the catalytic ability of the metal to decompose and trimerize thiocyanate (formation of 5-amino-

TABLE 3

Effect of osmium concentration on the extraction of 5×10^{-5} M ruthenium by polyurethane foam

Os(IV) present (M)	0.0	5×10^{-5}	1×10^{-4}	1.5×10^{-4}
Ru extracted (%)	97	97	98	98

1,2,4-dithiazole-3-thione) and reduces the interference caused by thiocyanic acid and the trimerization product.

The separation of osmium and ruthenium by polyurethane foam is highly efficient and has considerable advantages in comparison to the methods of selective distillation of the tetroxide which are commonly used. For example, chloroosmate $(OsCl_6)^{2-}$ is not easily converted to the tetroxide in the presence of excess of chloride [1], and in the selective distillation with nitric acid [12], the acid must be removed from the ruthenium fraction before RuO_4 can be volatilized quantitatively. The importance of polyurethane foam in the separation of ruthenium and osmium also arises from the fact that no successful application of either cation- or anion-exchange methods has been reported.

This work was supported by the Natural Science and Engineering Research Council of Canada.

REFERENCES

1 R. D. Sauerbrunn and E. B. Sandell, Anal. Chim. Acta, 9 (1953) 86.
2 J. H. Wiersma and P. F. Lott, Anal. Chem., 39 (1967) 674.
3 M. Qureshi and K. N. Mathur, Z. Anal. Chem., 242 (1968) 159.
4 V. I. Shlenskaya and V. P. Khvostova, J. Anal. Chem. USSR (Engl. Transl.), 23 (1968) 193.
5 V. Muralikrishna, K. V. Bapanaiah, N. S. N. Prasad and P. Kannarao, Indian J. Chem., Part A, 14 (1976) 291.
6 B. K. Pal, R. P. Chowdhury and B. K. Mitra, Talanta, 28 (1981) 62.
7 H. Meier, D. Bosche, E. Zimmerhackl, W. Albrecht, W. Hecker, P. Menge, A. Ruckdeschel, E. Unger and G. Zeitler, Mikrochim. Acta (Wien), (1969) 1083.
8 H. Meier, E. Zimmerhackl, W. Albrecht, D. Bosche, W. Hecker, P. Menge, A. Ruckdeschel, E. Unger and G. Zeitler, Mikrochim. Acta (Wien), (1969) 557.
9 S. Kalyanaraman and S. M. Khopkar, Anal. Chim. Acta, 78 (1975) 231.
10 H. Meier, E. Zimmerhackl, W. Albrecht, D. Bosche, W. Hecker, P. Menge, A. Ruckdeschel, E. Unger and G. Zeitler, Mikrochim. Acta (Wien), (1969) 826.
11 A. G. Saed, B. Z. Iofa and A. N. Nesmeyanov, Vestn. Mosk. Univ. Khim., 33 (1978) 222.
12 E. L. Steele and J. H. Yoe, Anal. Chem., 29 (1957) 1622.
13 A. D. Westland and F. E. Beamish, Mikrochim. Acta, (1957) 625.
14 Z. Marczenko and M. Balcerzak, Anal. Chim. Acta, 109 (1979) 123
15 W. Geilmann and R. Neeb, Fresenius Z. Anal. Chem., 156 (1957) 420.
16 S. J. Al-Bazi and A. Chow, Talanta, 29 (1982) 507.
17 I. P. Alimarin, V. P. Khvostova and G. I. Kadyrova, J. Anal. Chem. USSR (Engl. Transl.), 30 (1975) 1689.
18 H. H. Schmidtke and D. Garthoff, Helv. Chim. Acta, 50 (1967) 1631.
19 K. S. De Haas, J. Inorg. Nucl. Chem., 35 (1973) 3231.
20 W. H. Hall and I. R. Wilson, Aust. J. Chem., 22 (1969) 513.
21 R. F. Hamon, A. S. Khan and A. Chow, Talanta, 29 (1982) 313.
22 A. S. Khan, Ph.D. Thesis, University of Manitoba, 1982.
23 S. J. Al-Bazi and A. Chow, Talanta, 30 (1983) 487.
24 G. H. Ayres, Anal. Chem., 25 (1953) 1622.
25 S. J. Al-Bazi and A. Chow, Anal. Chem., 55 (1983) 1094.
26 S. J. Al-Bazi, Ph.D. Thesis, University of Manitoba, 1983.

Analytica Chimica Acta, 157 (1984) 91—97
Elsevier Science Publishers B.V., Amsterdam — Printed in The Netherlands

THE DETERMINATION OF TRACES OF FLUOROACETIC ACID BY EXTRACTIVE ALKYLATION, PENTAFLUOROBENZYLATION AND CAPILLARY GAS CHROMATOGRAPHY-MASS SPECTROMETRY

T. VARTIAINEN and P. KAURANEN
Department of Chemistry, University of Kuopio, Kuopio (Finland)
(Received 1st April 1983)

SUMMARY

A method is described for the extraction and determination of nanogram amounts of the highly toxic fluoroacetic acid in plant samples. The acid is extracted by ammonia solution and purified by repeated ether extractions. The fluoroacetate is then transferred to dichloromethane by using tetrahexylammonium as counter-ion, and finally derivatized by pentafluorobenzyl bromide. The determination is completed by capillary gas chromatography and single-ion monitoring mass spectrometry. Small amounts of fluoroacetate were found in many plant samples, including tea. The limit of detection was about 0.005 $\mu g\ g^{-1}$, the reproducibility about ±9% and the recovery of added fluoroacetate 89 ± 6%.

Fluoroacetic acid is a highly toxic compound that is synthesized in appreciable amounts by some tropical plants [1—3]. Small amounts of fluoroacetic acid are quite commonly found in a number of plants, especially in areas showing an elevated fluoride level [4]. However, because the fluoroacetate contents were extremely low, earlier analytical methods proved inadequate, and a more sensitive procedure had to be developed.

Several chromatographic methods have been published for the determination of small amounts of fluoroacetate in plants [5—7] or animal tissues [8—13]. The latter methods are mostly designed for the determination of "Compound 1080", which is sodium fluoroacetate and is used as a rodenticide. Because fluoroacetic acid is a rather strong acid (pK_a = 2.66), a suitable derivative must be prepared for gas chromatography. Highest sensitivity is apparently achieved by using for derivatization a reagent with high electron affinity, such as pentafluorobenzyl bromide (PFB-Br), which makes electron-capture detection of the derivative possible. This was done by Okuno et al. [13], who reported a detection limit of 0.1 $\mu g\ g^{-1}$ fluoroacetate in tissue, with a yield of 58 ± 8%. However, the chromatograms showed a large number of potentially interfering peaks around the PFB fluoroacetate peak, and the procedure required three different columns. Because the excess of PFB-Br reagent cannot be removed without losses, the PFB fluoroacetate derivative is eluted on the tailing part of the large reagent peak.

0003-2670/84/$03.00

For high-performance liquid chromatography (h.p.l.c.), fluoroacetic acid can be derivatized, e.g., with *p*-nitrobenzyl-N,N'-diisopropylisourea for u.v. detection [14] or with 4-bromomethyl-7-methoxycoumarin for fluorescence detection [15]. For the former method, the limit of detection is given as 0.1 mg l^{-1}, but no yield data were given below 1 mg l^{-1}.

Mass spectrometry offers very sensitive detection methods. Selected-ion monitoring mass spectrometry (m.s.) was used to detect methyl fluoroacetate by Stevens et al. [16]. However, they used the fragment FCH_2- (*m/z* = 33), which is very sensitive to interferences in biological samples. The lowest detectable fluoroacetate content was given as 0.1 μg g^{-1} and the yield as 50—55%.

None of the above-mentioned methods gave the sensitivity and reproducibility necessary for the present samples. Preliminary experiments indicated that only single-ion monitoring m.s. based on a large ion of a derivative would give the necessary sensitivity and selectivity. Extractive alkylation with PFB-Br to extract and esterize the acid after extensive clean-up was therefore adopted, followed by observation of the molecular ion of the pentafluorobenzyl ester of fluoroacetic acid (*m/z* = 258). The limit of detection of the method was 0.005 μg g^{-1} fluoroacetic acid in plant samples, and concentrations above 0.01 μg g^{-1} could be determined with good recovery and reproducibility.

EXPERIMENTAL

Reagents

Diethyl ether and dichloromethane (Merck p.a.) were redistilled in glass apparatus. A standard solution of fluoroacetic acid (Merck-Schuchardt) was prepared from 1 ml of the acid in 25 ml of dichloromethane; 1 g of 2,3,4,5,6-pentafluorobenzyl bromide (PFB-Br; Ega Chemie) was dissolved in 25 ml of dichloromethane; 1 ml of 2-chlorobutyric acid (Fluka) was dissolved in 10 ml of dichloromethane. Tetrahexylammonium hydroxide (THAH) solution was prepared as follows: 9.64 g of tetrahexylammonium iodide (Eastman) and 2.55 g of silver oxide were added to 200 ml of distilled water and the mixture was allowed to react for 2 h in an ultrasonic waterbath at room temperature. The solution was filtered and the filtrate was shaken twice with equal volumes of dichloromethane.

Gas chromatography/mass spectrometry (g.c.-m.s.)

A Carlo Erba Fractovap 2300 gas chromatograph was operated in connection with a JEOL JMS-D-300 mass spectrometer and a JMA-2000 mass data system, using helium carrier gas. The gas chromatographic columns and conditions were: a 40 m × 0.3 mm i.d. glass capillary column treated with OV-225, or a 30 m × 0.32 mm i.d. silica capillary column treated with Durawax 3 and 4, or a 30 m × 0.25 mm i.d. silica capillary column treated with SE-54. The injector temperature was 175°C and the temperature

program for the column oven was 1 min at 50°C, then 39°C min^{-1} to 100°C and then 8°C min^{-1} to 220°C. The sample was injected by the splitless technique. For the mass spectrometer, the ionization current was 300 μA and the ionization potential 23 eV; calibration was done with perfluorokerosene.

Procedures

Sample extraction and clean-up. Fluoroacetate was extracted from the air-dried, homogenized samples (about 0.5 g) with 100 ml of water, containing 50 μl of concentrated ammonia liquor, on a hot water bath. The mixture was centrifuged, the residue was washed twice with hot water and the combined extracts were acidified with 1 M sulphuric acid to pH 1.5. Organic acids were extracted into diethyl ether for 72 h (Fig. 1), using a continuous liquid-extraction apparatus; 50 ml of 1 M sodium hydrogencarbonate was added to the ether receiving flask of the extraction apparatus before extraction, to bind the fluoroacetic acid.

The ether extract was shaken three times with 50 ml of 1 M sodium hydrogencarbonate solution. All the hydrogencarbonate solutions were combined and acidified with 4 M sulphuric acid to pH 4.0. The solution was shaken with 150 ml of diethyl ether which was discarded. The water phase was then acidified to pH 1.9 by adding more sulphuric acid, and the fluoroacetic acid was again extracted for 72 h into ether using the extraction apparatus; 2 ml of THAH solution was added to the ether-receiving flask before this extraction.

Derivatization and g.c.-m.s. A further 2 ml of THAH solution was added to the ether flask. The ether was distilled off at reduced pressure, and the ion-pair, $(C_6H_{13})_4$ N-$OOCCH_2F$, was extracted into 3 ml of dichloromethane, which was then transferred to a test tube. The extraction was repeated 3 times, and the combined solutions were evaporated to dryness with a stream of nitrogen. A known amount (400 μl) of PFB-Br solution was added into the test tube, and the sample, containing the pentafluorobenzyl fluoroacetate, was then ready for injection. The final measurement was done by single-ion monitoring g.c.-m.s., the ions followed being m/z = 258 for PFB fluoroacetate and m/z = 302 for the internal standard, pentafluorobenzyl 2-chlorobutyrate.

In many cases, plenty of plant material was available, and a 2-g sample was then extracted, several aliquots of the dichloromethane solution being taken through the derivatization step.

RESULTS AND DISCUSSION

Problems are caused in determination of fluoroacetate by the volatility and strength of fluoroacetic acid. The extraction and esterification of small amounts of the acid easily lead to considerable losses [11, 15]. Extractive alkylation solves these problems, because the acid will be present as the non-

volatile salt during the concentrating step, and the extraction as the ion-pair is rapid and quantitative if a suitable counter-ion is used. Esterification can be done in a few minutes at room temperature. As counter-ions, the series tetrapropyl- to tetraheptyl-ammonium ions were tried. The best results were obtained with tetrahexylammonium (THA) ion. Tetrapentylammonium gave similar yields, but at a slower rate and at higher temperature, whereas tetraheptylammonium gave very low yields. Similar results were obtained by Dehmlow [17] and L'Emeillat et al. [18] in the determination of acetic acid ($pK_a = 4.74$).

Esterification with PFB-Br must be done in a small amount of dichloromethane, with no water present. This was achieved by evaporating the dichloromethane solution from the extraction step (about 12 ml) to dryness and by dissolving the residue in 200—400 μl of dichloromethane containing the PFB-Br reagent. A large amount of side-products is formed by PFB-Br [13]. The number of side-products can be decreased by lowering the reagent concentration, but the reaction time is then increased. However, practically no interfering peaks were seen, when the sample was first sufficiently cleaned by liquid extraction and then a large enough fragment was observed by m.s.

Fragmentation of PFB fluoroacetate at 70 eV is extensive, and the main fragment is the non-specific $C_6F_5CH_2^+$ (m/z = 181); the intensity of the molecular ion m/z = 258 is too low to be measured. An energy of 23 eV gives maximum intensity of the molecular ion, but it also puts strong demands on the apparatus and cleanness of the samples. A dirty sample contaminates the ionization chamber rapidly, sensitivity and linearity are lost, and interfering peaks may appear. These can only be identified by using columns of different polarity, because mass spectra could not be obtained on the picogram level. The risk of contaminating the ionization chamber was one reason for using the rather lengthy liquid extraction. Column clean-up could not be used, because the small amounts of fluoroacetate were lost. The extraction procedure adopted gave a reasonable purity and also a high and reproducible yield. The extraction time is long (Fig. 1) and depends on pH. If the pH is very low, more sulphuric acid is extracted and later consumes more of the THA reagent, increasing the volume of the aqueous phase. This explains the different pH values of 1.5 and 1.9 for the ether extractions; they are compromises between the extraction time and the problems caused by co-extracted sulphuric acid.

Recoveries of added fluoroacetic acid were 89.5 ± 6.1%, as can be seen from Table 1. Figure 2 shows two calibration graphs, run on glass and silica capillary columns. The latter shows higher sensitivity, because the open end of the flexible silica capillary can be drawn right into the ionization chamber. Figure 3 shows mass spectra of m/z = 258 for three plant samples with widely different fluroacetate concentrations.

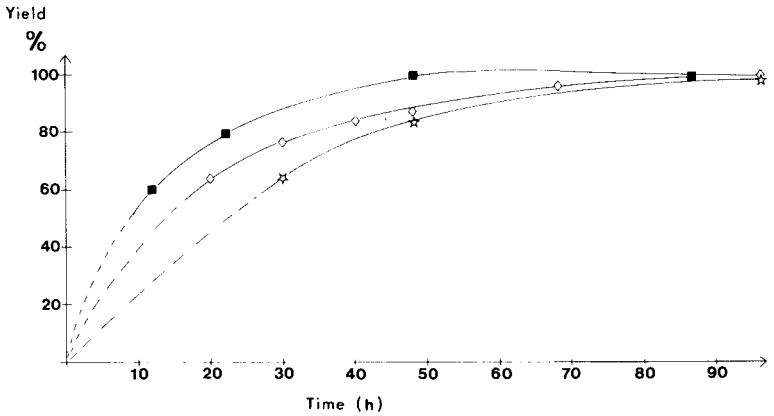

Fig. 1. Extraction of fluoroacetic acid into diethyl ether as a function of time and pH. The volume of aqueous phase in the extraction apparatus was 500 ml and the volume of the ether phase 200 ml. pH values: (■) 0.3; (△) 1.0; (☆) 2.3.

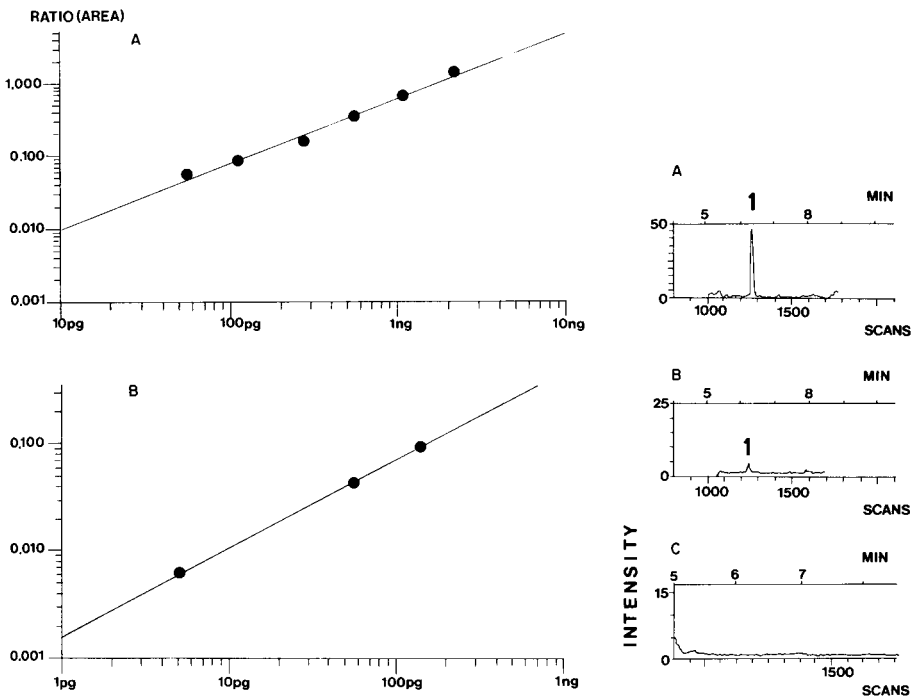

Fig. 2. Calibration graphs for fluoroacetate determinations. (A) OV-225 glass capillary column, connected to the ionization chamber by a thin glass tube; (B) SE-54 fused silica capillary column, connected directly into the ionization chamber.

Fig. 3. Recordings of m/z = 258 for three plant samples with different fluoroacetate concentrations: (a) 0.11 $\mu g\ g^{-1}$ (140 pg of fluoroacetate injected); (b) 0.010 $\mu g\ g^{-1}$ (12.6 pg of fluoroacetate injected); (c) <0.005 $\mu g\ g^{-1}$. The fluoroacetate peak at 6.3 min is marked by number 1.

TABLE 1

Recovery of fluoroacetate added to a 0.5-g tea sample containing 0.11 $\mu g\ g^{-1}$ fluoroacetate

Added ($\mu g\ g^{-1}$)	2.5	5.0	10.0	50.0	100.0
Recovery (%)[a]	89.3 ± 5.3	91.0 ± 9.3	87.0 ± 7.9	88.5 ± 6.5	91.3 ± 3.4

[a]Mean with standard deviation.

TABLE 2

Fluoroacetate content of plant samples

Samples	No. of samples	Fluoroacetate content ($\mu g\ g^{-1}$)		No. of samples below detection limit
		Range	Average	
Finnish plants from high-fluoride area	110	<0.005—0.21	0.034	26
Control plants from low-fluoride area	14	<0.005—0.04	0.008	12
Tea samples	21	0.06—0.48	0.19	—
"Flower tea" samples	5	<0.005	0.005	5
Australian plants with high fluoroacetic acid content	9	2.8—1009	260	—

Analysis of plant samples

The method was used to determine the fluoroacetate content of more than 150 plant samples. The results are summarized in Table 2. The concentrations observed in Finnish plants are very low and in many cases undetectable, but a slightly higher fluoroacetate level was observed for samples from areas with a high fluoride-containing bedrock. Tea samples appeared to contain small (toxicologically insignificant) amounts of fluoroacetate. The fluoroacetate content of the "poisonous" Australian plants was higher by many orders of magnitude. A detailed report of the fluoroacetate contents of the plant samples will be published separately.

The samples were mostly treated in duplicate, and the differences of the duplicate results gave a standard deviation (one sigma) of ±9%. Some of the samples were also analyzed by using two or three different columns. Polar liquid phases generally gave the best resolution from impurities.

Financial support of the Nessling Foundation is gratefully acknowledged. We are also thankful for Dr. D. R. King, Forrestfield Research Laboratories, W. Australia, for supplying the Australian plant samples.

REFERENCES

1 R. A. Peters and R. J. Hall, Nature (London), 187 (1960) 573.
2 L. R. Murray, J. D. McConnell and J. H. Whittem, Aust. J. Sci., 24 (1961) 41.
3 M. M. de Oliveira, Experientia, 19 (1963) 586.
4 T. Vartiainen and P. Kauranen, Kemia-Kemi, 12 (1980) 760.
5 B. Vickery, M. L. Vickery and J. T. Ashu, Phytochemistry, 12 (1973) 145.
6 M. H. Yu and G. W. Miller, Environ. Sci. Technol., 4 (1970) 492.
7 G. W. Miller, M. H. Yu and M. Psenak, Fluoride, 6 (1973) 203.
8 R. Sawyer, B. G. Cox, E. J. Dixon and J. Thomson, J. Sci. Food Agric., 18 (1967) 287.
9 H. M. Stahr, W. B. Buck and P. F. Ross, J. Assoc. Off. Anal. Chem., 57 (1974) 405.
10 H. M. Stahr, J. Assoc. Off. Anal. Chem., 60 (1977) 1434.
11 J. E. Peterson, Bull. Environ. Contam. Toxicol., 13 (1975) 751.
12 J. Okuno and D. L. Meeker, J. Assoc. Off. Anal. Chem., 63 (1980) 49.
13 J. Okuno, D. L. Meeker and R. R. Felton, J. Assoc. Off. Anal. Chem., 65 (1982) 1102.
14 A. C. Ray, L. O. Post and J. C. Reagor, J. Assoc. Off. Anal. Chem., 64 (1981) 19.
15 D. M. Collins, J. P. Fawcett and C. G. Rammell, Bull. Environ. Contam. Toxicol., 26 (1981) 669.
16 H. M. Stevens, A. C. Moffat and J. V. Drayton, Forensic Sci., 8 (1976) 131.
17 E. V. Dehmlow, Angew. Chem. Int. Ed. Engl., 16 (1977) 493.
18 Y. L'Emeillat, J. F. Ménez, F. Berthov and L. Bardov, J. Chromatogr., 206 (1981) 89.

Analytica Chimica Acta, 157 (1984) 99—115
Elsevier Science Publishers B.V., Amsterdam — Printed in The Netherlands

OPTIMAL DESIGNS WITH INFORMATION THEORY IN LEAST-SQUARES PROBLEMS

P. C. THIJSSEN* and G. KATEMAN

University of Nijmegen, Faculty of Sciences, Department of Analytical Chemistry, Toernooiveld, 6525 ED Nijmegen (The Netherlands)

H. C. SMIT

University of Amsterdam, Laboratory for Analytical Chemistry, Amsterdam (The Netherlands)

(Received 10th June 1983)

SUMMARY

The application of information theory in a recursive least-squares context is described. A theoretical discussion of the method is presented and its suitability for the optimal design problem is discussed. The resulting algorithms are simple, fast and easy to implement on a computer and may be used either in an on-line or an off-line fashion.

The scope of analytical chemistry may be described as development of the optimal means of obtaining and utilizing relevant information on the state and processes in material systems. Systems theory [1], information theory [2] and filtering theory [3] are of particular interest, as they provide an important basis for understanding effective applications of automation and determining and exploiting analytical data.

In many analytical situations the method of least squares is important; it is applied in linear calibration, multicomponent analysis and non-linear curve-fitting.

Within this context, little attention has been paid to the pattern of the experimental design, which influences the accuracy of the estimated parameters. Some exceptions are a study of the effects of experimental design in calibration [4] and on the optimization of choosing wavelengths in spectrophotometric analysis [5].

In the present paper, it will be shown that a general theoretical framework can be developed, and can be applied to the computation of optimal designs in a variety of experimental situations. The resulting algorithms are simple in design, rapidly evaluated and easy to implement on a computer either off-line or on-line. The application of information filtering leads to schemes for obtaining the maximum of relevant information with a minimum of computational and experimental effort.

0003-2670/84/$03.00

THEORY

Information theory

The first step in an analysis is usually the sampling of the system under investigation. By means of chemical or physical methods, the qualitative and/or quantitative composition of the sample is transformed to relevant information.

Assume a set of mutually exclusive events $\{i\}$, $i = 1,2, \ldots, n$, each with probability $0 \leqslant p \leqslant 1$. The amount of information is usually expressed in bits, represented by the dual logarithm $\mathrm{ld}\{\}$. The uncertainty or entropy H is defined as the average amount of information given by the probabilities $p(i)$ of all possible events $\{i\}$, with $\Sigma_{i=1}^{n} p(i) = 1$. For a finite discrete set of events, the Shannon formula is applicable by definition

$$H = -\sum_{i=1}^{n} p(i)\,\mathrm{ld}\{p(i)\} \tag{1}$$

For a continuous random variable x with a probability density function $p\{x\}$ the summation is replaced by the integral

$$H = -\int_{-\infty}^{+\infty} p(x)\,\mathrm{ld}\{p(x)\}\mathrm{d}x \tag{2}$$

The information yield, or more concisely the trans-information I, is defined as a change in uncertainty or entropy:

$$I = H_{\mathrm{before}} - H_{\mathrm{after}} \tag{3}$$

There is one subtle difference between the discrete and the continuous formulation. Unlike probabilities in the discrete situation, the probability density function in the continuous case is not dimensionless. As a result, the numerical value of the entropy or information yield will depend on the units in which the variable x is expressed.

If temporal or economic aspects are considered, additional useful information measures may be defined [6]. The information flow J can be represented by $J = \mathrm{d}I/\mathrm{d}t$, i.e., the amount of information transferred in a time unit $\mathrm{d}t$. For practical evaluations, a discrete formulation is self-evident. Similarly a specific information price can be defined.

Linear model

Many analytical relations are adequately described by means of the mathematical model

$$z = h_1 x_1 + h_2 x_2 + \ldots + h_n x_n + v \tag{4}$$

The contribution of each of the n parameters x_i ($i = 1, 2, \ldots, n$), is weighted by the coefficients h_i ($i = 1, 2, \ldots, n$), with the noise v added to result in a measured signal z. It is obvious that for the determination of the unknown

parameters several equations are required, thus Eqn. 4 can be written more concisely as

$$z(k) = \underline{h}^t(k)\underline{x} + v(k) \quad (k = 1, 2, \ldots, m) \tag{5}$$

where $\underline{x}$ is the n column vector with coefficients x_i, and $\underline{h}^t(k)$ is the n row vector, the transpose of the column vector $\underline{h}(k)$ with coefficients $h_i(k)$; k is an index denoting the kth equation. To establish the x_i values, the number of equations m must be at least as large as the number of the unknown parameters n, i.e., $m \geqslant n$. The mathematical model (Eqn. 5) is often designed in the form of a block diagram as shown in Fig. 1. Note that the parameter vector $\underline{x}$ remains constant as a function of the index k.

The equations together can be summarized in a single matrix vector equation: $Z(m) = H(m)\underline{x} + V(m)$, where $Z(m)$ is the m column vector with measurements $z(k)$, $V(m)$ is the m column vector with noise terms $v(k)$, and $H(m)$ is the $m*n$ design matrix with rows $\underline{h}^t(k)$. The design matrix $H(m)$ or the set $\{\underline{h}^t(k)\}$, $k = 1, 2, \ldots, m$; represents the combination of coefficients, factors or instrumental variables. Each row $\underline{h}^t(k)$ corresponds to a measurement, response or experimental result $z(k)$ with a noise term $v(k)$.

Least squares

Given the response vector $Z(m)$ and design matrix $H(m)$ the basic problem is to find an estimate of the parameter vector $\underline{x}$. The solution to this problem depends on the assumptions made: the structure of the mathematical model, a priori statistical knowledge and a suitable chosen optimization criterion. One implicit assumption has already been made. The model structure is linear, which means that in the additive Eqn. 4 the measurements z, coefficients h_i and the noise v contain no parameters x_i. In addition, the data set $H(m)$ is assumed to be deterministic and is obtained by some standard procedure. $H(m)$ has minimal rank n and maximal rank m, i.e., a proper solution from the given equations for the determination of the parameters exists.

It will be assumed that the noise $v(k)$ is not serially correlated, is independent of other quantities involved, and has a normal probability density function with zero mean and given variance $r(k)$. Because of the noise term, it is not possible to determine the unknown parameters uniquely. However, as there are more measurements than unknowns, an estimator $\underline{\hat{x}}(m)$ of $\underline{x}$ that minimizes in some arbitrary sense the effects of the experimental errors can be developed

$$e(k) = z(k) - \underline{h}^t(k)\underline{\hat{x}}(m) \quad k = 1,2, \ldots, m \tag{6}$$

For least-squares estimation the estimate is chosen to minimize the sum of squares of errors as a cost criterion. By choosing the weighted sum of products $e^t(i)e(j)$, $(i, j = 1, 2, \ldots, m)$, as a performance index, one achieves the weighted least-squares algorithm

$$\underline{\hat{x}}(m) = \{H^t(m)\,R(m)^{-1}\,H(m)\}^{-1}\,H^t(m)\,R(m)^{-1}\,Z(m) \tag{7}$$

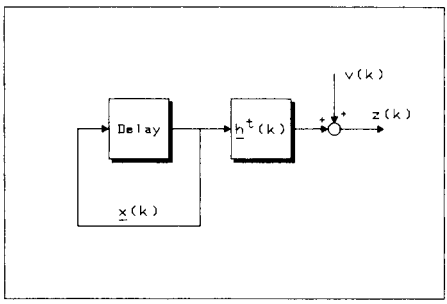

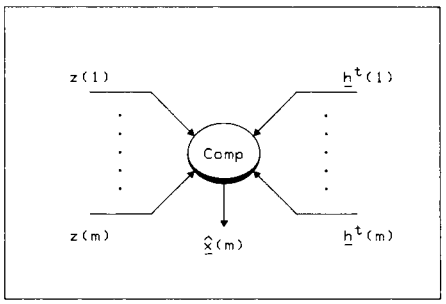

Fig. 1. A linear system model. $\underline{x}(k)$ represents the parameter vector, $\underline{h}^t(k)$ the design vector and $z(k)$ the measurement. The term $v(k)$ denotes the involved noise.

Fig. 2. The classical least-squares algorithm. $\underline{\hat{x}}(m)$ represents the estimated parameter vector and $\{\underline{h}^t(i)\}$, $\{z(i)\}$ $(i = 1, 2, \ldots, m)$ the design vectors with the measurements; Comp denotes a non-linear computation.

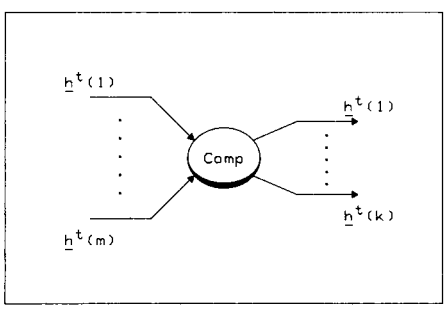

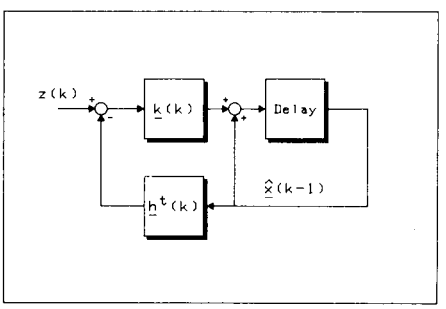

Fig. 3. The classical optimal design algorithm. $\{\underline{h}^t(i)\}$ $(i = 1, 2, \ldots, m)$ denotes the original design set, which results in an optimal set $\{\underline{h}^t(i)\}$ $(i = 1, 2, \ldots, k)$; Comp denotes the optimization computation.

Fig. 4. The recursive least-squares algorithm. $\underline{\hat{x}}(k-1)$ represents the last estimated state vector. The design vector $\underline{h}^t(k)$, the gain vector $\underline{k}(k)$ and the measurement $z(k)$ result in a new estimate $\underline{\hat{x}}(k)$. "Delay" denotes a time or sequence transition.

with $R(m)$ as a $m*m$ weighting matrix. A block diagram of the weighted least squares is shown in Fig. 2.

When the weighting matrix $R(m)$ is chosen as the noise covariance matrix, the estimate is in a statistical sense the best linear unbiased estimate with minimum variance. As a consequence, the $n*n$ dispersion matrix $P(m) = \{H^t(m)\,R(m)^{-1}\,H(m)\}^{-1}$ is the covariance matrix of the estimated parameters; here, $P(m)$, being a covariance matrix may serve as a measure of quality for the estimate $\underline{\hat{x}}(m)$. In general, the diagonal elements $p_{ii}(m)$ of $P(m)$ can be regarded as the variance in the ith coefficient $x_i(m)$ of $\underline{\hat{x}}(m)$, or var $\{x_i(m)\} = p_{ii}(m)$ $(i = 1, 2, \ldots, n)$. This relation is of importance when evaluating the gained accuracy with a preselected value, which can be used as a stop criterion. From the above, it can be concluded that it will only be possible to compute an estimate $\underline{\hat{x}}(m)$ of $\underline{x}$ if the inverse $P(m)$ exists.

Optimal designs

The experimental design affects directly the accuracy of the estimated parameters given by the covariance matrix $P(m)$. For an optimal design, the resulting covariance matrix must be minimized; i.e., the design matrix $H(m)$ and the weight matrix $R(m)$ must be chosen so that $P(m)$ is minimized. When the factors may be chosen without restriction from infinite areas, the dispersion matrix can be made always equal to the zero matrix. In practice, the factors are restricted within finite regions and depend on each other.

It is necessary to assume that $R(m)$ is a diagonal matrix (no serial correlation) and depends only on the measurements and not on the experimental design (linearity). An additional assumption is that the noise covariances in $R(m)$ or the set $\{r(k)\}$ $(k = 1, 2, \ldots, m)$ are equal. The covariance matrix $P(m)$ can then be written as $r(m)\{H^t(m)\, H(m)\}^{-1}$. Here the optimal choice of factors is found when the columns of $H(m)$ are orthogonal [7]. Some ways of formulating this mathematically are

minimize determinant $|\{H^t(m)H(m)\}^{-1}|$

or minimize trace $\mathrm{tr}(\{H^t(m)\, H(m)\}^{-1})$

or minimize norm $||\{H^t(m)H(m)\}^{-1}||$

Designs which minimize these criteria are called, respectively, D-optima, A-optima and E-optima [8].

An alternative criterion not based on statistical backgrounds is the condition $K\{H^t(m)H(m)\}$ [5]. It expresses the numerical (in)accuracy gained in the computation of the inverse and should only be used for the detection of numerical problems. The choice of a proper criterion is usually not critical and they correspond reasonably with each other. Some criteria, e.g., the trace, have to be viewed with some suspicion, because they may lead to designs with unidentifiable parameters. The determinant that represents the volume of the dispersion matrix is used mostly.

The classical approach to the optimal design problem is to use the determinant as a criterion formulated in the inverse way

$$\text{maximize } |P(m)^{-1}| = |H^t(m)\, R(m)^{-1}\, H(m)| \tag{8}$$

In the statistical literature, the matrix $M(m) = P(m)^{-1}$ is well known as the Fischer information matrix [7]. Because the main interest of optimization is only to minimize the second moment matrix, there are no serious consequences of the noise being non-Gaussian or using a non-linear model. However, in non-linear models the parameters that are required for computation of the dispersion matrix, can only be estimated by a preliminary experiment. A representation of the classical optimization procedure is shown in Fig. 3. To choose an optimal set $H(k)$ from a given data set $H(m)$ with $m > k$, one has to compute at least $m!/\{k!(m - k)!\}$ determinants of each possible permutation of the rows in the design matrix. Of course, this is an immense computational job. Therefore, optimised designs in a classical sense will only

be beneficial when a limited set of factors and not too many parameters are involved.

Recursive approach

The preceding approach and solution are commonly referred to as the "batch processing" least-squares algorithm, because the data $Z(m)$ are processed simultaneously. A disadvantage of this approach is that for each new entry $z(m+1)$ that becomes available, it is necessary to repeat the whole computational procedure. Again an $n*n$ matrix must be inverted and none of the employed calculations in Eqn. 7 can be used to facilitate the job. In essence, knowledge of the estimate $\underline{\hat{x}}(m)$ based on $Z(m)$ is disregarded completely, which explains the computational inefficiency. This waste of effort can be avoided by using a scheme of the following structure: new estimate = old estimate + correction. The old estimate is based on m measurements and the new estimate is based on $m+1$ measurements, while the correction is calculated from the information supplied by the new measurement. The solution is referred to as a sequential or recursive algorithm. As demonstrated in the Appendix, an important mathematical result for the development of a recursive structure is the matrix inversion lemma, based on the original relation between the old covariance matrix $P(m)$ and the new one $P(m+1)$.

In contrast to the batch algorithm, its recursive equivalent needs an additional statistical assumption: it is assumed that the parameter $\underline{x}$ is a random variable, which has a multivariate gaussian probability density function $p\{\underline{x}\}$. Initially the estimate and the covariance of $\underline{x}$ equals $\underline{\hat{x}}(0)$ and $P(0)$, respectively. As a result the recursive least-squares algorithm can be derived [10]

$$p\{\underline{x}|Z(k)\} = [(2\pi)^n |P(k)|]^{-1/2} \exp\{-1/2[\underline{x} - \underline{\hat{x}}(k)]^t P(k)^{-1} [\underline{x} - \underline{\hat{x}}(k)]\} \quad (9)$$

$$\underline{\hat{x}}(k) = \underline{\hat{x}}(k-1) + \underline{k}(k)\{z(k) - \underline{h}^t(k)\,\underline{\hat{x}}(k-1)\} \quad (10)$$

$$P(k) = P(k-1) - \underline{k}(k)\,\underline{h}^t(k)\,P(k-1) \quad (11)$$

$$\underline{k}(k) = P(k-1)\,\underline{h}(k)\{\underline{h}^t(k)\,P(k-1)\,\underline{h}(k) + r(k)\}^{-1} \quad (12)$$

where $p\{\underline{x}|Z(k)\}$ is the Gaussian density function calculated later. The n column vector $\underline{\hat{x}}(k)$ is the new estimate of $\underline{x}$ based on knowledge of the data $Z(k)$. A schematic representation of the recursive least-squares algorithm is shown in Fig. 4. As mentioned, the $n*n$ matrix $P(k)$ can be regarded as the error covariance of the difference between $\underline{x}$ and the estimate $\underline{\hat{x}}(k)$. In terms of probability, $\underline{\hat{x}}(k)$ and $P(k)$ can be interpreted as

$$\underline{\hat{x}}(k) = E\{\underline{x}|Z(k)\} \quad (13)$$

$$P(k) = E\{(\underline{x} - \underline{\hat{x}}(k))\,(\underline{x} - \underline{\hat{x}}(k))^t\,|Z(k)\} = E\{(\underline{x} - \underline{\hat{x}}(k))\,(\underline{x} - \underline{\hat{x}}(k))^t\}$$

$E\{\}$ denotes the expectation of the quantities within the braces. The correction in Eqn. 10 consists of two parts: the innovation $\nu(j)$ or the dif-

ference between the experimental and estimated measurement

$$v(k) = z(k) - \underline{h}^t(k)\hat{\underline{x}}(k-1) \tag{14}$$

and the n column vector $\underline{k}(k)$, the gain vector which weights the innovation $v(k)$.

The existence of the inverse matrix $P(k)$ is one way of formulating the "observability of the system", which expresses the necessity for a sufficient number of linear independent equations as an algebraic criterion. The observability condition defines the ability to determine $\underline{x}$ from the measurements [10]. A system is observable if rank $\{\underline{h}(k-n+1), \ldots, \underline{h}(k)\} = n$. Provided that the system is observable, for k to infinity, the matrix $P(k)$ will converge to the zero matrix and as a consequence the gain vector $\underline{k}(k)$ will become the null vector. In probability terms, it means that the algorithm knows the "state of $\underline{x}$" exactly. Because the quantity $\{\underline{h}^t(k)P(k-1)\underline{h}(k) + r(k)\}$ in Eqn. 12 is a scalar, no matrix inversion is needed in the computation. Moreover, there is no need for a growing computer memory, with increasing amount of processed data.

Given the preliminary assumptions, the recursive algorithm in Eqns. 10—12 represents the Kalman filter algorithm for the given problem of estimation. It reduces to the ordinary recursive least-squares algorithm when the weight $r(k) = 1$ for all k.

When no prior information is available, it is common practice to choose for the estimate $\hat{\underline{x}}(0)$ and covariance matrix $P(0)$ the initial values, $\hat{\underline{x}}(0) = 0$ and $P(0) = s_0^2 I_n$, where I_n is the $n*n$ identity matrix and s_0^2 the initial variance. Compromising statistical bias and numerical stability alike, a large value is chosen for s_0^2 [11, 12].

Information

According to information theory, the entropy of a multivariate probability density [3] is defined as

$$H = -\int_{-\infty}^{+\infty} p\{\underline{x}\} \operatorname{ld}(p\{\underline{x}\}) d\underline{x} \tag{16}$$

where $p\{\underline{x}\}$ is the probability density function of an n-dimensional random variable $\underline{x}$ and $d\underline{x}$ is the volume element. Assuming normal density $P\{\underline{x}|Z(k)\}$ (Eqn. 9), the mean and covariance matrix are defined by the integrals

$$\begin{aligned}
&\int_{-\infty}^{+\infty} p\{\underline{x}|Z(k)\}\, d\underline{x} = 1 \\
&\int_{-\infty}^{+\infty} \underline{x} p\{\underline{x}|Z(k)\}\, d\underline{x} = \hat{\underline{x}}(k) \\
&\int_{-\infty}^{+\infty} [\underline{x} - \hat{\underline{x}}(k)]\, [\underline{x} - \hat{\underline{x}}(k)]^t\, p\{\underline{x}|Z(k)\}\, d\underline{x} = P(k)
\end{aligned} \tag{17}$$

Applying Shannon's formula and using Eqn. 9 gives

$$H(k) = -\int_{-\infty}^{+\infty} p\{\underline{x}|Z(k)\}[-1/2\ \mathrm{ld}\{(2\pi)^n|P(k)|\}$$

$$-1/2\ \mathrm{ld}\{e\}(\underline{x}-\underline{\hat{x}}(k))^t P(k)^{-1}\ (\underline{x}-\underline{\hat{x}}(k))]\ d\underline{x}$$

$$= 1/2\ \mathrm{ld}\{(2\pi)^n|P(k)|\} + 1/2\ \mathrm{ld}\{e\}\mathrm{tr}\{P(k)^{-1}\ P(k)\} \tag{18}$$

Thus the entropy is

$$H(k) = 1/2\ \mathrm{ld}\{(2\pi e)^n\ |P(k)|\} \tag{19}$$

For the amount of information, $I(k) = H(k-1) - H(k)$, obtained by processing a new measurement $z(k)$ with corresponding design vector $\underline{h}(k)$

$$I(k) = -1/2\ \mathrm{ld}\ \{|P(k)|/|P(k-1)|\} \tag{20}$$

With use of the determinant product rule for the ratio $|P(k)|/|P(k-1)|$ in Eqn. 11 the information yield is given by

$$I(k) = -1/2\ \mathrm{ld}\ \{|I_n - \underline{k}(k)\underline{h}^t(k)|\} \tag{21}$$

The resulting relations for the information yield hold for the entire parameter space, i.e., for all parameters together. For the information yield of the specific parameters, the diagonal elements of the matrix $P(k)\cdot P(k-1)^{-1}$ or $\{I_n - \underline{k}(k)\underline{h}^t(k)\}$ can be used, ignoring correlational redundancy.

Equation 21 suggests the full use of recursive properties, which is confirmed in the appendix by another important mathematical result, the matrix determinant lemma

$$|P(k-1)| = \{\underline{h}^t(k)P(k-1)\underline{h}(k)/r(k) + 1\}|P(k)| \tag{22}$$

Incorporating this result in Eqn. 20 gives the information yield in the form

$$I(k) = 1/2\ \mathrm{ld}\ \{\underline{h}^t(k)P(k-1)\underline{h}(k)/r(k) + 1\} \tag{23}$$

Because the term between brackets is a scalar, the determinant computation is no longer required, which minimizes computational effort. The main term $\underline{h}^t(k)P(k-1)\underline{h}(k)/r(k)$ consists of three parts; the matrix $P(k-1)$ involved with the "old knowledge" of the algorithm, the design vector $\underline{h}(k)$ and the noise covariance $r(k)$, supplying the "new knowledge". Theoretically, it expresses the relation between the entropy gained in the previous experimental design, evaluating the information gain of the prevailing design vector and measurement noise. For k to infinity, the gain vector $\underline{k}(k)$ in Eqn. 21 converges to the null vector, thus the limiting value for the information yield is $\lim_{k\to\infty} I(k) = 1/2\ \mathrm{ld}\{|I_n|\} = 0$. This agrees with the expectation that for an infinite number of measurements the estimation algorithm knows the estimate $\underline{\hat{x}}(k)$ as $\underline{x}$ exactly, and no more information can be obtained.

Minimax optimization

The application of the recursive information approach for the computation of the optimal design will now be described. In analytical practice, the basic formula (Eqn. 23) can be used for a variety of experimental situations. Starting from the index $k = 1$, one could write for the total information yield $I_{tot}(k)$

$$I_{tot}(k) = 1/2 \text{ ld } \{|P(0)|/|P(k)|\}$$
$$= 1/2 \text{ ld } \{|P(0)|/|P(1)|\} + \ldots + 1/2 \text{ ld } \{|P(k-1)|/|P(k)|\}$$
$$= \sum_{i=1}^{k} I(i) = I_{tot}(k-1) + I(k) \tag{24}$$

The total information yield $I_{tot}(k)$ is the summation of all individual information yields $I(i)$, $i = 1, 2, \ldots, k$. Otherwise stated, $I_{tot}(k)$ is the sum of the preliminary information yield $I_{tot}(k-1)$ incorporating the entire previous experimental design and the new information yield $I(k)$ based on the new experimental choice.

According to information theory, the classical optimal design problem (Eqn. 8) amounts to minimizing the final entropy (Eqn. 19). As a consequence of the recursive formulation, the optimal design problem is especially involved with selecting an optimal experimental sequence. Alternatively the total information yield (Eqn. 24) can be maximized. In this sequence, each experimental possibility is rated with a specific information credit. The information $I_{tot}(k-1)$ is initially always the same, thus in the process of maximizing, the main term of interest is the information yield $I(k)$. All computed information yields $I(i)$, $i = 1, 2, \ldots, k$, are in sequence maximal and additive, so that the total information yield $I_{tot}(k)$ must be at a maximum. Hence, from recursive information theory, the classical optimal design is reformulated as a sequence of maximized experimental choices.

Reformulation of the information yield $I(k)$ (Eqn. 23), with omission of the dual logarithm, gives

$$\text{minimize } H(k) = -1/2 \text{ ld } \{(2\pi e)^n |P(k)|\}$$
$$\text{maximize } I_{tot}(k) = 1/2 \text{ ld } \{|P(0)|/|P(k)|\} = I_{tot}(k-1) + I(k)$$
$$\text{maximize } I(k) = 1/2 \text{ ld } \{\underline{h}^t(k)P(k-1)\underline{h}(k)/r(k) + 1\}$$
$$\text{maximize } \underline{h}^t(k)P(k-1)\underline{h}(k)/r(k) \tag{25}$$

Because every additional maximization is based on a previously minimized dispersion matrix, this procedure is known as minimax optimization. The minimax criterion is the quintessence to the recursive optimal design computation. For the choice of a new $\underline{h}(k)$, the whole design data set $\{\underline{h}(i), r(i)\}$ $(i = 1, 2, \ldots, m)$ has to be processed only once. This means for each value of k the computation of m times Eqn. 25; calculation of the determinant is no longer involved.

In order to initialize the recursive maximization algorithm, it is necessary to choose a covariance matrix $P(0)$ which expresses the initial entropy $H(0)$. In reality, the prior uncertainty or entropy of the system under investigation is infinite. By choosing a finite initial entropy, the maximization algorithm is in a classical sense suboptimal. This effect will be of less importance if initially a large variance s_0^2 is used in the equation $P(0) = s_0^2 I_n$. It can be proved that the maximization algorithm will converge asymptotically to the optimum for increasing index k. For comparative studies of various design computations, it is suggested that the same s_0^2 which gives as a reference entropy $H(0) = n/2 \text{ ld } \{2\pi e s_0^2\}$ should always be chosen, but naturally any value could be selected. The maximum amount of information, I_{max}, that can be experimentally obtained, is infinite. The relation between the total information gained and the reduction of the number of decimal digits of the preset accuracy is given by

$$I_{tot}(k) = n\, d/\log(2) \tag{26}$$

where d is the number of decimal digits and n the number of parameters. Upon incrementing index k, the additional information $I(k)$ converges to zero, which means that for every desired extension of the number of digits more measurements are required.

On-line computation

The assumption of covariances of equal value, such as are encountered in the classical optimal design formulation, is not necessary in the recursive approach. However, if the noise covariance depends on the measurement, the computation can only be done in an on-line fashion. A block diagram of the proposed optimization procedure integrated in the recursive least-squares algorithm is shown in Fig. 5. Based on the estimated parameters and the design vector of interest, it is possible to forecast the expected measurement with its probable noise covariance.

The procedure under consideration is again suboptimal but under the

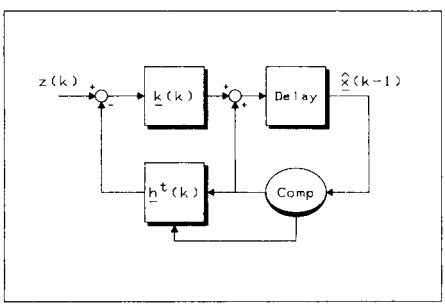

Fig. 5. The recursive optimal design algorithm. $\underline{\hat{x}}(k-1)$ represents the last estimated state vector. The design vector $\underline{h}^t(k)$, the gain vector $\underline{k}(k)$ and the measurement $z(k)$ produce a new estimate $\underline{\hat{x}}(k)$; Comp denotes the optimization computation, which controls the choice of the new design vector $\underline{h}^t(k)$.

experimental circumstances it makes the best choices based on all available information, with a compromise between design vector gains and estimated noise covariances. After a design vector has been chosen, the measurement with the correct noise covariance is used for updating the estimated parameters. In order to produce an entire suboptimal sequence, this procedure is repeated for each new measurement. The experiment can be terminated from a comparison of the total information yield $I_{tot}(k)$ with a predefined value (Eqn. 26). Alternatively, the diagonal elements of the covariance matrix with a desired accuracy for the parameters in the equation var$\{x_i(m)\} = p_{ii}(m)$ may be used as a stop criterion.

Off-line computation

Assuming equal noise covariances, one may compute in advance an optimal design before any experiment is done. Such a computation is referred to as an a priori processing algorithm. For the weight $r(k) = 1$, the covariance matrix $P'(k)$ in the recursive least-squares algorithm (Eqns. 10—12) is written as $P'(k) = r'P(k)$, where r' is the actual noise covariance and $P(k)$ is the computed dispersion matrix in Eqn. 11. By recycling through the maximization procedure, the chosen design vectors can be removed from the original design data base. Alternatively, the algorithm may have the freedom to reuse previously chosen design vectors. The final criterion in Eqn. 25 produces in sequential order the maximizations $k = 1, 2, \ldots$.

maximize $\underline{h}^t(i)P_{max}(k-1)\underline{h}(i)/r(i) \quad (i = 1, 2, \ldots, m)$

$$P_{max}(k-1) = \{P(0)^{-1} + \sum_{j=1}^{k-1} \underline{h}_{max}(j)r(j)^{-1}\,\underline{h}^t_{max}(j)\}^{-1} \tag{27}$$

After each maximization, the recursive Eqn. 11 updates the dispersion matrix $P_{max}(k-1)$ using the computed $\underline{h}_{max}(k)$. For clarity, the alternative formula is given.

The first maximizations $\underline{h}_{max}(j)$ are of course suboptimal, because of the initial dispersion matrix $P(0) = I_n s_0^2$. The effect of the initial $P(0)$ decreases upon incrementing index k, whereas the influence of the summation $\Sigma_{j=1}^{k-1}\underline{h}_{max}(j)h \cdot r(j)^{-1} \cdot h^t\underline{h}^t_{max}(j)$ increases.

After each maximization, the new computed design vector will be a better choice, because of the effect of the preliminary suboptimal choices $\underline{h}_{max}(j)$. In the iteration, the procedure tunes itself to the minimal optimal solution, provided that the algorithm may re-use previously chosen design vectors. Essentially, the presented a priori algorithm can be described as a self-optimizing process.

To be optimal, the computed solution should comprise a minimal set of Eqns. 5, which must be observable. After a number of iterations, the maximized solution repeats itself and equals the classically determined optimal design. The iterative process considered may be terminated if the following condition is satisfied

$$(|P_{max}(k)| - |P_{max}(k-1)|)/|P_{max}(k)| \leqslant \delta \tag{28}$$

or

$$\underline{h}^t_{max}(k) P_{max}(k-1) \underline{h}_{max}(k)/r(k) \leqslant \delta \tag{29}$$

with δ as a very small value. A mathematical proof of the convergence property is available [9].

Extension to any over-determined optimal design could be done easily after computation of the optimal determined design. The chosen design vectors are removed from the original data base after each maximization. Because the determined solution is optimal, each extension with a design vector $\underline{h}^t_{max}(k)$ in the sequence is also optimal. The computed matrix $P_{max}(k-1)$ is no longer a covariance matrix, because it can only be computed after starting removal of design vectors from the original data base. The off-line optimization procedure can be represented by the classical scheme shown in Fig. 3.

In order to select a new $\underline{h}_{max}(k)$ the entire design data set has to be processed once only, involving for every cycle the computation of m times the final Eqn. 25 but no determinant computation. For a large initial s_0^2, about $2*n$ iterations are required in order to find the optimal determined solution. For an optimal experimental sequence, $i = 1, 2, \ldots, k$, the computations are reduced to $m(2n + k)$ times Eqn. 25. In comparison with the classical approach, there is a remarkable reduction of the computational efforts. This new feature provides a strong argument in favor of the recursive approach. For timing comparisons, the proposed algorithm has a linear dependency with the target dimension k and data-base dimension m, while it depends quadratically on the number of involved parameters n.

Basic properties

If equal noise covariances are assumed, some additional properties can be formulated, which could be of analytical importance. For clarity, it is sometimes easier to return to the classical formulation of least squares, which has essentially the same properties. An interesting property can be described as "permutation freedom". For the total information yield $I_{tot}(k)$, it is possible to derive

$$I_{tot}(k) = 1/2 \operatorname{ld} \{|I_n + P(0) \sum_{i=1}^{k} \underline{h}(i) r(i)^{-1} \underline{h}^t(i)|\} \tag{30}$$

The term $\Sigma_{i=1}^{k} \underline{h}(i) r(i)^{-1} \underline{h}^t(i)$ is important. The total information yield is invariant under permutation of design vectors $\underline{h}(i)$ and corresponding noise covariance $r(i)$. When the same design considerations are used, in practice this means that the experiment could be performed in any sequential order. This conclusion is of importance when time-dependent effects are of analytical interest.

As demonstrated in the appendix, the optimal design computation is

not dependent on a multiplication factor a_i on every coefficient $h_i(j)$, ($j = 1, 2, \ldots, m$) in the data base. A practical consequence of the multiplication rule is that relative design vectors will have no effect on the optimal design computation. However, this means that only relative parameters can be estimated by the least-squares algorithm (the parameter x_i divided by the constant). Another result is that the optimal design computation is independent of an additive factor b_i on every coefficient $h_i(j)$ ($j = 1, 2, \ldots, m$) in the entire data base, provided that an extra coefficient ($\underline{h}^t(j)$, 1) is included. Because of the extension of the model with one parameter, the computed optimal design will be different, owing to correlational effects of the dummy with the original parameters. Therefore the estimated parameters will also be different. In practical situations, the additive rule means that the design vectors and measurements could contain different baselines.

The combination of the multiplicative and additive property deals with the most advanced practical situation of relative design vectors and measurements with different baselines. They will be of use when the aim is to compute an optimal design without estimating the exact parameters.

POSSIBLE APPLICATIONS

If the model structure is correct and if the noise covariances are either known or constant, the theory may be of some use in the following examples. First, it should be useful in multicomponent spectrophotometric analysis for the proper selection of wavelengths. As an example, if 4 components are to be measured and known pure spectra at 30 wavelengths are available with 6 wavelengths to be selected, then the classical optimization procedure involves the computation of almost 600 000 4*4 determinants and requires a few days computation. The recursive procedure offers the same solution in about 420 times Eqn. 25 plus some minor computations for updating the covariance matrix, requiring less than a minute on the same computer (HP-9845B). There are no differences in memory requirements.

Other potential uses are in calibration problems [4]. It is well known that the optimal design for a linear calibration graph is given by the boundaries of the concentration range. For a quadratic curve, the concentration at the centre of the range will also be found. If the static model is replaced and stochastic behaviour of the parameters is assumed, as used for on-line calibration, assessment and quality control with possible extension to drift [17], this generalization still holds. However, it is not known in advance which of the "good" concentrations will be the optimal choice. The generalized standard addition method [18, 19] and non-linear curve-fitting are other possible areas of application.

Conclusions

The classical optimal design problem is reformulated in terms of recursive information theory as a sequence of maximized experimental choices.

If equal noise covariances are assumed, it is possible to compute off-line an optimal design before any experiment is done. When the original data base is a relative one or contains different baselines, these effects on the computation can be eliminated. With inclusion of the same design considerations, the experiment could be performed in any sequential order. The algorithms presented yield a considerable reduction of the computational effort, which permit the application of informative filtering in either an on-line or an off-line fashion.

Appendix A. Some vector and matrix fundamentals [13, 14]

Scalar. A scalar is defined as a single element with a numerical value and is denoted by a lower-case letter.

Vector. A vector is an array of elements arranged in a column. It is designated by an underlined lower-case letter and referred to as a vector $\underline{x}$. The number of elements in the vector is its dimension.

Matrix. A matrix is an $m*n$ rectangular array of elements, denoted by a capital letter. The matrix A, consisting of m rows and n columns is defined as $\{a_{ij}\}$, where a_{ij} is the i, jth element for $i = 1, 2, \ldots, m$ and $j = 1, 2, \ldots, n$. A column vector may be considered as a matrix with n rows and 1 column and a scalar as a $1*1$ matrix.

Transpose. The superscript "t" denotes the transpose of a matrix or a vector. This linear operation can be formulated as interchanging rows and columns. A column vector $\underline{x}$ becomes a row vector $\underline{x}^t$, and an $m*n$ matrix A becomes an $n*m$ matrix A^t after transposition.

Trace. The trace of a matrix is designated as "tr $\{\}$" and is defined as the sum of the diagonal elements a_{ii} of an $n*n$ square matrix A: $\mathrm{tr}\{A\} = \Sigma_{i=1}^{n} a_{ii}$.

Addition. The addition of two vectors $\underline{x}$ and $\underline{y}$ with the same dimension is:

$$\underline{x} + \underline{y} = \begin{pmatrix} x_1 + y_1 \\ \cdot \\ \cdot \\ \cdot \\ x_n + y_n \end{pmatrix}$$

Vector subtraction is defined in a similar manner. Equivalently, the subtraction and addition of two matrices is defined, when they have identical dimensions.

Product. If $\underline{x}$ and $\underline{y}$ are column vectors with elements x_i and y_i, respectively, then the vector product, $\underline{x}^t\underline{y} = \Sigma_{i=1}^{n} x_i y_i$, is a scalar, whereas the product

$$\underline{x}\,\underline{y}^t = \begin{pmatrix} x_1y_1 & \cdot & \cdot & \cdot & x_1y_n \\ \cdot & & & & \cdot \\ \cdot & & & & \cdot \\ \cdot & & & & \cdot \\ x_ny_1 & \cdot & \cdot & \cdot & x_ny_n \end{pmatrix}$$

yields a matrix. The same rules hold for vector × matrix and matrix × matrix products.

Norm. The norm of a vector denoted by "|| ||" defines a measure of distance or magnitude. Various definitions of the norm are possible. For the present purpose, the Euclidian norm is used. The norm of a vector $\underline{x}$ is the square root of the sum of squared elements or as a vector product: $\|\underline{x}\| = (\underline{x}^t\underline{x})^{1/2}$. The norm of an arbitrary matrix A used here is $\|A\| = \{\lambda_{\max}(A^tA)\}^{1/2}$, where $\lambda_{\max}$ is the largest eigenvalue of the matrix product A^tA.

Condition. The condition of a matrix denoted by "$K(\ )$" is defined as the product of the norm of a matrix with the norm of its inverse or equivalently as the square root of the ratio of the largest and smallest eigenvalue: $K(A) = \|A\|\,\|A^{-1}\| = \{\lambda_{\max}(A^tA)/\lambda_{\min}(A^tA)\}^{1/2}$. The condition number is a measure of the numerical difficulties encountered

in obtaining the inverse of a matrix. As $K(A)$ increases, the matrix A is said to be increasingly ill-conditioned.

Determinant. To every square matrix, the determinant is an associated scalar quantity denoted by "| |". It is defined as the sum of all products of different sign:

$$|A| = \sum_{p=1}^{n!} (-1)^p a_{p_1} a_{p_2} \cdot \ldots \cdot a_{pn}$$

where p denotes all permutated terms within the matrix A. If in a matrix every element of a row (column) of a square matrix is zero, then the determinant $|A| = 0$. Two identical rows or columns also produce a zero determinant. The determinant of the product AB is defined as $|AB| = |A||B|$. If each element of a row (column) is multiplied by a scalar a_i, the determinant is multiplied by that factor. For ease, the matrix A is defined as a set of column vectors $\underline{x}_j$:

$$|\underline{x}_1, \ldots, a_i \underline{x}_i, \ldots, \underline{x}_n| = a_i |\underline{x}_1, \ldots, \underline{x}_i, \ldots, \underline{x}_n|$$

If in a matrix a scalar b_i is added to every element of a row or a column, the resulting determinant is invariant under this operation, provided that the matrix is extended with a dummy column (row) $\underline{1}$.

$$|\underline{x}_1, \ldots, \underline{x}_i + \underline{b}_i, \ldots \underline{x}_n, \underline{1}| = |\underline{x}_1, \ldots \underline{x}_i, \ldots \underline{x}_n, \underline{1}| + |\underline{x}_1, \ldots, \underline{b}_i, \ldots, \underline{x}_n, \underline{1}|$$

$$= |\underline{x}_1, \ldots, \underline{x}_i, \ldots \underline{x}_n, \underline{1}| + b_i |\underline{x}_1, \ldots, \underline{1}, \ldots, \underline{x}_n, \underline{1}|$$

The second term vanishes because of the two identical columns.

Rank. The rank of a matrix is the dimension of the largest square matrix in A formed by deleting rows and columns, which has a non-zero determinant. An $n*n$ matrix A has a rank m with $m \leqslant n$.

Inversion. The superscript "—1" denotes the inverse of an $n*n$ matrix. The inverse is only defined for a square matrix, having linear independent rows or columns. The inverse of a matrix A is given by the relation $AA^{-1} = A^{-1}A = \mathrm{I}_n$. For inversion, the $n*n$ matrix A must have a rank n or a non-zero determinant.

Appendix B. Recursive vector and matrix results [15, 16]

The parameter $\underline{x}$ is estimated in such a way that the estimator $\underline{\hat{x}}(m)$ minimizes the cost index $J(m)$ as a weighted sum of products:

$$J(m) = \sum_{k=1}^{m} (z(k) - \underline{h}^t(k)\underline{\hat{x}}(m))^t r(k)^{-1} (z(k) - \underline{h}^t(k)\underline{\hat{x}}(m)) \tag{B1}$$

Consequently $\underline{\hat{x}}(m)$ should satisfy $\mathrm{d}J(m)/\mathrm{d}\underline{\hat{x}}(m) = 0$ such that:

$$\underline{\hat{x}}(m) = \left\{ \sum_{k=1}^{m} \underline{h}(k) r(k)^{-1} \underline{h}^t(k) \right\}^{-1} \sum_{k=1}^{m} \underline{h}(k) r(k)^{-1} z(k) \tag{B2}$$

or equivalently $\underline{\hat{x}}(m) = \{H^t(m)R(m)^{-1}H(m)\}^{-1} H^t(m)R(m)^{-1} Z(m)$.

Redefining (B2): $\underline{\hat{x}}(m) = P(m)\underline{b}(m)$

where

$$P(m)^{-1} = \sum_{k=1}^{m} \underline{h}(k) r(k)^{-1} \underline{h}^t(k) \text{ and } \underline{b}(m) = \sum_{k=1}^{m} \underline{h}(k) r(k)^{-1} z(k),$$

gives the analogous recursive relations:

$$P(m)^{-1} = P(m-1)^{-1} + \underline{h}(m) r(m)^{-1} \underline{h}^t(m) \tag{B3}$$

$$\underline{b}(m) = \underline{b}(m-1) + \underline{h}(m) r(m)^{-1} z(m) \tag{B4}$$

Recursive alternatives from the previous relations are now derived. In succession, multiply both sides of Eqn. B3 by $P(m)$ at the left, then by $P(m-1)$ at the right and finally by $\underline{h}(m)$ at the left:

$$I_n = P(m)P(m-1)^{-1} + P(m)\underline{h}(m)r(m)^{-1}\,\underline{h}^t(m) \tag{B5}$$

$$P(m-1) = P(m) + P(m)\underline{h}(m)r(m)^{-1}\,\underline{h}^t(m)P(m-1)$$

$$P(m-1)\underline{h}(m) = P(m)\underline{h}(m) + P(m)\underline{h}(m)r(m)^{-1}\,\underline{h}^t(m)P(m-1)\underline{h}(m)$$

$$= P(m)\underline{h}(m)\{r(m)^{-1}\,\underline{h}^t(m)P(m-1)\underline{h}(m) + 1\}$$

The term $\{r(m)^{-1}\,\underline{h}^t(m)P(m-1)\underline{h}(m) + 1\}$ is a scalar, thus

$$P(m-1)\underline{h}(m) = \{r(m)^{-1}\,\underline{h}^t(m)P(m-1)\underline{h}(m) + 1\}P(m)\underline{h}(m)$$

Dropping $\underline{h}(m)$ on both sides and introducing determinants yields the matrix determinant lemma

$$|P(m-1)| = \{\underline{h}^t(m)P(m-1)\underline{h}(m)/r(m) + 1\}\,|P(m)| \tag{B6}$$

Going back to Eqn. B5 and writing $r(m)^{-1}$ out of the scalar term:

$$P(m-1)\underline{h}(m) = P(m)\underline{h}(m)r(m)^{-1}\,\{\underline{h}^t(m)P(m-1)\underline{h}(m) + r(m)\} \tag{B7}$$

Multiplying both sides by $\{\underline{h}^t(m)P(m-1)\underline{h}(m) + r(m)\}^{-1}\,\underline{h}^t(m)P(m-1)$ at the right yields

$$P(m-1)\underline{h}(m)\,\{\underline{h}^t(m)P(m-1)\underline{h}(m) + r(m)\}^{-1}\,\underline{h}^t(m)P(m-1)$$

$$= P(m)\underline{h}(m)r(m)^{-1}\,\underline{h}^t(m)P(m-1) \tag{B8}$$

Substituting $P(m)\underline{h}(m)r(m)^{-1}\,\underline{h}^t(m)P(m-1)$ from Eqn. B5 gives

$$P(m) = P(m-1) - P(m-1)\underline{h}(m)\,\{\underline{h}^t(m)P(m-1)\underline{h}(m) + r(m)\}^{-1}\,\underline{h}^t(m)P(m-1)$$

Reformulating gives the matrix inversion lemma

$$P(m) = P(m-1) - \underline{k}(m)\underline{h}^t(m)P(m-1) \tag{B9}$$

$$\underline{k}(m) = P(m-1)\underline{h}(m)\{\underline{h}^t(m)P(m-1)\underline{h}(m) + r(m)\}^{-1} \tag{B10}$$

Eliminating on both left sides of equation (B8) the term $\underline{h}^t(m)P(m-1)$ gives an alternative formula for $\underline{k}(m)$, viz. $\underline{k}(m) = P(m)\underline{h}(m)r(m)^{-1}$. Considering Eqn. B3 from an initial $P(0)$

$$P(m) = \left\{P(0)^{-1} + \sum_{k=1}^{m} \underline{h}(k)r(k)^{-1}\underline{h}^t(k)\right\}^{-1} \tag{B11}$$

For the estimator of the parameter, vector $\underline{\hat{x}}(m)$ follows directly

$$\underline{\hat{x}}(m) = P(m)\underline{b}(m) = P(m)\underline{b}(m-1) + P(m)\underline{h}(m)r(m)^{-1}z(m)$$

$$= P(m)\underline{b}(m-1) + \underline{k}(m)z(m) = P(m-1)\underline{b}(m-1) - \underline{k}(m)\underline{h}^t(m)P(m-1)\underline{b}(m-1)$$

$$+ \underline{k}(m)z(m)$$

This yields

$$\underline{\hat{x}}(m) = \underline{\hat{x}}(m-1) + \underline{k}(m)\{z(m) - \underline{h}^t(m)\underline{\hat{x}}(m-1)\} \tag{B12}$$

Equations B9, B10 and B12 describe the recursive least-squares algorithm.

The authors thank Dr. F. W. Pijpers for his contributions to theoretical discussions, Drs. H. S. Scholberg for evaluating the manuscript, and the Netherlands Z.W.O. for financial support.

REFERENCES

1 G. Gottschalk, Talanta, 20 (1973) 811.
2 H. Malissa and J. Rendl, Talanta, 22 (1975) 597.
3 R. E. Kalman, P. L. Falb and M. A. Arbib, Topics in Mathematical System Theory, McGraw-Hill, New York, 1969.
4 L. Aarons, Analyst, 106 (1981) 1249.
5 S. Ebel, E. Glasen, S. Abdulla, U. Steffens and V. Walter, Fresenius Z. Anal. Chem., 313 (1982) 24.
6 K. Eckschlager and V. Stepaneck, Anal. Chem., 54 (1982) 1115A.
7 C. R. Rao, Linear Statistical Interference and its Applications, Wiley, New York, 1965.
8 D. A. Harville, in J. N. Srivastava (Ed.), Statistical Design and Linear Models, North Holland America/Elsevier, New York, 1975.
9 V. V. Fedorov, Theory of Optimal Experiments, Academic Press, New York, 1972.
10 A. Gelb (Ed.), Applied Optimal Estimation, MIT Press, Cambridge, MA, 1974.
11 H. N. J. Poulisse, Anal. Chim. Acta, 112 (1979) 361.
12 H. N. J. Poulisse and P. Engelen, Anal. Lett., 13 (1980) 921.
13 F. Ayres, Matrices, Schaum Outline Series, McGraw-Hill, New York, 1974.
14 S. Lipschutz, Linear Algebra, Schaum Outline Series, McGraw-Hill, New York, 1968.
15 H. W. Sorenson, Parameter Estimation, M. Dekker, New York, 1980.
16 D. Graupe, Identification of Systems, R. E. Krieger, New York, 1972.
17 P. C. Thijssen, S. M. Wolfrum, G. Kateman and H. C. Smit, Anal. Chim. Acta, 156 (1984) in press.
18 J. H. Kalivas, Anal. Chem., 55 (1983) 565.
19 B. Vandeginste, J. Klaessens and G. Kateman, Anal. Chim. Acta, 150 (1983) 71.

Analytica Chimica Acta, 157 (1984) 117—124
Elsevier Science Publishers B.V., Amsterdam — Printed in The Netherlands

A RAPID-SCANNING ELECTRON PARAMAGNETIC RESONANCE SPECTROMETER WITH STOPPED-FLOW MIXING

STEPHEN A. JACOBS, GARY W. KRAMER, ROBERT E. SANTINI and DALE W. MARGERUM*

Department of Chemistry, Purdue University, West Lafayette, IN 47907 (U.S.A.)

(Received 18th August 1983)

SUMMARY

Modifications to a commercial electron paramagnetic resonance (e.p.r.) spectrometer are described which allow data to be obtained from 64 e.p.r. spectra (0.1—100 gauss per scan) with scan times of 0.010—0.900 s and with 0.020—900 s delay times between scans. Reagents are delivered into an e.p.r. cell from a stopped-flow mixer that triggers the generation of a microprocessor-controlled waveform to drive a rapid-scan unit. This digitally synthesized waveform is designed to correct inherent imperfections in the Helmholtz-type sweep coil circuit in the rapid-scan unit. The spectra are digitized (250 points per scan) and can be processed to determine rates of reaction. Performance of the system is demonstrated by the determination of the kinetics of rearrangement of a bis(dipeptide)nickelate(III) complex.

Methods which can identify the properties of transient intermediates are valuable in the characterization of rapid chemical processes. A common approach is to trap the intermediate, e.g., use of radical stabilizers or freeze-quenching. A more desirable approach is to examine directly the intermediates without disturbing their chemical or physical environment. Continuous- or stopped-flow techniques have been used in conjunction with a variety of spectrometers to study rapid reactions [1, 2]. Only a few kinetic techniques have been shown to produce complete time-resolved spectra: ultraviolet-visible [3], infrared [4], and electron paramagnetic resonance spectroscopy (e.p.r.) [5—8].

Several approaches have been used to obtain time-resolved e.p.r. spectra. Shiga [5] used a continuous flow of reagents to observe reactions which occurred within 5—30 ms after mixing. Spectral windows of up to 250 gauss were recorded in 2.5 min while consuming about 1 l of each reagent per determination. Kinetic information was obtained by varying the flow rate so that a different portion of the reaction profile was sampled. Although this approach is capable of millisecond time resolution [6], it requires prohibitively large volumes of reagents.

Gascoyne [7] has reported an instrument capable of obtaining time-resolved e.p.r. spectra while consuming 200 ml of each reagent. This was accomplished by collecting small spectral slices as a function of time which

0003-2670/84/$03.00

were later sorted into complete spectra. A computer-controlled stopped-flow arrangement was used to perform 400 experiments over 12.5 h. This novel approach reduces the amount of reagents consumed, but is appropriate only if the reactants are stable for many hours.

Sohma et al. [8] demonstrated that rapid sequential observation of e.p.r. spectra could be accomplished by repeatedly sweeping the magnetic flux in a sample using a pair of Helmholtz coils. Scan times as short as 20 ms, with an interval of 1.5 s between scans, were reported. Spectral windows as large as 250 gauss were generated with a saw-tooth waveform. Unfortunately, the generated fields were linear only up to 50 gauss.

The major disadvantages of the Shiga and Gascoyne techniques are the requirements for large reagent volumes and long measurement periods. These disadvantages become crucial for the characterization of costly and moderately stable systems, such as nickel(III) peptide complexes. The goals of the current work were to minimize the reagent volume and time required for a kinetic determination. An instrument is described which combines the rapid-scanning approach used by Sohma, with an improved waveform for field linearity, and the stopped-flow technique for low reagent consumption. This system permits rapid and repetitive e.p.r. scans of a reaction system. Stored data can be used for kinetic analysis.

Recently, the less common trivalent oxidation state of nickel (d^7 system) has been identified by e.p.r. to be present in biological systems [9—13]. Work in this laboratory has characterized nickel(III)—oligopeptide complexes in aqueous media [14, 15]. A novel series of bis(dipeptide)nickelate(III) complexes has been found, members of which are relatively stable in neutral solution, but undergo rapid rearrangement in acid followed by redox decomposition [16]. The mechanism of decomposition involves a transient intermediate, which has been shown to be also a nickel(III) complex by using the rapid-scan e.p.r. instrument described here.

EXPERIMENTAL

A Varian E-109 X band e.p.r. spectrometer, equipped with a phase-sensitive receiver referenced to 100-kHz fast field modulation, was modified in order to perform the rapid-scan, stopped-flow experiment.

A hand-driven pushblock, which simultaneously drives two 10-ml glass syringes, delivers the solutions into a quartz mixing/observation cell (Model WG-804 Wilmad). This cell is positioned in a Varian E-238, T_m mode cavity. A 0.05-ml dead volume exists between the observation chamber and two tangential mixing jets. Flow volumes up to 15 ml s^{-1} are possible, with a minimum dead time of approximately 3 ms. The dead time is the time required to fill the cavity from the point of mixing to the point of observation. Only 2—3 ml of each reagent are consumed per experiment. The flow is stopped at the drive syringes in order to minimize stress and mechanical vibration on the mixing/observation cell. A microswitch with an adjustable

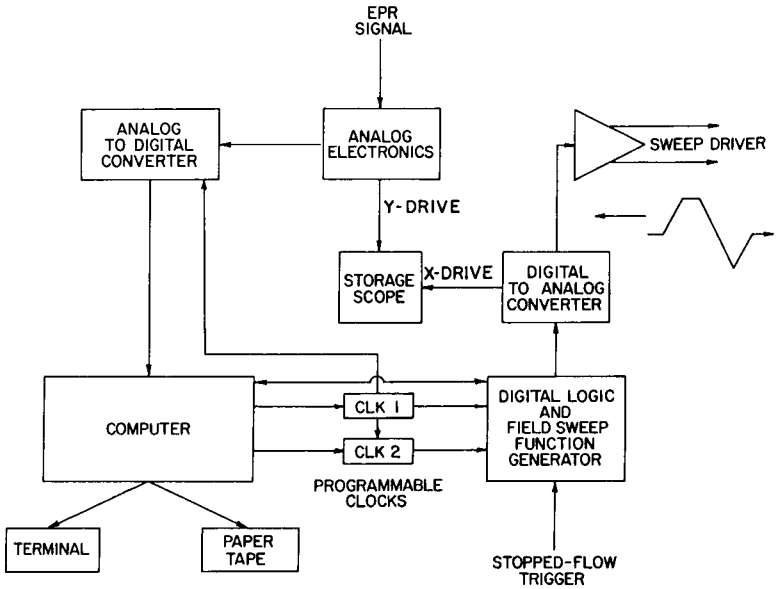

Fig. 1. Schematic diagram of the rapid-scanning e.p.r. instrument.

trigger point is located on the syringe drive pushblock to activate the rapid-scan sequence. A block diagram of the instrument is given in Fig. 1.

The demodulated signal from the e.p.r. spectrometer is amplified (—5 to +5 V full scale) and filtered (0.0—20.0 kHz; Frequency Devices 744 PB-5; adjustable low-pass, active filter). The conditioned signal is directed to the y-axis of a storage oscilloscope (Tektronix Model 603 A-21), and to a sample-and-hold amplifier (S/H; Analog Devices Model AD 583KD). The S/H feeds directly into a 10-bit analog-to-digital converter (ADC; Analog Devices Model AD571JD). Only the most significant bits of the ADC were actually used because the host microcomputer is based on an 8-bit processor. A signal proportional to the field sweep drives the x-axis of the storage oscilloscope. This provides a real-time display of the data.

The microcomputer is constructed around an 8080A microprocessor with 17K bytes of random-access memory and 2K bytes of programmable read-only memory. Four input/output ports and associated electronics were constructed to communicate with a system terminal, a paper-tape punch, the ADC and two programmable clocks.

After data acquisition is complete, the e.p.r. spectra (signal vs. field) vs. time data along with the experimental parameters (file name, identification code, data, cavity temperature, bulk field, scan time, delay time, scan amplitude, number of scans, filter frequency and cavity type) are transferred to paper-tape. These data were transferred to a remotely located Hewlett-Packard 2100 computer for processing and permanent storage. The system provides for subsequent implementation of a high-speed serial data link to the remote computer.

The programmable clocks are designed around a single 20.000-MHz crystal oscillator (Motorola K 1091A), countdown registers, digital multiplexers, down counters and pulse generators. The two clocks are programmed to set the times for the field sweep and the delay between scans. These two periods are the variable portions of the rapid-scan waveform.

Initiation of the rapid-scan sequence and data acquisition comes from the trigger pulse generated at the end of the stopped-flow push. Figure 2 gives one cycle of a voltage vs. time waveform which controls the magnetic field sweep. There is a pre-scan delay (10 ms) prior to the actual field sweep for data acquisition. This delay consists of a 1 V ms^{-1} slew to the initial voltage (i.e., magnetic field value) followed by a 5-ms pause to allow the magnetic field to stabilize. This set-up sequence is crucial to avoid ringing or other non-linearities in the response of the sweeping magnetic field with respect to the input waveform. A similar 10-ms sequence is used at the end of each full sweep as a reset action which returns the drive voltage to zero output (i.e., center field). Returning the sweeping field to zero eliminates resistive heating in the field sweep coils during idle periods. After the reset sequence, there is a wait period which is controlled by the delay programmable clock.

The actual field sweep voltage is a digitally synthesized waveform consisting of 500 steps. The pulses from the programmable field-sweep clock cycle an 8-bit up/down counter. The value from the counter feeds an 8-bit digital-to-analog (DAC) converter. The resulting analog voltage is buffered and passes through an electronic polarity switch. The polarity switch determines the sign of the sweeping field. At the beginning of the sweep, the counter is loaded with a value of 250 and the polarity switch is set positive. The analog voltage output is initially +5 V; the counter is then counted down to zero. A digital zero detector circuit then switches the polarity

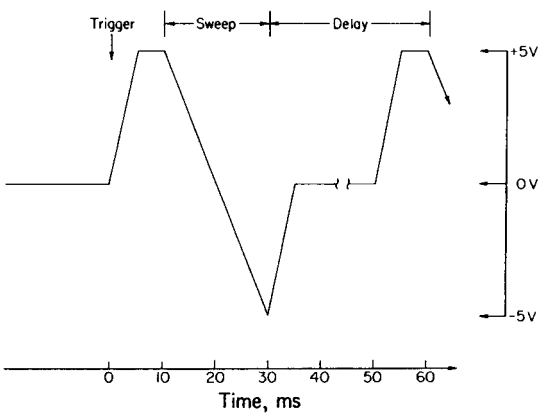

Fig. 2. One cycle of the rapid-scan voltage vs. time waveform.

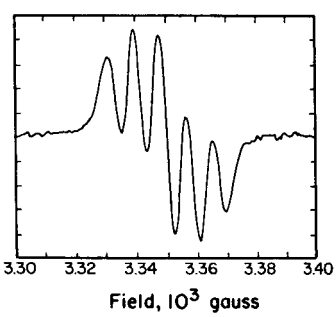

Fig. 3. Calibration spectrum of DPPH in benzene with a scan time of 0.1 s.

switch to a negative output and causes the counter to count up. The next 250 clock pulses generate the 0 to −5 V portion of the waveform. The result is a digital voltage vs. time waveform from +5 to −5 V with a resolution of 20 mV/step and a slew rate defined by the programmable clock.

The field sweep coil driver is based on a Varian E-271 power amplifier. The amplifier is configured, for this application, as an operational current source with the sweep coils in the feedback loop. Appropriate external compensation was provided to optimize the linearity of the sweeping magnetic field.

The sweep coils are mounted coaxially with a T_m mode e.p.r. cavity (Varian E-238) and outside the 100-kHz field modulation coils. The field sweep, as described above, is intended to drop to one-half the value of the selected sweep range, sweep through the center field, and on up to one-half of the selected sweep range, before settling back to the center field. The center field value of the e.p.r. magnet is regulated with a Hall sensor. This sensor is located off-axis in the magnet gap, beyond the fringing field of the sweep coils. The exact position of the Hall sensor was chosen empirically in order to minimize interaction between the magnet field regulation control loop and the sweeping field. Scan times as short as 10 ms do not degrade the linearity of the field. The characteristics of the final system are listed in Table 1.

Calibration

The adjustment procedures necessary for calibration of the E-271 unit were as described by the manufacturer. The scan amplitude and field calibrations were done with a dilute sample of DPPH (α,α'-diphenyl-β-picrylhydrazyl) in benzene. Scans from the E-109 console operated in its standard mode were comparable to those from the rapid-scan unit. A field sweep of 100 gauss was used. This required 4 min for the E-109 normal mode and 0.1 s for the rapid-scan mode. The output from the rapid-scan measurement (Fig. 3) was found to be symmetrical when either phase or scan direction was reversed. This indicates that the induced field produced by the rapid-scan coils is both homogeneous and linear.

Microwave frequencies were routinely measured with an adjustable absorption type cavity (Microlab FXR, Model X410B). The calibration of this cavity was confirmed by using a Hewlett-Packard 5342A direct-reading microwave counter. In normal use, the adjustable cavity is inserted into a

TABLE 1

Characteristics of rapid-scan e.p.r. system

Scan time	0.01—0.900 s	Field sweep	0.1—100 gauss
Delay time	0.02—900 s	No. of scans	1—64
Minimum half-life	$\geq$0.07 s	No. of points/scan	250
Maximum k	$\leq 10\ s^{-1}$ (first-order)	Signal band width	0.0—20.0 kHz

nulling circuit which normalized its frequency response such that the circuit indicated an unbalanced reading only when the cavity was correctly tuned to the frequency of the e.p.r. microwave source.

Application

The rapid-scanning stopped-flow e.p.r. spectrometer has been used in this laboratory to identify a transient intermediate in the decomposition of bis(dipeptide)nickelate(III) complexes [16]. There are two major sequential steps which are detachable by this technique. Typical results are given in Figs. 4—6. Figure 4 shows that the first step in the decomposition process is an intramolecular rearrangement or similar process which does not alter the trivalent oxidation state of the nickel. Figure 5 shows that the nickel(III) intermediate undergoes a redox reaction which results in diamagnetic products. The general scheme is

$$^{A}\text{Ni(III)} \rightarrow {}^{B}\text{Ni(III)} \rightarrow {}^{C}\text{Ni(II)}$$

Based on the u.v.-visible kinetic studies, the assignment of the +3 oxidation state to intermediate (B) was not possible, but it is clearly seen in the rapid-scan e.p.r. results. Kinetic information is also present in the e.p.r. rapid-scan data. Figure 6 shows the response vs. time profile for the data given in Fig. 5 where the dashed vertical line indicates the field value used for kinetic studies. Also included in Fig. 6 are the residuals (calculated − observed)

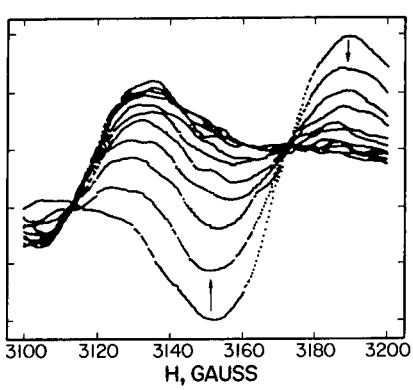

Fig. 4. Rapid-scan spectra of the first step in the acid-catalyzed decomposition of a bis(dipeptide)nickelate(III) complex. Scan time 0.020 s; delay time 0.050 s; every sixth spectrum displayed starting with scan number 2; 0.35 s between spectra.

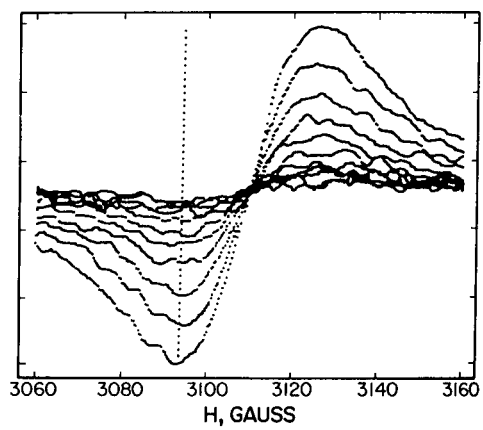

Fig. 5. Rapid-scan spectra for the second step in the acid-catalyzed decomposition of a bis(dipeptide)nickelate(III) complex. Scan time 0.100 s; delay time 0.510 s; every sixth spectrum displayed starting with scan number 2; 3.05 s between spectra.

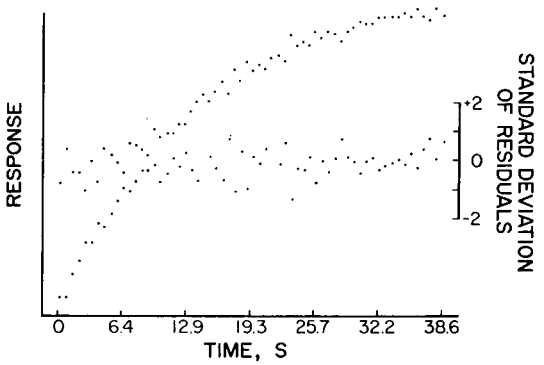

Fig. 6. Response vs. time, for the data in Fig. 5: 3094 gauss; 0.61 s between points; $k_{obs} = 0.075 \pm 0.001\ s^{-1}$.

from fitting the data to the model given by

$$(R_t - R_\infty)/(R_0 - R_\infty) = \exp(-kt) \quad (1)$$

where R_0 is the response at zero time, R_∞ is the response at infinite t, R_t is the response as a function of t, and k is the first-order rate constant. No values were assumed for R_0, R_∞, or k. Rather, Eqn. 1 was treated as a non-linear model and the variables were resolved using the approach developed for optical spectroscopy [17]. The resolved rate constants were independent (less than 5%) of scan time, delay time, and field value.

Conclusion

The rapid-scanning stopped-flow e.p.r. apparatus has been shown to be useful for both qualitative and quantitative investigations of the kinetics and mechanism of a reaction involving a paramagnetic center. Table 1 summarizes the characteristics of the system. Additional versatility is inherent from the modular nature of the system. For example, the stopped-flow portion can be replaced by an electrolytic cell assembly or the sample can be optically irradiated. In this configuration, simultaneous e.p.r. spectra and voltammograms or optical spectra could be recorded.

This investigation was supported by Public Health Grant No. GM-12152 from the National Institute of General Medical Sciences.

REFERENCES

1 J. J. Gettings and E. Wyn-Jones (Eds.), Techniques and Application of Fast Reactions in Solution, Reidel, Boston, MA, 1979.
2 B. Chance, R. H. Eisenhart, Q. H. Gibson and K. K. Louberg-Holm (Eds.), Rapid Mixing and Sampling Techniques in Biochemistry, Academic Press, New York, 1964.
3 H. L. Pardue, in J. K. Foreman and P. B. Stockwell (Eds.), Topics in Automatic Chemical Analysis, E. Horwood, Chichester, 1979, pp. 163—207.

4 J. P. Maher, in B. Chance, R. H. Eisenhart, Q. H. Gibson and K. K. Louberg-Holm (Eds.), Rapid Mixing and Sampling Techniques in Biochemistry, Academic Press, New York, 1964, pp. 29–34.
5 T. Shiga, J. Phys. Chem., 69 (1965) 3805.
6 T. Shiga and K. Imaizumi, Arch. Biochem. Biophys., 167 (1975) 469.
7 P. R. C. Gascoyne, J. Phys. E. Sci. Instrum., 14 (1981) 62.
8 J. Sohma, T. Komatsu and Y. Kanda, Jpn. J. Appl. Phys., 7 (1968) 298.
9 A. J. Thomson, Nature, 298 (1982) 602.
10 R. Cammack, D. Patil, R. Aguirre and E. C. Hatchikian, FEBS Lett., 142 (1982) 289.
11 J. LeGall, P. O. Ljungdahl, I. Moura, H. D. Peck, A. V. Xavier, J. J. Moura, M. Teixera, B. H. Huynh and D. V. DeVartanian, Biochem. Biophys. Res. Commun., 106 (1982) 610.
12 S. P. J. Albracht, E. G. Graf and R. K. Thauer, FEBS Lett., 140 (1982) 311.
13 J. R. Lancaster, FEBS Lett., 115 (1980) 285.
14 C. K. Murray and D. W. Margerum, Inorg. Chem., 21 (1982) 3501; 22 (1983) 463.
15 D. W. Margerum, Pure Appl. Chem., 55 (1983) 23; ACS Adv. Chem. Ser., No. 198 (1982) 3.
16 S. A. Jacobs and D. W. Margerum, Inorg. Chem., 23 (1984) in press.
17 G. M. Ridder, Ph. D. Thesis, Purdue University, 1977.

Analytica Chimica Acta, 157 (1984) 125—133
Elsevier Science Publishers B.V., Amsterdam — Printed in The Netherlands

ENZYMATIC FLUORIMETRIC DETERMINATION OF CHOLIC ACID AND CHENODEOXYCHOLIC ACID IN AQUEOUS SOLUTIONS AND BLOOD SERUM USING A DIFFERENTIAL KINETIC METHOD

A. PAPANASTASIOU-DIAMANDI, P. A. SISKOS and T. P. HADJIIOANNOU*

Laboratory of Analytical Chemistry, University of Athens, 104 Solonos Str., Athens 144 (Greece)

(Received 14th July 1983)

SUMMARY

An enzymatic fluorimetric method is described for the determination of chenodeoxycholic acid and its conjugates and of cholic acid and its conjugates in aqueous solutions and serum. The method is based on the oxidation of 7α-hydroxy bile acids by β-NAD^+ in the presence of 7α-hydroxysteroid dehydrogenase; the NADH produced is monitored fluorimetrically. Chenodeoxycholic acid is determined in the presence of cholic acid by a differential kinetic procedure; the sum of the two acids (primary bile acids) is determined by an equilibrium procedure, and cholic acid is calculated by difference. The r.s.d. was ca. 3% and 10% for aqueous solutions and sera, respectively. Recoveries of chenodeoxycholic acid, cholic acid and primary bile acids added to serum samples averaged 100.5, 105.1, and 102.9%, respectively. Ten samples can be analyzed per working day.

The determination of serum total bile acids in the postprandial state is a sensitive screening test for hepatobiliary disease [1]. The determination of cholic acid (CA) and chenodeoxycholic acid (CDCA), the two predominant bile acids of serum, has additional diagnostic value in differentiating various forms of liver disease [2, 3]. Several methods have been developed for the determination of bile acids, such as gas-liquid chromatography [3, 4], high-performance liquid chromatography [5], radioimmunoassay [6, 7], fluoro-immunoassay [8] and various enzymatic methods [9—15]. The enzymatic methods are most suitable for routine clinical determination because they combine simplicity with low cost [16]. They are based on the conversion of the 3α-, 7α- or 12α-hydroxy bile acids to 3-oxo, 7-oxo or 12-oxo bile acids by β-NAD^+, in the presence of 3α-, 7α- or 12α-hydroxysteroid dehydrogenase (HSD), respectively, and measurement of the generated NADH by u.v. or fluorescence spectrometry. At present, only the total 3α-bile acids (cholic acid, CDCA, deoxycholic acid, and their tauro- or glyco-conjugates), or the total 7α-bile acids (cholic acid, CDCA and their conjugates) have been determined with commercially available enzymes. All published enzymatic methods are end-point methods.

0003-2670/84/$03.00

In this paper, a differential kinetic enzymatic method is described for the determination of cholic acid and chenodeoxycholic acid and their conjugates without prior separation of the acids. The bile acids react with β-NAD^+ in the presence of 7α-HSD and the NADH produced is measured fluorimetrically. The CDCA is determined by a differential kinetic method using proportional equations, and the total primary bile acids (cholic acid and CDCA) is determined by an equilibrium procedure; cholic acid is calculated by difference.

EXPERIMENTAL

Apparatus

A Perkin-Elmer Model 512 double-beam fluorescence spectrometer with a 150-W xenon lamp was used. All measurements were done with standard rectangular cells of 1.000-cm path length, made of fluorescence-free fused silica. The cell compartment was modified so that a magnetic stirrer could be placed under the sample cell holder. A constant temperature of 25.0 ± 0.1°C in the sample cell was maintained by using a water bath (Model ST, Sargent, Chicago). The fluorimetric signals were recorded on a Perkin-Elmer Model 56 potentiometric recorder. The following instrumental settings were used: ratio mode, dynode voltage 750 V, excitation wavelength 350 nm with a slit-width of 20 nm, emission wavelength 455 nm with a slit-width of 20 nm. The sensitivity scaling factor used to measure fluorescence intensity was at the X10 and X3 positions for the kinetic and equilibrium measurements, respectively.

Reagents

All solutions were prepared in deionized, twice-distilled water from reagent-grade materials, unless otherwise stated. 7α-Hydroxysteroid dehydrogenase (HSD; E.C. 1.1.1.159; Worthington Biochemicals Corp., Freehold, NJ) was supplied as powder obtained from *E. coli* with an activity of 0.5 U mg^{-1}. An enzyme stock solution (3.0 U ml^{-1}) was prepared in 0.020 M Tris—0.0020 M EDTA buffer, pH 7.2. This solution was frozen at —20°C when not in use and was stable for at least a week. A working enzyme solution of 0.125 U ml^{-1} was prepared daily by dilution of the stock solution with the above buffer [17].

A 0.0100 M solution of β-NAD^+ (Calbiochem, San Diego, CA) was prepared by dissolving 0.0717 g of β-NAD^+ (grade A) in 10.0 ml of water. When refrigerated this solution is stable for at least 2 weeks. A 0.10 M glycine buffer, pH 9.5, containing EDTA (0.005 M) was prepared by dissolving 1.88 g of glycine and 0.465 g of $Na_2EDTA \cdot 2H_2O$ in ca. 200 ml of water, adjusting the pH to 9.5 with 5 M sodium hydroxide and diluting to 250 ml. A 1.5 M hydrazine solution, pH 9.5, was prepared by dissolving 19.5 g of hydrazine sulfate in ca. 80 ml of water, adjusting the pH to 9.5 with 5 M sodium hydroxide and diluting to 100 ml.

Bile acids were purchased from Calbiochem; 1.000×10^{-3} M stock solutions of cholic acid, glycocholic acid, taurocholic, chenodeoxycholic acid, glycochenodeoxycholic acid and taurochenodeoxycholic acid were prepared

by dissolving appropriate amounts of their sodium salts in water. More dilute solutions were prepared as needed by dilution with water. The CDCA solutions containing 5% albumin were prepared by mixing appropriate volumes of the stock solution and a 25% bovine albumin solution and diluting with water.

Zinc sulfate solution was prepared by dissolving 10.0 g of $ZnSO_4 \cdot 7H_2O$ in 100 ml of water. The barium hydroxide solution was prepared by dissolving 6.0 g of $Ba(OH)_2 \cdot 8H_2O$ in 100 ml of freshly boiled water. This solution was filtered through glass wool and stored in a firmly stoppered plastic container. The ether/heptane mixture was 1:1 (v/v).

Procedures

Kinetic studies. Pipet into the cell 1.60 ml of glycine buffer, 0.200 ml of bile acid solution (cholic acid or CDCA) and 0.100 ml of enzyme solution, and start the stirrer. After the fluorescence signal has stabilized (ca. 1 min), inject 0.100 ml of β-NAD^+ solution and record the fluorescence intensity for about 2 min.

Sequential determination of CDCA and cholic acid in aqueous mixtures (equilibrium procedure). Pipet into the cell 1.60 ml of glycine buffer, 0.200 ml of CDCA standard or sample solution and 0.100 ml of 0.125 U ml^{-1} enzyme solution, and start the stirrer. After the fluorescence signal has stabilized, inject 0.100 ml of β-NAD^+ solution and record the fluorescence intensity for 2 min. Change immediately the instrumental sensitivity from X10 to X3, inject 0.100 ml of 3.0 U ml^{-1} enzyme solution and 0.100 ml of hydrazine sulfate solution, and record the fluorescence intensity until the signal reaches its maximum value (ca. 2 min).

Determination of CDCA and cholic acid in serum. For the isolation of bile acids, transfer 5.0 ml of absolute ethanol to a 25-ml centrifuge tube and boil in a boiling water bath. Add dropwise while stirring 1.00 ml of standard CDCA solution in 5% albumin or serum. Add 0.40 ml of barium hydroxide solution and boil the mixture in the boiling water bath for 2 min. Add 0.20 ml of zinc sulfate solution and mix thoroughly. Centrifuge at 3000 rpm for 10 min and decant the supernatant liquid into a 15-ml stoppered centrifuge tube. Wash the residue with 2.0 ml of absolute ethanol, boil in the boiling water bath for 2 min, centrifuge again and add the supernatant liquid to the stoppered tube. Evaporate the ethanolic solution to dryness at 70°C under a nitrogen stream and dissolve the residue in 3.0 ml of 50%(v/v) ethanol. Add 6.0 ml of ether/heptane mixture and shake in a shaker for 20 min. Centrifuge at 1500 rpm for 5 min and discard the upper phase. Evaporate the ethanolic (lower) phase to dryness as above and dissolve the residue in 5.00 ml of glycine buffer (this gives solution A).

For the kinetic determination of CDCA, pipet into the cell 2.00 ml of solution A and 0.100 ml of β-NAD^+ solution, and start the stirrer. After the fluorescence signal has stabilized, inject 0.100 ml of 0.125 U ml^{-1} enzyme solution and record the fluorescence intensity for ca. 3 min. Empty the cell by aspiration and wash it with water.

For the equilibrium determination of CDCA and cholic acid, pipet into the cell 2.0 ml of solution A, 0.100 ml of 3.0 U ml^{-1} enzyme solution and 0.100 ml of hydrazine sulfate solution, and start the stirrer. After the fluorescence signal has stabilized, inject 0.100 ml of β-NAD^+ solution and record the fluorescence intensity until the signal reaches its maximum value (5—10 min).

RESULTS AND DISCUSSION

The enzymatic fluorimetric method was developed in two stages. The first stage involved optimization of the quantitative aspects of the enzymatic reaction in known aqueous bile acid solutions in the presence and absence of compounds that could affect the kinetics and fluorescence of the enzymatic reaction of bile acids in serum samples. The second step was to establish the applicability of the newly developed enzymatic procedures to the determination of individual primary bile acids in serum, after removal of interferences, without prior separation of the acids.

Studies of the bile acids/β-NAD^+/7α-HSD reaction

7α-Hydroxysteroid dehydrogenase can be obtained from different bacterial strains [10, 18—21]. The commercial 7α-HSD from *E. coli* exhibits satisfactory kinetic differences for cholic acid and CDCA [21] and this enzyme was therefore chosen for these kinetic studies. In order to establish the optimal experimental conditions for the differential kinetic method, various parameters were studied [18]. The optimal pH for the kinetic determination of CDCA in the presence of cholic acid is 9.5, within the range 8.5—10.0 studied. This gives the maximum difference in reaction rates for the two acids and is also the optimum pH for the enzyme 7α-HSD [21]. At a final β-NAD^+ concentration $>5 \times 10^{-4}$ M (range studied 2.5×10^{-4}—2.5×10^{-3} M) the reaction rates for CDCA and cholic acid were constant, whereas the background fluorescence increased with increasing β-NAD^+ concentration. Therefore, a 5×10^{-4} M final concentration was chosen as optimal. Glycine, pyrophosphate and ethanolamine buffers were tested. Although the ratio of the apparent reaction rate constants [22] for CDCA and cholic acid is 43% larger in ethanolamine than in glycine or pyrophosphate buffer, ethanolamine is not the best buffer because of its relatively high background fluorescence. Therefore, a 0.10 M glycine buffer was chosen for the quantitative applications. The reaction rates of glycochenodeoxycholic acid and glycocholic acid increased with increasing enzyme concentration, but the ratio of their rate constants remained constant. A final concentration of 0.00625 U ml^{-1} was chosen so as to obtain a high fluorescence change in a short time interval.

Calibration graphs of initial reaction rate (ΔF min^{-1}) vs. bile acid concentration (where ΔF is the fluorescence change) obtained with equimolar aqueous solutions of CDCA and its glyco- and tauro-conjugates, were identical. Typical calibration equations for CDCA and cholic acid (CA) in aqueous

solution are $\Delta F\ min^{-1} = 0.290[CDCA] + 0.600$ and $\Delta F\ min^{-1} = 0.035[CA] - 0.260$.

Thus CDCA reacts with β-NAD^+ in the presence of 7α-HSD 8.3 times faster than cholic acid. When CDCA is determined kinetically in the presence of cholic acid, a positive error results which is proportional to the cholic acid concentration (Table 1). However, this error can be eliminated (Table 1, last column), if the contribution of cholic acid to the total reaction rate is taken into consideration as follows

$$[CDCA]_{uncorr.} = [CDCA] + R[CA] \quad (1)$$

where $[CDCA]_{uncorr.}$ is the uncorrected concentration of CDCA determined from a kinetic calibration graph (initial reaction rate vs. [CDCA]), and R is the ratio of the proportionality constants in the calibration equations above (in the present case, $R = 0.035/0.290 = 0.121$).

Typical recorded curves of the change in fluorescence with time for the sequential determination of CDCA and the sum of CDCA and cholic acid are shown in Fig. 1. From the equilibrium calibration graph (maximum fluorescence intensity vs. [PBA], with CDCA solutions used for calibration) [PBA] is determined. As [PBA] = [CA] + [CDCA], Eqn. 1 can be rewritten so that the concentrations of CDCA and cholic acid in mixtures can be calculated:

$$[CA] = ([PBA] - [CDCA]_{uncorr.})/(1 - R) \quad (2)$$

$$[CDCA] = [PBA] - ([PBA] - [CDCA]_{uncorr.})/(1 - R) \quad (3)$$

Table 2 shows the results for the sequential determination of CDCA and cholic acid in aqueous solutions of known concentrations. The relative standard deviation for 30 μM CDCA was 2.5% (n = 8) and 1.5% (n = 5) for the kinetic and equilibrium procedures, respectively.

Determination of CDCA and cholic acid in serum

After conditions had been established for the measurement of CDCA and cholic acid in aqueous mixtures without prior separation, the applicability of

TABLE 1

Results for the kinetic determination of CDCA in the presence of cholic acid (CA) in aqueous solutions

[CDCA]/[CA][a]	$\Delta F\ min^{-1}$	$[CDCA]^{b}_{uncorr.}$ (μM)	Error (%)	$[CDCA]_{corr.}$ (μM)	Error (%)
1:0	10.4	30.4	+1.3	30.4	+1.3
1:1	11.6	33.8	+12.7	30.2	+0.7
1:2	12.6	36.7	+22.3	29.4	−2.0
1:3	13.8	40.1	+33.7	29.2	−2.7

[a][CDCA] = 30 μM. [b]From calibration graph.

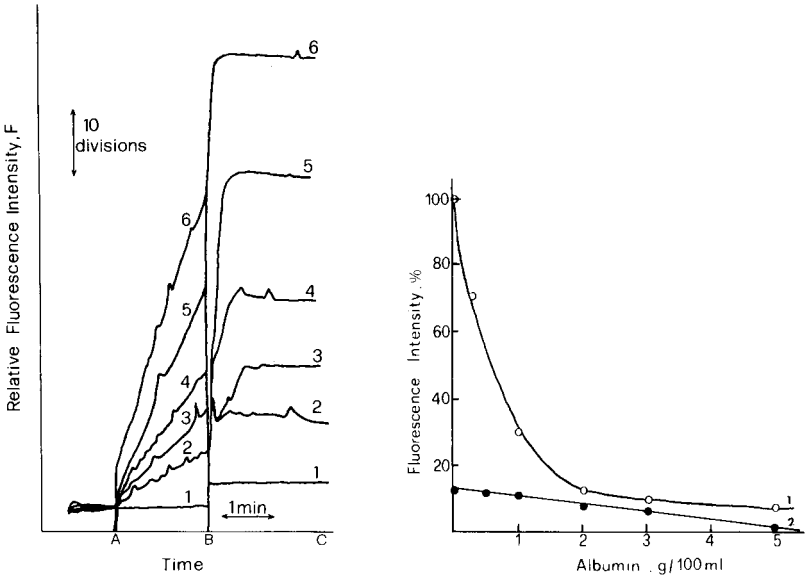

Fig. 1. Recorded fluorescence changes for the sequential determination of chenodeoxycholic acid (AB) and the sum of cholic acid and chenodeoxycholic acid (BC) in aqueous solutions in the same cuvette. Standard solutions of CDCA: (1) blank; (2) 12; (3) 24; (4) 36; (5) 60; (6) 84 μM.

Fig. 2. Effect of albumin concentration on the initial reaction rate of: (○) chenodeoxycholic acid; (●) cholic acid. The initial rate for CDCA is taken as 100%; [CDCA] = [CA] = 84 μM. Other conditions as in procedure for kinetic studies.

TABLE 2

Results for the sequential determination of CDCA and cholic acid in aqueous solutions

Bile acid concentration (μM)								
Taken[a]			Found[b]			Error (%)		
[CDCA] + [CA]	[CDCA]	[CA]	[CDCA] + [CA][c]	[CDCA][d]	[CA][e]	[CDCA] + [CA]	[CDCA]	[CA]
12.0	9.6	2.4	11.8	9.6	2.2	−1.7	—	−8.3
30.0	15.0	15.0	31.4	13.9	17.5	+4.7	−7.3	+16.7
42.0	8.4	33.6	41.5	10.0	31.5	−1.2	+19.0	−6.2
42.0	21.0	21.0	41.5	21.2	20.3	−1.2	+1.0	−3.3

[a]Initial concentrations. [b]Single runs. [c]Equilibrium procedure; the equation of the calibration graph is $\Delta F = 0.845[PBA] - 1.18$. [d]Calculated from the equation of the kinetic calibration graph and Eqn. 3. [e]Calculated from Eqn. 2.

these procedures to the determination of these acids in serum was examined. The method involves the removal of proteins, bilirubin and lipids, prior to the measurement steps, because it was found that they interfere with the kinetic determination. The effect of albumin on the reaction rate is shown in Fig. 2. A similar effect was observed with 3α-HSD [12, 23]. The presence of bilirubin led to negative errors in both the kinetic and equilibrium procedures because bilirubin quenches both the excitation and emission photons for NADH fluorescence [12]. Lipids quenched the fluorescence and gave turbid solutions. Proteins were removed with ethanol, whereas bilirubin was removed partly during deproteinization and partly by treatment with the barium hydroxide/zinc sulfate mixture. Lipids were removed by extraction with a 1:1 ether/heptane mixture [24, 25].

The calibration graphs for the kinetic and equilibrium determinations were obtained from measurements made on standard aqueous solutions of CDCA containing 5% bovine albumin. The standards were treated in the same manner as the serum samples. The linearity of both graphs extended up to 84 μM. The relative standard deviations for a 32 μM equimolar mixture of CDCA and cholic acid in 5% albumin were 10% (n = 9) and 3.7% (n = 9) for the kinetic and equilibrium procedures, respectively. The accuracy of the method was checked with recovery experiments in which CDCA or cholic

TABLE 3

Recovery of CDCA and cholic acid added to serum samples (differential kinetic—equilibrium procedure)

Bile acid concentration (μM)						Recovery (%)	
Initially present		Added		Found[a]		[CDCA]	[CA]
[CDCA]	[CA]	[CDCA]	[CA]	[CDCA][b]	[CA][c]		
3.3	2.7	8.80	3.00	12.04	5.86	99	105
3.3	2.7	28.6	—	31.2	2.7	98	—
3.3	2.7	33.3	10.1	71.3	20.5	114	103
2.7	2.9	40.4	20.3	39.4	25.0	91	109
2.7	2.9	52.2	26.1	61.1	30.2	112	105
4.0	4.0	28.6	—	27.5	8.0[d]	82	—
4.0	4.0	16.5	33.0	23.7	39.6	119	108
4.0	4.0	5.40	22.9	9.40	30.4	100	115
2.0	2.0	11.1	—	12.9	2.0	98	—
2.0	2.0	21.4	—	23.4	2.0	100	—
2.0	2.0	15.7	15.7	19.1	17.0	109	96
2.0	2.0	40.9	—	42.9	2.0	100	—
4.0	4.0	11.0	—	13.7	4.0	88	—
4.0	4.0	—	21.4	4.0	24.4	—	95
4.0	4.0	—	40.9	4.0	49.0	—	110
					Mean ± s.d.	100.5 ± 10.2	105.1 ± 6.5

[a]Single runs. [b]From Eqn. 3. [c]From Eqn. 2.

TABLE 4

Recovery of PBA added to serum samples (equilibrium procedure)

Primary bile acid concentration (μM)				Recovery (%)
Initially present	Added	Total	Found[a]	
6.0	11.8	17.8	17.9	101
6.0	28.6	34.6	33.9	98
6.0	43.4	49.4	54.4	112
5.6	60.7	66.3	64.4	97
5.6	78.3	83.9	91.3	109
8.0	28.6	36.6	36.6	100
8.0	49.5	57.5	63.3	112
8.0	28.3	36.3	39.8	112
4.0	11.1	15.1	14.9	98
4.0	21.4	25.4	25.4	100
4.0	31.4	35.4	36.1	102
4.0	40.9	44.9	44.9	100
8.0	11.0	19.0	17.7	88
8.0	40.9	48.9	54.3	113
8.0	21.4	29.4	28.4	95
8.0	40.9	48.9	53.0	110
			Mean ± s.d.	102.9 ± 7.5

[a]Single runs.

acid or both were added to serum samples. The recoveries ranged from 82 to 119% for CDCA (average 100.5%), from 95 to 115% for cholic acid (average 105.1%), and from 95 to 113% for PBA (average 102.9%). Tables 3 and 4 show typical results from the recovery studies. Results for four normal serum samples were found to be below 9 μM (5.9 ± 1.6) and compared well with normal values obtained by enzymatic fluorimetry [26]. The method is therefore suitable for the determination of chenodeoxycholic acid and cholic acid in serum without prior separation. It can be used for routine clinical purposes; ten samples can be analyzed in a working day.

The authors thank Dr. D. S. Papastathopoulos for technical assistance in adapting the magnetic stirrer to the instrument.

REFERENCES

1 S. Barnes, G. A. Gallo, D. B. Trash and J. S. Morris, J. Clin. Pathol., 28 (1975) 506.
2 J. B. Carey Jr., J. Clin. Invest., 37 (1958) 1494.
3 G. P. Van Berge-Henegouwen, A. Ruben and K.-H. Brandt, Clin. Chim. Acta, 54 (1974) 249.
4 G. Karlaganis and G. Paumgartner, J. Lipid Res., 19 (1978) 771.
5 F. Nakagama and M. Nakagaki, J. Chromatogr., 183 (1980) 287.

6 L. M. Demers and G. Hepner, Clin. Chem., 22 (1976) 602.
7 S. W. Scalm, G. P. Van Berge-Henegouwen, A. F. Hosmann, A. E. Couwen and J. Turcotte, Gastroenterology, 73 (1977) 285.
8 F. A. Shridi, A. Chitranukroh, M. Pourfarzaneh, B. H. Billing and G. Ekeke, Ann. Clin. Biochem., 17 (1980) 188.
9 G. A. D. Haslewood, G. M. Murphy and J. M. Richardson, Clin. Sci., 44 (1973) 95.
10 B. A. Skalhegg and O. Fausa, Scand. J. Gastroenterol., 12 (1977) 433.
11 O. Fausa and B. A. Skalhegg, Scand. J. Gastroenterol., 12 (1977) 441.
12 P. A. Siskos, P. T. Cahill and N. B. Javitt, J. Lipid Res., 18 (1977) 666.
13 F. Mashige, N. Tanaka, A. Maki, S. Kamei and M. Yamanaka, Clin. Chem., 27 (1981) 1352.
14 M. J. Crowell and I. A. Macdonald, Clin. Chem., 26 (1980) 1298.
15 I. A. Macdonald, N. C. Williams and B. C. Musial, J. Lipid Res., 21 (1980) 381.
16 N. B. Javitt, K. Budai, P-Y. Shan, P. A. Siskos and P. T. Cahill, in G. Paumgartner, A. Stiehl and W. Gerak (Eds.), Biological Effects of Bile Acids, MTP Ltd., Lancaster, 1979, p. 267.
17 L. A. Deker (Ed.), The Worthington Enzyme Manual, Worthington Biochemical Corp., Freehold, NJ, 1977.
18 H. U. Bergmeyer (Ed.), Principles of Enzymatic Analysis, Verlag-Chemie, Weinheim, 1978, pp. 13—91.
19 I. A. Macdonald, N. C. Williams, D. E. Mahony and W. M. Christie, Biochim. Biophys. Acta, 384 (1975) 12.
20 J. A. Sherrod and P. B. Hylemon, Biochim. Biophys. Acta, 486 (1977) 351.
21 I. A. Macdonald, C. N. Williams and D. E. Mahony, Biochim. Biophys. Acta, 309 (1973) 243.
22 P. A. Siskos, S. M. Tzouwara and S. M. Phillianos, Anal. Lett., 13(B18) (1980) 1589.
23 H. Steensland, Scand. J. Clin. Lab. Invest., 38 (1978) 447.
24 E. J. Mroszzak and S. Riegelman, Clin. Chem., 18 (1972) 987.
25 G. M. Murphy, B. H. Billing and D. N. Baron, J. Clin. Pathol., 23 (1970) 594.
26 K. Kobayashi, R. M. Allen, J. R. Bloomer and G. Klatskin, J. Am. Med. Assoc., 241 (1979) 2043.

Analytica Chimica Acta, 157 (1984) 135—142
Elsevier Science Publishers B.V., Amsterdam — Printed in The Netherlands

THE ATOMIC ABSORPTION SPECTROMETRIC DETERMINATION OF ARSENIC AND SELENIUM IN MINERAL WATERS BY ELECTROTHERMAL ATOMIZATION

V. HUDNIK and S. GOMIŠČEK*

Boris Kidrič Institute of Chemistry and Department of Chemistry and Chemical Technology, Edvard Kardelj University, Ljubljana (Yugoslavia)

(Received 13th June 1983)

SUMMARY

A procedure for the determination of arsenic and selenium in mineral waters based on electrothermal atomic absorption spectrometry is described. Because of matrix effects and the inadequate detection limits for direct determinations, both elements are separated from the macrocomponents by co-precipitation in hydrated iron(III) oxide. The precipitate is dissolved in 0.2 M sulphuric acid for injection. The detection limits are 0.2 and 0.5 $\mu g\ l^{-1}$ for arsenic and selenium, respectively.

The determination of trace metals in mineral waters requires the use of sensitive analytical methods and the development of procedures with very low detection limits. Electrothermal atomic absorption spectrometry (a.a.s.) is suitable for such determinations provided that the trace metals are first separated from matrix components and preconcentrated in order to improve the often inadequate detection limits [1].

The determination of arsenic and selenium levels in water is of considerable interest because they are essential elements as well as being toxic or possibly carcinogenic [2]. Several sensitive methods are available for the determination of arsenic and selenium. Arsenic has often been determined by spectrophotometry [3—5] and selenium fluorimetrically [6, 7]. Neutron activation analysis [8, 9], voltammetric methods [10, 11] and atomic absorption spectrometry are now often applied for these determinations. The application of flame a.a.s. is limited because of insufficient sensitivity, interferences and appreciable background noise. Therefore hydride generation or electrothermal atomization techniques are generally preferred for the determination of low arsenic and selenium concentrations [12—17].

The present paper reports the determination of arsenic and selenium in mineral waters by the application of electrothermal a.a.s. after their separation by co-precipitation.

0003-2670/84/$03.00

EXPERIMENTAL

Apparatus and chemicals

Measurements were made with a Perkin-Elmer graphite tube furnace, HGA-72, in conjunction with a Perkin-Elmer 300-S atomic absorption spectrometer. Perkin-Elmer high-frequency electrodeless lamps were used.

All chemicals were of analytical reagent quality. Redistilled water from a Heraeus quartz apparatus was used.

Procedure

Iron(III) standard solution (0.5 ml of a 1 mg ml^{-1} solution prepared from iron wire) was added to 200 ml of the sample, carbon dioxide was boiled out, and hydrated iron(III) oxide was precipitated at pH 6—7 with diluted ammonia liquor (1 + 3). The precipitate was collected on a filter, washed with dilute ammonia solution (1 + 10) and dissolved in 10 ml of nitric acid (1 + 3). The solution was evaporated to dryness and the residue dissolved in 5 ml of 0.2 M sulphuric acid. An aliquot (10 μl) of the solution was injected into the graphite furnace and the absorption of the element under test was measured. For both selenium and arsenic, the drying temperature was 100°C for 30 s, the ashing temperature was 1000°C for 60 s and the atomization temperature was 2400°C for 20 s. Arsenic was measured at 193.7 nm and selenium at 196.0 nm.

Calibration. Appropriate amounts of a standard solution of the test elements were transferred to 25-ml measuring flasks, 2.5 ml of the standard iron(III) solution (1 mg ml^{-1}) was added, and the mixture was diluted to the mark with 0.2 M sulphuric acid. These solutions were then taken through the recommended procedure, including the co-precipitation.

RESULTS AND DISCUSSION

Even a brief survey of the literature [18—21] is sufficient to show that the determination of arsenic and selenium by electrothermal a.a.s. is complicated by interferences because of the uncontrollable volatility of arsenic and selenium compounds, especially in complex inorganic and organic matrices. Mineral waters contain alkali metals, alkaline-earth metals, sulphate, chloride, and hydrogencarbonate ions in high and changeable concentrations, whereas the concentrations of arsenic and selenium are normally very low [1]. The results of experiments shown in Figs. 1 and 2 justify these predictions. Moreover, in highly mineralized waters, the measurement is often impossible owing to the decomposition and evaporation of the main components. Therefore direct electrothermal a.a.s. determinations are not practically feasible.

To avoid these difficulties and sources of errors, co-precipitation with hydrated iron(III) oxide was applied. In contrast to the unsatisfactory results for Cd, Co, Cu, Ni and Pb ions found in our previous work [1], the

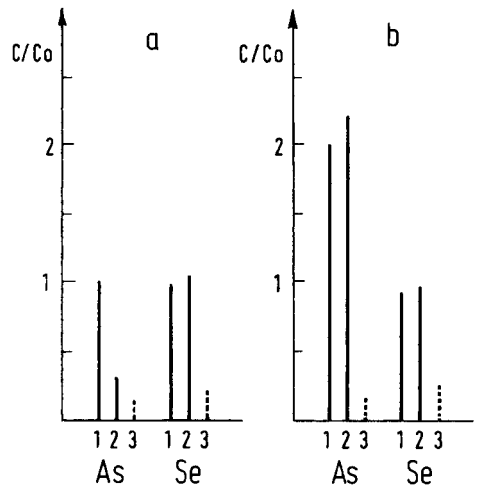

Fig. 1. The influence of (a) sodium and (b) calcium on the absorption of arsenic and selenium. Lines: (1) 5 mg l^{-1} Na^+ or Ca^{2+}; (2) 500 mg l^{-1} Na^+ or Ca^{2+}, (3) 5000 mg l^{-1} Na^+ or Ca^{2+}; (---) nonspecific absorption. C/C_0 is the ratio of apparent and real concentrations.

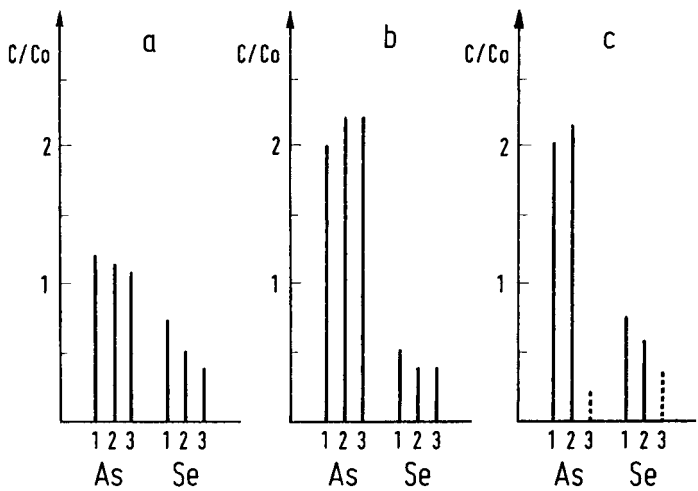

Fig. 2. The influence of (a) hydrochloric, (b) nitric, and (c) sulphuric acid on the absorption of arsenic and selenium. Lines: (1) 0.2 M; (2) 1 M; (3) 2 M acid. For (-----) and C/C_0, see Fig. 1.

co-precipitation of arsenic(III) and (V), as well as selenium(IV) and (VI) in hydrated iron(III) oxide was quantitative. The recoveries were 97% for arsenic and 100% for selenium.

Because the precipitate must be dissolved prior to injection into the graphite tube, the suitability of some acids was investigated. Figure 3 summarizes the behaviour of arsenic and selenium in dependence on the temperature during

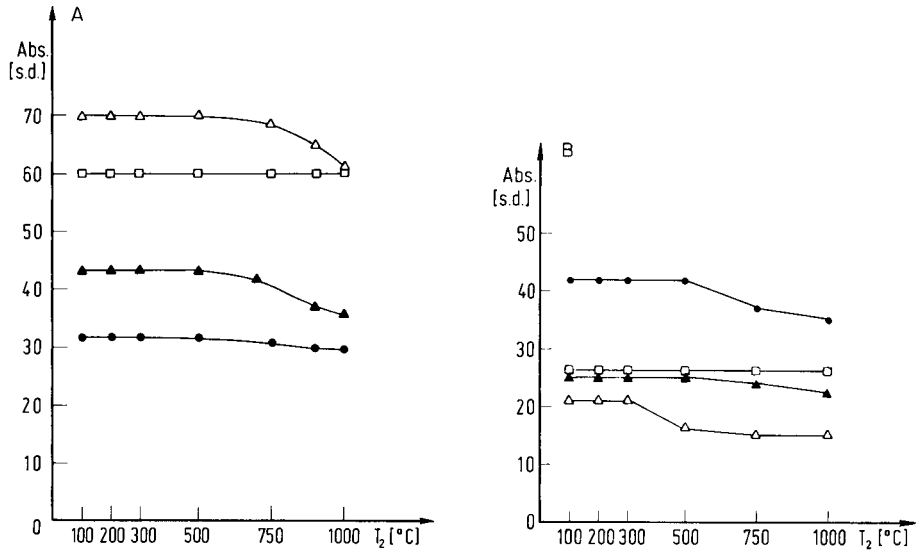

Fig. 3. The influence of ashing temperature on the absorption of (A) arsenic and (B) selenium. Solvent: (•) H_2O; (□) 0.2 M H_2SO_4; (△) 0.2 M HNO_3; (▲) 0.2 M HCl.

the ashing step in different media. It is obvious that sulphuric acid is the most suitable solvent for the dissolution of the precipitate, for there are no losses of arsenic and selenium in the temperature range between 100 and 1000°C. However, sulphuric acid can influence the absorption of arsenic and selenium, having enhancing and depressing effects, respectively, with increasing acid concentrations. As is shown in Fig. 4, the influence of sulphuric acid on the absorption of arsenic and selenium becomes constant at concentrations higher than 0.5 mol l^{-1}. However, to keep the concentration of sulphuric acid as low as possible in order to avoid undesirable nonspecific absorption effects, 0.2 M sulphuric acid solutions were used in further experiments.

The solutions in which arsenic and selenium were determined contained 0.1—0.2 mg ml^{-1} iron(III). Therefore the effect of iron(III) on the absorption of the test elements was examined. Figure 5 shows the influence of iron on the absorption of both elements. It can be seen that iron does not affect the absorption of arsenic, whereas it diminishes the absorption of selenium. However, the depressing effect is constant in the concentration range of interest.

In addition, hydrated iron(III) oxide precipitates adsorb ions of the main constituents. The amount of these in the precipitate will depend on their concentrations in the mineral water. Table 1 shows experimentally obtained concentration ranges of some adsorbed ions for different mineral water samples. In the case of these elements which can affect the atomization of arsenic and selenium, the sulphuric acid has a compensating effect.

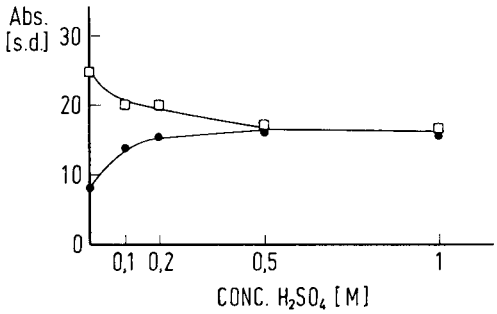

Fig. 4. The influence of sulphuric acid concentration on the absorption of (•) arsenic and (▫) selenium.

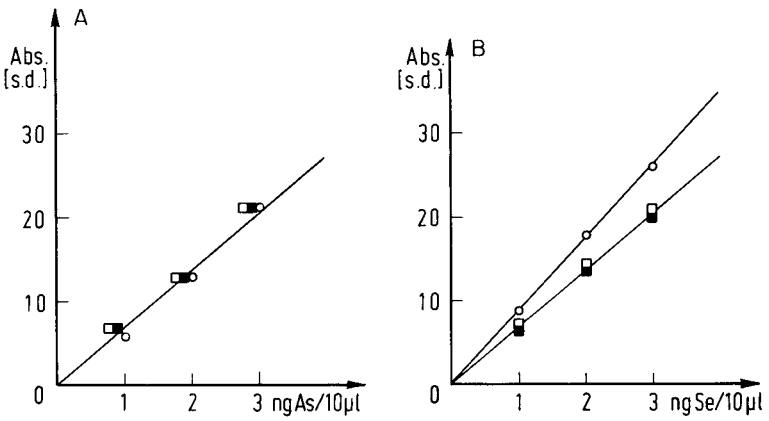

Fig. 5. The influence of Fe(III) on the absorption of (A) arsenic and (B) selenium: (○) 0.2 M H_2SO_4; (▫) 0.2 M H_2SO_4 + 0.1 mg Fe^{3+} ml^{-1}; (▪) 0.2 M H_2SO_4 + 0.2 mg Fe^{3+} ml^{-1}.

Further experiments showed that only sodium in concentrations over 10 mg l^{-1} exerted a depressing effect on arsenic absorption, whereas aluminium, calcium, magnesium, potassium and manganese did not have any significant influence (Fig. 6). The situation with the atomization of selenium is even better. All the above-mentioned elements, including

TABLE 1

Analysis of hydrated iron(III) oxide pricipitates

Element	Concentration range (mg l^{-1})	Element	Concentration range (mg l^{-1})
Al	<0.3—2	Mg	2—110
Ca	20—100	Mn	0.1—1
K	<0.1—4	Na	0.3—20

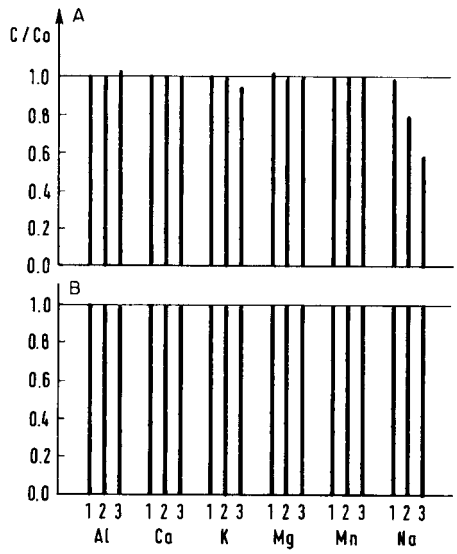

Fig. 6. The influence of some metals on the absorption of (A) arsenic and (B) selenium in the presence of 0.2 M H_2SO_4. Lines: (1) 1 mg l^{-1} Al^{3+}, 20 mg l^{-1} Ca^{2+}, 2 mg l^{-1} K^+, 20 mg l^{-1} Mg^{2+}, 0.2 mg l^{-1} Mn^{2+} or 10 mg Na^+; (2) 6 mg l^{-1} Al^{3+}, 200 mg l^{-1} Ca^{2+}, 10 mg l^{-1} K^+, 200 mg Mg^{2+}, 2 mg l^{-1} Mn^{2+} or 20 mg l^{-1} Na^+; (3) 10 mg l^{-1} Al^{3+}, 400 mg l^{-1} Ca^{2+}, 20 mg l^{-1} K^+, 400 mg l^{-1} Mg^{2+}, 10 mg l^{-1} Mn^{2+} or 100 mg l^{-1} Na^+. For C/C_0, see Fig. 1.

sodium, had no effect on atomization. It is necessary to point out that the concentrations of sodium in the precipitates obtained in the analysis of real samples were very seldom critical.

Blanks for arsenic and selenium after co-precipitation in hydrated iron(III) oxide obtained from ten parallel determinations as well as the relative standard deviations and statistically calculated detection limits are given in Table 2. The high blank for arsenic can be ascribed to impurities in the iron wires which were used for the preparation of the iron standard solution. This level could be minimized by subsequent evaporation of the solution in the presence of hydrochloric acid.

TABLE 2

Blanks and detection limits for arsenic and selenium after co-precipitation in hydrated iron(III) oxide

Element	$\bar{x}$ (ng/10 μl)	s_r (%)	D.l. (μg l^{-1})
As	0.13[a]	10	0.2
Se	<0.2	—	0.5

[a]Mean of 10 measurements; range 0.10—0.15 ng/10 μl.

TABLE 3

Accuracy of the procedure

Element	Added (ng/10 μl)	Found (ng/10 μl)
As(III)	2.0	1.95
As(V)	2.0	1.90
Se(IV)	2.0	2.0
Se(VI)	2.0	2.0
As	250[a]	246[b]

[a]Proposed method. [b]Spectrophotometry.

TABLE 4

Results for some mineral waters from Slovenia

Spring	As (μg l^{-1})	Spring	As (μg l^{-1})	Spring	As (μg l^{-1})
1	0.8	5	1.6	9[a]	2.0
2	0.5	6	190	10[a]	55
3	1.5	7	250	11[a]	3.7
4	3.0	8[a]	<0.2		

[a]Bottled.

The accuracy of the procedure was established by spike tests. Additionally, the results for arsenic were compared with spectrophotometric results [3]. The results obtained are presented in Table 3.

The method proposed was used in the analysis of some mineral waters from Slovenia. The results obtained for arsenic are given in Table 4. The samples were acidified with sulphuric acid to pH 2 immediately after sampling. It can be concluded that the procedure is suitable for the determination of arsenic in mineral waters. The determination of selenium, which is present in lower concentrations, is more difficult. For all the mineral waters tested (springs 1—11, Table 4), the selenium content was <0.5 μg l^{-1}. The method makes it possible to determine total concentrations of arsenic and selenium. As can be seen from Table 4, concentrations of arsenic can be relatively high, which means that the speciation could be of interest in some cases. With the application of ammonium tetramethylenedithiocarbamate extraction in combination with the procedure proposed, arsenic(III) and arsenic(V) could be distinguished in such waters.

REFERENCES

1 V. Hudnik, S. Gomišček and B. Gorenc, Anal. Chim. Acta, 98 (1978) 39.
2 T. D. Luckey and B. Venugopal, Metal Toxicity in Mammals, Plenum Press, New York, 1977.
3 W. Fresenius and W. Schneider, Z. Anal. Chem., 203 (1961) 27.
4 D. L. Johnson, Environ. Sci. Technol., 5 (1971) 411.
5 H. Woidich and W. Pfannhauser, Z. Lebensm. Unters. Forsch., 159, 323 (1975) 327.
6 J. M. Rankin, Environ. Sci. Technol., 7 (1973) 823.
7 J. H. Wiersma and F. G. Lee, Environ. Sci. Technol., 5 (1971) 1203.
8 E. Heuss and K. H. Lieser, J. Radioanal. Chem., 50 (1979) 289.
9 K. Lenvik, E. Steinnes and A. C. Pappas, Anal. Chim. Acta, 97 (1978) 295.
10 G. Henze, P. Monks and G. Tölg, Z. Anal. Chem., 295 (1969) 1.
11 P. L. Buldini, D. Ferri and Q. Zini, Mikrochim. Acta, 1 (1980) 71.
12 K. G. Brodie, Int. Lab., (1977) 65.
13 K. C. Tam, Environ. Sci. Technol., 8 (1974) 734.
14 G. C. Kunselman and E. A. Huff, At. Absorpt. Newsl., 15 (1976) 29.
15 E. L. Henn, Anal. Chem., 47(3) (1975) 428.
16 K. S. Sulzamanian and J. C. Meranger, Anal. Chim. Acta, 124 (1981) 131.
17 R. R. Brooks, D. E. Ryan and H. Zhang, Anal. Chim. Acta, 131 (1981) 1.
18 F. D. Pierce and H. R. Brown, Anal. Chem., 49(9) (1977) 1417.
19 P. R. Walsh and J. L. Fasching, Anal. Chem., 48(7) (1976) 1014.
20 J. Korečkova, W. Freck, E. Lundberg, J. A. Persson and A. Cedergren, Anal. Chim. Acta, 130 (1981) 267.
21 K. Saeed and Y. Thomassen, Anal. Chim. Acta, 130 (1981) 281.

Analytica Chimica Acta, 157 (1984) 143—150
Elsevier Science Publishers B.V., Amsterdam — Printed in The Netherlands

THE DETERMINATION OF TRACE METALS IN HUMAN FLUIDS AND TISSUES

Part 1. Estimation of "Normal Values" for Copper, Zinc, Cadmium and Manganese in Blood Serum and Liver Tissue

V. HUDNIK

Boris Kidrič Institute of Chemistry, Ljubljana (Yugoslavia)

M. MAROLT-GOMIŠČEK

Faculty of Medicine, Edvard Kardelj University, Ljubljana (Yugoslavia)

S. GOMIŠČEK*

Faculty of Natural Sciences and Technology, Edvard Kardelj University, Ljubljana (Yugoslavia)

(Received 26th July 1983)

SUMMARY

The procedures for the determination of copper, zinc, cadmium and manganese in human blood serum and liver tissue with use of flame and electrothermal atomic absorption spectrometry are presented and discussed. The procedures were applied for the estimation of "normal" levels of these elements in human serum and liver tissue.

Studies of the role of trace elements in animals, including man, demonstrate their importance for life [1]. Consequently, increasing interest has been shown in analytical investigations in the field of biological materials, and in particular, animal and human fluids and tissues. Very many procedures for the determination of toxic and essential elements have been proposed, "classical" as well as the most modern instrumental methods being applied [2—4]. Recent studies have been concerned with the reliability of analytical procedures and their usability in clinical chemistry and medical investigations [5, 6].

The determination of trace elements is increasingly considered as a useful and important test in medicine, because the levels of some elements can be related to various pathological conditions in man. Therefore the results obtained for trace metal levels can contribute to the diagnosis, prognosis and treatment of particular diseases [7, 8].

In accordance with the above, the present study was concentrated on the development of reliable procedures for the determination of trace elements which are applicable in clinical laboratories and are practicable under normal hospital conditions. The analytical steps and factors which influence the

0003-2670/84/$03.00

accuracy of the results, e.g., sampling, storage, homogeneity and contamination, will be examined in later parts of this series. Additionally, the procedures proposed were used to establish the "normal" values for particular trace elements. This paper reports the normal values for copper, zinc and cadmium in serum and for copper, zinc, cadmium and manganese in liver tissue for a mixed population of 35—40 individuals. The procedures based on atomic absorption spectrometry (a.a.s.) and their analytical limitations are described and discussed.

EXPERIMENTAL

Apparatus and chemicals

Measurements were made with a Varian Techtron AA-6 (flame), and a Perkin-Elmer 300-S atomic absorption spectrometer in conjunction with a Perkin-Elmer HGA-72 graphite tube furnace. The Perkin-Elmer spectrometer was provided with automatic deuterium background correction. Westinghouse (Zn, Cu, Mn) hollow-cathode lamps, and a Perkin-Elmer cadmium high frequency electrodeless lamp were used.

All chemicals were A.R. quality. Redistilled water from a Heraeus quartz apparatus was used.

All containers used were washed with diluted nitric acid and rinsed thoroughly with redistilled water.

Samples

Venous blood samples were taken with disposable needles from healthy blood donors. The blood was centrifuged for 10 min at 3000 rpm. Liver tissue samples were obtained by autopsy from cases of accidental death and were lyophilized. The time between death and sample collection was as short as possible (5—20 h) and no significant histological changes of tissue were observed.

All samples were stored in polystyrene vessels (Spex) at −20°C until required for analysis.

Procedures

Serum. For copper and zinc, 0.5 ml of serum was diluted with 0.1% (w/v) Triton X-100 solution to 5 ml and aspirated into the air-acetylene flame.

For cadmium, 0.1 ml of serum was decomposed in a sealed glass ampoule with 0.1 ml of HNO_3—$HClO_4$ mixture (3:1) at 140°C. Then the ampoule was opened, 20 μl of concentrated sulphuric acid was added, and the solution was evaporated to dryness. The residue was dissolved with 0.4 ml of 0.1 M hydrochloric acid and then 25 μl of the solution was injected into the graphite tube furnace for the absorption measurement [9, 10].

For manganese, 25 μl of serum was injected into the graphite tube furnace and the absorption was measured.

Liver. The liver tissue (5—10 mg) was treated as described above for the

determination of cadmium in serum. After evaporation the residue was dissolved in 3 ml of 0.1 M hydrochloric acid.

The absorption of the particular element was measured under the conditions summarized in Table 1. The concentrations of elements were calculated on the basis of calibration curves prepared with metal standard solutions in 0.1 M hydrochloric acid. Zinc and copper in serum, as well as zinc in liver tissue samples, were determined by the flame technique, an air-acetylene flame being used.

RESULTS AND DISCUSSION

Although numerous papers have been published on the determination of trace elements in human fluids and tissue, as well as on analytical data related to "normal" and pathological states, a critical review of the state of the art leads to the conclusion that much further study is necessary. The need for further work on the methods available and on the estimation of "normal" concentrations and imbalances of trace element levels related to pa'hological states becomes even clearer at symposia concerning the role of trace elements in medicine and biology.

The medical studies which should give a decisive answer on the role of trace elements in the diagnosis, prognosis and treatment of particular diseases must be done in hospitals, thus involving all the requirements of clinical work and medical ethics. Accordingly, the factors affecting the reliability of the results under these conditions must be carefully monitored and studied and the procedures have to be simple enough to allow precise and accurate routine work. For this purpose, flame and electrothermal a.a.s. in combination with normal sampling was applied and found to be suitable except for the determination of manganese in human serum (see Part 3 of this series).

The determination of copper and zinc in serum which are present in relatively high concentrations presents no serious difficulties for flame a.a.s.,

TABLE 1

Conditions for electrothermal a.a.s. measurements

		Cd	Cu	Mn
Wavelength (nm)		228.8	324.7	279.5
Drying	T_1 (°C)	100	100	100
	t_1 (s)	30[a]	30[a]	30[a]
		30[b]	—	60[b]
Ashing	T_2 (°C)	300	750[a]	1100
	t_2 (s)	30[a]	30[a]	30[a]
		30[b]	—	60[b,c]
Atomization	T_3 (°C)	1600	2400[a]	2300
	t_3 (s)	10	10[a]	10

[a]Liver tissue. [b]Serum. [c]HGA-72, ramp 5.

whereas the determination of cadmium and manganese is much more demanding, as regards sensitivity and contamination, and therefore electrothermal a.a.s. must be applied. The concentrations of cadmium, copper, manganese and zinc in liver tissue are higher. However, if one takes into account that only the part of the sample taken by biopsy would normally be used in the analysis, the application of electrothermal a.a.s. is to be preferred for copper, cadmium and manganese whereas zinc should be determined by the flame technique. Therefore the main problem is the dissolution and mineralization of the organic matter. In the present work, this is achieved by pressurized dissolution, which is particularly characterized by low blanks [9, 10].

Precision and accuracy

The precision and accuracy of the procedures applied are summarized in Tables 2—4. The precision of the procedures is satisfactory, the relative standard deviations corresponding to the values normally obtained for the particular concentration range. The detection limits ensure reliable determinations of most elements, even at the low concentrations occurring in particular cases, but there may be occasional problems with low levels of manganese and cadmium in serum. The accuracy of the procedures for serum was checked by comparison with the results obtained by anodic stripping voltammetry (copper, zinc) and differential-pulse anodic stripping voltammetry (cadmium). For liver tissue, the accuracy was estimated by analyses of the standard reference material Bovine liver SRM 1577.

Estimation of "normal" values in blood sera and liver tissue

"Normal" values in a local context were estimated by the analysis of serum of 35 male (m) and 5 female (f) blood donors; liver tissue was ob-

TABLE 2

The precision (s_r) and detection limits (d.l.) for copper, zinc, cadmium and manganese in blood serum ($\mu g\ ml^{-1}$) and liver tissue ($\mu g\ g^{-1}$)

	Element	D.l.	s_r (%)	Occurrence in the human body[a]
Serum	Cd	0.0003	12	0.0004—0.004
	Cu	0.2[b]	2	0.7—1.5
	Mn	0.0003	14	0.0004—0.003
	Zn	0.1[b]	3	0.7—1.4
Liver tissue (5 mg)	Cd	0.06	2	0.44—34
	Cu	2	3	8—42
	Mn	0.2	2	2.8—6.9
	Zn	6[b]	3	23—312

[a]Literature values. [b]Flame.

TABLE 3

The accuracy of the procedure for the determination of copper, zinc and cadmium in blood serum

Sample	Zn (μg ml^{-1})		Cu (μg ml^{-1})		Cd (ng ml^{-1})	
	A.a.s.	A.s.v.[a]	A.a.s.	A.s.v.	A.a.s.[b]	D.p.a.s.v.[c]
1	1.35	1.30	0.85	0.80	2.2	2.0
2	0.90	0.95	1.15	1.10	1.6	2.1
3	1.15	1.20	1.05	0.95	1.4	1.7
4	0.80	0.75	0.90	0.80	2.5	1.7
5	0.95	0.90	1.20	1.20	0.88	0.95

[a]Anodic stripping voltammetry. [b]Electrothermal method. [c]Differential-pulse anodic stripping voltammetry.

TABLE 4

The accuracy of the procedure for the determination of copper, zinc, cadmium and manganese in liver tissue (in μg g^{-1}); Bovine Liver SRM 1577

Sample	Cd	Cu	Mn	Zn
Present data	0.29 ± 0.01	186 ± 5.2	10.6 ± 0.19	130 ± 4.5
Certificate	0.27	193	10.3	130

TABLE 5

"Normal" values for copper, zinc and cadmium in blood serum

Age (Years)	Sex	N	Range	$\bar{x}$	s
Copper (μg ml^{-1})					
22—30	m + f	13	0.82—1.38	1.08	0.16
30—40	m + f	16	0.95—1.40	1.13	0.15
40—52	m + f	11	0.75—1.21	1.05	0.14
22—52	m + f	40	0.75—1.40	1.09	0.15
22—52	m	35	0.82—1.40	1.10	0.14
23—42	f	5	0.75—1.30	1.09	0.23
Zinc (μg ml^{-1})					
22—30	m + f	13	0.67—1.05	0.87	0.16
30—40	m + f	16	0.73—1.15	0.92	0.12
40—52	m + f	11	0.63—1.05	0.86	0.12
22—52	m + f	40	0.63—1.15	0.89	0.13
22—52	m	35	0.67—1.15	0.90	0.12
23—42	f	5	0.63—1.05	0.78	0.16
Cadmium (mg ml^{-1})					
22—30	m + f	13	<0.3—2.0	—	—
30—40	m + f	16	<0.3—2.3	—	—
40—52	m + f	11	<0.3—1.1	—	—
22—52	m + f	40	<0.3—2.3	—	—
22—52	m	35	<0.3—2.0	—	—
23—42	f	5	0.3—2.3	—	—

TABLE 6

"Normal" values for copper, zinc, cadmium and manganese in liver tissue (dry tissue, $\mu g\,g^{-1}$)

Age (Years)	Sex	N	Range	$\bar{x}$	s	Range	$\bar{x}$	s
			Copper			*Zinc*		
14—25	m + f	13	10.7—63.0	38.6	13.9	156—395	233	68
25—35	m + f	11	10.1—71.0	27.5	19.8	92—268	162	50
35—45	m + f	7	16.9—57.9	31.0	15.4	90—280	172	68
over 45	m + f	4	8.2—27.2	14.2	8.9	68.8—201	117	59
14—60	m + f	35	8.2—71.0	30.8	17.1	68.8—395	185	72
14—60	m	27	8.2—71.0	33.5	17.4	90—395	185	72
22—59	f	8	8.3—45.9	21.6	13	68.8—280	183	77
			Cadmium			*Manganese*		
14—25	m + f	13	2.3—18.2	6.4	4.5	4.5—8.3	5.8	1.4
25—35	m + f	11	2.0—17.4	6.9	5.6	2.7—8.0	4.8	1.5
35—45	m + f	7	1.2—9.7	5.8	2.8	3.0—9.4	4.7	2.1
over 45	m + f	4	2.0—12.9	6.2	3.2	2.9—5.2	4.7	1.3
14—60	m + f	35	1.2—18.2	6.4	4.4	2.7—9.4	5.2	1.6
14—60	m	27	1.2—18.2	6.8	4.8	2.7—8.3	5.2	1.5
22—59	f	8	2.0—7.5	5.0	2.0	2.9—9.4	4.9	2.0

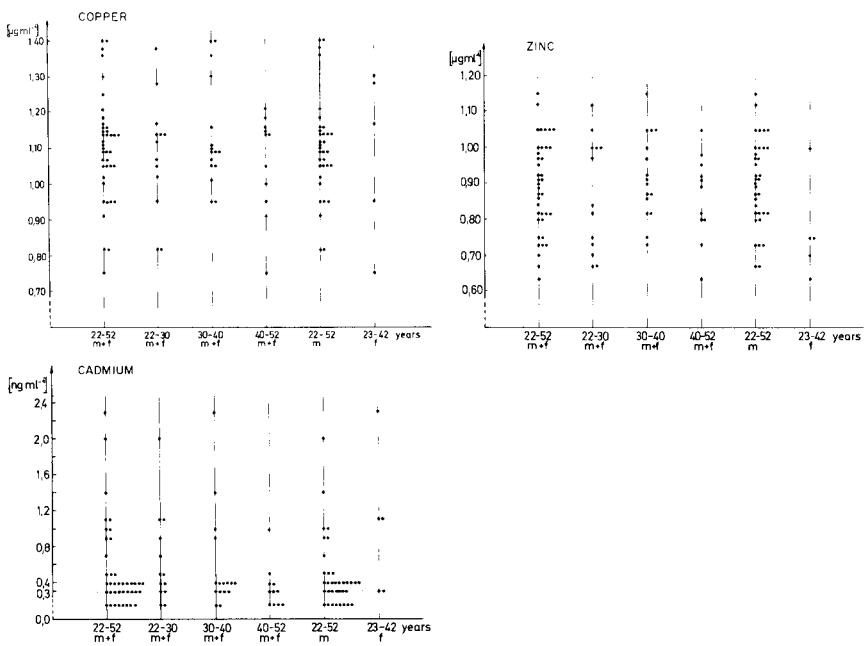

Fig. 1. Distribution of "normal" levels of copper, zinc and cadmium in blood serum.

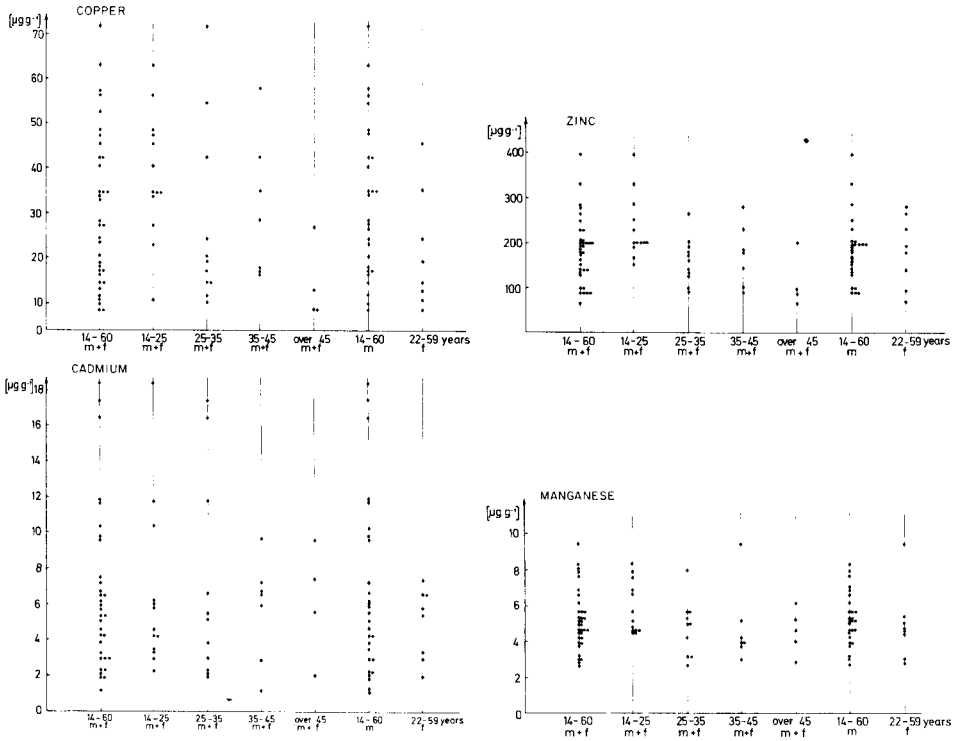

Fig. 2. Distribution of "normal" levels of copper, zinc, cadmium and manganese in liver tissue.

tained by autopsy from 35 accident victims in otherwise healthy individuals. In these investigations, only liver samples with normal histological structure were accepted. The results obtained are presented in Tables 5 and 6 and in Figs. 1 and 2. The values for manganese in serum are omitted because they may have been burdened by systematic error caused by contamination in sampling (see Part 3).

The estimated "normal" values for this local population are within the limits reported by other authors in recent years [11—14]. On the basis of all these data, it can be concluded that in spite of the multitude of factors that can influence trace metal levels in a healthy individual, the "normal" ranges proposed can be accepted as the most probable concentrations for copper, zinc and cadmium in human serum and for copper, zinc, cadmium and manganese in liver tissue. These values can be used as a starting point for medical investigations.

The authors are grateful to the Research Community of Slovenia for financial support. We also thank Dr. Jacques Versieck for his critical review of this manuscript.

REFERENCES

1 E. J. Underwood, Trace Elements in Human and Animal Nutrition, Academic Press, London, 1977.
2 S. S. Brown (Ed.), Clinical Chemistry and Chemical Toxicology of Metals, Elsevier, Amsterdam, 1977.
3 T. D. Luckey, B. Venugopal, Metal Toxicity in Mammals, Plenum Press, New York, 1977.
4 P. Brätter and P. Schramel (Eds.), Trace Element Analytical Chemistry in Medicine and Biology, W. de Gruyter, Berlin, 1980.
5 Workshop on Research Needed to Improve Data on Mineral Content of Human Tissues, Fed. Proc. Fed. Am. Soc. Exp. Biol., 40(8) (1981) 2111.
6 V. Iyengar, Anal. Chem., 54(4) (1982) 554.
7 A. S. Prasad and D. Oberleas (Eds.), Trace Elements in Human Health and Disease, Vols. I and II, Academic Press, New York, 1976.
8 N. Kharasch (Ed.), Trace Metals in Health and Disease, Raven Press, New York, 1979.
9 S. Gomišček, V. Hudnik and M. Veber, in S. S. Brown (Ed.), Clinical Chemistry and Chemical Toxicology of Metals, Elsevier/North-Holland Biomedical Press, Amsterdam, 1977, p. 319.
10 V. Hudnik, S. Gomišček and M. Katič, VSKDAA 25, 4 (1978) 391.
11 J. Versieck and R. Cornelis, Anal. Chim. Acta, 116 (1980) 217.
12 D. Brune and B. Bivered, Anal. Chim. Acta, 85 (1976) 411.
13 C. A. Johnson, Anal. Chim. Acta, 81 (1976) 69.
14 W. Koenig, F. W. Richter, B. Meine and J. Ch. Bode, in P. Brätter and P. Schramel (Eds.), Trace Element Analytical Chemistry in Medicine and Biology, W. de Gruyter, Berlin, 1980, p. 381.

Analytica Chimica Acta, 157 (1984) 151—156
Elsevier Science Publishers B.V., Amsterdam — Printed in The Netherlands

Short Communication

CATION SELECTIVITY OF LIQUID-MEMBRANE ELECTRODES BASED ON MACROCYCLIC LACTONES AND LACTONELACTAMS

A. V. BOGATSKY, N. G. LUKYANENKO*, V. N. GOLUBEV, N. YU. NAZAROVA, L. P. KARPENKO, YU. A. POPKOV and V. A. SHAPKIN

Physico-Chemical Institute, Academy of Sciences of the Ukr.S.S.R., 270080 Odessa (U.S.S.R.)

(Received 22nd August 1983)

Summary. Selectivity coefficients are reported for liquid membranes containing 27 macrocyclic lactones and lactonelactams with respect to alkali and alkaline-earth metal ions. It is shown that introduction of amide and ester groups into cyclic polyethers can modify the cation selectivity over a wide range. The results indicate the possibility of obtaining various highly selective membrane electrodes based on these neutral macroheterocyclic compounds.

One of the most striking features of crown ethers, cryptands and similar macrocyclic compounds is their ability to form lipophilic stable complexes with alkali and alkaline-earth metal ions as well as to form complexes selectively with various cations. This property has provided interesting possibilities for these compounds as the active components in ion-selective electrodes [1—3]. Generally, the ion-selectivity of liquid or polyvinyl chloride membranes containing macrocyclic ligands is similar to that observed for complexation with metal ions in aqueous solutions. As a rule, ordinary macrocyclic polyethers show some K/Na selectivity depending on the structural changes of the molecule [4, 5].

The introduction of ester and amide groups provides additional binding sites for complexation which in some cases results in selective interaction with alkaline-earth metal ions [5, 6]. Macrocyclic compounds of this type can be considered as bifunctional ligands capable of forming complexes with different structures.

This communication is concerned with an investigation of electrode properties of liquid membranes containing novel macrocyclic ligands, and with the influence of ligand structure on the cation selectivity of such membranes in solutions of alkali and alkaline-earth metal ions.

Experimental

Macrocyclic compounds **I—XXVII** were chosen for investigation. The synthesis and properties of these compounds have been described [7, 8].

0003-2670/84/$03.00

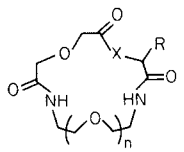

I n = 1, X = O, R = H
II n = 1, X = O, R = $CH_2C_6H_5$
III n = 1, X = S, R = H
IV n = 2, X = O, R = H
V n = 2, X = O, R = $CH_2C_6H_5$
VI n = 2, X = S, R = H
VII n = 3, X = O, R = H
VIII n = 3, X = O, R = $CH_2C_6H_5$
IX n = 4, X = O, R = H

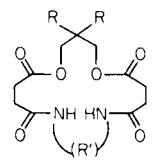

X R = CH_3, R′ = $(CH_2)_4$
XI R = CH_3, R′ = $(CH_2CH_2)O$

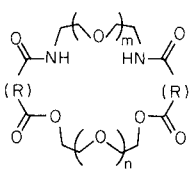

XII m = 1, n = 1, R = $(CH_2)_2$
XIII m = 3, n = 3, R = $(CH_2)_2$
XIV m = 2, n = 3, R = $(CH_2)_2$
XV m = 1, n = 2, R = $(CH_2)_2$
XVI m = 1, n = 3, R = $(CH_2)_2$
XVII m = 2, n = 2, R = CH_2OCH_2
XVIII m = 3, n = 3, R = CH_2OCH_2
XIX m = 2, n = 1, R = CH_2OCH_2
XX m = 3, n = 1, R = CH_2OCH_3

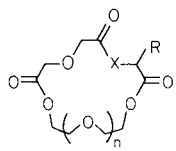

XXI n = 1, X = O, R = H
XXII n = 1, X = O, R = $CH_2C_6H_5$
XXIII n = 1, X = S, R = H
XXIV n = 2, X = O, R = $CH_2C_6H_5$
XXV n = 2, X = S, R = H
XXVI n = 4, X = O, R = $CH_2C_6H_5$
XXVII n = 2, X = O, R = H

The ion-selective properties of compounds **I**—**XXVII** with respect to alkali and alkaline-earth metal ions were determined potentiometrically [9]. The liquid membranes containing the ligands were investigated in cells of the following type

Ag, AgCl | $Me_i^{n+}Cl_n^-$ || liquid membrane || $Me_j^{n+}Cl_n^-$ | AgCl, Ag

The e.m.f. of the cell was measured with an OP 208/1 (Radelkis) pH meter at 22°C. A solution of the macrocyclic ligand (5×10^{-3} M) in dry solvent (chloroform, 1,2-dichloroethane or nitrobenzene) was used to prepare the liquid membranes. The liquid membrane was separated from the electrolyte solutions by cellophane films (20 μm thick).

The separate solutions method with 0.01 M solutions of the chlorides was applied for determining the potentiometric selectivity coefficients given by the equation [4]

$$\log k_{M_iM_j} = [(E_j - E_i)z_iF/2.303\,RT] - (z_i/z_j)\log a_j + \log a_i$$

Results and discussion

The data in Table 1 show that the selectivity of compounds **I**, **IV**, **VII** and **IX** for alkali and alkaline-earth metal ions changes regularly with an

increase in the size of the macrocycle from 15 to 21. Thus the 15-membered lactonelactam shows selectivity for rubidium ions while the 21-membered compound (**VII**) shows selectivity for cesium ions. Further increase in size to a 24-membered macrocycle (**IX**) changes the sequence of cation selectivity again. The membrane based on **IX** shows preference for potassium ions. Such inversion of ion selectivity is due to the structural change and stoichiometry. Lactonelactam **IX** can form 1:1 inclusion complexes whereas sandwich-type 2:1 complexes cannot be ruled out for compounds **I**, **IV** and **VII**. This suggestion is confirmed by examination of CPK models.

Compounds **I**, **IV**, **VII** and **IX** exhibit a pronounced increase in the selectivity for barium ions compared to other alkaline-earth metals, and compounds **I** and **IX** are of particular interest.

Introduction of a sulfur atom into the macrocycle (**III** and **VI**) leads to a slight decrease in selectivity for alkali metal ions with respect to alkaline-earth metal ions, although there is not very much difference from the behaviour of their oxygen analogs **I** and **IV**.

The introduction of a benzyl group on the polyether macrocycle has an unfavourable effect on the selectivity for alkaline-earth metal ions in the case of **II** and **VIII**, whereas it increases the preference for Ba^{2+} in the case of lactonelactam **V**. Lactonelactam **II** exhibits high selectivity towards K^+ compared to other alkali metal ions. Interestingly, that interaction with rubidium ions is weak, regardless of the macrocycle size, whereas the selectivity for cesium ions increases regularly with growing size of the macrocycle. The highest selectivity for Cs^+ was observed with the 21-membered compound **VIII**.

In the series of macrocyclic lactonelactams derived from succinic acid, compounds **XIII**—**XVI** show higher selectivity for alkali metal ions compared to alkaline-earth metals whereas compounds **X**—**XII** show preference for barium ions.

Among the alkali metal ions, the 25-membered macrocycle **XV** exhibits high selectivity towards K^+, similarly to ordinary crown ethers. An increase in macrocycle size results in selectivity enhancement for Rb^+ and Cs^+. Notably 34-membered lactonelactam **XIII** shows high selectivity for rubidium ions. In contrast to the case with **XII**—**XVI**, the macrocyclic lactonelactams **XVII**—**XX** show selectivity for alkaline-earth metal ions. Ligands **XVIII** and **XX** show a high preference for calcium ions over alkali and other alkaline-earth metal ions and would repay further investigation. It is of interest that the 30-membered lactonelactams **XVII** and **XX**, differing only in molecular symmetry, show different cation selectivities.

Except for compound **XXII**, which exhibits higher selectivity towards Sr^{2+}, the macrocyclic lactones (**XXI**, **XXIII**—**XXV**) show preference for alkali metal ions, and in particular for potassium ions. The striking differentiation between K^+ and Na^+ shown by lactones **XXI**, **XXIII**, **XXV**, **XXVI** is higher than in the case of some common cyclic polyethers [5].

Table 2 demonstrates the effect of the solvent on the ion-selective properties

TABLE 1

Selectivity coefficients, $k_{M_iM_j}$, of crown compounds in 1,2-dichloroethane

Crown compound	Li^+	Na^+	K^+	Rb^+	Cs^+	NH_4^+	Mg^{2+}	Ca^{2+}	Sr^{2+}	Ba^{2+}
I	0.181	0.295	0.372	0.958	0.497	0.474	0.160	0.220	0.183	1.000
II	0.007	0.028	1.000	0.016	0.078	0.015	0.004	0.028	0.043	0.052
III	0.402	0.641	0.544	0.350	0.838	0.029	0.528	0.760	0.618	1.000
IV	0.312	0.413	0.186	0.144	0.473	0.181	0.604	1.000	0.647	1.000
V	0.002	0.076	0.349	0.087	0.117	0.037	0.097	0.358	0.221	1.000
VI	0.067	0.084	0.063	0.243	0.452	0.008	0.167	1.000	0.485	0.616
VII	0.289	0.233	0.408	0.500	1.075	0.036	0.127	0.226	0.257	1.000
VIII	0.035	0.092	1.000	0.057	0.936	0.076	0.058	0.149	0.037	0.058
IX	0.227	0.747	1.067	0.501	0.522	0.370	0.811	0.665	0.589	1.000
X	0.056	0.137	0.368	0.391	0.555	0.006	0.178	0.305	0.359	1.000
XI	0.106	0.268	0.351	0.432	0.482	0.254	0.202	0.621	0.561	1.000
XII	0.179	0.303	0.878	0.216	0.557	0.296	0.288	0.421	0.374	1.000
XIII	0.067	0.252	0.578	1.000	0.463	0.156	0.067	0.052	0.108	1.000
XIV	0.211	0.075	1.000	0.756	0.801	0.308	0.046	0.146	0.068	0.135
XV	0.008	0.016	1.000	0.066	0.069	0.004	0.003	0.195	0.009	0.425
XVI	0.147	0.367	0.915	1.000	0.664	0.263	0.208	0.351	0.307	0.355
XVII	0.147	0.188	0.967	0.255	0.288	0.078	0.169	0.204	0.163	1.000
XVIII	0.311	0.387	0.416	0.400	0.462	0.137	0.336	1.000	0.246	0.436
XIX	0.086	0.126	0.101	0.280	0.133	0.067	0.109	0.112	0.096	1.000
XX	0.188	0.232	0.255	0.251	0.284	0.075	0.319	1.000	0.220	0.412
XXI	0.032	0.020	1.000	0.181	1.000	0.029	0.119	0.021	0.032	0.150
XXII	0.051	0.127	0.068	0.133	0.285	0.057	0.176	0.436	1.000	0.028
XXIII	0.005	0.017	1.000	0.167	0.201	0.033	0.008	0.006	0.028	0.500
XXIV	0.255	0.200	0.689	0.338	1.000	0.034	0.055	0.090	0.013	0.089
XXV	0.002	0.012	1.000	0.204	0.422	0.031	0.003	0.009	0.005	0.021
XXVI	0.009	0.021	1.000	0.110	0.316	0.025	0.078	0.092	0.080	0.218

TABLE 2

Selectivity coefficients, $k_{M_iM_j}$, of crown compounds in nitrobenzene or chloroform

Crown compound	Li^+	Na^+	K^+	Rb^+	Cs^+	NH_4^+	Mg^{2+}	Ca^{2+}	Sr^{2+}	Ba^{2+}
Nitrobenzene as solvent										
II	0.013	0.025	0.112	0.180	1.000	0.029	0.012	0.034	0.016	0.052
XXI	0.005	0.009	0.131	0.282	1.000	0.014	0.017	0.020	0.032	0.021
XXII	0.003	0.007	0.063	0.981	1.000	0.020	0.003	0.004	0.007	0.016
XXIII	0.021	0.025	0.072	0.210	1.000	0.028	0.012	0.034	0.119	0.022
XXIV	0.021	0.020	0.214	0.342	1.000	0.033	0.009	0.011	0.015	0.038
Chloroform as solvent										
XXI	0.418	0.362	0.754	0.348	0.492	0.480	0.518	0.853	0.531	1.000
XXII	0.018	0.026	1.000	0.031	0.078	0.026	0.017	0.027	0.017	0.043
XXIII	0.052	0.108	0.474	0.562	0.729	0.151	0.158	0.639	0.433	1.000
XXVII	0.028	0.069	0.362	0.120	0.178	0.049	0.057	0.103	0.127	1.000

of liquid membranes. In nitrobenzene, the cation selectivity of lactones **XXI, XXIII, XXIV** changes from potassium to cesium, whereas that of compound **XXII** goes from strontium and rubidium to cesium. No essential difference in cation selectivity of **XXI** and **XXIII** for alkali metal ions was observed when chloroform was used instead of 1,2-dichloroethane. However, these compounds in chloroform show preference for Ba^{2+} over other alkaline-earth metal ions. The exception is compound **XXII** which shows higher selectivity for K^+ in chloroform. Similar effects connected with the inversion of cation selectivity sequence of liquid membrane electrodes containing crown ethers have been reported previously [6] and can be attributed to different solvation of macrocyclic ligands and their complexes in liquid membranes.

REFERENCES

1 N. Lakshminarayanaiah, Membrane Electrodes, Academic Press, New York, 1976.
2 Y. Petranek and O. Ryba, Anal. Chim. Acta, 72 (1974) 375.
3 W. E. Morf, D. Ammann, R. Bissig, E. Pretsch and W. Simon, in R. M. Izatt and J. J. Christensen (Eds.), Progress in Macrocyclic Chemistry, Vol. 1, J. Wiley, New York, 1979.
4 Yu. A. Ovchinnikov, V. T. Ivanov, A. M. Shkrob, in B. A. Library (Ed.), Membrane Active Complexones, Vol. 12, Elsevier, New York, 1974.
5 Y. Petranek and O. Ryba, Collect. Czech. Chem. Commun., 45 (1980) 1567.
6 W. E. Morf, D. Ammann, E. Pretsch and W. Simon, Pure Appl. Chem., 36 (1973) 421.
7 A. V. Bogatsky, N. G. Lukyanenko, Yu. A. Popkov, K. S. Zaharov and V. M. Varava, Zh. Org. Khim. USSR, 17 (1981) 1062.
8 N. G. Lukyanenko, A. V. Bogatsky, V. A. Shapkin and Yu. A. Popkov, Zh. Org. Khim., USSR, 17 (1981) 1069.
9 H. K. Frensdorff, J. Am. Chem. Soc., 93 (1971) 600.

Analytica Chimica Acta, 157 (1984) 157—162
Elsevier Science Publishers B.V., Amsterdam — Printed in The Netherlands

Short Communication

ION-SELECTIVE ELECTRODES FOR SOME β-ADRENERGIC AND CALCIUM BLOCKERS

LARRY CUNNINGHAM and HENRY FREISER*
Department of Chemistry, University of Arizona, Tucson, AZ 85721 (U.S.A.)
(Received 17th June 1983)

Summary. Potentiometric sensors based on dinonylnaphthalene sulfonic acid (DNNS) were prepared for several recently developed drugs used in the treatment of cardiovascular disorders. Thus, incorporation of DNNS along with the β-adrenergic blocker Acebutalol, or calcium-channel blockers Verapamil, Diltiazem, Nicardipine, or Lidoflazine into a plasticized poly(vinyl chloride) membrane resulted in coated-wire ion-selective electrodes which displayed nearly Nernstian response in the concentration range 10^{-3}—10^{-5} M and quantitatively useful responses down to 10^{-6} M. Selectivity behavior for each set of electrodes was accurately predicted from calculated distribution constants for the respective drugs. Application of these electrodes to pharmaceutical preparations is discussed, as is their utility in pharmacokinetic studies.

Incorporation of dinonylnaphthalene sulfonic acid as an extractant in PVC membranes plasticized with dioctylphthalate has led to coated-wire electrodes having extremely high selectivity for organic cations over common inorganic cationic species [1]. Previous work has focused on the role of analyte structure on the selectivity behavior of these devices [2] and on development of electrodes selective to many important drugs of abuse [3] and other pharmaceuticals [4, 5]. In each of these studies, it was shown that the selectivity of an electrode increases with the analyte extractability, i.e., with its distribution constant. Therefore, the selectivity depends not only on molecular weight, but on the degree of nitrogen substitution and branching of hydrocarbon chains. A more important consideration with pharmaceutical compounds is the influence of hydrophilic substituents, because among a group of drugs similar in size, such factors prevail in determining overall membrane selectivity with respect to either metabolites or other potential interferents. As demonstrated in earlier work, interference from common inorganic and hydrophilic organic cations is not measureable [1, 2].

In this work, coated-wire electrodes were prepared for several drugs used in treatment of cardiovascular diseases [6, 7]; among them are drugs awaiting FDA approval for commercial introduction as well as some available for prescription. The existence of widely varying structures (e.g., I—V) among the calcium channel blockers has puzzled researchers who are trying to

0003-2670/84/$03.00

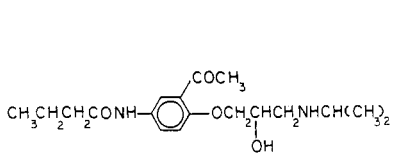

I

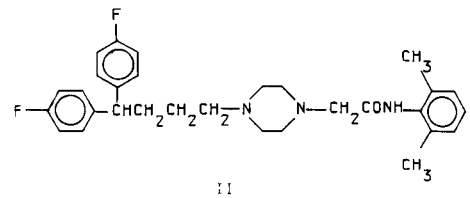

II

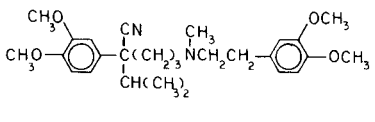

III

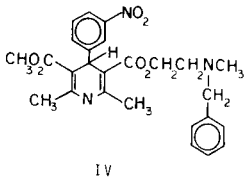

IV

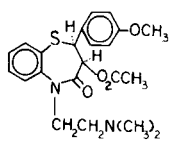

V

elucidate a well-defined mechanism of action. The electrodes described here could prove useful in future investigations because of their low cost, small size, durability, sensitivity and selectivity. All of these compounds are monovalent cations at physiological pH values which make them amenable to ion-selective electrode potentiometry. Structural differences will influence drug extractability and hence electrode response characteristics. Response characteristics were critically evaluated in this study in the context of their potential application to pharmaceutical assay and in-vivo or in-vitro drug monitoring. In anticipation of routine use with pharmaceutical preparations, the effect of high background levels of α-lactose, a common packing material, was also determined.

Recent studies [8, 9] have shown that incorporation of a lipophilic base such as tridodecylamine into plasticized PVC results in a pH-responsive electrode having little or no interference from inorganic anions provided that sufficient amounts of a lipophilic anion such as tetraphenylborate are also included. Because the electrodes reported here are analogous to these systems, having a lipophilic amine in the form of a high-molecular-weight pharmaceutical and a lipophilic anion as DNNS, some kind of pH response might be expected. If so, an optimum pH region would exist for each electrode.

Experimental

Reagents. The drugs investigated here were Acebutalol (Ives) (I), a β-adrenergic blocker; and the calcium-channel blockers Lidoflazine (Janssen) (II), Verapamil (Searle, Knoll) (III), Nicardipine (Syntex) (IV), and Diltiazem (Marion) (V), which were kindly supplied by the manufacturers. These were dried over calcium chloride prior to use. Free bases were converted to their hydrochloride forms by dissolving in a minimum of concentrated hydrochloric acid; all solutions were prepared at pH 4.0 in 0.01 M acetate buffer. Chromatographic grade poly(vinyl chloride) (Polysciences, Warrington, PA) was used as obtained, as was practical-grade dioctyl phthalate (J. T. Baker, Phillipsburg, NJ) Dinonylnaphthalene sulfonic acid (Henkel Chemical) was purified by the ion-exchange method of Danesi et al. [10]. All other chemicals were reagent grade.

Electrode preparation and handling. The coated-wire electrodes were constructed as described earlier [11], except that PVC-insulated copper wires were substituted for coaxial cables. This facilitated the fabrication of large numbers of electrodes (20 for each drug) with a negligible increase in noise from the absence of shielded wire. After manufacture, it was necessary to bathe the electrodes in 10^{-3}—10^{-4} M solutions of the protonated analyte species for several days before stable responses could be obtained, during which time hydration of the polymer membrane occurred. As was the case in earlier work [5], soaking in blank buffer for several minutes prior to calibration resulted in best reproducibility.

Apparatus and e.m.f. measurements. Previously described micro- and minicomputer systems were used to perform all calibrations within user-specified concentration limits [2, 12]. Except for pH response, all potentials reported were measured at pH 4.0 against a double-junction calomel electrode having 0.1 M ammonium nitrate in the external junction. Electrode equilibrium was assumed when a maximum of 0.4 mV min^{-1} drift was measured. All measurements were made at 25.0 ± 0.5°C.

Detection limits were measured by extrapolating the linear segments of plots of potential vs. log concentration to meet another plot taken from the points in the region of no response [13], typically at concentration levels below 10^{-6} M.

At the end of a calibration run, electrodes were placed in a solution of known primary ion concentration. Specified ratios of primary to interfering ion concentration were made by adding standard interferent solution from a second digital burette, after which responses of each electrode were measured and stored. Selectivity coefficients were then calculated using software based on the two-solution method of Srinivasan and Rechnitz [14].

The pH responses were also evaluated under computer control. The coated-wire electrode potentials were read vs. a Ag/AgCl reference contained in a Radiometer/Copenhagen glass combination electrode, which was used simultaneously to monitor pH. Starting at a low initial pH value (<4.0), small increments (0.2 ml) of 0.1 M sodium hydroxide were added to the blank buffer solution until a minimum specified pH change was achieved, at which point electrodes were sampled until each equilibrated. This process was repeated until the desired pH limit was reached. Profiles of mV vs. pH were then plotted on a digital plotter.

Results and discussion

All electrodes displayed logarithmic response of nearly Nernstian character in the concentration of analyte above approximately 10^{-5} M as shown in Table 1. Because these pharmaceuticals have low water solubility, an upper limit of only 10^{-3} M was possible for each calibration, though Nicardipine and Lidoflazine could be measured only to $10^{-3.2}$ M. Detection limits of at least 10^{-5} M were observed for all electrodes. Somewhat lower detection limits were obtained with electrodes for Nicardipine which displayed values

TABLE 1

Electrode response characteristics

Drug	Slope (mV/log C)	S.d.[a]	Y-intercept (mV)	S.d.[a]
Acebutalol	57.7	3.0(1.7)	156	23(22)
Diltiazem	60.1	1.7(1.8)	274	10(9)
Lidoflazine	60.0	1.5(1.6)	311	8(7)
Verapamil	58.7	1.7(1.0)	310	5(5)
Nicardipine	58.8	1.6(1.4)	393	11(8)

[a]Standard deviations for individual electrodes after repeated calibrations over several months and, in parentheses, average standard deviations among 20 electrodes.

down to 10^{-6} M (Fig. 1). Response times ranged from a few seconds for concentrations greater than 10^{-5} M to several minutes for lower concentrations.

It is expected that these electrodes would be exposed to a variety of matrices during analysis of pharmaceutical preparations. The effects of high background levels of neutral compounds were assessed by comparison of calibrations in absence and in presence of 10^3- to 10^4-fold excess concentrations of α-lactose relative to the highest concentration of the drug of interest. It was found that repeated calibrations of various electrodes were virtually identical, demonstrating that no interference is measurable from high levels of this substance in the sample matrix.

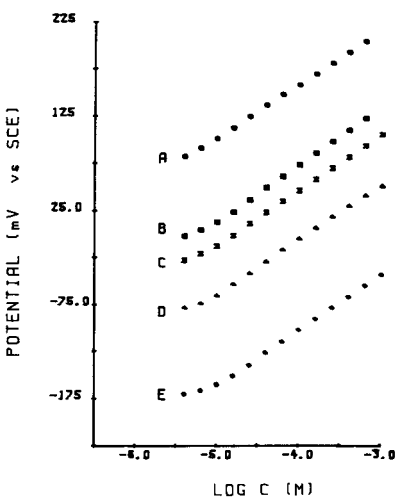

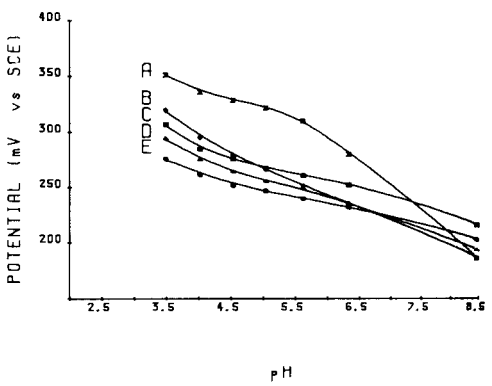

Fig. 1. Calibration curves of coated-wire electrodes for Nicardipine (A), Lidoflazine (B), Verapamil (C), Diltiazem (D) and Acebutalol (E).

Fig. 2. pH responses of coated-wire electrodes for Nicardipine (A), Acebutalol (B), Verapamil (C), Diltiazem (D) and Lidoflazine (E).

TABLE 2

Selectivity coefficients of each electrode vs. tributylammonium

Drug	Log $k^{pot}_{i,TBA}$	S.d.[a]	Log K_D
Acebutalol	2.44	0.2	—0.2
Diltiazem	0.71	0.02	2.3
Lidoflazine	0.30	0.02	5.3
Verapamil	—0.32	0.02	5.9
Nicardipine	—0.89	0.02	6.3

[a]Average standard deviation after five measurements with ten electrodes for each compound.

Relative selectivity was determined by measuring responses in solutions containing various ratios of tributylammonium to the primary ion. Log $k^{pot}_{i,TBA}$ values which were calculated from the electrode responses and known activities of each ion are given in Table 2 along with respective log K_D values calculated by the Hansch correlation method [15]. The increase in selectivity with drug lipophilicity was consistent with prior investigations of homologous series of alkylated ammonium ion interferents and for electrodes selective to other drugs [5]. Because drug metabolites are usually more hydrophilic than their parent compounds, they would exhibit negligible interference.

Response to pH was also a function of the primary ion. A decrease in e.m.f. readings with increasing pH was observed (Fig. 2), though these were not linear over the entire pH range studied and were sub-Nernstian even in regions where there was a highly pH-dependent response (50 mV/pH unit maximum). Because pH can be accurately maintained to ±0.02 units, an uncertainty of ±1 mV is expected for the latter region. This corresponds to a concentration error of ±4%. However, errors of less than 1% would be expected in regions of lesser pH dependence, i.e., 10—15 mV/pH unit.

The electrodes reported here provide a rapid, inexpensive, and reliable method of determination with minimum sample preparation and high selectivity. Detection limits of 10^{-5} M or lower along with stability in various matrices further enhances their practicality in assays of these and other pharmaceuticals which are protonated amines. Though no commercial preparations were tested here, a suitable procedure would simply involve sample dissolution into an appropriate pH buffer followed by potentiometric measurement. As demonstrated, neutral fillers need not be extracted or accounted for. It is, of course, recommended that electrode calibration be confirmed periodically.

Perhaps of greater interest is the use of potentiometric sensors for monitoring the concentration of these drugs during pharmacological or related studies. The way in which each of these drugs inhibit Ca^{2+} uptake by smooth muscle cells, a required step for cellular contraction, is as yet unknown

[16, 17]. For this reason, a drug monitor would be beneficial in investigations aimed at resolving such problems.

This research was funded by a grant from the United States Office of Naval Research.

REFERENCES

1 C. R. Martin and H. Freiser, Anal. Chem., 52 (1980) 562.
2 L. Cunningham and H. Freiser, Anal. Chim. Acta, 132 (1981) 43.
3 C. R. Martin and H. Freiser, Anal. Chem., 52 (1980) 1772.
4 T. Yamada and H. Freiser, Anal. Chim. Acta, 125 (1981) 179.
5 L. Cunningham and H. Freiser, Anal. Chim. Acta, 139 (1982) 97.
6 N. A. Awan, A. N. DeMaria and D. T. Mason, Drugs, 23 (1982) 235.
7 H. J. Sanders, Chem. Eng. News, 60(28) (1982) 26.
8 P. Schulthess, Y. Shijo, H. V. Pham, E. Pretsch, D. Ammann and W. Simon, Anal. Chim. Acta, 131 (1981) 111.
9 D. Ammann, F. Lanter, R. A. Steiner, P. Schulthess, Y. Shijo and W. Simon, Anal. Chem., 53 (1981) 2267.
10 P. R. Danesi, R. Chirizia and G. Scibona, J. Inorg. Nucl. Chem., 35 (1973) 3926.
11 C. R. Martin and H. Freiser, J. Chem. Educ., 57 (1980) 512.
12 C. R. Martin and H. Freiser, Anal. Chem., 51 (1979) 803.
13 International Union of Pure and Applied Chemistry, Pure Appl. Chem., 48 (1976) 129.
14 K. Srinivasan and G. Rechnitz, Anal. Chem., 41 (1969) 1203.
15 C. Hansch and A. J. Leo, Substituent Constants for Correlation Analysis in Chemistry and Biology, Wiley, New York, 1979.
16 A. Schwartz, Am. J. Cardiol., 49 (1982) 497.
17 R. W. Millard, D. A. Lathrop, G. Grupp, M. Ashraff, I. Grupp and A. Schwartz, Am. J. Card., 49 (1982) 499.

Analytica Chimica Acta, 157 (1984) 163—169
Elsevier Science Publishers B.V., Amsterdam — Printed in The Netherlands

Short Communication

QUANTITATION OF SULPHUR IN XYLENE WITH AN INDUCTIVELY-COUPLED PLASMA PHOTODIODE-ARRAY SPECTROMETER

M. W. BLADES* and PETER HAUSER

Department of Chemistry, University of British Columbia, Vancouver, B.C. V6T 1Y6 (Canada)

(Received 28th March 1983)

Summary. The application of an inductively-coupled plasma spectrometer with a photodiode-array detection system to the direct quantitation of total sulphur in xylene is described. The emission lines utilized are the near-infrared atomic sulphur (S I) lines at 921.29, 922.81, and 923.75 nm. Structure in the background emission spectrum in this region is attributed to the Philips molecular C_2 band. The best spatial zone to observe is at 12 mm above the load coil. The detection limit for sulphur at the 921.29-nm line is 100 mg l^{-1}.

There is considerable interest in the application of atomic spectrometric techniques to the determination of metals in petroleum-based samples [1]. Inductively-coupled plasma emission spectrometry (i.c.p.e.s.) is attractive for these determinations [2, 3], and studies on the optimized design and operation of an i.c.p. torch for use with organic solvents have recently been reported [4]. The application of i.c.p.e.s. for quantifying sulphur in organic solvents has not received much attention. Windsor and Denton [5] evaluated i.c.p.e.s. for quantifying nonmetals, including sulphur, introduced as vapours from a heated vaporizing block, and Ward [6] reported results for sulphur in residual fuel oil. Windsor and Denton used the 190.03-nm line. In aqueous solvents, the spectral lines normally used are 180.73, 182.04, and 182.63 nm [7]; these resonance lines lie in the vacuum ultraviolet so that the spectrometer must be either evacuated, or purged with nitrogen to prevent atmospheric absorption of emitted radiation.

The use of a linear, self-scanned, photodiode array to quantify nonmetals, including sulphur, using near-infrared, nonresonant transitions has been suggested [8, 9]. The photodiode array has its maximum response in the 700—800-nm region and thus is a good detector for near-infrared emissions. In addition, a linear photodiode array such as the Reticon 1024S can simultaneously monitor a relatively wide spectral region, thus offering the potential for simultaneous multielement quantitation combined with inherent background correction capability.

In a previous study [9], the most sensitive emission lines for atomic sulphur

0003-2670/84/$03.00

(S I) were identified by injecting hydrogen sulfide into the argon aerosol gas stream. The present study focuses on the utilization of these lines for quantitation in nebulized organic samples. Xylene was used as solvent because it is a very common diluent for oils and gas-oils [1]. The introduction of a hydrocarbon, like xylene, can alter the characteristics of the i.c.p. quite substantially so that these characteristics must be studied in establishing optimum conditions.

Experimental

The radio-frequency (r.f.) inductively-coupled plasma, the photodiode array spectrometer, and the data acquisition system are outlined in Table 1. The system has been described [10], but in the present study, the photodiode array is mounted horizontally in the exit focal plane of the monochromator. The spectral range is about 38 nm at 900 nm. All facets of the operation of the photodiode array can be controlled from the Apple computer keyboard. The integration time is supervised by the computer, which can be programmed to allow integration times from 50 ms to 10 s in 50-ms increments.

Xylene solutions containing sulphur were prepared using diphenyldisulphide dissolved in a mixture of the reagent-grade xylene isomers.

The i.c.p. is initiated using isopropanol as a solvent aerosol and, after tuning, is switched to xylene. The automatic matching network compensates for changes in reflected power and the plasma can normally be operated at less than 10 W reflected power by fine tuning. Stability of the "organic" i.c.p. is very sensitive to the type of quartz torch used; the Sherritt-Gordon torch was found to be far superior in terms of plasma stability and reflected power compared to a torch of more conventional dimensions [11]. The deposition of carbon soot at the inner edges of the quartz tubes can be a problem when organic materials are aspirated [2, 4] with the latter torches; the Sherritt-Gordon torch is much less susceptible to this buildup, at the gas flows recommended.

Spectra are obtained by integrating emission intensities for a fixed period of time. This signal is stored in the computer memory. Effects of fixed-pattern signal associated with the array are reduced by subtracting the dark current from the signals for the samples. The background signal for xylene is subtracted from the signal for sulphur in xylene.

Results and discussion

In agreement with Hughes et al. [8, 9], it was observed that the most sensitive sulphur lines in the near-infrared region (0.7—1 μm) were the non-resonant $4s$—$4p$ atomic transitions at 921.29, 922.81, and 923.75 nm. The spectrum monitored by the photodiode array, centered at 915 nm, is plotted in Fig. 1. For xylene alone (Fig. 1A), the principal emission lines are those from atomic carbon (C I) and atomic argon (Ar I). Figure 1B is the emission spectrum observed for 1% sulphur (as diphenyldisulphide) in xylene; Fig. 1C is the background-corrected spectrum of this solution, obtained by acquiring

TABLE 1

System components

I.c.p.	Plasma-Therm (Kresson, NJ), HFP-2500E RF generator (2.5 kW), AMN-2500E automatic matching network, APCS-1 automatic power control unit, PR-1 pressure regulator
Quartz torch	All quartz low gas flow torch from Sherritt-Gordon Mines (Fort Saskatchewan, Alberta, Canada)
Nebulizer	Plasma-Therm Model GN5601 glass concentric
R.f. power	1.75—2.0 kW forward, < 10 W reflected
Argon flow rates (l min^{-1})	Plasma 8, auxiliary 2, nebulizer 0.8
Observation zone	2.5 mm vertical section centered at 12 mm above the load coil
Focusing optics	150-mm focal length, 50-mm diameter plano-convex fused silica lens, 1:1 magnification
Monochromator	GCA-McPherson Model 270, 0.35-m focal length, Czerny-Turner
Grating	1200 lines per mm blazed at 500.0 nm
Detector	Reticon RL-1024S linear photodiode array (Sunnyvale, CA)
Readout	Reticon RC-1024S-3 evaluation board
Entrance slit	100 mm wide
Data system	Apple II plus computer-based data-acquisition system
ADC	Interactive Structures AI13, 12-bit ADC
Diode array clock rate	17.5 kHz

a xylene background emission spectrum at an integration time of 1.22 s and subtracting it from the sample spectrum. The sulphur transitions at 921.29 and 923.75 nm are essentially free of major spectral overlap, but the 922.81-nm transition has a significant spectral overlap with the Ar I 922.45-nm line.

The lower region of the aerosol channel has very intense molecular C_2 emission in a zone extending to about 12 mm above the load coil. This C_2 emission creates the characteristic green "bullet" (Swan bands). The spectrum in Fig. 2 shows the (0,0) and (1,0) bandheads of C_2 which cause this emission. It is important to view the S I emission in a spectral region in which C_2 emission is minimized because it is the main contributor to spectral background in the 900-nm region. The Philips band caused by the $b^1\Pi_u$—$x^1\Sigma_g$ transition has two bandheads at 875.08 nm and 898.04 nm [12]. These bands are degraded to the red and present a significant rotational structure in the 920-nm region. The C_2 emission spectrum is shown in Fig. 3. The lower limit of detection will be dictated by the flicker noise in the C_2 background. In agreement with previous workers [8, 9] it was found that the intensity of the nonresonant sulphur emission is also greatest in the region 0—12 mm above the load coil. Thus a compromise must be reached which will minimize the C_2 background and maximize the S I line intensity.

The spatial distributions of C_2 and S I emission are shown in Fig. 4. These distribution profiles were measured as follows: the i.c.p. torch enclosure

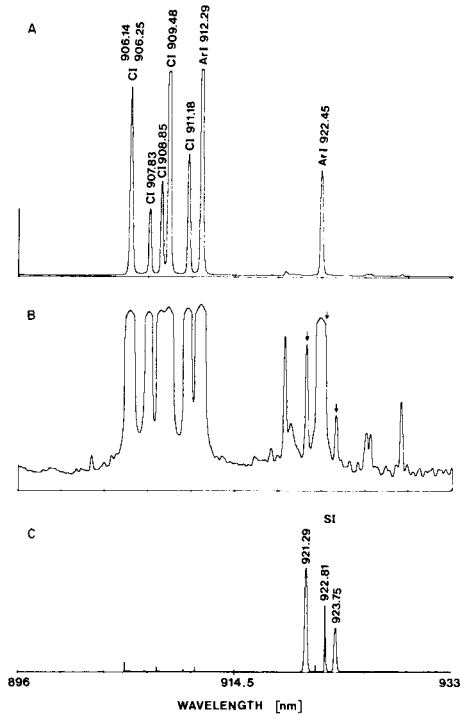

Fig. 1. Emission spectra centered at 915 nm. Sample aerosol: (A) xylene, integration time 0.24 s; (B) xylene plus 1% sulphur, integration time 1.22 s; (C) spectrum of 1% sulphur with the background removed. The S lines in (B) are marked with arrows.

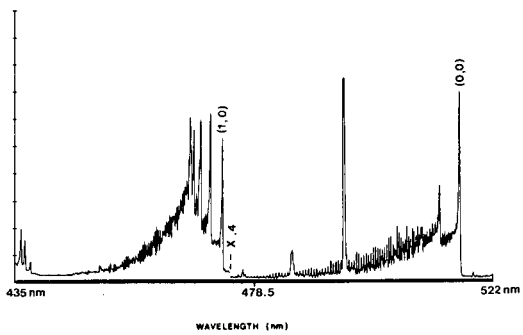

Fig. 2. Emission spectrum from 435 to 522 nm showing the (0,0) and (1,0) emission bands of C_2, with xylene as aerosol. The (0,0) band was recorded at 0.4 times the sensitivity of the (1,0) band and is thus 2.5 times more intense.

was mounted on a linear translation stage (Daedel Model 4979, Harrison City, PA) capable of moving the enclosure horizontally relative to the entrance slit of the monochromator. The Apple computer controlled this motion to the nearest 0.025 mm via a stepper motor interface. The stage

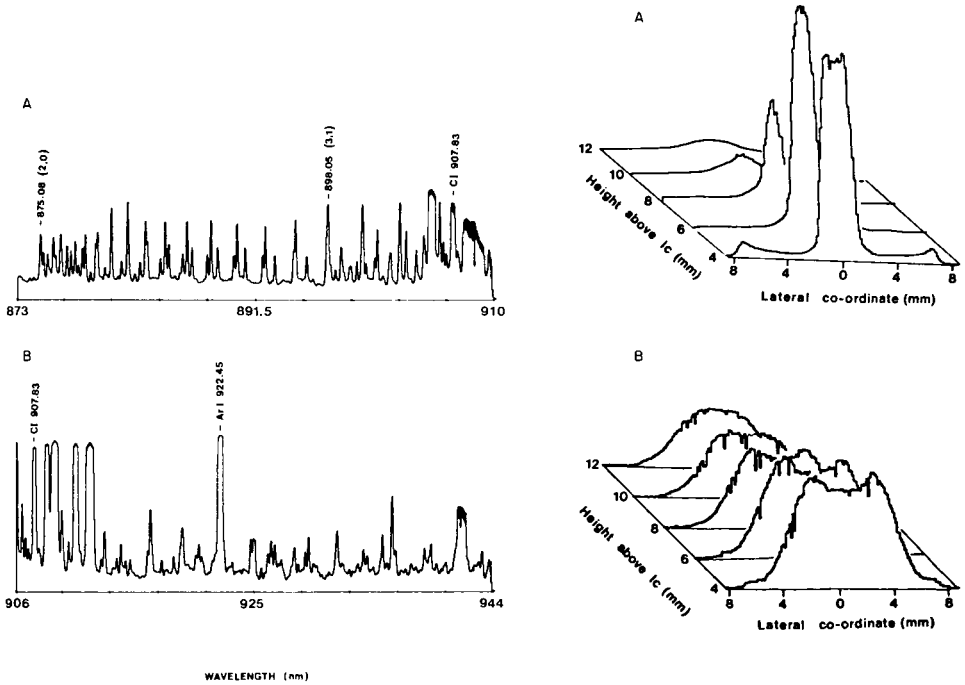

Fig. 3. Emission spectrum of the Philips band, $b^1\Pi_\mu - x^1\Sigma_g^+$, showing the (2,0) band at 875.08 nm, and the (3,1) band at 898.05 nm (integration time 3.05 s).

Fig. 4. Spatial emission profiles of: (A) C_2 473.71 nm, and (B) S I 921.29 nm. See text for discussion.

was positioned so that a set of spectral lines near the edge of the discharge could be measured. The emission intensity of the selected line was measured and stored; the stage was moved a short distance and the process was repeated. Thus the spatial emission intensity distribution was collected for a set of lines for up to 200 points across the discharge for each height. Figure 4A and B are the spatial distributions of the C_2 Swan bandhead and of the S I line at 921.29 nm, respectively.

Several features of these diagrams are important. The C_2 emission is essentially confined to the aerosol channel. There is some slight skirting of the aerosol around the outer edges of the discharge, which produces a small amount of C_2 emission at a lateral displacement of about ±7.5 mm from the center at 4 mm above the load coil. In contrast, the S I emission is not confined to the aerosol channel but originates from within the annular region of the plasma, a feature that has been observed for emission from states with high excitation energies [13]. This is a curious property of high-energy lines, because it is not clear how the analyte can migrate to a position within the annular region; perhaps there is more mixing of aerosol and plasma gases than one would expect. However, the C_2 emission essentially disappeared

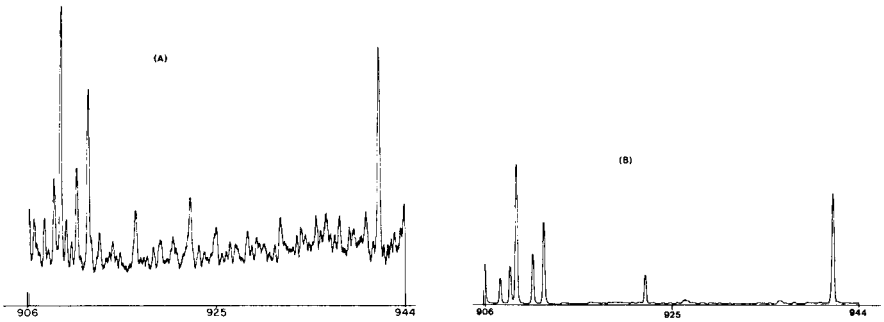

Fig. 5. Effect of adding oxygen to the aerosol stream on background emission intensity from xylene. Sample: (A) aerosol argon only; (B) argon plus 5% O_2. Taken at 10 mm above the load coil, 1.75 kW.

at 12 mm above the load coil and thus this height was chosen for quantitative measurements.

To establish the quantitative capability for sulphur determinations in xylene, a working curve was constructed using diphenyldisulphide dissolved in xylene at 921.29 nm. The plot was linear over the concentration range 0.05—1 wt.% sulphur in xylene. Linear regression provided the following statistics: slope = 1.013, intercept = 3.125×10^{-4} (with the emission intensity at 1% sulphur set to 1.0 and other intensities normalized to this value), correlation coefficient = 0.998, and the standard error of estimate = 0.0299. The estimated detection limit for sulphur in xylene was 0.01 wt.% or 100 mg l^{-1}, which is significantly worse than the detection limit of 0.024 mg l^{-1} achieved for aqueous samples at 180.731 nm [14]. The principal reasons for the higher detection limits are that the 921.19-nm line is less intense than the 180.731-nm line and that the aspirated xylene creates an intense spectral background at 921 nm, significantly reducing the signal-to-background ratio compared with aqueous aerosols.

The detection limit can obviously be improved by reducing the background C_2 emission. An attempt was therefore made to produce an oxidizing atmosphere in the i.c.p. discharge by adding oxygen to the aerosol [15]. The spectra of Fig. 5 demonstrate the utility of this approach for reducing the background structure from C_2 emission in the region 906—944 nm. The detection limit for the 921.29-nm S I line with oxygen added was not improved, however, when the operational parameters were the same as with no oxygen, the line intensity for sulphur was reduced by a factor of 1.8, probably because of changes in the spatial emission structure for the S I line. This effect has been observed for metals in the i.c.p. [16].

Conclusions

The approach may be useful, for the direct quantitation of total sulphur in crude and refined petroleum samples where the sulphur concentrations are

often in the range 0.1—5 wt.%; this is being evaluated using National Bureau of Standards petroleum standards.

The low-to-medium resolution photodiode array spectrometer could be extremely useful as an extra channel on existing direct-reading systems. The ability to determine the nonmetals in the near-infrared region is one application for such an extra channel. In addition, because the linear photodiode array is responsive over the entire spectral range from 200 to 1000 nm, this extra channel could also be applied as a quick, qualitative tool for estimating the composition of a sample. Finally, because the diode array-based spectrometer can simultaneously measure the emission spectrum over 35—50 nm, the spectral background structure in the region of a line of interest can be quickly examined.

The authors thank the Natural Sciences and Engineering Research Council of Canada for financial support. We also thank Sherritt-Gordon Mines for the donation of the quartz torch used. This paper was presented in part at the 1982 Pacific Conference on Chemistry and Spectroscopy, San Francisco, October, 1982.

REFERENCES

1 V. Sychra, J. Land and G. Sebov, Prog. Anal. At. Spectrosc., 4 (1981) 341.
2 V. A. Fassel, C. A. Peterson, F. N. Abercrombie and R. N. Kniseley, Anal. Chem., 48 (1976) 516.
3 R. N. Merryfield and R. C. Lloyd, Anal. Chem., 51 (1979) 1965.
4 P. W. J. M. Boumans and M. Ch. Lux-Steiner, Spectrochim. Acta, Part B, 37 (1978) 97.
5 D. L. Windsor and M. B. Denton, Appl. Spectrosc., 32 (1978) 366.
6 A. F. Ward, Am. Lab., Nov., (1978) 79.
7 G. F. Kirkbright, A. F. Ward and T. S. West, Anal. Chim. Acta, 62 (1972) 241.
8 S. K. Hughes and R. C. Fry, Appl. Spectrosc., 35 (1981) 493.
9 S. K. Hughes, R. M. Brown and R. C. Fry, Appl. Spectrosc., 35 (1981) 396.
10 M. W. Blades, Appl. Spectrosc., 37 (1983) 371.
11 V. A. Fassel and R. N. Kniseley, Anal. Chem., 46 (1974) 1110A, 1155A.
12 J. G. Phillips, Astrophys. J., 107 (1942) 389.
13 N. Furuta and G. Horlick, Spectrochim. Acta, Part B, 34 (1982) 53.
14 T. Hayakawa, F. Kikui and S. Ikeda, Spectrochim. Acta, Part B, 37 (1982) 1069.
15 D. Truitt and J. W. Robinson, Anal. Chim. Acta, 51 (1970) 61.
16 E. H. Choot, Ph.D. Thesis, University of Alberta, 1982.

Analytica Chimica Acta, 157 (1984) 171—176
Elsevier Science Publishers B.V., Amsterdam — Printed in The Netherlands

Short Communication

THE DETERMINATION OF INORGANIC PHOSPHORUS COMPOUNDS BY USING MOLECULAR EMISSION CAVITY ANALYSIS

A. C. CALOKERINOS* and T. P. HADJIIOANNOU
Laboratory of Analytical Chemistry, University of Athens, Athens (Greece)
(Received 14th July 1983)

Summary. The chemical and spectral interferences on the HPO emission within the cavity are investigated. Alkali metals, copper, manganese, iron and sulphate all interfere spectrally, and the alkali metals also suppress the HPO emission. A standard addition method after a batch ion-exchange resin treatment of the sample solution is proposed for the determination of phosphorus (1—1000 mg l^{-1} P) in solutions of inorganic samples (e.g., rocks).

The determination of phosphorus compounds by cool-flame spectrometry with generation of HPO emission is simple, fast and requires minimal sample preparation compared to conventional spectrophotometric methods. Aspiration of aqueous orthophosphoric acid solutions into a hydrogen-nitrogen flame has been proposed for determinations in the range 0.2—500 mg l^{-1} phosphorus (as phosphate) with a limit of detection of 0.1 mg l^{-1} [1]; this was lowered to 7 μg l^{-1} by using a heated nebulization chamber and a simple filter photometer [2]. Formation of refractory compounds within the cool flame severely decreases the HPO emission, and batch treatment with a cation-exchange resin was recommended to eliminate these depressive effects [1, 2]. Removal of sodium and potassium ions was not complete and calibration against pure orthophosphoric acid solutions was impossible. A standard addition batch method was suggested for the determination of phosphorus in lubricating oils [3].

Conventional molecular emission cavity analysis (m.e.c.a.) [4, 5] allows the determination of low levels of phosphorus with a limit of detection of 0.5 ng [6, 7]. Addition of sulphuric acid eliminates the formation of refractory compounds in the cavity [6] but severe spectral interference occurs from S_2 emission [8]. Treatment of the sample solution with a cation-exchange resin has been proposed [8, 9] but the procedure has not previously been applied to real samples.

In this communication, chemical and spectral interferences on the HPO emission from inorganic phosphorus compounds are investigated. Batch treatment with a cation-exchange resin is proposed for the determination of phosphorus in the range 1—1000 mg l^{-1}. The method is applied to the determination of phosphorus in rocks by using standard additions.

0003-2670/84/$03.00

Experimental

Apparatus. The apparatus and cavity used were the same as previously reported [10]. The solution is aspirated into the hydrogen-nitrogen flame and the HPO emission generated on the cool cavity surface is measured at 528 nm [10]. In this system, a solid residue does not form on the inner surface of the cavity and the reflectivity remains constant [4].

Reagents. Analytical-grade reagents and deionized-distilled water were used throughout. A stock orthophosphoric acid solution containing 5 mg P ml^{-1} was prepared by diluting 11 ml of concentrated orthophosphoric acid (Ferak Berlin, 85%) with water to 1 l; the solution was standardized titrimetrically with standard sodium hydroxide solution (glass electrode). All standard solutions were then prepared by appropriate dilution.

Batch treatment of solutions with cation-exchange resin. Add 2 g of dry Dowex 50W-X8 (200—400 mesh, Fluka) resin to about 40 ml of solution in a 50-ml beaker and stir with a glass stirrer for 15 min. Leave to settle for 5 min and filter through a Whatman No. 41 filter paper. Aspirate the filtrate and measure the HPO emission.

Determination of phosphorus in rocks. Weigh accurately about 2 g of finely powdered sample and transfer to a 250-ml beaker. Add 10 ml of water, 20 ml of concentrated nitric acid and 10 ml of concentrated hydrochloric acid and cover with a watch glass. Heat the mixture to dissolve the sample, preferably on an oscillating hot plate, and boil gently until no fumes of hydrochloric acid can be detected. Add 10 ml of water and 5 ml of 1 M nitric acid and heat to dissolve the soluble salts. Filter through a Whatman No. 41 filter paper into a 100-ml volumetric flask. Wash the residue with 10 ml of warm 1 M nitric acid to remove any traces of phosphate and make up to volume with water (solution A). Transfer 10.00-ml aliquots of solution A into three 100-ml volumetric flasks (A1, A2, A3). Add 1.00 ml and 2.00 ml of stock orthophosphoric acid solution to A2 and A3, respectively, so that after dilution the solutions contain 50 and 100 mg l^{-1} phosphorus added. After dilution to volume, treat with resin and measure the HPO emission.

Results and discussion

Optimization and calibration. The effect of the hydrogen dilution function D [10] on the HPO emission intensity at various hydrogen flows is shown in Fig. 1. Intense emissions are obtained at 2.60 l H_2 min^{-1} and $D = 0.480$ which corresponds to 2.82 l N_2 min^{-1}. These flows were used for all subsequent measurements.

The position of the cavity in the flame determines the cavity temperature, the nature and concentration of flame species (unburnt gas, radicals) and the amount of analyte that enters the cavity space. Table 1 shows the effect of vertical and horizontal displacement of the cavity in the flame. All subsequent measurements were made with the cavity fixed at the flame centre, 14 mm above the burner head. Cooling water was supplied to the cavity at 440 ml min^{-1}.

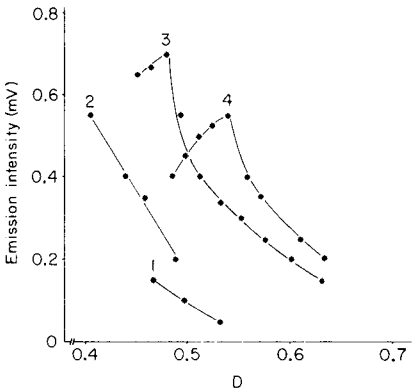

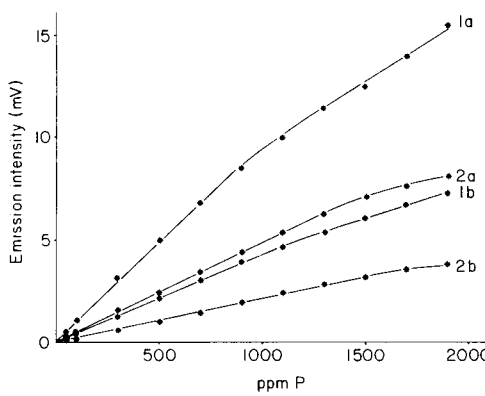

Fig. 1. The effect of the hydrogen dilution function D on the HPO emission intensity from 100 mg l^{-1} P as orthophosphoric acid at: (1) 1.50; (2) 1.80; (3) 2.60; (4) 3.30 l H_2 min^{-1}.

Fig. 2. HPO calibration graph from aqueous orthophosphoric acid: (1) pure; (2) in the presence of 0.3 M sulphuric acid, at: (a) 2 mm; (b) 1.3 mm slit width.

TABLE 1

HPO emission intensity (I) from 100 mg l^{-1} P as a function of (a) vertical, (b) horizontal displacement of cavity

(a) *Vertical displacement of cavity*

Height (mm)[a]	0	2	4	6	8	10	12	14	16	18	20
I (mV)	0.45	0.35	0.20	0.25	0.35	0.40	0.50	0.70	0.60	0.40	0.35

(b) *Horizontal displacement of cavity*

Distance (mm)[b]	0	1	2	3	4	5
I (mV)	0.20	0.60	0.65	0.65	0.65	0.45

[a]Measured from burner head, cavity 3 mm into flame. [b]Measured from flame edge away from detector towards the detector (centre of flame is ca. 3 mm), height = 14 mm.

The calibration graph had two linear ranges, 1—50 and 50—1000 mg l^{-1} P, at a slit-width of 2 mm (Fig. 2). Negative deviations were observed at higher concentrations, probably because of flame saturation. The limit of detection (signal-to-noise ratio = 2) was 1 mg l^{-1} P. The sensitivity decreased at a slit width of 1.3 mm (Fig. 2).

Spectral and chemical interferences. Sodium ion, in samples and in chemical reagents, is the commonest chemical and spectral interferent on the HPO emission. Formation of refractory sodium compounds may severely decrease the molecular emission; sulphuric acid (0.3 M final concentration) has been recommended as a releasing agent [6, 8]. The sodium emission shows

measurable intensities at 528 nm which cannot totally be eliminated by slit-width reduction (Table 2). Weak sodium emission is generated even after addition of sulphuric acid to the analyte solution. Therefore, the same concentration of sodium ions must be present in standards and unknowns to compensate for this radiation.

When aqueous sulphuric acid solutions were aspirated into the flame, the characteristic S_2 emission was generated on the surface of the cavity, showing measurable intensities at 528 nm, even at narrow slit-widths (Table 2). Addition of sulphuric acid to aqueous solutions of orthophosphoric acid reduced the net HPO emission (Fig. 2), probably because it alters the flame radical concentration and/or flame temperature at the region of HPO formation.

Hydrochloric acid did not affect the emission, whereas 0.2, 0.5 and 1 M nitric acid decreased the emission from 300 mg l^{-1} P by 15%, 25% and 40%, respectively. This decrease might be due to the catalytic effect of NO radicals on the recombination of atomic hydrogen and hydroxyl radicals to water vapour [11] with subsequent decrease in flame radical concentration. Therefore, if nitric acid is used to dissolve samples, reference to a calibration for pure orthophosphoric acid will give erroneous results.

The use of sulphuric acid as a releasing agent for phosphorus compounds is associated with spectral interferences and decreased HPO emission, as already stated. Therefore, metal ions that interfere spectrally or chemically with the emission must be removed from the sample solution prior to aspiration.

The effect of various cations on the HPO emission before and after the proposed resin treatment is shown in Table 3. Potassium ions show stronger spectral and weaker chemical interferences than sodium ions; they are also more effectively removed by the resin treatment than sodium ions but neither ion is eliminated completely when present in high concentrations, and calibration graphs for pure solutions cannot be used. Copper(II), manganese(II) and iron(III) as chlorides generate characteristic emissions with maxima at 488, 500 and 515 nm, respectively [12, 13] and cause severe spectral interferences at 528 nm. However, they are completely eliminated by the resin treatment.

TABLE 2

Emission intensities from sodium atoms and S_2 molecules at 528 nm with various slit widths

Compound	Concn. (M)	Emission intensity (mV)			Compound	Concn. (M)	Emission intensity (mV)		
		Slit width (mm)					Slit width (mm)		
		1.300	0.650	0.325			1.300	0.650	0.325
NaCl	0.5	0.75	0.25	0.05	H_2SO_4	0.1	0.50	0.10	0.03
	1.0	1.25	0.35	0.06		0.3	0.65	0.20	0.05
	2.0	1.75	0.45	0.11		0.6	0.80	0.20	0.05
	3.0	2.00	0.50	0.15		1.0	0.90	0.20	0.05

TABLE 3

The effect of various cations on the HPO emission intensity from 100 mg l^{-1} P before and after treatment with the resin

Interferent[a]	Relative emission intensity[b]			
	Interferent alone		Interferent +100 mg l^{-1} P	
	Before	After	Before	After
0.01 M Na^+	4.50	0	4.50	77.3
0.1 M Na^+	50.0	22.7	50.0	22.7
0.01 M K^+	18.2	0	22.7	91.0
0.1 M K^+	109	45.4	109	50
Ba^{2+}	0	0	78.8	100
Ca^{2+}	0	0	34.6	100
Cu^{2+}	63.1	0	105	100
Cr^{3+}	0	0	10.5	100
Co^{2+}	0	0	89.5	100
Mn^{2+}	5.30	0	63.1	100
Al^{3+}	0	0	0	100
Fe^{3+}	2.60	0	68.4	100

[a]All added as chlorides. Apart from alkali metals, all metals were added at 100 mg l^{-1} concentrations.
[b]The emission intensity from the pure solution of 100 mg l^{-1} P (1.30 mV) was arbitrarily taken as 100.

TABLE 4

Determination of phosphorus in aqueous orthophosphoric acid solutions

P added (mg l^{-1})	Calibration graph		Standard addition	
	P found (mg l^{-1})	Rel. error (%)	P found (mg l^{-1})	Rel. error (%)
5.00[a]	5.12	+2.4	5.13	+2.6
10.0[a]	10.2	+2.0	10.1	+1.0
25.0[a]	24.5	−2.0	25.0	0.0
50.0[a]	50.0	0.0	50.5	+1.0
100[b]	100	0.0	99.0	−1.0
200[b]	199	−0.5	197	−1.5
350[b]	352	+0.6	351	+0.3
500[b]	498	−0.4	504	+0.8
800[b]	802	+0.2	796	−0.5
1000[b]	1000	0.0	1000	0.0
50.0[c]	45.8	−8.4	50.0	0.0
50.0[d]	41.7	−16.6	51.0	+2.0

[a]From 1—50 mg l^{-1} P calibration graph.
[b]From 50—1000 mg l^{-1} P calibration graph. [c]0.15 M HNO_3 present. [d]0.5 M HNO_3 present.

TABLE 5

Determination of phosphorus in phosphate rocks[a]

P_2O_5 (%) present	17.35	22.80	25.19	26.69	32.80
Found	17.50	22.97	24.67	27.32	31.78
Relative error (%)	+0.9	+0.7	−2.1	+2.4	−3.1

[a]T. Smith Analyzed Standards.

Applications of the method. The results obtained for aqueous orthophosphoric acid solutions by using the calibration graph and standard addition procedures are shown in Table 4. The standard addition procedure (with additions before the resin treatment) is necessary if nitric acid is present, otherwise low results are obtained.

The proposed method was applied to the determination of phosphorus in analyzed phosphate rocks. The results were in good agreement with the expected values (Table 5). The accuracy of the method was further checked with recovery experiments in which phosphate was added to a concentrated liquid detergent, after treatment with concentrated hydrochloric acid. The recoveries ranged from 97 to 103% with an average of 100.2% (5 results).

This paper was presented at the 6th SAC Conference, Edinburgh, 1983.

REFERENCES

1 R. M. Dagnall, K. C. Thompson and T. S. West, Analyst, 93 (1968) 72.
2 K. M. Aldous, R. M. Dagnall and T. S. West, Analyst, 95 (1970) 417.
3 W. N. Elliott, C. Heathcote and R. A. Mostyn, Talanta, 19 (1972) 359.
4 S. L. Bogdanski, M. Burguera and A. Townshend, CRC Crit. Rev. Anal. Chem., 10 (1981) 185.
5 A. C. Calokerinos and A. Townshend, Prog. Anal. At. Spectrosc., 5 (1982) 63.
6 O. Osibanjo, Proc. Anal. Div. Chem. Soc., 13 (1976) 127.
7 R. Belcher, S. L. Bogdanski, O. Osibanjo and A. Townshend, Anal. Chim. Acta, 84 (1976) 1.
8 D. J. Knowles, P. Marriott and S. J. E. Slater, Proc. Anal. Div. Chem. Soc., 15 (1978) 62.
9 I. H. El-Hag, Anal. Proc., 19 (1982) 320.
10 A. C. Calokerinos and T. P. Hadjiioannou, Anal. Chim. Acta, 148 (1983) 277.
11 E. M. Bulewicz and T. M. Sugden, Proc. R. Soc. Ser. A, 277 (1964) 143.
12 R. Belcher, S. L. Bogdanski, S. A. Ghonaim and A. Townshend, Nature, 248 (1974) 326.
13 R. Belcher, S. L. Bogdanski, I. H. B. Rix and A. Townshend, Anal. Chim. Acta, 81 (1976) 325.

Analytica Chimica Acta, 157 (1984) 177—181
Elsevier Science Publishers B.V., Amsterdam — Printed in The Netherlands

Short Communication

DETERMINATION OF SULPHUR ANIONS BY FLOW INJECTION WITH A MOLECULAR EMISSION CAVITY DETECTOR

J. L. BURGUERA and M. BURGUERA

Departamento de Quimica, Facultad de Ciencias, Universidad de Los Andes, Apartado Postal 542, Mérida 5101-A (Venezuela)

(Received 30th August 1983)

Summary. A molecular emission cavity detector is attached to a flow injection system for the determination of sulphide, sulphite and sulphate in the ranges 2—130, 3—150 and 5—250 ng S, respectively, in 3-μl samples. The sample throughput is about 100 h^{-1}. Resolution of mixtures of these anions is also possible, based on the sequential appearance of their S_2 emission peaks. The use of a hydrogen peroxide carrier stream allows the determination of total sulphur.

All sulphur compounds give the characteristic blue S_2 emission with maximum intensity at 384 nm, when the cavity containing the sample for molecular emission cavity analysis (m.e.c.a.) is inserted into a hydrogen diffusion flame [1]. The determination of sulphur anions by m.e.c.a. is well documented [2—4]. Their mixtures can be resolved on the basis of their t_m values (time elapsed between introducing the cavity into the flame and achieving the maximum emission intensity). These values depend on the thermal stability of the particular sulphur compounds used and, depending on the flame conditions, binary [2] and some ternary [3] mixtures give resolved peaks.

Flow injection analysis (f.i.a.) has recently been used in conjunction with several other techniques, such as atomic absorption spectrometry [5—7], potentiometry with ion-selective electrodes [8], polarography [9] and chemiluminescent measurements [10] to produce useful solutions to a broad range of problems. Good sensitivity, high sampling rate and reproducibility are considered to be the main advantages. A combination of m.e.c.a. with f.i.a. has not been reported before. This communication describes the advantages of a f.i.a-m.e.c.a. system for determining nanogram levels of some sulphur anions.

Experimental

The instrument for m.e.c.a. measurements was a Varian atomic absorption spectrometer (model AA-1475) operated in the emission mode and equipped with a specially designed sample holder support device and a circular emission burner positioned 95 mm from the entrance slit [11].

0003-2670/84/$03.00

The water-cooled steel cavity (5 mm diameter, 8 mm deep) used had a side tube (0.5 mm i.d., unless otherwise stated) screwed into a hole drilled on its wall, in order to connect the f.i.a. system to the centre of the rear wall of the cavity (Fig. 1). All measurements were made at 384 nm. Hydrogen and nitrogen were supplied to the burner through separate inlets, and the flows were controlled with Manostat Series 100 Century flow meters.

A Sage pump (model 375-A) with adjustable flow control was used; the pump tubing was 0.5 mm i.d. The sample was injected into a stream of water or 1.0 M hydrogen peroxide via a rotary valve (Rheodyne, model 7125), to which a loop of given volume was attached. Teflon tubing (1.0 mm i.d.) connected the carrier solution reservoir to the injector (l_1 = 30 cm, Fig. 1). A stainless steel tube (0.5 mm i.d.) through which the carrier stream flowed (l_2), connected the injector to the cavity; its length was varied as required.

All reagents were of analytical grade and deionized, double-distilled water was used throughout. Preliminary tests and optimization of the experimental parameters were done with a 30 ng S μl^{-1} solution as sodium sulphate. Sodium sulphide and sulphite were used in other experiments.

Results and discussion

Response signals. In the system described (Fig. 1), the cavity was continuously situated within the flame, and the sample was introduced into it with the carrier stream. Such introduction of the sample gives a peak response as illustrated in Fig. 2. The peak height and form would be expected to vary according to the parameters governing f.i.a. (sample volume, carrier flow rate, length and diameter of tubing l_2) and m.e.c.a. (cavity position, flame composition, water cooling rate). The highest peaks with least tailing were obtained under the optimum conditions listed in Table 1.

As expected, the solution flow rate has a great influence on the signals obtained. The maximum peak heights were obtained at 0.14 ml min^{-1}.

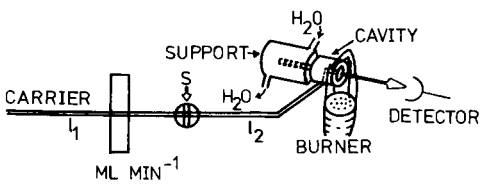

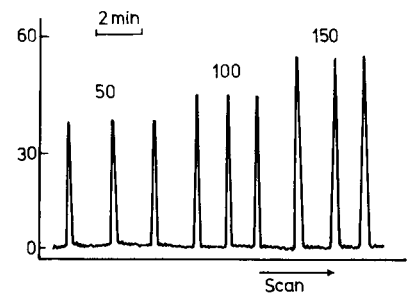

Fig. 1. Schematic diagram of the m.e.c.a.-f.i.a. system. S, rotary sample injector.

Fig. 2. Reproducibility of response peaks for the determination of sulphate (numbers on the peaks indicate ng S as sulphate). Conditions as in Table 1; the arrows indicate the times of sample injection.

TABLE 1

Experimental parameters used in the m.e.c.a.-f.i.a. system for the determination of sulphur anions

M.e.c.a.		F.i.a.	
Wavelength (nm)	384	Sample volume (μl)	3.0
Slit width (nm)	1.0	Carrier flow rate (ml min^{-1})	0.14
Cavity at flame centre		l_2 tube length (cm)	20
Burner diam. (cm)	1.5	l_2 tube i.d. (mm)	0.5
Cavity angle below horizontal	2.5°		
Flame l H_2 min^{-1}	0.80		
Flame l N_2 min^{-1}	2.56		
Water cooling flow rate (ml min^{-1})	285		

At lower flow rates there was a decrease and broadening of the signals because of the decreasing rate of sample flow into the cavity (Fig. 3A). When the flow rate was >0.15 ml min^{-1}, lower irreproducible multi-peaked responses were obtained. This effect is partly due to an increase in sample dispersion in l_2, but mainly due to an excessive amount of solvent reaching the cavity so that the efficiency of sample vaporization decreases and becomes erratic. Thus, at $\geqslant 0.18$ ml min^{-1}, the cavity flooded, the unvaporized liquid sputtered and no emission was obtained. In order to obtain maximum reproducible intensity, the rate at which the carrier stream reaches the cavity must be strictly related to the rate of solvent evaporation in the cavity.

The effect of sample volume was investigated. The sensitivity increased with increasing sample volumes (Fig. 3B) but the injection of larger volumes (>5 μl) into the carrier stream led to less intense multi-peaked signals. Variation of the length of tube l_2 between 10 and 30 cm did not affect the m.e.c.a. signal; this indicates that the sample was not significantly diluted

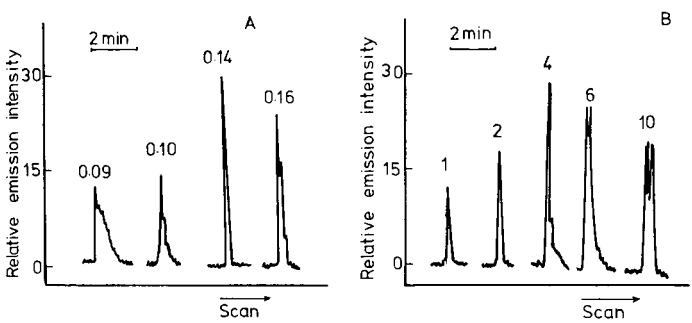

Fig. 3. Effect on (A) pumping rate and (B) sample volume on peak height and shape for 30 ng S as sulphate. The numbers on the peaks represent: (A) flow rate in ml min^{-1}; (B) volume injected in μl. (Other experimental conditions as in Table 1.)

during the flow. The instrumentation did not allow the use of tubing shorter than 10 cm. Peak broadening and tailing were observed when l_2 exceeded 30 cm, because of increased dispersion of the sample zone. Broadening and tailing were also found when the internal diameter of the l_2 tubing was increased to 0.75 or 1.0 mm; this again is due to increased dispersion.

A linear log-log calibration graph was obtained for peak heights and the amount of sulphur as sulphate in the range 5—250 ng; the slope was 1.60. The method showed good reproducibility, with a relative standard deviation of 2.0% for 3 ng of sulphur (8 determinations). The analytical signal is available within 30 s after sample injection permitting about 100 measurements per h.

Sulphite and sulphide can be determined in a similar way. The time of appearance of the peaks is faster than in the case of sulphate because of the more rapid generation of emissions within the cavity [2, 3]. The analytical characteristics for all three systems are summarized in Table 2. The poorer precision obtained for sulphide and sulphite probably arises because the cavity and flame conditions were optimized for the determination of sulphate. Table 2 also indicates that it should be possible to determine simultaneously mixtures of sulphide, sulphite and sulphate, as in conventional m.e.c.a. [3]. This is confirmed in Fig. 4, which shows the separate peaks obtained from the three anions in one sample.

By changing the carrier stream from water to hydrogen peroxide only one peak was obtained from a binary mixture (S^{2-} + SO_3^{2-}) or a ternary mixture (S^{2-} + SO_3^{2-} + SO_4^{2-}), the peak corresponding to that of sulphate. When the sulphate calibration graph previously obtained was used to determine the amount of sulphate formed, apparently poor recoveries (<50%) were obtained. This probably happened because the products of hydrogen peroxide decomposition (oxygen in particular) in the flame increase the flame temperature and diminish the S_2 emission [12]. Therefore, a calibration graph for sulphate in the peroxide carrier stream was prepared, which indicated 95 and 92% recoveries for sulphite and sulphide, respectively. These results suggested that total sulphur may be determined in this way.

TABLE 2

Analytical characteristics of the m.e.c.a.-f.i.a. system for the determination of sulphur anions

Compound	t[a] (s)	Linear range (ng S)	Detection limit (ng S)[b]	R.s.d.[c] (%)	Slope of log-log plot
Na_2S	17	2—130	0.06	4.0	1.90
Na_2SO_3	20	3—150	0.09	3.5	1.83
Na_2SO_4	26	5—250	0.15	2.0	1.60

[a]Time from injection to peak response. [b]2σ value. [c]For 8 determinations of 3 ng S.

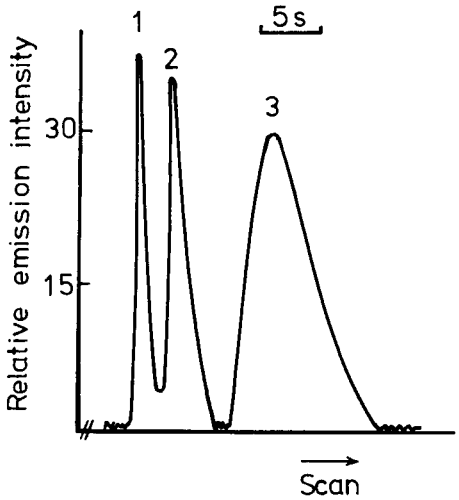

Fig. 4. Response from a mixture of sulphur anions: 30 ng S as (1) S^{2-}; (2) SO_3^{2-}; (3) SO_4^{2-}. Conditions as in Table 1.

The advantage of this method, apart from the fact that it can discriminate between different sulphur anions, is that it continuously monitors the S_2 emission without the necessity of cooling the cavity between injections as in conventional m.e.c.a.

REFERENCES

1 R. Belcher, S. L. Bogdanski and A. Townshend, Anal. Chim. Acta, 67 (1973) 1.
2 R. Belcher, S. L. Bogdanski, D. J. Knowles and A. Townshend, Anal. Chim. Acta, 79 (1975) 292.
3 M. Q. Al-Abachi, R. Belcher, S. L. Bogdanski and A. Townshend, Anal. Chim. Acta, 86 (1976) 139.
4 T. J. Cardwell, P. J. Marriott and D. J. Knowles, Anal. Chim. Acta, 121 (1980) 175.
5 K. Fukamachi and N. Ishibashi, Anal. Chim. Acta, 119 (1980) 383.
6 B. F. Rocks, R. A. Sherwood and C. Riley, Clin. Chem., 28 (1982) 440.
7 J. L. Burguera, M. Burguera and M. Gallignani, An. Acad. Bras. Cienc., 55 (1983) in press.
8 E. H. Hansen, J. Růžička and A. K. Ghose, Anal. Chim. Acta, 100 (1978) 151.
9 B. Persson and L. Rosen, Anal. Chim. Acta, 123 (1981) 115.
10 J. L. Burguera, A. Townshend and S. Greenfield, Anal. Chim. Acta, 114 (1980) 209.
11 M. Burguera and J. L. Burguera, Anal. Chim. Acta, in press.
12 R. Belcher, S. L. Bogdanski, D. J. Knowles and A. Townshend, Anal. Chim. Acta, 77 (1975) 53.

Analytica Chimica Acta, 157 (1984) 183—186
Elsevier Science Publishers B.V., Amsterdam — Printed in The Netherlands

Short Communication

THE DETERMINATION OF TRACE METALS IN HUMAN FLUIDS AND TISSUES
Part 2. The Homogeneity of Liver Tissue for Sampling

V. HUDNIK

Boris Kidrič Institute of Chemistry, Ljubljana (Yugoslavia)

M. MAROLT-GOMIŠČEK

Faculty of Medicine, Edvard Kardelj University, Ljubljana (Yugoslavia)

S. GOMIŠČEK*

Faculty of Natural Sciences and Technology, Edvard Kardelj University, Ljubljana (Yugoslavia)

(Received 26th July 1983)

Summary. The homogeneity of liver tissue of healthy persons is examined with regard to the distribution of copper, zinc, cadmium and manganese. The relative standard deviations of results for particular samples of the same human liver were 6.1—9.9, 4.0—6.0, 6.2—8.7 and 6.2—10.3% for copper, zinc, cadmium and manganese, respectively. Comparison of these values with those obtained for the standard reference material NBS Bovine Liver 1577 (2.8, 3.5, 3.4 and 1.8%, respectively) indicates that small samples of liver tissue can be accepted, with some limitations, as representative of the whole organ for the metals investigated.

The first condition for the reliable investigation of any material is the production of a representative sample. The representativeness of biological materials is often critical, and this is an important problem in clinical work, especially in the determination of trace metals. The representativeness of liver tissue samples has often been discussed and must be accepted as a decisive factor in the applicability of trace element results in medical investigations.

Kostič et al. [1] examined the iron, zinc and cobalt contents in tissue samples taken from different parts of healthy and cirrhotic livers; they found that a representative sample of healthy liver tissue was obtained, irrespective of the site. In cirrhotic liver tissue, however, heterogeneous pathological structures were involved, and the distribution of these trace elements was not the same in the tissue samples selected as in the whole liver. Lievens et al. [2] determined the concentrations of 25 trace elements in five normal human livers, taking eight samples from each; the relative standard deviations found for iron and zinc in the same liver were less than 10%, but those for cobalt were higher. Schicha et al. [3] observed a heterogeneous but parallel distribu-

0003-2670/84/$03.00

tion of cobalt, iron, phosphorus, selenium and zinc, whereas van Eijk et al. [4] concluded from their results that there were no differences in the iron contents between the left, right and central parts of human liver. Koenig et al. [5] determined 18 elements in homogenized samples taken from three different areas of a single human liver, and concluded that the results obtained for small liver samples were, except for lead, fairly representative of the whole organ.

The aim of this study was to obtain additional data on the homogeneity of liver tissue of healthy persons, regarding the distribution of copper, zinc, cadmium and manganese.

Experimental

Tissue specimens were obtained at autopsy from victims of accidental death. In the initial tests (Table 1), only one specimen was taken from each liver; in further tests, 4—6 specimens were taken from different areas of one particular liver by surgical techniques. Each of these specimens was divided into four samples. These samples were lyophilized and stored in polystyrene vessels at −20°C until required for the determination of copper, zinc, cadmium and manganese. The procedures applied have been described [6].

Results and discussion

Homogeneity can be critical in the sampling of liver tissue. In hospitals, such samples are obtained by biopsy, which can be done in diagnosing hepatic disease; only the residual sample is then available for the determination of metals. In addition to contamination during sampling, the representativeness of the small sample (0.5—5 mg) is decisive for reliable results. In order to elucidate this problem, the series of tests outlined above were done. In all cases, the specimens were taken at autopsy with surgical instruments. Afterwards, the upper layers were removed with quartz scalpels in the laboratory before lyophilization in order to avoid the risk of contamination from the surgical instruments. Only samples without any pathological changes

TABLE 1

The homogeneity of liver samples[a]

		Cd	Cu	Mn	Zn
Human liver	$\bar{x}$ ($\mu g\ g^{-1}$)	7.07	34.5	5.18	183
$N = 120$	s ($\mu g\ g^{-1}$)	0.76	2.7	0.43	12
$k = 30$	s_r (%)	10.7	8.5	8.3	6.5
Bovine liver[b]	$\bar{x}$ ($\mu g\ g^{-1}$)	0.29	186	10.6	130
NBS 1577	s ($\mu g\ g^{-1}$)	0.01	5.2	0.19	4.5
$N = 10$	s_r (%)	3.4	2.8	1.8	3.5

[a]N is the number of determinations and k the number of different livers examined. [b]Certified content. Cd 0.27, Cu 193, Mn 10.3, Zn 130 μg^{-1}.

were accepted for examination. The results obtained were statistically evaluated; the deviations calculated by the equation for pooled data [7] were taken as a measure of the homogeneous distribution of the metals in the liver tissues.

The initial tests were designed to obtain an overall view of the homogeneity of normal liver tissue. The results are shown in Table 1. The standard deviations and relative standard deviations obtained for the human liver samples are higher than those obtained for the NBS Bovine Liver, but not excessively so. Considering all the efforts put into the preparation of standard reference materials with the highest possible homogeneity, it appears that the liver tissues studied were reasonably homogeneous.

In further experiments, the homogeneity of the distribution of copper, zinc, cadmium and manganese in different parts of the same liver was examined. The results are shown in Table 2, where the spread is the difference between the lowest and the highest mean values for each specimen and standard and relative standard deviations are calculated from pooled data of all specimens. From the results obtained, it is obvious that the variations in the contents of copper, zinc, cadmium and manganese in the investigated specimens

TABLE 2

Homogeneity of liver tissue with regard to copper, zinc, cadmium and manganese

Liver	N	k	Spread ($\mu g\ g^{-1}$)[a]	$\bar{x}$ ($\mu g\ g^{-1}$)	s ($\mu g\ g^{-1}$)	s_r (%)
Copper						
1	23	6	14.1—16.6	14.8	1.47	9.9
2	22	6	32.6—36.9	34.9	3.17	9.0
3	16	4	21.9—27.5	24.4	1.48	6.1
4	19	5	10.0—13.7	11.9	0.79	6.6
Zinc						
1	24	6	139—147	142	8.6	6.0
2	22	6	158—177	166	9.9	6.0
3	15	4	234—294	265	11.7	4.4
4	16	4	121—149	137	5.5	4.0
Cadmium						
1	23	6	6.0—7.6	6.6	0.44	6.6
2	24	6	3.6—5.4	4.6	0.30	6.5
3	16	4	4.2—6.6	5.5	0.34	6.2
4	19	5	3.1—4.3	3.9	0.34	8.7
Manganese						
1	23	6	4.5—5.4	5.0	0.32	6.4
2	24	6	4.6—5.6	5.1	0.50	9.8
3	16	4	5.2—5.5	5.3	0.55	10.3
4	19	5	4.9—6.7	5.8	0.36	6.2

[a]Calculated for dry tissue.

of the same liver are small. Therefore it can be concluded that small samples of liver tissue can be accepted, at least for the metals investigated, as representative of the whole organ. These conclusions can be related to samples obtained by biopsy if they are not contaminated during sampling. The differences between particular samples of the same liver are negligible, particularly if one recalls that the concentrations of the trace elements under investigation in liver tissues from different people vary significantly [6].

The authors are grateful to the Research Community of Slovenia for financial support. We also thank Dr. Jacques Versieck for his critical review of this manuscript.

REFERENCES

1 K. Kostić, R. Ristanović, V. Obradović, M. Djordjević and R. Drašković, in Trace Element Analytical Chemistry in Medicine and Biology, Walter de Gruyter, Berlin, 1980, p. 601.
2 P. Lievens, J. Versieck, R. Cornelis and J. Hoste, in Proc. 1976 Int. Conf. Modern Trends in Activation Analysis, Vol. 1, 1976, p. 311.
3 H. Schicha, L. E. Feinendegen, K. Kasperek, H. J. Klein and V. Siller, Beitr. Pathol., 141 (1970) 227.
4 H. G. van Eijk, W. F. Wilting, G. Bos and J. P. Goossens, Clin. Chim. Acta, 50 (1974) 275.
5 W. Koenig, F. W. Richter, B. Meinel and J. Ch. Bode, J. Clin. Chem. Clin. Biochem., 17 (1979) 23.
6 V. Hudnik, M. Marolt-Gomišček, Anal. Chim. Acta, 157 (1984) 143.
7 D. A. Skoog and D. M. West, in Fundamentals of Analytical Chemistry, Holt, Rinehart & Winston, New York, 1971, p. 39.

Analytica Chimica Acta, 157 (1984) 187—191
Elsevier Science Publishers B.V., Amsterdam — Printed in The Netherlands

Short Communication

THE SEPARATION OF TELLURIUM(IV) FROM WATER AND SEA WATER BY FLOTATION WITH HYDRATED IRON(III) OXIDE

SUSUMU NAKASHIMA* and MASAKAZU YAGI

Institute of Agricultural and Biological Sciences, Okayama University, Kurashiki-shi, Okayama 710 (Japan)

(Received 12th July 1983)

Summary. A flotation separation is described for sub-microgram levels of tellurium(IV) from 1-l samples of water and sea water. Tellurium(IV) is coprecipitated with hydrated iron(III) oxide at pH 8—9. The precipitate is floated with the aid of surfactant solutions and small nitrogen bubbles, separated and dissolved in dilute hydrochloric acid. Tellurium is then converted to hydrogen telluride with sodium tetrahydroborate and measured by atomic absorption spectrometry. Recovery of added tellurium (0.4 and 0.8 $\mu g\ l^{-1}$) was about 83%. The time required for the preconcentration is 30 min per sample, including 15 min stirring.

There is an increasing need for rapid and accurate methods of determining low parts per billion ($\mu g\ l^{-1}$) of trace elements in water. At tellurium levels below 1 $\mu g\ l^{-1}$, precise direct determination is difficult even by atomic absorption spectrometry of hydrogen telluride, which is very sensitive [1—8]. Preconcentration of tellurium(IV) from aqueous solution has been achieved by coprecipitation with hydrated iron(III) oxide [9, 10] or hydrated lanthanum oxide [8, 11, 12]. These bulky amorphous precipitates, however, are difficult to filter, and centrifugation is cumbersome for large volumes.

Flotation separation techniques have been widely used to concentrate trace elements from aqueous systems. Applications of flotation techniques have been reviewed by Karger and De Vivo [13], Lemlich [14], Grieves [15] and Mizuike and Hiraide [16, 17]. However, the flotation separation of low $\mu g\ l^{-1}$ levels of tellurium(IV) in water does not seem to have been reported previously. In previous papers [18—23], a flotation technique [24—28] in which the precipitate of hydrated iron(III) oxide is floated with the aid of surfactant and small air bubbles, was used for the preconcentration of arsenic(III, V) [18], selenium(IV) [19], tin(II, IV) [20], bismuth(III) [21] and antimony(III, V) [22, 23] in water and sea water. The present communication describes the application of this technique [18—23] for the preconcentration of trace amounts of tellurium(IV) from water and sea water. The precipitate is readily separated from the mother liquor and then dissolved in dilute hydrochloric acid for hydride-generation atomic absorption spectrometry (a.a.s.). The method developed is simple and rapid, and

0003-2670/84/$03.00

applicable to the separation of tellurium at low $\mu g\ l^{-1}$ levels from large volumes of water and sea water.

Experimental

Apparatus. The flotation and separation apparatus has been described [19—23]. Nitrogen was used as the inert gas instead of air. The atomic absorption equipment, including a long absorption tube (60 cm long, 1.2 cm i.d.) and hydride measurement unit, was similar to that described previously [18, 19], except for the light source, which was a Westinghouse tellurium hollow-cathode lamp.

Reagents. All reagents were of analytical-reagent grade except for sodium dodecyl sulphate (sodium lauryl sulphate) and sodium oleate. Aqueous solutions were prepared in deionized distilled water. A tellurium(IV) stock solution (1 mg Te ml^{-1}) was prepared from tellurium(IV) oxide; standard solutions were freshly prepared by diluting this stock solution. An iron(III) solution (5 mg Fe ml^{-1}) was prepared from ammonium iron(III) sulphate. Sodium dodecyl sulphate and sodium oleate solutions (1 mg ml^{-1}) were prepared by dissolving each surfactant (powder, extra-pure reagent, Wako Pure Chemical Industries) in 99.5% (v/v) ethanol. A sodium tetrahydroborate solution (5% w/v) in a 0.1 M sodium hydroxide was freshly prepared.

Procedure and flotation. A 1-l sample of acidified water was placed in a 1-l beaker and the pH of the solution was adjusted to 8—9 with aqueous ammonia. Hydrated iron(III) oxide suspension (pH 8—9), preformed by adding aqueous ammonia to iron(III) solution (10 mg Fe), was added and the mixture was stirred magnetically for about 15 min. Sodium dodecyl sulphate solution (1 ml) and sodium oleate solution (1 ml) were added, the mixture was transferred to the flotation cell, and the residue in the beaker was washed into the cell with three small portions of water. Nitrogen was passed at 20 ml min^{-1} from the lower end of the cell for about 3 min to obtain complete mixing and flotation of the precipitate. While the nitrogen was passed at 10 ml min^{-1}, most of the mother liquor was drained from the side arm by opening the tap on the drain pipe. After the tap had been closed, the residual mother liquor was sucked off through the sintered-glass disk. The precipitate adhering to the wall of the cell was washed down by spraying with water, and the precipitate was washed with 30 ml of water. A 5-ml portion of 7 M hydrochloric acid was added to the cell to dissolve the precipitate. The filtrate was collected by suction in a 10-ml volumetric flask, the sintered-glass disk was washed with water, the washings were added to the flask, and the mixture was diluted to the mark with water. For natural sea water, the above procedure was modified so that 4 ml of sodium dodecyl sulphate solution and 2 ml of sodium oleate solution were added to the flotation cell.

Procedure for the measurement of tellurium. The a.a.s. procedure was almost the same as those for bismuth [21] and antimony [22, 23].

A calibration graph was constructed using 3.5 M hydrochloric acid solution containing 1 mg ml^{-1} of iron(III) and 0—0.10 μg ml^{-1} of tellurium(IV); the graph was nearly linear over this range.

The atomic absorption equipment was operated under the following conditions: wavelength, 214.3 nm; lamp current, 12 mA; gas flow rates, nitrogen 1.0, hydrogen 1.0, and auxiliary nitrogen 6 l min^{-1}; spectral bandwidth, 1 nm. No difference in sensitivity and precision was found between argon and nitrogen. The recommended 60-cm tube system [18, 19] cannot be used with most commercial atomic absorption spectrometers. However, the tellurium in a sample solution can also be measured by a.a.s. by using an electrically or flame-heated silica tube.

Results and discussion

Optimum conditions for the a.a.s. measurement of tellurium. The effect of the sodium tetrahydroborate concentration on the evolution of hydrogen telluride was investigated. A reductant concentration exceeding 3% (w/v) (1-ml volume) sufficed for quantitative reduction of up to 0.10 μg of tellurium(IV) to hydrogen telluride; 1 ml of 5% (w/v) sodium tetrahydroborate solution is recommended.

The flow rate of auxiliary nitrogen was important. The absorbance of tellurium increased as this nitrogen flow increased, the optimal absorbance being obtained with auxiliary nitrogen flow rates of 6—8 l min^{-1} along with carrier nitrogen and hydrogen flow rates of 1.0 l min^{-1} each; an auxiliary nitrogen flow rate of 6.0 l min^{-1} is recommended.

The optimal concentration of hydrochloric acid was 3—7 M; a concentration of 3.5 M was preferred in further work.

Optimum conditions for the flotation of tellurium. When tellurium was floated with hydrated iron(III) oxide, it was necessary to raise the pH of the solution to >4 immediately after iron(III) solution had been added to the acidic water samples, resulting in the formation of hydrated iron(III) oxide. Otherwise, the recoveries of tellurium were low and irreproducible; recoveries were worse for water than sea water. This result is considered to indicate that trace levels of tellurium(IV) in the acidic solution are oxidized to tellurium(VI) in the presence of iron(III) ion. Therefore, except when the effect of pH was being examined, the preferred routine was to adjust the pH of the acidic sample solution to 8—9 with aqueous ammonia, add preformed hydrated iron(III) oxide suspension at pH 8—9 (see Procedure), stir the mixture, and then float the precipitate.

The effect of pH on the coprecipitation and flotation of tellurium(IV) was examined for 1 l of solution containing 0.8 μg of tellurium; 2 ml of iron(III) solution was added to 1 l of acidified sample and immediately the pH of the solution was adjusted to values within the range 3.8—9.6 by adding aqueous ammonia. Constant recoveries (83 ± 4%) of tellurium were obtained over the pH range 3.8—9.6. When the mixed surfactant (sodium dodecyl sulphate and sodium oleate) solution was used, the surface foam

TABLE 1

Recovery of tellurium(IV) added to water[a] and sea water[a,b]

Water[a]								
Added (μg)	0.4	0.8	1.0	1.2	1.6	2.0	10	
Recovery (%)	82	84	83	84	85	84	91	
Added (μg)	20	40	60	80	100	150		
Recovery (%)	90	92	94	93	93	94		
Sea water[a,b]								
Added (μg)	0.4	0.8	1.0	5.0	10	20	50	100
Recovery (%)	83	83	84	89	94	92	94	95

[a]Solution containing 10 mg of iron(III); pH 8—9; volume 1 l. [b]This sample was taken at Shibukawa, Okayama Prefecture, Japan.

layer supporting the precipitate was stable within this pH range. In all further work, pH 8—9 was used for coprecipitation and flotation.

The recovery of tellurium was investigated as a function of the amount of iron(III) added to 1 l of solution. Constant recoveries of 0.8 μg of tellurium were obtained with >7.5 mg of iron(III). For routine work, 10 mg of iron(III) was added to 1 l of sample. Complete flotation of the precipitate in 1 l of water was obtained by using 1 ml of sodium dodecyl sulphate solution and 1 ml of sodium oleate solution. For 1 l of sea water, 4 ml of sodium dodecyl sulphate solution and 2 ml of sodium oleate solution produced complete flotation of the precipitate and a stable foam layer supporting the precipitate at pH 8—9.

Coprecipitation was found to be constant over a time of 5—40 min. In practice, stirring for 15 min was used.

Recovery of tellurium. Recoveries of known amounts of tellurium(IV) added to water and sea-water samples were examined by the described procedure. Sea water was treated with 3 ml of hydrochloric acid per liter of sample immediately after collection. Aliquots (1 l) of clear sea water were filtered through 0.45-μm Millipore filters. Table 1 presents the recovery data for tellurium. Recoveries of the added tellurium(IV) exceeded 82% in all instances. When ⩾10 μg of tellurium was added, recoveries exceeded 90%. The blank value of the whole process was <10 ng Te l^{-1}. The concentration of tellurium(IV) in the sea water sample was <10 ng l^{-1}. At such extremely low concentrations, the determination of tellurium is difficult even by the highly sensitive method described here.

Conclusions

The flotation of tellurium(IV) coprecipitated with hydrated iron(III) oxide at pH 8—9 offers a useful procedure for isolation of low levels of tellurium(IV). The subsequent atomic absorption measurement of hydrogen telluride is rapid and sensitive.

The time required for the preconcentration of tellurium from a 1-l volume

of solution is about 30 min per sample, including 15 min of stirring. In practice, of course, flotation from one sample can be done while the next sample is being stirred.

The authors thank Professor Atsushi Mizuike and Dr. Masataka Hiraide, Nagoya University, for their helpful advice on the flotation technique. One of the authors (S.N.) also thanks the Japanese Ministry of Education, Science and Culture for financial support through a Grant-in-Aid for Scientific Research.

REFERENCES

1 K. C. Thompson and D. R. Thomerson, Analyst, 99 (1974) 595.
2 H. D. Fleming and R. G. Ide, Analyst, 83 (1976) 67.
3 J. A. Fiorino, J. W. Jones and S. G. Caper, Anal. Chem., 48 (1976) 120.
4 L. P. Greenland and E. Y. Campbell, Anal. Chim. Acta, 87 (1976) 323.
5 K. Jin, M. Taga, H. Yoshida and S. Hikime, Bull. Chem. Soc. Jpn., 52 (1979) 2276.
6 M. Ikeda, J. Nishibe and T. Nakahara, Bunseki Kagaku, 30 (1981) 368.
7 R. Kobayashi, M. Imai and Y. Hashimoto, Bunseki Kagaku, 31 (1982) 467.
8 W. A. Maher, Analyst, 108 (1983) 305.
9 E. M. Donaldson, Talanta, 23 (1976) 823.
10 J. D. Mullen, Talanta, 23 (1976) 846.
11 W. Reichel and B. G. Bleakly, Anal. Chem., 46 (1974) 59.
12 M. Thompson, B. Pahlavanpour, S. J. Walton and G. F. Kirkbright, Analyst, 103 (1978) 705.
13 B. L. Karger and D. G. De Vivo, Sep. Sci., 3 (1968) 393.
14 R. Lemlich (Ed.), Adsorptive Bubble Separation Techniques, New York, Academic Press, 1972.
15 R. B. Grieves, Chem. Eng. J., 9 (1975) 93.
16 A. Mizuike and M. Hiraide, Pure Appl. Chem., 54 (1982) 1556.
17 M. Hiraide and A. Mizuike, Rev. Anal. Chem., 6 (1982) 151.
18 S. Nakashima, Analyst, 103 (1978) 1031; Bunseki Kagaku, 28 (1979) 561.
19 S. Nakashima, Anal. Chem., 51 (1979) 654.
20 S. Nakashima, Bull. Chem. Soc. Jpn., 52 (1979) 1844.
21 S. Nakashima, Fresenius Z. Anal. Chem., 303 (1980) 10.
22 S. Nakashima, Bull. Chem. Soc. Jpn., 54 (1981) 291.
23 S. Nakashima and M. Yagi, Fresenius Z. Anal. Chem., 314 (1983) 155.
24 M. Hiraide, Y. Yoshida and A. Mizuike, Anal. Chim. Acta, 81 (1976) 185.
25 M. Hiraide and A. Mizuike, Bunseki Kagaku, 29 (1980) 84.
26 M. Hiraide, T. Ito, M. Baba, H. Kawaguchi and A. Mizuike, Anal. Chem., 52 (1980) 804.
27 E. H. DeCarlo, H. Zeitlin and Q. Fernando, Anal. Chem., 53 (1981) 1104; 54 (1982) 898.
28 R. S. S. Murthy and D. E. Ryan, Anal. Chem., 55 (1983) 682.

Analytica Chimica Acta, 157 (1984) 193—197
Elsevier Science Publishers B.V., Amsterdam — Printed in The Netherlands

Short Communication

ELECTROTHERMAL ATOMIC ABSORPTION SPECTROMETRIC DETERMINATION OF TRACES OF CHROMIUM, NICKEL, IRON AND BERYLLIUM IN ALUMINUM AND ITS ALLOYS WITHOUT PRELIMINARY SEPARATION

KOJI MATSUSAKI*

Department of Industrial Chemistry, Technical College, Yamaguchi University, Tokiwadai, Ube 755 (Japan)

TAKASHI YOSHINO

Department of Industrial Chemistry, Faculty of Engineering, Yamaguchi University, Tokiwadai, Ube 755 (Japan)

(Received 31st August 1983)

Summary. Graphite-furnace a.a.s. is used for the determination of >0.0007% Cr, >0.01% Ni, >0.007% Fe and >0.0002% Be in aluminum and its alloys. The samples are dissolved in hydrochloric acid and processed directly after addition of a slight molar excess of diammonium-EDTA over aluminum.

Rapid simple methods are required for the determination of traces of metals in metallurgical materials and electrothermal atomic absorption spectrometry (a.a.s.) is probably the best technique for this purpose. However, interferences from chloride are frequently encountered [1—4], which is unfortunate, as many metals and alloys are readily dissolved in hydrochloric acid. In previous reports [5, 6], diammonium-EDTA was found to be the most suitable additive for removal of chloride interferences; it was applied to the determination of trace lead, copper and manganese in aluminum and its alloys. These metals have a relatively low atomization temperature. In the present communication, metals having a high atomization temperature corresponding to that of aluminum (i.e., chromium, nickel, iron and beryllium) are determined, and diammonium-EDTA is again applied in their direct determination in aluminum and its alloys after dissolution of the sample in hydrochloric acid. The detection limits for these elements in aluminum were found to be similar to those obtained by flame a.a.s. with liquid-liquid extraction [7—10].

Experimental

The apparatus was as described previously [6], except for the radiation sources; Hitachi chromium, nickel, iron and beryllium hollow-cathode lamps were used.

0003-2670/84/$03.00

All solutions were prepared from analytical-reagent grade chemicals and demineralized water, and stored in polyethylene bottles. The 1000 mg l^{-1} stock solutions for chromium, nickel, iron and beryllium were prepared by dissolving each pure metal in the minimum of nitric acid and diluting with 0.1 M nitric acid.

The sample (ca. 1 g) was dissolved as described previously [6]. To aliquots of the sample solution containing 0.2—3.0 μg of chromium, 1.0—20 μg of nickel, 0.2—2.4 μg of iron and 0.05—1.0 μg of beryllium, 3.7×10^{-2} mol or slightly more $(NH_4)_2EDTA$ was added per gram of metal sample. The pH was adjusted with ammonia, if necessary, to 2—6 for beryllium and 2—10 for the other metals and the volume was made up to 25 ml with water. Calibration solutions for nickel and beryllium were prepared similarly, using the appropriate stock solutions and the same weights of aluminum (as aluminum chloride) and $(NH_4)_2EDTA$, as those taken above. Solutions for chromium and iron were prepared using only the metal stock solutions. A 5-μl aliquot of the sample solution was processed as described previously, under the conditions given in Table 1.

Results and discussion

The concentrations of the analyte elements in the test solutions, unless otherwise specified, were 0.1, 0.4, 0.1 and 0.02 μg ml^{-1} for chromium, nickel, iron and beryllium, respectively. The effects of drying, ashing and atomization conditions and of nitrogen flow rate were examined for each element solution containing 0.1 M aluminum chloride and 0.1 M $(NH_4)_2EDTA$. Throughout this study, the same instrumental conditions except for the wavelength were applied to all the analytes in order to simplify the procedure. Under the conditions shown in Table 1, the calibration graphs were linear over the ranges 0.01—0.15 μg Cr ml^{-1}, 0.04—0.8 μg Ni ml^{-1}, 0.01—0.12 μg Fe ml^{-1} and 0.002—0.04 μg Be ml^{-1}.

Prior to the examination for the effect of EDTA, the effects of aluminum chloride concentration on the atomic absorption signal of the analyte elements in the absence of EDTA were investigated. Curves 1—4 in Fig. 1 show that the signal for iron is suppressed by $\geqslant 10$ μg ml^{-1} aluminum and for other elements by $\geqslant 40$ μg ml^{-1} aluminum (as chloride). Addition of masking agents such as EDTA, therefore, is necessary for the determination of traces of chromium, nickel, iron and beryllium in aluminum and its alloys after dissolution in hydrochloric acid.

TABLE 1

Instrumental conditions

Wavelength	Cr 357.9; Ni 232.0; Fe 248.3; Be 234.9 nm
N_2 flow rate	6.0 l min^{-1}
Drying	110°C (0.65 V) for 30 s
Ashing	620°C (1.7 V) for 30 s
Atomization	8.0 V for 4 s

The effect of $(NH_4)_2EDTA$ concentration was investigated for each element solution containing 0.01 or 0.04 M aluminum chloride under the recommended conditions. In all cases, the analyte atomic absorbance increased with increasing concentration of EDTA, and became constant when more than a 1:2 mole ratio of EDTA to aluminum was present. Thus the interference of aluminum chloride can be removed by addition of about an equimolar concentration of EDTA to aluminum, as in the determination of lead, copper and manganese [6]. In the absence of aluminum chloride, EDTA did not affect the signals of chromium, nickel and iron, but >0.01 M EDTA slightly suppressed the beryllium signal.

In the presence of equimolar amounts of EDTA and aluminum, the effects of aluminum chloride and EDTA concentrations on the atomic absorbance of the analytes were investigated. Curves 7 and 5 in Fig. 1 show that EDTA completely removed the chloride interferences for chromium and iron, but incompletely removed that for nickel. In contrast, an enhancing effect was observed for beryllium (curve 6). Aluminum nitrate had a similar effect on beryllium [11] and nickel. Therefore such an enhancing effect for beryllium and suppressing effect for nickel may arise from aluminum oxide formed, for example, by thermal decomposition of the EDTA complex of aluminum during the ashing step. In order to standardize the amount of EDTA added, all samples were regarded as pure aluminum, and the amount of EDTA added was calculated of that basis, i.e., 3×10^{-2} mol g^{-1} of sample. For the calibration solutions for nickel and beryllium, equal concentrations of aluminum and EDTA were added to compensate for any interfering effects. The maximum concentration of EDTA was about 0.1 M, because at higher concentrations, the reproducibility of the signals was invariably poor.

The effect of the pH of the test solution on the atomic absorbance was

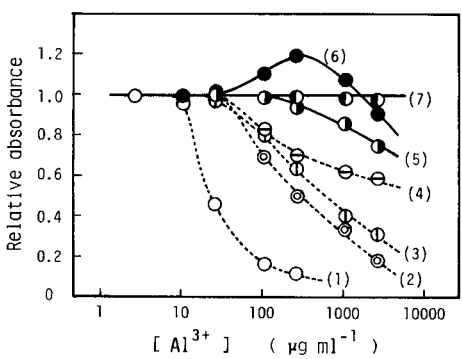

Fig. 1. Effects of aluminum concentration (as chloride) on the absorbances of: (4, 7) chromium, 0.1 $\mu g\ ml^{-1}$; (3, 5) nickel, 0.4 $\mu g\ ml^{-1}$; (1, 7) iron, 0.1 $\mu g\ ml^{-1}$; (2, 6) beryllium, 0.002 $\mu g\ ml^{-1}$, relative to those when EDTA and aluminum chloride were absent. (1—4) Without EDTA; (5—7) equimolar amounts of EDTA and aluminum added.

investigated for a synthetic sample solution containing aluminum chloride (270 μg Al ml^{-1}). The pH was adjusted with hydrochloric acid or ammonia. Between pH 2 and 6 for beryllium and 2 and 10 for other analytes, no variation in the signals was observed.

The conditions described above were used in the investigation of the effects of major metals in aluminium alloys on the recovery of the analyte, as described previously [6]. The results showed no significant effects of other elements on the determination of chromium, nickel, iron and beryllium.

The detection limits for each analyte in aluminum, established as before [6], were 0.0007% for chromium, 0.01% for nickel, 0.007% for iron and 0.0002% for beryllium in aluminum. These values are comparable with those obtained by flame a.a.s. using liquid-liquid extraction [7—10].

The proposed procedure was applied to the determination of traces of the four metals in several standard aluminum and alloy samples. These

TABLE 2

Determination of traces of chromium, nickel, iron and beryllium in aluminum and its alloys

Element	Sample	Found (%)[a]	Certified value (%)
Cr	ALCOA-WA-1199-L	0.00080 ± 0.00003	0.0008
	ALCOA-WA-1000-K	0.0125 ± 0.0003	0.012
	ALCOA-SS-2018-E (4% Cu—2% Ni—Al alloy)	0.063 ± 0.002	0.060
Ni	BCS 262/1 (10% Mg—Al alloy)	0.069 ± 0.002	0.071
	ALCOA-SS-360-AB (10% Si—Al alloy)	0.175 ± 0.004	0.18
	ALCOA-WA-1000-K	0.011 ± 0.001	0.011
	ALCOA-KF-380-N (8% Si—3% Cu—3% Zn—Al alloy)	0.106 ± 0.003	0.11
Fe	BAM 301	0.054 ± 0.002	0.054
	BCS 195g	0.081 ± 0.002	0.08_0
	ALCOA-WA-1199-L	0.0022 ± 0.0001	0.0021
Be	BCS 263/1 (5% Mg—Al alloy)	0.0041 ± 0.0002	0.004
	MBH 05H1 (2% Mg—Al alloy)	0.00069 ± 0.00002	0.0007
	MBH 05H2 (3% Mg—Al alloy)	0.0021 ± 0.0001	0.002
	MBH 10H1 (8% Mg—Al alloy)	0.00094 ± 0.00002	0.001
	ALCOA-KB-514-C (5% Mg—Al alloy)	0.0054 ± 0.0002	0.005

[a]Mean and standard deviation calculated from five replicate measurements.

results are presented in Table 2. They show good reproducibility, and good agreement with certificate values.

REFERENCES

1 K. Garbett, G. I. Goodfellow and G. B. Marshall, Anal. Chim. Acta, 126 (1981) 147.
2 E. J. Czobik and J. P. Matousek, Anal. Chem., 50 (1978) 2.
3 K. Matsusaki, T. Yoshino and Y. Yamamoto, Anal. Chim. Acta, 124 (1981) 163.
4 K. Matsusaki, N. Kameshima, S. Murakami and T. Yoshino, Nippon Kagaku Kaishi, (1981) 1715.
5 K. Matsusaki, Anal. Chim. Acta, 141 (1982) 223.
6 K. Matsusaki, T. Yoshino and Y. Yamamoto, Anal. Chim. Acta, 144 (1982) 189.
7 T. Kono, Bunseki, Kagaku, 22 (1973) 55.
8 T. Goto and N. Unohara, Bunseki Kagaku, 27 (1978) 264.
9 A. Gómez Ceodo, M. T. Dorado and J. L. Jiménez Seco, Rev. Met. (Madrid), 8 (1972) 343.
10 K. Matsusaki, Bunseki Kagaku, 24 (1975) 442.
11 S. Shimomura, H. Morita and M. Kubo, Bunseki Kagaku, 25 (1976) 539.

Analytica Chimica Acta, 157 (1984) 199—202
Elsevier Science Publishers B.V., Amsterdam — Printed in The Netherlands

Short Communication

HIGH-PERFORMANCE LIQUID CHROMATOGRAPHY OF SOME NOVEL DIASTEREOMERIC TRICYCLIC 1,2,4-TRIOXANES

CHARLES W. JEFFORD*, JOHN BOUKOUVALAS, SHIGEO KOHMOTO and HAMISH G. GRANT

Department of Organic Chemistry, University of Geneva, 1211 Geneva 4 (Switzerland)

(Received 17th August 1983)

Summary. A series of 4a,10b-dihydronaphtho-[2,1-e]-1,2,4-trioxanes were examined by h.p.l.c. Compounds existing as a pair of diastereomers are only resolved when hydrogen is a substituent at the C3 position. The separations actually observed may arise from conformational differences rather than simple diastereoisomerism.

Several novel *cis*-fused 4a,10b-dihydronaphtha-1,2,4-trioxanes having different substituents at the C3 position have recently been described [1]. Their synthesis was undertaken to evaluate the role of the 1,2,4-trioxane moiety in Qinghaosu or artemisinine (**10**) which has potent antimalarial activity [2]. Although artemisinine and some of its derivatives have been analyzed by high-performance liquid chromatography (h.p.l.c.) on silica gel and C-18 type columns [3], little is known about simple members of this class of oxygen heterocycles [4]. Consequently, studies of a series of *cis*-fused trioxanes (**1**—**9**) are reported here.

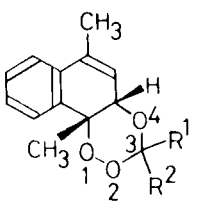

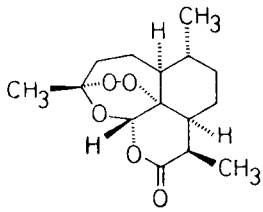

10

1 $R^1 = R^2 = H$
2 $R^1 = R^2 = CH_3$
3 $R^1 = H$, $R^2 = CH_3$
4 $R^1 = H$, $R^2 = C_6H_5$
5 $R^1 = H$, $R^2 = C_6H_4$-p-NO_2
6 $R^1 = H$, $R^2 = C_6H_4$-p-Cl
7 $R^1 = H$, $R^2 = C(CH_3)_3$
8 $R^1 = CH_3$, $R^2 = COCH_3$
9 $R^1 = CH_3$, $R^2 = CO_2CH_3$

0003-2670/84/$03.00

Experimental

The trioxanes were pre-purified by multiple recrystallization and by thin-layer chromatography before being injected for h.p.l.c. A Waters Associates μBondapak C-18 (10 μm) column and a refractive index detector were used.

Results and discussion

The method of synthesis of the trioxanes results in the unique formation of *cis*-fused bicyclic derivatives. With the exception of the reference structures **1** and **2**, which exist as pairs of enantiomers, the rest of the series form diastereomeric pairs by virtue of substitution at the C3 position.

Various binary and tertiary solvent mixtures using columns of both types including partially and completely end-capped C-18 columns were evaluated and it was found that all trioxanes examined were chemically stable under the conditions used. For quantitative purposes, acetonitrile/water (1+1) and a fully end-capped C-18 column were found to be the most effective. However, small-scale (5 mg) semi-preparative separations were best accomplished by using a ternary mixture of acetonitrile/methanol/water (1+1+1). Solvent mixtures containing methanol compared to aqueous acetonitrile resulted in substantial peak broadening owing to increased interactions between the sample and the mobile phase. Separations were nonetheless enhanced at the expense of increased peak width.

Separations were also critically dependent on the nature of the substituent at C3 (Table 1). All compounds showed a large spread of retention times, except the mixture of **6** and **7** which by coincidence gave identical values for each pair of diastereomers. Significantly, no resolution of peaks was observed for diastereomers not having a C3-H substituent, e.g., **8** and **9**. All the other compounds, regardless of the size and nature of the C3 substituents, exhibited distinct peaks for each diastereomer. Resolution was unexpectedly sharp reaching to the baseline (Fig. 1).

In general, separation of diastereomers depends on the substituents at the epimeric centers and their mutual spatial relations [5]. From n.m.r. evidence

TABLE 1

Retention times (t_R, s) for some 4a,10b-dihydronaphtho-[2,1-e]-1,2,4-trioxanes in acetonitrile/water (2+1) (A) and methanol/acetonitrile/water (1+1+1) (B) at 1.0 ml min^{-1}

Compound	C3 Substituents	t_R (A)	t_R (B)
1	H, H	370	431
9	CH_3, CO_2CH_3	396	594
8	CH_3, $COCH_3$	422	528
3	H, CH_3	468, 507	518, 583
2	CH_3, CH_3	528	594
5	H, $p$$NO_2$-$C_6H_4$	780, 564	1212, 1440
4	H, C_6H_5	804, 905	1086, 1242
6	H, pCl-C_6H_4	1072, 1224	1674, 2082
7	H, $C(CH_3)_3$	1072, 1224	1674, 2082

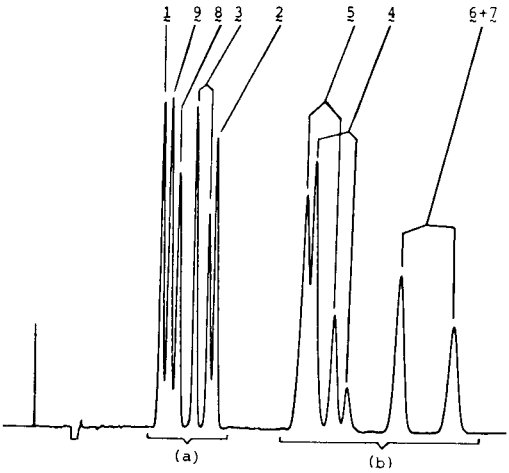

Fig. 1. Combined chromatograms of two mixtures of trioxanes 1, 2, 3, 8 and 9 (a) and 4, 5, 6 and 7 (b). Conditions: Waters μBondapak-C18 column; acetonitrile/water (2+1) at 1.0 ml min^{-1}; refractive index detection.

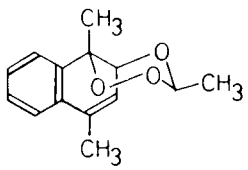

3c R_t=507 s

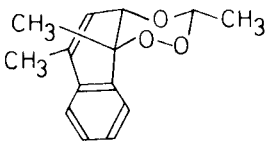

3t R_t = 468s

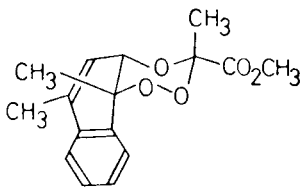

9c

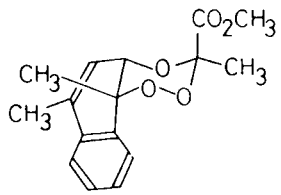

9t

and x-ray spectrometry [6], it is known that the *trans* and *cis* epimers of 3 adopt two different chair conformations, 3t and 3c respectively. In both cases, the C3 substituents occupy an equatorial position, whereas the benzene part of the *cis*-fused ring is joined to the two chair conformations of the trioxane ring via an axial (3t) and an equatorial bond (3c), respectively. Similar pairs of conformations exist for the rest of the series (4—7). However, for the C3 geminally-substituted deriviatives 8 and 9, the same chair conformation is adopted for each pair of diastereomers. Clearly, the intramolecular spatial relationships in each pair will be similar; 9c and 9t, for

example, only differ in configuration at the C3 position, leaving the overall molecular shape unchanged. Therefore, chromatographic interactions are poorly differentiated, resulting in little or no separation.

It can be concluded that conformational isomerism in the *cis*-fused trioxane ring derivatives is the structural element responsible for chromatographic resolution. Conversely, separability should also be useful as an index of conformational isomerism.

We are indebted to the Swiss National Science Foundation (Grant No. 2.201-0.81) for the support of this work.

REFERENCES

1 C. W. Jefford, D. Jaggi, J. Boukouvalas and S. Kohmoto, J. Am. Chem. Soc., 105 (1983) 6497.
2 G. Schmid and W. Hofheinz, J. Am. Chem. Soc., 105 (1983) 624.
3 Z. Wang, Y. Zhu, S. Zhang and X. Lu, Yaoxue Xeubao, 16 (1981) 466; Chem. Abstr., 97, 61086g.
4 G. B. Payne and C. W. Smith, J. Org. Chem., 22 (1957) 1682; W. Adam and A. Rios, J. Chem. Soc. Chem. Commun., (1971) 822; K. Maruyama, M. Muraoka and Y. Naruta, J. Chem. Soc. Chem. Commun., (1980) 1282; H. Yamamoto, M. Akutagawa, H. Aoyama and Y. Omote, J. Chem. Soc. Perkin Trans 2, (1980) 2300.
5 R. W. Souter, J. Chromatogr., 134 (1977) 187; M. G. Young, J. Chromatogr., 150 (1978) 221; F. Salto, J. Chromatogr., 161 (1978) 379; E. P. Kroeff and D. J. Pietrzyk, Anal. Chem., 50 (1978) 1353; H. H. Wittenkind and B. Testa, J. Chromatogr., 179 (1979) 370.
6 C. W. Jefford, J. Boukouvalas, S. Kohmoto, U. Burger, O. Kennard, F. H. Allen and S. Bellard, unpublished work.

Analytica Chimica Acta, 157 (1984) 203—206
Elsevier Science Publishers B.V., Amsterdam — Printed in The Netherlands

Short Communication

EFFECTS OF POLYACRYLIC ACID ON THE ROOM-TEMPERATURE PHOSPHORESCENCE OF SELECTED COMPOUNDS

V. P. SENTHILNATHAN, S. M. RAMASAMY[a] and R. J. HURTUBISE*
Department of Chemistry, The University of Wyoming, Laramie, WY 82071 (U.S.A.)
(Received 14th July 1983)

Summary. Polyacrylic acid solutions of 4-phenylphenol, *p*-aminobenzoic acid, 1,2-benzocarbazole, and 5,6-benzoquinoline were spotted on filter paper and the results obtained by room-temperature phosphorescence were compared with similar samples spotted on filter paper without polyacrylic acid. Improvements in sensitivity ranged from 26 times to 1.1 times and limits of detection from 100 times to 1.1 times for the samples on filter paper with polyacrylic acid. The relative standard deviations for the samples with polyacrylic acid added were also improved.

There has been considerable recent research activity in the area of room-temperature phosphorescence (r.t.p.) [1—3]. Because analytical r.t.p. is still a developing area, it is important to continue to investigate new materials and experimental conditions so that sensitivity, selectivity, reproducibility, and sample-handling techniques can be improved. Recently, there was an extensive evaluation of cellulose as a substrate for r.t.p. [4], and a quantitative study of r.t.p. by the internal standard and standard addition techniques [5]. In this work, the new technique of spotting polyacrylic acid solutions of phosphors on filter paper is discussed. Notable improvements in sensitivity, limits of detection, and relative standard deviation have been achieved.

Experimental

Apparatus. All intensity data were obtained with a Schoeffel SD3000 spectrodensitometer equipped with a SDC-300 density computer (Schoeffel Instruments, Westwood, NJ) and a phosphoroscope assembly. Details of instrumental set-up were reported previously [6]. Relative signal measurements were made with inlet and exit slits set at 2 mm and 3 mm, respectively. A 200-W Xe-Hg lamp (Conrad Hanovia, Newark, NJ) was used in the spectrodensitometer. An ultrasonic bath (Branson Cleaning Equipment Co., Shelton, CT) was used in preparing some of the solutions.

Reagents. Ethanol was purified by distillation; 4-phenylphenol, *p*-aminobenzoic acid, 1,2-benzocarbazole and phenanthrene were recrystallized from

[a]Present address: Department of Chemistry, Gobi Arts College, Gobichettipalayam 638452, India.

0003-2670/84/$03.00

ethanol. 5,6-Benzoquinoline (Gold Label, Aldrich Chemical Co.) and polyacrylic acid (secondary standard, Scientific Polymer Products, Ontario, NY) were used as received. The filter paper (Whatman No. 1) was developed in ethanol to collect impurities at one end prior to use.

Procedure. A stock solution of polyacrylic acid in ethanol (1 g/25 ml) was prepared by sonification over a period of 6 h. The stock solution was used to dilute ethanolic neutral or hydrobromic acid (0.1 M) solutions containing the required amount of phosphor. The phosphor solution (1 μl) containing 20 μg of polyacrylic acid was allowed to form a drop at the blunt tip of a Hamilton syringe (Model No. 701N) and then placed on the filter paper. The stem (stainless steel) of the Hamilton syringe had an external sleeve of tightly fitted teflon tubing to prevent reactions with some solutions that interfered with r.t.p. studies. The filter paper containing the sample was heated to 80°C for 15—20 min in an open air oven or placed in a vacuum oven at room temperature for 30 min. The r.t.p. intensities were measured as described earlier [6].

The following excitation and emission wavelengths were used: 5,6-benzoquinoline, 370 nm, 510 nm; 4-phenylphenol, 285 nm, 480 nm; *p*-aminobenzoic acid 290 nm, 430 nm; 1,2-benzocarbazole, 300 nm, 500 nm; phenanthrene, 300 nm, 500 nm.

Results and discussion

Mixtures of polyacrylic acid (PAA) and salt, and silica gel chromatoplates containing a salt of PAA as a binder have been used to induce r.t.p. from a variety of compounds [1, 7—10]. In this work, phosphors in ethanolic PAA solutions were spotted on filter paper.

Table 1 compares r.t.p. data for four compounds of widely different structural features adsorbed on filter paper and filter paper with PAA. Several concentrations of PAA were investigated and 20 $\mu g\ \mu l^{-1}$ in the sample solution was found to give the optimal r.t.p. for the compounds investigated. The phosphors were adsorbed onto the surfaces from ethanol, ethanol/0.1 M HBr, ethanol/PAA and ethanol/PAA/0.1 M HBr solutions (Table 1). Ethanol has been used routinely in r.t.p. work and ethanolic 0.1 M HBr solutions have been important in yielding strong r.t.p. from some phosphors [1, 7, 10]. Table 1 shows that the linear ranges for the phosphors were either 0—60 ng or 0—80 ng. The results in Table 1 show an enhancement in sensitivity for all the phosphors adsorbed with PAA onto filter paper. Sensitivity enhancements varied from 26-fold to 1.1-fold.

Table 1 shows that in all but one case the limits of detection were improved with the PAA addition. It should be noted that quantitatively useful signals were not obtained for 4-phenylphenol adsorbed with PAA on filter paper from ethanolic 0.1 M HBr solution. The r.t.p. of hydroxyl aromatics has been discussed [9]. Also, no useful r.t.p. signals were obtained from *p*-aminobenzoic acid adsorbed from ethanolic 0.1 M HBr solutions. For most phosphors, the relative standard deviations were lower when PAA was added.

TABLE 1

Comparison of quantitative data for phosphors adsorbed with and without PAA on filter paper

Compound and solution[a]	Sensitivity enhancement[b]		Detection limit (ng)[e]			
			With PAA		Without PAA	
	Air[c]	Vacuum[d]	Air[c]	Vacuum[d]	Air[c]	Vacuum[d]
5,6-Benzoquinoline						
Ethanol	26	16	0.04(2.9)	0.10(3.2)	4.0(5.9)	3.2(4.6)
0.1 M HBr-ethanol	2.0	1.3	0.07(3.8)	0.24(1.7)	0.14(4.3)	0.6(3.6)
1,2-Benzocarbazole						
Ethanol	1.1	1.2	0.70(2.0)	0.70(3.8)	0.70(5.8)	0.90(3.2)
0.1 M HBr-ethanol	1.9	1.5	1.4(4.9)	1.5(3.7)	4.0(6.2)	4.0(6.4)
4-Phenylphenol						
Ethanol	1.2	1.7	17(5.9)	24(4.1)	20(6.0)	40(4.9)
0.1 M HBr-ethanol	—	—	—	—	17(6.8)	30(6.4)
p-Aminobenzoic acid						
Ethanol	1.2	1.3	0.90(6.1)	1.1(2.0)	1.0(5.8)	1.5(4.2)
0.1 M HBr-ethanol	—	—	—	—	—	—

[a]Linear range 0—80 ng except for 5,6-benzoquinoline (0.1 M HBr-ethanol, vacuum-dried), 1,2-benzocarbazole (0.1 M HBr-ethanol, air-dried and vacuum-dried), and 4-phenylphenol (ethanol, vacuum-dried) which were 0—60 ng. [b]The sensitivity enhancement is the ratio of the slope of the calibration graph obtained with PAA to the slope of the calibration curve obtained without PAA. [c]Dried in an open air oven at 80°C for 15—20 min. [d]Dried in a vacuum oven at room temperature for 30 min. [e]Limit of detection (ng) based on a signal-to-noise ratio of 3, with relative standard deviation (%) in parentheses.

The vacuum-dried samples with PAA addition generally showed the lowest relative standard deviations. The relative standard deviations were calculated on the basis of the relative response of the various samples. The lower relative standard deviations with the PAA addition apparently result from the smaller spot size relative to the spot size without the addition of PAA.

The standard deviations for the relative response of the samples were also compared. Comparisons were made between combinations of vacuum-dried and air-dried spots on filter paper with and without addition of PAA. For the samples listed in Table 1, six of the pairs of samples spotted with PAA showed lower standard deviations than the samples without PAA. The other six pairs of samples showed the opposite trend with standard deviations lower without PAA than with PAA. Application of the F-test showed that eight pairs of the standard deviations were significantly different at the 95% confidence level. Yet the relative standard deviations were lower for the PAA-containing samples in most cases (Table 1).

The results in Table 1 generally show improved sensitivity, limits of detection and relative standard deviations when PAA is added to the sample. It is clear from Table 1 that no one set of conditions will give the "best" data for all the compounds studied. Probably, experiments with other phosphors

would yield improved data with PAA addition on filter paper. It was found that the r.t.p. of phenanthrene was decreased considerably when adsorbed from the PAA solution onto filter paper or a silica gel chromatoplate. It appears the new approach works best with phosphors that have polar functionality.

Finally, the above results should be put in perspective with other r.t.p. results. A limit of detection of 1.2 ng (S/N of 3) was obtained here for 5,6-benzoquinoline adsorbed on a silica gel chromatoplate. A relative standard deviation of 3.2% (16 samples at 100 ng each) was reported for 5,6-benzoquinoline on a silica gel chromatoplate [6]. Table 1 shows a lower limit of detection and a lower relative standard deviation for 5,6-benzoquinoline adsorbed from ethanol on filter paper with PAA. No comparable data have been published for 1,2-benzocarbazole. With 4-phenylphenol, a limit of detection of 1.1 ng (S/N of 3) was reported for the compound adsorbed on filter paper from an ethanolic sodium bromide solution [9]; the relative standard deviation was 5.5% (average of two sets of ten samples at 100 ng each). The data in Table 1 show an improvement in relative standard deviation but not in the limit of detection for 4-phenylphenol. With *p*-aminobenzoic acid adsorbed on sodium acetate, a limit of detection of 0.4 ng was obtained and the relative standard deviation was 5% (10 samples at 100 ng each) [11]. Table 1 indicates an improvement in the relative standard deviation but no improvement in the limit of detection. The main purpose of the present work was to compare the performance of filter paper with and without addition of PAA because filter paper is the most widely used surface to induce r.t.p. The results in Table 1 suggest that addition of PAA to the sample improves the performance of filter paper as a surface for inducing r.t.p.

Financial support for this project was provided by the Department of Energy, Division of Basic Energy Sciences, Contract No. DE-AC02-80ER10624.

REFERENCES

1 R. J. Hurtubise and R. A. Dalterio, Am. Lab., 13 (11) (1981) 58.
2 R. T. Parker, R. S. Freedlander and R. B. Dunlap, Anal. Chim. Acta, 119 (1980) 189; 120 (1980) 1.
3 R. J. Hurtubise, Solid Surface Luminescence Analysis: Theory, Instrumentation, Applications, M. Dekker, New York, 1981, Ch. 3, 5, and 7.
4 R. P. Bateh and J. D. Winefordner, Talanta, 29 (1982) 713.
5 M. W. Warren II, J. P. Avery and H. V. Malmstadt, Anal. Chem., 54 (1982) 1853.
6 C. D. Ford and R. J. Hurtubise, Anal. Chem., 51 (1979) 659.
7 R. J. Hurtubise, Talanta, 28 (1981) 145.
8 R. J. Hurtubise and G. A. Smith, Anal. Chim. Acta, 139 (1982) 315.
9 R. A. Dalterio and R. J. Hurtubise, Anal. Chem., 54 (1982) 224.
10 S. M. Ramasamy and R. J. Hurtubise, Anal. Chem., 54 (1982) 1642.
11 R. M. A. von Wandruska and R. J. Hurtubise, Anal. Chem., 48 (1976) 1784.

Analytica Chimica Acta, 157 (1984) 207—210
Elsevier Science Publishers B.V., Amsterdam — Printed in The Netherlands

Short Communication

THE DETERMINATION OF VANADIUM IN STEEL SAMPLES BY X-RAY FLUORESCENCE SPECTROMETRY AFTER PRECIPITATION WITH 4-CAPRINOYL-3-METHYL-1-PHENYL-5-PYRAZOLONE

YOSHIFUMI AKAMA*, MASARU HAYAKAWA, TOSHIO NAKAI and FUMIKAZU KAWAMURA

Department of Chemistry, Meisei University, Hino, Tokyo 191 (Japan)

(Received 27th January 1983)

Summary. Vanadium(V) is quantitatively precipitated from aqueous solution with 4-caprinoyl-3-methyl-1-phenyl-5-pyrazolone at pH 1, and collected as a film on a membrane for x-ray fluorescence spectrometry. The limit of detection is ca. 2 μg of vanadium. The procedure gave satisfactory results on standard steels containing 0.003—0.091% vanadium.

X-ray fluorescence (x.r.f.) spectrometry is frequently used for the direct determination of metals in alloys, plants, rocks, etc. without preliminary digestion of samples; the risk of contamination of the sample is thus considerably reduced. Direct x.r.f. methods, however, are not successful if standard samples are not available, and are difficult to apply to low metal concentrations because the method lacks sensitivity. Therefore, a preliminary coprecipitation is often preferred [1—3] for the concentration and separation of trace elements from complex matrices.

In this communication, the preconcentration of vanadium(V) is done by precipitation with 4-caprinoyl-3-methyl-1-phenyl-5-pyrazolone (CMPP). 4-Benzoyl-3-methyl-1-phenyl-5-pyrazolone (BMPP) has been extensively used for the extraction [4—10] of metals, but CMPP has rarely been applied [11, 12]. The latter compound is easily prepared from 3-methyl-1-phenyl-5-pyrazolone and possesses good chemical stability and reasonable solubility in organic solvents. Vanadium(V) is chelated with CMPP at pH 1 and precipitated. The precipitate is collected as a thin film for x.r.f. spectrometry. In steel analysis, agreement with the certified values was good and the recovery of vanadium(V) from spiked samples was 97—108%.

Experimental

Reagents. The CMPP was synthesized as described by Jensen [13], purified by recrystallizing from methanol, and dried under reduced pressure. (Found 72.6% C, 8.65% H, 8.5% N; required 73.2% C, 8.5% H, 8.5% N.) A 0.3% (w/v) solution of CMPP was prepared in acetone; this solution was stable for several months. A stock solution (1.00 g l^{-1}) of vanadium(V) was

0003-2670/84/$03.00

prepared by dissolving 2.298 g of ammonium metavanadate in 100 ml of 9 M sulfuric acid and diluting to 1 l with distilled water. Dilute standards were prepared by suitable dilution with water. Buffer solutions for the pH range 0.5—2 were prepared from 1 M hydrochloric acid and 1 M sodium acetate, and for the pH range 3—6 from 1 M sodium acetate and 1 M acetic acid. All other solvents and reagents were of reagent-grade.

Apparatus. The x.r.f. measurements were done with a Rigaku-Denki KG-4 spectrometer. The operating conditions used are shown in Table 1.

General procedure. Pipette a portion of the sample solution containing 5—200 μg of vanadium(V) into a 300-ml beaker, dilute to 300 ml with distilled water and adjust to pH 1 with the hydrochloric acid/acetate buffer. Add 2 ml of the 0.3% (w/v) CMPP solution and stir for a few minutes. Leave overnight at 4°C. Filter through a membrane filter (1.0-μm pore size, 47-mm diameter, Toyo Roshi Co.). Measure the intensity of the V $K\alpha$ line and its background under the conditions listed in Table 1.

Procedure for steels. Dissolve the sample (0.5—1.0 g) in 20 ml of aqua regia by heating on a hot-plate at 150°C, then evaporate to dryness, and cool. If dissolution is incomplete, add 2 ml of perchloric acid and evaporate to dryness again. Dissolve the residue in 10 ml of concentrated hydrochloric acid and repeat the evaporation. Finally, dissolve the residue in 35 ml of 7 M hydrochloric acid, transfer to a 100-ml separating funnel, add 30 ml of 4-methylpentan-2-one and shake the funnel vigorously for a few minutes to remove the iron. Heat the separated aqueous phase to remove any dissolved solvent and dilute to exactly 100 ml with water. Oxidize any vanadium(IV) to vanadium(V) by addition of 0.1% (w/v) potassium permanganate solution and then measure total vanadium as described above.

Results and discussion

4-Caprinoyl-3-methyl-1-phenyl-5-pyrazolone forms insoluble metal complexes and is itself only slightly soluble in water at lower pH. Thus vanadium(V) is quantitatively precipitated as a vanadium(V)—CMPP complex. If the vanadium(V) content in the solution is low, the complex is co-deposited with the excess of CMPP.

Interferences. Various ions were examined for their effect on the precipitation of 100 μg vanadium(V). Among the ions examined, Al, Ba, Ca, Cd, Co(II), K, Mg, Mn(II), Ni(II), Pb and Zn ions were not precipitated at pH 1, and did not interfere even at 50-fold (mass) ratios to vanadium(V). As can be

TABLE 1

Operating conditions for vanadium determination

X-ray tube	Philips tungsten target (2 kW)	Counter	Scintillation counter
Voltage and current	42.5 kV, 28 mA	Line	V $K\alpha$ ($2\theta = 76.92^\circ$)
Collimator	Primary 0.45 mm × 10 cm, Secondary 0.15 mm × 10 cm	Background	$2\theta = 78.00^\circ$
		Counting	Fixed time method (40 s)
Analyzing crystal	LiF (200)	Path	Vacuum

TABLE 2

Determination of vanadium(V) (100 μg) in the presence of diverse ions

Ion	Amount added (mg)	V found (μg)	Ion	Amount added (mg)	V found (μg)
Cr(VI)	3	98	Mo(VI)	0.05	95
	5	79		0.1	88
Cu(II)	0.1	96	W(VI)	0.1	99
	0.3	38		0.3	92
Fe(III)	1	99		0.5	83
	5	90			

seen from Table 2, W(VI), Mo(VI) and Cu(II) interfered seriously even at moderate concentrations, and so require separation or masking.

Effect of pH and CMPP concentration. A study of the effect of pH in the range 0.5—6 on the precipitation of vanadium(V) showed that constant maximum intensity of the V $K\alpha$ line was obtained for pH 0.5—4. All later precipitations were therefore done at pH 1.

It was found that 2 ml of 0.1% (w/v) CMPP solution in acetone sufficed for quantitative precipitation of 100 μg of vanadium(V). A large excess (up to 2 ml of 1%) had no adverse effect, and 2 ml of 0.3% (w/v) reagent solution is recommended. Variation of the aqueous solution volume did not influence the precipitation of 100 μg of vanadium(V) in the range 100—1000 ml.

Calibration graph. Under the recommended conditions, the calibration graph was linear over the range 0—200 μg of vanadium(V) per 300 ml. The relative standard deviation of the intensity of the V $K\alpha$ line was calculated to be 1.0% for five separate measurements of 50 μg of vanadium(V).

Application. Four Japanese Iron and Steel Standards (JSS) were chosen for testing; the concentrations of interfering elements such as W, Mo, Cu, in

TABLE 3

Determination of vanadium in selected steel samples

Sample	Taken (g)	Vanadium content (%)		
		Proposed method[a]	Other method[b]	Certified
JSS 503-4	1.2673	0.003	—	0.004
JSS 102-3	0.9101	0.035	0.036	0.035
JSS 151-7	0.4994	0.052	0.058	0.053
JSS 175-3	0.5039	0.091	0.091	0.093

[a]A 1/20 aliquot of the sample solution was used. The values given are the mean of 5 determinations. [b]Spectrophotometric method [10] with CMPP.

TABLE 4

Recovery of vanadium(V) added to standard steel samples

Sample	Taken[a] (g)	Vanadium(V) (μg)		
		Added	Found	Recovery (%)
JSS 151-7	0.4994	0	13	—
		50	67	108
		100	110	97
JSS 175-3	0.5039	0	23	—
		50	72	98
		100	129	106
		150	179	104

[a]A 1/20 aliquot of steel solution was used.

these steels are lower than the above tolerance limits. The interference of large amounts of iron was prevented by extraction with 4-methylpentan-2-one as outlined above. The results obtained by the recommended method are in good agreement with the certificate values (Table 3). The recoveries of vanadium(V) added to the steel samples after acid digestion were reasonable (Table 4).

The proposed method is suitable for the determination of vanadium in the range 0.003—0.1%. It is reproducible and accurate, and can be used down to 2 μg of vanadium. More accurate determinations of lower concentrations will be obtained by taking larger sample weights.

The authors thank Dr. H. Kanno for helpful comments and Dr. M. Kajitani for doing the elemental analysis of CMPP. The present work was partly supported by a Grant-in-Aid for Scientific Research from the Ministry of Education, Science and Culture.

REFERENCES

1 C. L. Luke, Anal. Chim. Acta, 41 (1968) 237.
2 H. Watanabe, S. Berman and D. S. Russell, Talanta, 19 (1972) 1363.
3 S. Takemoto, H. Kitamura, Y. Kuge, S. Nakagawa, K. Murata and S. Ikeda, Bunseki Kagaku, 25 (1976) 40.
4 S. Umetani, M. Matsui, J. Tôei and T. Shigematsu, Anal. Chim. Acta, 113 (1980) 315.
5 S. Umetani, K. Sasayama and M. Matsui, Anal. Chim. Acta, 134 (1982) 327.
6 M. Y. Mirza, Talanta, 25 (1978) 685.
7 M. Y. Mirza and F. Ik. Nwabue, J. Inorg. Nucl. Chem., 43 (1981) 1817.
8 E. Uhlemann, B. Maack and M. Raab, Anal. Chim. Acta, 116 (1980) 153.
9 J. P. Brunette, M. Lakkis, G. Goetz-Grandmont and M. J. F. Leroy, Polyhedron, 1 (1982) 461.
10 Y. Akama, T. Nakai and F. Kawamura, Analyst, 106 (1981) 250.
11 Y. Akama, T. Nakai and F. Kawamura, Fresenius Z. Anal. Chem., 310 (1982) 429.
12 Y. Akama, H. Naka, T. Nakai and F. Kawamura, Bunseki Kagaku, 27 (1978) 680.
13 B. S. Jensen, Acta Chem. Scand., 13 (1959) 1668.

Vol. 157, No. 1

ACA announcements

AWARD

DAL NOGARE AWARD

Dr. Hamish Small is the recipient of the 1984 Dal Nogare Award sponsored by the Chromatography Forum of the Delaware Valley. The award is given annually, in memory of Stephen Dal Nogare, one of the outstanding innovators in gas chromatography and the first elected president of the forum. The award will be presented during the Pittsburgh Conference on Analytical Chemistry and Applied Spectroscopy, Tuesday afternoon, March 6, 1984, in Atlantic City, NJ, U.S.A., as part of a special award symposium.

Dr. Hamish Small was born and educated in Northern Ireland. He has B.S. and M.S. degrees from the Queen's University, Belfast. During 1949–1955 he worked at the AERE Harwell. In 1955 he emigrated to the U.S.A. and joined the Dow Chemical Company. He worked in Dow's Central Research Department until 1983 when he retired to pursue professional and private interests.

His work on ion chromatography and hydrodynamic chromatography has earned him a number of awards including the Pittsburgh Applied Analytical Chemistry award and the Albert F. Sperry award of the Instrument Society of America. His address at the Dal Nogare Award Symposium will be "Practical and Theoretical Challenges in the Chromatography of Colloidal Particles".

ANNOUNCEMENTS OF MEETINGS

INTERNATIONAL SYMPOSIUM ON QUANTITATIVE LUMINESCENCE SPECTROMETRY IN BIOMEDICAL SCIENCES, GHENT, BELGIUM, SEPTEMBER 3–6, 1984

An international symposium on quantitative luminescence spectrometry in biomedical sciences, sponsored by the Faculty of Pharmaceutical Sciences of the State University of Ghent, the National Foundation of Scientific Research (N.F.W.O. – F.N.R.S.), and the Ministry of Education, will be held at the Farmaceutisch Instituut in Ghent.

Contributed papers will cover the following topics: drug and bioanalysis via fluorescence and phosphorescence; fluorescence and chemiluminescence immunoassays; detection techniques in chromatography (fluorescence, r.t.p.l., etc.); solid-surface luminescence methods; chemical derivatization methods; luminescence applications and drug metabolism, clinical chemistry, biochemistry, pharmacokinetics, toxicology, ecology, protein tagging. The conference will be conducted in English and no simultaneous translation will be provided. Facilities for technical exhibitions will be arranged.

Five plenary lectures will be presented: R.P. Ekins (fluoroimmunoassays), R.W. Frei (detection techniques), G.G. Guilbault (fluorescence techniques), J.N. Miller (solid-surface methods), and J.S. Woodhead (chemiluminescence immunoassays).

Further information: Dr. W. Baeyens, Symposium Chairman, Laboratoria voor Farmaceutische Chemie en voor Ontleding van Geneesmiddelen, Rijksuniversiteit Gent, Harelbekestraat 72, B-9000 Ghent, Belgium.

1984 EASTERN ANALYTICAL SYMPOSIUM, NEW YORK, NY, U.S.A., NOVEMBER 13–16, 1984

A limited number of oral and poster presentations on new developments in analytical chemistry will be accepted for the 1984 Eastern Analytical Symposium. These presentations will be grouped into several sessions to complement the symposium's invited technical sessions. Prospective authors should submit a 50- to 100-word abstract before April 1st, 1984, indicating preference of oral or

poster format, to Mr. Thomas Kometani, EAS Program Chairman, Bell Laboratories RM1A-378, 600 Mountain Avenue, Murray Hill, NJ 07974, U.S.A. Tel.: (201) 582-6559. Care should be exercised in considering the title and authors of the proposed presentation; if the presentation is accepted, both title and authors will be considered final. Authors of accepted presentations will receive forms for submission of a 200- to 300-word abstract which will appear in the final program.

3rd INTERNATIONAL CONGRESS ON ANALYTICAL TECHNIQUES IN ENVIRONMENTAL CHEMISTRY, BARCELONA, SPAIN, NOVEMBER 21–23, 1984

The above congress, to be held in conjunction with the 14th Annual Symposium on the Analytical Chemistry of Pollutants, will take place at the Congress Centre, Barcelona. The congress will be devoted to invited plenary lectures, invited and submitted research lectures and poster presentations covering the whole field of environmental analytical chemistry.

Further details, together with registration form and preliminary programme, may be obtained from: Dr. J. Albaiges, Expoquimia, Avenida Reina Ma. Cristina, Barcelona 4, Spain.

CALENDAR OF FORTHCOMING MEETINGS

March 5–9, 1984 Atlantic City, NJ, U.S.A.	**35th Pittsburgh Conference and Exposition on Analytical Chemistry and Applied Spectroscopy** Contact: Linda Briggs, Pittsburgh Conference, 437 Donald Road, Dept. J-005, Pittsburgh, PA 15235, U.S.A. (Further details published in Vol. 155.)
March 26–30, 1984 London, Great Britain	**APCOM '84 – 18th International Symposium on the Application of Computers and Mathematics in the Mineral Industries** Contact: The Conference Office, The Institute of Mining and Metallurgy, 44 Portland Place, London W1N 4BR, Great Britain.
April 8–13, 1984 St. Louis, MO, U.S.A.	**187th National Meeting of the American Chemical Society** Contact: Meetings Department, American Chemical Society, 1155 Sixteenth Street, NW, Washington, DC 20036, U.S.A.
April 10–13, 1984 Munich, G.F.R.	**9th Conference on Biochemical Analysis (BIOCHEMISCHE ANALYTIK 84) & ANALYTICA 84 Exhibition** Contact: Secretary General, Dr. Rosmarie Vogel, Abteilung für Klinische Chemie und Klinische Biochemie in der Chirurgischen Klinik Innenstadt der Universität München, Nussbaumstrasse 20, D-8000 München 2, G.F.R. Tel.: (089) 15 30 32, Telex: 5 216 018 bird d. (Further details published in Vol. 151, No. 1.)
April 16–18, 1984 Neuherberg, F.R.G.	**3rd International Workshop on Trace Element Analytical Chemistry in Medicine and Biology** Contact: Dr. P. Schramel, Gesellschaft für Strahlen- und Umweltforschung, Institut für Angewandte Physik, Physikalisch-Technische Abteilung, Ingolstädter Landstrasse 1, D-8042 Neuherberg, F.R.G.
April 16–19, 1984 Exeter, U.K.	**Royal Society of Chemistry Annual Congress** Contact: Royal Society of Chemistry, Burlington House, London W1V 0BN, U.K. Tel.: 01-734 9971.
April 16–19, 1984 New York, NY, U.S.A.	**20th International Symposium on Advances in Chromatography** Contact: Professor A. Zlatkis, Chemistry Department, University of Houston, Houston, TX 77004, U.S.A. (Further details published in Vol. 155.)

April 17–19, 1984 Noordwijkerhout, The Netherlands	**Analytical Methods and Problems in Biotechnology – An International Symposium** Contact: W.A. Scheffers, Symposium Analytical Methods and Problems in Biotechnology, Delft University of Technology, Laboratory of Microbiology, Julianalaan 67A, NL-2628 BC Delft, The Netherlands. Tel.: (015)-782411. (Further details published in Vol. 152.)
April 29–May 4, 1984 Rio de Janeiro, Brazil	**12th International Congress of Clinical Chemistry, 7th Latin American Congress of Clinical Biochemistry, & 12th Brazilian Congress of Clinical Analysis** Contact: 12th International Congress of Clinical Chemistry, Rua Vicente Licinio 95, Tijuca, 20270 Rio de Janeiro, RJ, Brazil.
May 9–11, 1984 Dourdan, France	**4th Weurman Flavour Research Symposium** Contact: J. Adda, Laboratoire de Recherches sur les Arômes, 17 rue Sully, 21034 Dijon Cedex, France.
May 15–18, 1984 Ghent, Belgium	**5th International Symposium on Mass Spectrometry in Life Sciences** Contact: Prof. Dr. A. De Leenheer, Symposium Chairman, Laboratoria voor Medische Biochemie en voor Klinische Analyse, Harelbekestraat 72, B-9000 Ghent, Belgium. Tel.: (091) 21.89.51. (Further details published in Vol. 155.)
May 20–25, 1984 New York, NY, U.S.A.	**8th International Symposium on Column Liquid Chromatography** Contact: Professor Cs. Horváth, Mason Laboratory, Yale University, P.O. Box 2159, Yale Station, New Haven, CT 06520, U.S.A. (Further details published in Vol. 146.)
June 12–14, 1984 Szeged, Hungary	**2nd Symposium on the Analysis of Steroids** Contact: Professor S. Görög, Chairman of the Organizing Committee of the 2nd Symposium on the Analysis of Steroids, c/o Hungarian Chemical Society, H-1061 Budapest, Anker köz 1, Hungary.
June 28–20, 1984 Milan, Italy	**2nd International Conference on Chromatography and Mass Spectrometry in Biomedical Sciences** Contact: Dr. Alberto Frigerio, Italian Group for Mass Spectrometry in Biochemistry and Medicine, Via Eustachi 36, I-20129 Milan, Italy; or, Dr. Hubert Milon, P.O. Box 88, CH-1814 La Tour-de-Peilz, Switzerland. Tel: (24) 42 11 91; Telex: 457302 lino ch. (Further details published in Vol. 155.)
June 18–21, 1984 Ronneby, Sweden	**International Symposium on Liquid Chromatography in the Biomedical Sciences** Contact: Swedish Academy of Pharmaceutical Sciences, P.O. Box 1136, S-111 81 Stockholm, Sweden. (Further details published in Vol. 152.)
June 24–28, 1984 Jerusalem, Israel	**9th International CODATA (Committee on Data for Science and Technology) Conference** Contact: Kopel Tours Ltd. – Conventions, P.O. Box 4413, 61 044 Tel Aviv, Israel. Tel.: (03) 653616; Telex: 35562 ktor il; Cable: Kopel Tel Aviv.
July 10–13, 1984 Leeds, U.K.	**2nd Biennial National Atomic Spectroscopy Symposium** Contact: Mr. F. Buckley, Department of Earth Sciences, University of Leeds, Leeds, W. Yorks. LS2 9JT, U.K. Tel. 0532-431751, ext. 6464 or 6465. (Further details published in Vol. 155.)
Aug. 21–24, 1984 Colombo, Sri Lanka	**Analytical Chemistry in Development** Contact: Centre for Analytical Research and Development, Department of Chemistry, University of Colombo, Colombo, Sri Lanka; or, Trace Analysis Research Centre, Chemistry Department, Dalhousie University, Halifax, N.S. B3H 4J1, Canada. (Further details published in Vol. 151, No 1.)

Aug. 26–31, 1984 Philadelphia, PA, U.S.A.	**188th National Meeting of the American Chemical Society** Contact: A.T. Winstead, American Chemical Society, 1155 16th Street, NW, Washington, DC 20036, U.S.A.
Aug. 26–Sept. 1, 1984 Cracow, Poland	**EUROANALYSIS V – 5th European Conference on Analytical Chemistry** Contact: Professor Zygmunt Kowalski, Secretary-General, Euroanalysis V, Academy of Mining and Metallurgy, Mickiewicza 30, 30-059 Kraków, Poland. (Further details published in Vol. 148.)
Aug. 27–31, 1984 Göttingen, F.R.G.	**Electrophoresis 84. 4th International Meeting of the Electrophoresis Society** Contact: Dr. V. Neuhoff, Max-Planck-Institut für experimentelle Medizin, Hermann-Rein-Strasse 3, D-3400 Göttingen, F.R.G. Tel.: 0551-303248.
Sept. 2–6, 1984 Hradec Králové, Czechoslovakia	**4th International Symposium on Isotachophoresis – ITP 84** Contact: ITP 84, Dr. Z. Prusik, C.Sc., Institute of Organic Chemistry and Biochemistry, Czechoslovak Academy of Sciences, Flemingovo nám. 2, CS-166 10 Praha 6, Czechoslovakia. (Further details published in Vol. 146.)
Sept. 3–6, 1984 Ghent, Belgium	**International Symposium on Quantitative Luminescence Spectrometry in Biomedical Sciences** Contact: Dr. W. Baeyens, Symposium Chairman, Laboratoria voor Farmaceutische Chemie en voor Ontleding van Geneesmiddelen, Rijksuniversiteit Gent, Harelbekestraat 72, B-9000 Ghent, Belgium.
Sept. 23–28, 1984 Philadelphia, PA, U.S.A.	**11th Annual Meeting of the Federation of Analytical Chemistry and Spectroscopy Societies** Contact: R.F. Hirsch, Division of Analytical Chemistry, American Chemical Society, 304 Beach Wood, Orange, NJ 07050, U.S.A.
Oct. 1–5, 1984 Nürnberg, G.F.R.	**15th International Symposium on Chromatography** Contact: Gesellschaft Deutscher Chemiker, Abteilung Fachgruppen, Postfach 90 04 40, Varrentrappstrasse 40–42, D-6000 Frankfurt (Main) 90, G.F.R.
Oct. 8–10, 1984 Tarrytown, NY, U.S.A.	**3rd International Symposium on Capillary Chromatography** Contact: Dr. A. Zlatkis, Chemistry Department, University of Houston, Houston, TX 77004, U.S.A.
Oct. 13–18, 1984 Mátrafüred, Hungary	**4th Scientific Session on Ion-Selective Electrodes** Contact: Organizing Committee, 4th Scientific Session on Ion-Selective Electrodes, Institute for General and Analytical Chemistry, Technical University, 1502 Budapest, Gellért tér 4, Hungary. (Further details published in Vol. 155.)
Oct. 24–26, 1984 Montreux, Switzerland	**Third Workshop on LC–MS and MS–MS** Contact: Professor Dr. R.W. Frei, Department of Analytical Chemistry, Free University, De Boelelaan 1083, 1081 HV Amsterdam, The Netherlands. (Further details published in Vol. 151, No. 1.)
Nov. 13–16, 1984 New York, NY, U.S.A.	**1984 Eastern Analytical Symposium** Contact: Dr. S. David Klein, EAS Publicity, Merck & Co., Inc., P.O. Box 2000/R80L-106, Rahway, NJ 07065, U.S.A. Tel.: (201) 846-1582.
Nov. 19–24, 1984 Barcelona, Spain	**EXPOQUIMIA 84 – Salón Internacional de la Quimica** Contact: EXPOQUIMIA, Feria de Barcelona, Barcelona 4, Spain.

Nov. 21–23, 1984 Barcelona, Spain	**3rd International Congress on Analytical Techniques in Environmental Chemistry** Contact: Dr. J. Albaiges, Expoquimia, Avenida Reina Ma, Cristina, Barcelona 4, Spain; or Instituto de Quimica Bio-organica, Jorge Girona Salgado S/N, Barcelona-34, Spain. Tel.: 204 06 00.
Nov. 22–24, 1984 Barcelona, Spain	**14th Annual Symposium on Analytical Chemistry of Pollutants** Contact: 3rd International Congress on Analytical Techniques in Environmental Chemistry/EXPOQUIMIA, Av. Reina Ma. Christina, Palacio No. 1, Barcelona 4, Spain. Tel.: 223.31.01; telex: 50458 FOIMB-E.
Nov. 22–24, 1984 Barcelona, Spain	**3rd International Congress on Analytical Techniques in Environmental Chemistry** Contact: 3rd International Congress on Analytical Techniques in Environmental Chemistry/EXPOQUIMIA, Av. Reina Ma. Christina, Palacio No. 1, Barcelona 4, Spain. Tel.: 223.31.01; telex: 50458 FOIMB-E.
Dec. 10–12, 1984 Baltimore, MD, U.S.A.	**4th International Symposium on HPLC of Proteins, Peptides, and Polynucleotides** Contact: Shirley E. Schlessinger, Symposium Manager, Fourth International Symposium on HPLC of Proteins, Peptides, and Polynucleotides, 400 East Randolph, Chicago, IL 60601, U.S.A. Tel.: (312) 527-2011.
Feb. 25–March 1, 1985 New Orleans, LA, U.S.A.	**36th Pittsburgh Conference and Exposition on Analytical Chemistry and Applied Spectroscopy** Contact: Linda Biggs, Pittsburgh Conference, 437 Donald Road, Dept. J-005, Pittsburgh, PA 15235, U.S.A.
April 28–May 3, 1985 Miami Beach, FL, U.S.A.	**189th National Meeting of the American Chemical Society** Contact: Meetings Department, American Chemical Society, 1155 Sixteenth Street, NW, Washington, DC 20036, U.S.A.
July 1–5, 1985 Edinburgh, Scotland, Great Britain	**9th International Symposium on Column Liquid Chromatography** Contact: J.H. Knox, Department of Chemistry, University of Edinburgh, Edinburgh EH9 3JJ, Scotland, Great Britain.
Sept. 8–13, 1985 Chicago, IL, U.S.A.	**190th National Meeting of the American Chemical Society** Contact: Meetings Department, American Chemical Society, 1155 Sixteenth Street, NW, Washington, DC 20036, U.S.A.
Sept. 9–13, 1985 Manchester, Great Britain	**30th International Congress of Pure and Applied Chemistry** Contact: The Royal Society of Chemistry, Burlington House, London W1V 0BN, Great Britain. (Further details published in Vol. 155.)
Sept. 15–21, 1985 Garmisch-Partenkirchen, F.R.G.	**Colloquium Spectroscopicum Internationale XXIV** Contact: CSI XXIV, Organisationsbüro, Institut für Spektrochemie und angewandte Spektroskopie, Postfach 778, D 4600 Dortmund 1, F.R.G.
Nov. 11–16, 1985 Yalta, U.S.S.R.	**5th Danube Symposium on Chromatography** Contact: Dr. L.N. Kolomiets, The Scientific Council of Chromatography, Academy of Sciences of the U.S.S.R., Institute of Physical Chemistry, Lenin-Prospect 31, Moscow 117312, U.S.S.R.

(Continued from outside back cover)

Short Communications

 0003-2670/84/$03.00

rinted in The Netherlands

CONTENTS

(Abstracted, Indexed in: Anal. Abstr.; Biol. Abstr.; Chem. Abstr.; Curr. Contents Phys. Chem. Earth Sci.; Life Sci.; Index Med.; Mass Spectrom. Bull.; Sci. Citation Index; Excerpta Med.)

(Continued on inside back cov